



Centro Brasileiro de Pesquisas Físicas
Coordenação de Formação Científica
Coordenação de Cosmologia, Astrofísica e Interações
Fundamentais

Luiz Filipe de Oliveira Guimarães

On the degeneracy between inflationary and bouncing cosmologies

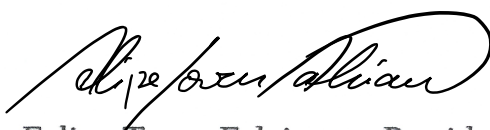
Rio de Janeiro - RJ

August 26, 2022

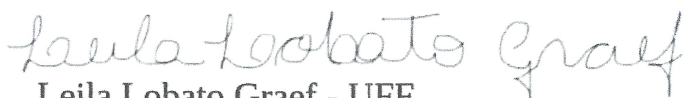
**“ON THE DEGENERACY BETWEEN INFLATIONARY AND BOUNCING
COSMOLOGIES”**

LUIZ FILIPE DE OLIVEIRA GUIMARÃES

Tese de Doutorado em Física apresentada no
Centro Brasileiro de Pesquisas Físicas do
Ministério da Ciência Tecnologia e Inovação.
Fazendo parte da banca examinadora os seguintes
professores:



Felipe Tovar Falciano – Presidente/Orientador/CBPF



Leila Lobato Graef - UFF

Documento assinado digitalmente



RUDNEI DE OLIVEIRA RAMOS
Data: 14/04/2022 16:08:39-0300
Verifique em <https://verificador.iti.br>

Rudnei de Oliveira Ramos - UERJ



Nelson Pinto Neto – CBPF



Clécio Roque De Bom - CBPF

Rio de Janeiro, 12 de abril de 2022.

Luiz Filipe de Oliveira Guimarães

**On the degeneracy between inflationary and
bouncing cosmologies**

Tese apresentada ao curso de Pós-Graduação em Física do Centro Brasileiro de Pesquisas Físicas, como requisito parcial para a obtenção do Título de doutor em Física.

Orientador:

Prof. Dr. Felipe Tovar Falciano

August 26, 2022

The billboard said "The End Is Near"
I turned around, there was nothing there
Yeah, I guess the end is here
The end is here
The end is here
The end is here
The end is...ahh
('I Know the End' - Phoebe Bridgers)

Agradecimentos

Primeiramente devo agradecer a minha família por tudo que representam para mim. Dedico esta tese a meu irmão Carlos Augusto, minha mãe, Graça, meu pai, Carlos Gabriel e minha avó, Maria Alice. Serei sempre grato pela força que eles demonstraram no período de saúde mais delicada de meu pai, em 2020, enquanto eu ainda estava fora do país. Também dedico esta tese ao meu avô José, que nos deixou em 2018;

Agradeço aos meus amigos de Niterói, de quem o doutorado sanduíche e a pandemia afastaram de mim, mas apenas geograficamente. A todos meus amigos e amigas, Brasil e mundo a fora;

Ao meu orientador, Felipe Tovar, por toda essa segunda etapa de orientação pela qual passamos juntos. Meu pai acadêmico para sempre. E ao meu co-orientador no exterior, Giovanni Marozzi, e esposa, por terem me recebido tão bem na Itália;

Ao meu irmão de orientação Guilherme Brando (GB), por todo incentivo, ajuda e zoações. Aos meus co-irmãos, Chiara Animalì e Matheus Rodrigues, pelo acolhimento, almoços, e amizade. Aos meus demais amigos de pós graduação, tanto os brasileiros do Rio, como Felipe Monteiro (FMA), quanto italianos de Pisa, como Gianfranco, Tiziano, Giovanni e Lorenzo. Aos meus colegas de apartamento, Gianfranco di Salle e Paolo Surdi, e ao proprietário, Carlo la Bella, e família. Aos meus amigos da UNIPI e de demais universidades brasileiras e estrangeiras. Em especial aos demais intercambistas de doutorado sanduíche na Itália, cujo grupo no WhatsApp foi de tremenda ajuda.

Aos meus colaboradores, em especial ao Nelson, por toda a ajuda. A todos os funcionários do CBPF – da limpeza, da COEDU, secretárias e seguranças.

Por fim, agradeço ao CNPq pela bolsa de doutorado. O presente trabalho foi realizado com apoio da Coordenação de Aperfeiçoamento de Pessoal de Nível Superior - Brasil (CAPES) - Código de Financiamento 001.

Contents

| | |
|--|------------|
| Resumo | x |
| Abstract | xii |
| 1 Introduction | 1 |
| 1.1 Hot Big-Bang Model | 4 |
| 1.1.1 Cosmological Puzzles | 4 |
| 1.2 Inflationary Scenario | 8 |
| 1.2.1 Inflationary Paradigm | 9 |
| 1.2.2 The Inflaton | 12 |
| 1.2.3 Inflaton dynamics | 14 |
| 1.2.4 Inflation Phenomenology | 15 |
| 1.2.5 Multi-Field Inflation | 18 |
| 1.3 Bouncing Cosmologies | 20 |
| 1.3.1 Bouncing Scenario | 21 |
| 1.3.2 Matter Bounce Scenario | 24 |
| 1.3.3 Realizing the bounce | 25 |
| 1.4 Inflation vs. Bounce | 26 |
| 2 Cosmological Perturbations | 28 |
| 2.1 Newtonian Perturbations | 29 |
| 2.2 Cosmological Perturbations in GR | 30 |
| 2.2.1 Linear Metric Perturbations | 31 |
| Scalar Perturbations | 32 |
| Tensor Perturbations | 33 |
| 2.2.2 Perturbation in the Matter Content | 33 |

| | | |
|----------|--|------------|
| 2.2.3 | Gauge Invariance | 34 |
| 2.2.4 | Adiabatic and Non-Adiabatic Perturbations | 35 |
| 2.2.5 | Entropic Mechanism | 45 |
| 2.3 | Perturbation Theory for $f(R)$ Gravity | 46 |
| 2.3.1 | Quantum Perturbations in $f(R)$ | 47 |
| 2.4 | Observations | 49 |
| 2.4.1 | Cosmological Perturbations Statistics | 49 |
| 2.4.2 | Non-Gaussianities | 55 |
| 2.4.3 | δN formalism | 59 |
| 2.4.4 | Current Observational Results | 62 |
| 2.4.5 | Cosmological Perturbations for Inflation | 64 |
| 2.4.6 | Cosmological Perturbations for Bouncing Cosmologies | 66 |
| 3 | Starobinsky-like Bouncing Model | 69 |
| 3.1 | Introduction | 69 |
| 3.2 | Starobinsky Inflation | 70 |
| 3.3 | Wands Duality | 78 |
| 3.4 | Starobinsky Inflation Parametrization | 82 |
| 3.5 | Starobinsky-like bounce | 84 |
| 3.5.1 | Scalar Duality vs. Tensor Duality | 89 |
| 3.6 | Cosmological Perturbations | 91 |
| 3.6.1 | Crossing the Bounce | 91 |
| 3.6.2 | Scalar Perturbations in Bounce Models | 95 |
| 3.6.3 | Tensor Perturbations | 99 |
| 3.7 | Results on the reconstruction of bouncing cosmologies from inflationary models | 103 |
| 4 | Reconstructed Self-Interacting Curvaton | 105 |
| 4.1 | Introduction | 105 |
| 4.2 | CMB Anomalies | 107 |
| 4.3 | Curvaton Scenario | 110 |
| 4.3.1 | Linear Cosmological Perturbations | 111 |
| 4.3.2 | Non-Gaussianities | 114 |

| | | |
|----------|--|------------|
| 4.4 | Curvaton Reconstruction Procedure | 116 |
| 4.4.1 | Crossing f_{NL} parameter | 116 |
| 4.4.2 | Constructing the curvaton potential | 117 |
| 4.4.3 | Observables from the reconstruction | 119 |
| 4.4.4 | Reconstructing a polynomial potential | 120 |
| 4.5 | Reconstructed Curvaton Model | 121 |
| 4.5.1 | Example A: $b = -20/e$, $c = 216/e$ | 123 |
| 4.6 | Producing the CMB Anomalies | 126 |
| 4.7 | Results on the non-Gaussianities and CMB anomalies in curvaton models | 129 |
| 5 | Bouncing Curvaton Scenario | 132 |
| 5.1 | Introduction | 132 |
| 5.2 | de Broglie-Bohm Scenario | 134 |
| 5.2.1 | Background Evolution | 134 |
| 5.2.2 | Cosmological Perturbations | 135 |
| 5.2.3 | Initial Conditions for the Perturbations of Massive Fields | 136 |
| 5.3 | Mixed Fluid-Curvaton Bouncing Scenario | 137 |
| 5.3.1 | Background Evolution | 137 |
| 5.3.2 | Mixed Fluid-Field Perturbations | 138 |
| 5.3.3 | Mixed Perturbations | 138 |
| 5.4 | Negative Mexican Hat Potential Model | 139 |
| 5.4.1 | Background | 139 |
| 5.4.2 | Scalar Field Cosmological Perturbations | 140 |
| 5.4.3 | Cosmological Perturbations: Fluid + Field | 141 |
| 5.5 | Revisiting the Negative Mexican Hat Model: Corrections to the case $m = 2$ | 142 |
| 5.5.1 | Background | 142 |
| 5.5.2 | Cosmological Perturbations | 144 |
| 5.5.3 | Total Spectral Index | 145 |
| 5.5.4 | The issue of the field initial conditions | 146 |
| 5.6 | Preliminary results for the mixed fluid-field dBB bounce cosmology | 148 |
| 6 | Conclusion | 150 |
| A | Introduction to Cosmology | 154 |

| | | |
|----------|---|------------|
| B | Computation of $z(\eta)$ | 158 |
| C | Fluid and field perturbations in the dBB quantum cosmology | 160 |
| C.1 | Mixed fluid-field scalar perturbations | 160 |
| C.1.1 | Mukhanov-Sasaki equations | 161 |
| C.1.2 | The power spectrum for each component | 164 |
| C.1.3 | Spectral index | 165 |
| C.1.4 | Total power spectrum | 166 |
| C.2 | Additional details about the scalar perturbations | 168 |
| C.2.1 | Field spectral index | 168 |
| C.2.2 | Revisiting the mixed inflaton-curvaton scenario | 169 |

List of Figures

| | | |
|-----|--|-----|
| 1.1 | Types of inflationary potentials: (a) Old Inflation, (b) New Inflation (hybrid of small field), and (c) Chaotic inflation (large field). | 15 |
| 2.1 | Decomposition of the entropy perturbation. | 43 |
| 2.2 | CMB temperature Fluctuations using the SMICA method. | 51 |
| 2.3 | CMB angular power spectrum (top) and its residual (bottom). | 54 |
| 2.4 | 68% and 95% confidence levels for n_s and r from the combination of Planck, BICEP2/Keck Array and BAO results, in comparison to theoretical predictions from different inflationary models. | 66 |
| 3.1 | Scalar field potential for the Starobinsky inflation in the Einstein frame. . . | 74 |
| 3.2 | Wands' duality maps an equation of state ω into $\tilde{\omega}$. There are only two fixed points that mapped into itself given by $\omega = -\frac{1}{3}$ and 1. The solid lines represent the map according to Eq. (3.51). The dots mark conventional equation of states in cosmology such as $\omega = -1, -\frac{1}{3}, 0, 1$ | 80 |
| 3.3 | Phase portrait of $\dot{\varphi}$ versus φ for the potential Eq. (3.99) using the values $V_0 = \varphi_* = 1$. One can see that the dynamics generated by this reconstructed potential are very similar to the exact dust ($p = 0$) potential showing that the square root deformation of the exponential potential works as a small correction. | 89 |
| 4.1 | Final allowed region for b in green, when $\sigma_{\max} = 0.15$, $c > 0$, including all constraints. The red grid lines indicate the point $(b, c) = (-20/e, 216/e)$ for the model in Sec. 4.5.1. | 122 |

| | | |
|-----|--|-----|
| 4.2 | Top: curvaton potential $V(\sigma)$ for example A, where $b = -20/e$, $c = 216/e$. The inflection point is located at $V_{\sigma\sigma} = 0$. Bottom: reconstructed (blue dash-dotted line), ansatz (red solid line), and quadratic potential (black dashed line) solutions for the curvaton slow-roll equation results in terms of σ_k | 124 |
| 4.3 | Top: reconstructed f_{NL} (dash-dotted) parameter for example A in comparison to the ansatz (solid) with $b = -20/e$ and $c = 216/e$. Bottom: the same for g_{NL} | 125 |
| 4.4 | Numerically computed zeros of f_{osc} , as a function of b , from ansatz (red, circle) and reconstructed (blue, square) solutions. The ratio $-b/c$ is the black dotted line, while the ratio $b = -\sqrt{2c/e}$ is the gray dashed line. $c = 216/e$ | 126 |
| 4.5 | Reconstructed f_{osc} (solid lines) and $V_{\sigma\sigma}$ (dotted lines) for varying b , $a = 1/e$, and $c = 216/e$. Their magnitudes grow with $ b $. The distance between the crossing position decreases with growing $ b $ for the chosen parameter range. In the highlight, we show the point where both are equal, which happens for a value a bit above $V_{\sigma\sigma} = 1$ | 127 |
| 4.6 | Non-Gaussianity parameters f_{NL} (solid lines) and g_{NL} (dotted lines) for the model example A. We vary b by $\pm 10\%$. The slow-roll parameters were chosen as $\epsilon_0 = 1/128$ and $\bar{\eta}_\sigma = 0.01$. k_0 is the pivot scale 0.05Mpc^{-1} , defined as the scale at which $f_{\text{NL}} = 0$ | 128 |
| 4.7 | Non-Gaussianity parameters f_{NL} (dashed lines) and g_{NL} (solid lines) for $b = -20/e$ and different values of c . Note that a change in c causes g_{NL} to drop below the observational constraints – i.e., $g_{\text{NL}} = (-5.8 \pm 6.5) \times 10^4$ | 129 |

Resumo

Neste trabalho, investigamos as conexões e degenerescências entre modelos inflacionários e de ricochete. Na primeira etapa do trabalho, analisamos a degenerescência entre esses modelos de universo primordial, com respeito às perturbações escalares de primeira ordem. Focamos em uma simetria presente nas equações de Mukhanov-Sasaki. Baseado nesta simetria, e utilizando o contexto de *Loop Quantum Cosmology* para realizar o ricochete, desenvolvemos um procedimento para construir um universo com ricochete cujas perturbações escalares são as mesmas do modelo inflacionário de Starobinsky. Na etapa seguinte, analisamos como funções de correlação de ordem superior ajudam a diferenciar entre os cenários. Em particular, investigamos a produção da modulação dipolar da CMB a partir de não-Gaussianidade dependente de escala em uma classe particular de modelos de inflação de vários campos, o cenário de curvaton. Desenvolvemos um procedimento para recuperar modelos de curvaton a partir de um parâmetro f_{NL} desejado. Então, aplicamos um *ansatz* para f_{NL} no procedimento e recuperamos o respectivo modelo de curvaton. Confirmamos que o modelo recuperado resulta em não-Gaussianidade dependente de escala e no comportamento correto para a modulação dipolar. Finalmente, investigamos se campos tipo-curvaton em uma cosmologia de ricochete com várias componentes resulta em fenomenologia que diferencia modelos de inflação e de ricochete. Como trabalho em andamento, analisamos o caso de um universo com ricochete de de Broglie-Bohm que possui fluido de matéria e um campo escalar. Encontramos as condições necessárias ao campo escalar para que o espectro de potência de curvatura possua um *red-tilt*.

Palavras-chave: Cosmologia; Inflação; Curvaton; Ricochete.

Abstract

In the present work we investigate the connections and degeneracies between inflationary and bouncing cosmologies. In the first stage of our work, we analyze the degeneracy between these early universe scenarios with respect to first order scalar perturbations. We focus on a symmetry that is present in the Mukhanov-Sasaki equation. Based on this symmetry, and using Loop Quantum Cosmology to realize the bounce, we develop a procedure to build a bouncing universe whose scalar perturbations were the same as a the Starobinsky model of inflation. In the next stage, we analyze how higher order correlation functions help differentiate between the scenarios. In particular, we investigate the production of the CMB dipolar modulation from the scale-dependent non-Gaussianity in a particular class of multi-field models of inflation, the curvaton scenario. We develop a procedure to recover curvaton models from a desired f_{NL} parameter. Then, we apply a scale-dependent ansatz for f_{NL} to such procedure and recover the respective curvaton model. We confirm that the reconstructed model results in scale-dependent non-Gaussianity and in the correct behavior for the dipolar modulation. Finally, we investigate if curvaton-like fields in a multi-component bouncing cosmology result in phenomenology that would disentangle inflationary and bouncing models. As a work in progress, we analyze the case of a de Broglie-Bohm bouncing universe doted with a matter fluid and a scalar field. We find the necessary conditions on the scalar field in order to a slight red-tilted curvature power spectrum to be present.

Keywords: Cosmology; Inflation; Curvaton; Bounce.

Chapter 1

Introduction

Throughout history, the origin and evolution of the universe have played a crucial role in the culture and identity of multiple societies and groups. Religion and Philosophy were the root of the first paradigms concerning cosmogony and have remained so for millennia. General Relativity (GR) and Cosmology allowed the construction of the first mathematically rigorous models for the universe's history and evolution. However, it has not taken long for paradoxes and problems to arise.

Among a wide range of proposals, as the Einstein models and the Stationary universe, the Hot Big-Bang (HBB) model was the one that prevailed. Midway through the XXth century, no consensus was built, with huge names in the area, such as Bondi and Einstein, defending alternate scenarios. The discovery of the Cosmic Microwave Background (CMB) radiation by Penzias and Wilson demarcates the consolidation of the Big-Bang model.

Analyzing the Friedmann equation solutions, it is shown that the HBB model has lots of conceptual problems. First of all, as it happens in the context of GR, a singularity is present – cosmological singularity – at time $t = 0$. We expect that this issue may only be solved by the advent of quantum gravity (QG). Additionally, to explain the universe as it is today, the HBB scenario encounters problems in the form of the fine-tuning of the initial conditions of the universe. Among those issues are the origin of cosmological perturbations and the flatness and horizon problems ¹.

The years between the '70s and the '80s marked the revival of the interest in alternatives to the HBB model. Starobinsky's model from 1979 [2] tried, unsuccessfully, to solve the cosmological singularity by using modifications of the Einstein-Hilbert (EH) action.

¹Other issues in the intersection between particle physics and cosmology can be found on Ref. [1].

However, it succeeded in unveiling crucial advantages of inserting a de Sitter phase of expansion in the early universe. In 1981, Guth's paper [3] cemented the use of such phase, by noting that the exponential expansion – that would be known as inflation – present in such space-time would be enough to solve the different puzzles from the HBB model. That marked the birth of the inflationary scenario.

It is worth highlighting that Guth's scenario has fatal inconsistencies. It makes use of a phase transition that would result in bubbles, necessary for the reheating of the universe. However such bubble and reheating mechanisms would destroy the universe's homogeneity and isotropy. Despite such flaws, the model was essential for the development of the area, culminating in the current state of affairs.

Other models, with different ideas and mechanisms, were being developed at the same time. Before the Guth paper, Novello and Salim [4] achieved the first analytic solution for a contracting universe that included a bounce. Models that presented a stage of contraction for the universe were already known by that time, and a bouncing phase had already been theorized. In such a scenario, the HBB model problems are different in comparison to the inflationary scenario. Despite not have been studied as much as inflation in the subsequent decades, universes with a bouncing phase have been analyzed in different contexts and theories, including quantum cosmology [5, 6, 7], matter bounces [8, 9], d-branes [10], among others [11, 12, 13, 14, 15, 16, 17].

In this thesis, we explore the connection and differences between inflationary and bouncing models. Our goal is to better understand the degeneracies between those scenarios, so that we can distinguish and separate them.

The first chapter introduces the historical setting of early universe cosmology, in particular the HBB model and its puzzles. We then present theory for inflationary and bouncing models. In the second chapter, we introduce the theory of cosmological perturbations in GR and in $f(R)$ theories ². Then, we present the connection between perturbation theory and the CMB observations. We highlight the general predictions for some CMB observables for both types of scenario.

In the third chapter, we present the first work developed during the Ph.D., in which we reconstruct a matter bounce model from an inflationary one. The work is motivated by a duality between both scenarios, thanks to a symmetry that is present in the Mukhanov-

²Necessary for our first work, shown in Chapter 3.

Sasaki equations. According to this duality, an inflationary model has a dual matter bounce model, that predicts the same quasi scale-invariant spectrum of scalar perturbations. We show that from this duality it is possible to use the dynamics of an inflationary model to build the dual bounce model from scratch. Such reconstructed model, in terms of scalar perturbations, is indistinguishable from its inflationary parent model. That highlights the fact that, for the degeneracies between inflationary and bouncing models to be solved, higher order correlation functions are needed. That is one of the main motivations for our subsequent work.

Then, in the fourth chapter, we present my work on a particular set of multi-field inflationary models, named the curvaton scenario. We introduce how the curvaton produces scale-dependent non-Gaussianities and how it leads to the observed CMB dipolar modulation. To do so, and still respect the most recent observational results, the non-linearity parameter f_{NL} must be small around the pivot scale - for example, by changing its sign. By using the curvaton slow-roll equation of motion and a desired functional form of f_{NL} , We developed a reconstruction procedure that results in the curvaton potential that leads to the desired f_{NL} parameter. We present a model from an ansatz for f_{NL} and show that, by a correct choice of free parameters, the model respects the Planck constraints and the correct behavior for the CMB dipolar modulation.

In the last chapter, we present a work in progress, in which a multi-component bouncing cosmology is constructed. The goal of this work is to investigate if bouncing cosmologies could present scale-dependent non-Gaussianities. However, as a first stage, we need to guarantee that the working models are predicting a red-tilted spectra of density perturbations. The model consists of a matter fluid, which behaves like dust ($\omega \simeq 0$), plus a scalar field, that we also call a curvaton (as it is auxiliary in terms of the spectral index). We compute the curvature perturbations, which has contribution from both components. We find a general form for the spectral index of the scalar power spectrum. Then, we investigate two concrete examples of scalar field. Preliminary results indicate that the second model results in a slightly red-tilted power spectrum, as long as quantum diffusion effects in the remote past can be neglected.

Finally, we sum up the results of my work during the Ph.D. in Chapter 6.

Over the next sections, we will establish the needed tools for studying inflationary and bouncing universes. First, we will review the HBB model in order to better understand its

issues. Next, we detail the inflationary universe, starting from the resolution of the HBB puzzles and how to construct such models. Then, we introduce bouncing cosmologies and what they present as possible solutions to the HBB problems. Finally, we present some conceptual issues that haunt both inflationary and bouncing proposals in general.

In this work we use the Planck units where $M_{\text{Pl}} = c = \hbar = 1$, unless we want to better highlight the units of a physical quantity, in which case we leave M_{Pl} explicit.

1.1 Hot Big-Bang Model

The decades following Friedmann's pioneering work, even though there was still no answer to the initial cosmological singularity, were filled with proposals for the model of the universe. The academic discourse was uncertain. There were those models in which the universe was cold, as Einstein's, Milne's, and Stationary proposals. On the other hand, there was the hot universe proposal from the HBB model. It was in this latter context that works on particle physics and grand unification were situated. In those works, the early universe was extremely hot, had restored symmetries, and was in a bath of ultra-relativistic particles. The discovery of the CMB radiation, already predicted by those kinds of models, solidified the HBB scenario. The universe would have started really hot, radiation-dominated, and would gradually lower its temperature as it expanded, eventually becoming matter-dominated. The thermal history description was established, but the initial behavior of some other physically relevant quantities (such as the curvature of the universe) were not yet determined.

The need for a fine-tuning of some of the properties of the universe, or at least a more complete theory explaining such specific values, was already being hinted at since the earliest observations. Evidence of a fine-tuning of initial conditions mounted over time, and it became clear that a shift in the standard scenario of the early universe was needed.

1.1.1 Cosmological Puzzles

The root of the problems of the HBB model lies in its spatial distribution of matter, i.e. its energy density and velocity field. From the aforementioned puzzles, the horizon and the initial fluctuations problems are derived from matter and its spatial distribution, while the flatness problem comes from the precision needed for initial velocities.

Horizon Problem

In the FLRW model, the universe's matter distribution at really large scale is isotropic and homogeneous – an approximation that is named as the cosmological principle. Even though at small scales the universe consists of voids, clusters, and galaxies, at larger scales the cosmological principle is verified with extreme precision [18]. In the remote past, primordial universe phenomena (such as particle production) are all isotropic, hence it is expected that they keep the universe isotropic as well. However, that is only the case for a single particle horizon, in which case there is causal contact between its regions.

The CMB is highly homogeneous and isotropic [18, 19], apart from the small temperature fluctuations, of magnitude of order 10^{-5} . The degree of homogeneity could only be possible if all regions present in the CMB must have been in causal contact, to the point that they could have homogenized. However, that is not what is predicted by the HBB model evolution.

The current observable universe has approximately the same radius as the particle horizon, where the limit of observation is the CMB (as far as photons are concerned, because primordial GWs freely propagate since inflation and neutrinos decouple a lot earlier than the CMB). We can then compute what was the size of the current particle horizon, push backward in time, when the CMB was formed. In terms of the temperature, the so called last-scattering surface was

$$R_{LSS} = R_H(t_0) \left(\frac{a_{LSS}}{a_0} \right) = R_H(t_0) \left(\frac{T_0}{T_{LSS}} \right) \quad (1.1)$$

The particle horizon through time has a different dynamic, as it is proportional to H^{-1} . Through the time dependence of $H(T)$ during the matter domination epoch ³, once again in terms of temperature

$$H^2 \propto a^{-3} \propto T^3 \quad (1.2)$$

$$R_H(t_{LSS}) = R_H(t_0) \left(\frac{T_0}{T_{LSS}} \right)^{3/2} \quad (1.3)$$

Comparing the LSS radius 1.1 with the particle horizon radius 1.3, we see that there

³Between today and the last scattering surface, we can set dark matter as dominant in the universe, despite the recent time of dark energy domination.

are more regions without causal contact (outside the horizon) than the opposite. The ratio between them is

$$\frac{R_{LSS}^3}{R_H^3(t_{LSS})} = \left(\frac{T_0}{T_{LSS}}\right)^{-3/2} \approx 10^6 \quad (1.4)$$

Therefore, the observable universe (i.e., what is registered in the CMB) has 10^6 regions that were not in causal contact during recombination. Hence, we cannot explain the CMB's homogeneity, as most of its regions were deprived of contact with each other. There is no known physical process that could explain this. Either the universe was already homogeneous throughout it all (beyond the particle horizon) and all CMB regions have almost the same temperature by sheer luck (probability of such is of order 10^{-27}); or the evolution of the aforementioned quantities is different. In this case, all of those regions must have been inside the same horizon, so that thermal equilibrium could have been reached.

Primordial Density Fluctuations

In the context of the HBB model, there is no origin for the small non-homogeneities, the sources of the temperature fluctuations of the CMB, which later become galaxies, clusters, and other structures. Not only the fluctuations had to exist before the CMB was formed, but they must also had to have the exact observed magnitude of order 10^{-5} . Additionally, they had to present an almost scale-invariant spectrum.

Those constraints are imposed over the whole extent of the LSS – which was, at that time, larger than the particle horizon. The existence and characteristics of the density fluctuations make the horizon problem even stronger: not only should we explain why the temperature across the CMB is almost homogeneous, but how its deviations also share the same global characteristics.

In the early developments of alternatives to the HBB model, the primordial density fluctuations had not been yet detected. After their discovery, the absence of any physical mechanism to explain their existence became arguably the greatest problem for the HBB model.

Flatness Problem

The flatness problem arises from the fact that the spatial curvature of the universe cannot be pre-determined by some physical motivation. The Friedmann equations for a generic curvature, in terms of the density parameters, result in

$$\frac{H^2}{H_0^2} = \frac{\Omega_{r,0}}{a^4} + \frac{\Omega_{m,0}}{a^3} + \Omega_{\Lambda,0} + \frac{1 - \Omega_0}{a^2} \quad (1.5)$$

$$1 - \Omega = \frac{-k}{(aH)^2} = \frac{\rho_{\text{crit.}} - \rho}{\rho_{\text{crit.}}} \quad (1.6)$$

where the $\Omega_{i,0} = \rho_{i,0}/\rho_{\text{crit},0}$ are the density parameters for the fluids that compose the universe, computed today (all cosmological quantities with subscript 0 refer to today's value), while Ω is the total density parameter. The subscript 'r' stands for radiation, 'm' for non-relativistic matter (baryonic and dark matter), while λ stands for the cosmological constant. $\rho_{\text{crit},0}$ is the total energy density of the universe in case that the curvature is flat, which means that $1 - \Omega = 0$, see (1.6).

Both in the radiation dominated ($H^2 \propto a^{-4}$) and matter-dominated epochs ($H^2 \propto a^{-3}$), we have that $1 - \Omega$ grows in time. Nowadays, $1 - \Omega_0 \approx 10^{-3}$, which indicates that at early times this value should have been even smaller. Comparing the current value with the one during nucleosynthesis (both during matter domination), we get

$$\frac{|1 - \Omega|_{\text{Nucl.}}}{|1 - \Omega|_0} \approx \left(\frac{a_{\text{Nucl.}}^2}{a_0^2} \right) \approx \mathcal{O}(10^{-16}) \quad (1.7)$$

Beyond that, towards grand unification epochs,

$$\frac{|1 - \Omega|_{\text{GUT}}}{|1 - \Omega|_0} \approx \left(\frac{a_{\text{GUT}}^2}{a_0^2} \right) \approx \mathcal{O}(10^{-55}) \quad (1.8)$$

The above result demonstrates how fine-tuned the value of $1 - \Omega$ must be to obtain its current value. Any vestige of global curvature today implies that the universe was even flatter in the past (despite not being completely flat). The small value around zero also shows that the divergences in the density could have moved the universe above/below $\rho_{\text{crit.}}$, which would result in largely different evolution for the universe; it could have led the universe to a fast collapse/expansion, that we do not observe.

The density parameter Ω can be interpreted as the ratio between potential and ki-

netic energy in the universe. The conditions (1.7) and (1.8) then imply a high degree of similarity between both types of energies. In a fluid, the potential energy comes from gravitational interaction, while the kinetic energy comes from the velocity. That is why the flatness problem is related to the matter velocity field.

Other puzzles

Other difficulties in adjusting the HBB model to what we observe concerns particle and high-energy physics. One example for general unification theories and standard model extensions is the existence of monopoles and other thermal relics. The absence of such in observations means that either the universe has some mechanism that dilutes them, or new theories are needed.

The flatness problem is also associated with the so-called entropy problem. Near the Planck scale, if the universe is dominated by radiation, an adiabatic process to the entropy S leads to

$$|1 - \Omega|_{\text{Pl.}} = \frac{1}{S^{2/3}} \approx \mathcal{O}(10^{-68}) \quad (1.9)$$

Hence, the flatness problem can be translated into how the primordial universe entropy is so high. The entropy would be responsible for the smallness of $1 - \Omega_0$.

The baryon asymmetry is another phenomenon out of the HBB scope, although being closely related to the nonexistence of a fundamental theory in order to explain it. The asymmetry is not automatically solved by the proposal described in the next sections, but a program that lists the basic necessary ingredients for it are the Sakharov conditions [20].

1.2 Inflationary Scenario

It is, then, possible to sum up the desirable features that the universe should have to avoid the problems cited in the previous section. The flatness and entropy problems are intimately connected, so we conclude that a non-adiabatic expansion phase could at least partially solve those problems. Alternatively, a period in which the universe had a decreasing $|1 - \Omega|$ would also be a solution.

Another characteristic is related to the Horizon problem. As previously anticipated – and thoroughly used in the Cosmological Perturbations chapter 2 – a period when the perturbations in the CMB were in causal contact could be enough to solve it. This behavior can be obtained by a stage where physical scales grow beyond the particle horizon, evolving faster than it. During this period, we require that regions that were once in causal contact be separated, as physical distances grew. Hence, during CMB formation, they would not be casually connected, but they could still be in thermal equilibrium thanks to the time when they do were connected.

These are the consequences of what such stage of evolution would allow, to avoid the need of fine-tuned of initial conditions. Next, we need to present the mathematical description of how this stage could take place. From the second-mentioned characteristic, we can obtain how the scale factor should behave. Physical scales evolve proportionally to the scale factor, $\sim a$, while the horizon evolves with $\sim H^{-1}$. The time evolution of the ratio between both evolve as

$$\frac{d}{dt} \left(\frac{a}{H^{-1}} \right) = \frac{d}{dt} (\dot{a}) = \ddot{a} > 0 \quad (1.10)$$

As discovered by Guth [3], an accelerated, almost exponential phase of expansion would solve the HBB puzzles. Such a regime came to be known as inflation.

1.2.1 Inflationary Paradigm

Accelerated expansion is not the only defining detail from the inflationary regime of the universe. A non-adiabatic expansion, as previously mentioned, is lacking. However, the inflationary program offers a natural solution to this conundrum, the so-called reheating, that we will briefly explain later in this section.

From the acceleration requisition and the Friedmann equations, we can obtain information about the leading fluid during inflation

$$\frac{\ddot{a}}{a} = \frac{-4\pi G}{3} (\rho + 3p) > 0 \quad (1.11)$$

$$\Rightarrow (\rho + 3p) < 0 \quad (1.12)$$

In other words, in order to realize inflation, it is necessary to have a fluid doted with

negative pressure, $p < -\rho/3$. It was already known, from research conducted in earlier decades, that vacuum energy had an equation of state $p = -\rho$. Other proposals that achieved the same equation of state were constructed since then (we detail some of them in section 1.2.2.)

A fluid with such behavior dominates the universe and respects the previous requirements, leading to a so-called de Sitter expansion. There, we have constant ρ and H . Therefore,

$$\frac{\dot{a}}{a} = H_i \tag{1.13}$$

$$\Rightarrow a = a_i \exp^{H_i(t-t_i)}, \tag{1.14}$$

where a_i and H_i are, respectively, the values of the scale factor and Hubble parameter at the beginning of inflation.

The de Sitter regime is marked by an exponential expansion of the scale factor. Rigorously, inflationary models should actually follow a quasi-de Sitter regime, because an exact de Sitter expansion has no graceful exit; the Hubble parameter does not evolve and, therefore, we have an eternal expansion. In a quasi-de Sitter expansion, the graceful exit is reached, and the reheating phase of inflation kicks in. Different inflationary scenarios require additional assumptions in order to completely solve the HBB puzzles. We detail some peculiarities on Section 1.4.

Horizon Problem

As previously mentioned, the resolution of the horizon problem is centered on the acceleration of the universe during inflation. If the present horizon scale is inside the particle horizon at the beginning of inflation, it is a first step to explain the CMB homogeneity. Using the de Sitter expansion (1.14) we can compute how long inflation should have lasted to solve the horizon problem.

The particle horizon at the beginning of inflation was ⁴

⁴We used $R_H \sim H^{-1}$

$$\lambda_{RH}(t_i) = H_0^{-1} \left(\frac{a_{t_i}}{a_{t_0}} \right) = H_0^{-1} \left(\frac{a_{t_f}}{a_{t_0}} \right) \left(\frac{a_{t_i}}{a_{t_f}} \right) = H_0^{-1} \left(\frac{T_0}{T_f} \right) e^{-N} \lesssim H_I^{-1} \quad (1.15)$$

$$N = H_I (t_f - t_i) \quad (1.16)$$

where N is the number of e-folds, t_i the time when inflation starts, t_f the time when it ends, and H_I is the Hubble parameter during inflation. For the horizon problem to be solved and (1.15) to be satisfied, we need $N \gtrsim 70$.

In order to prove it, we use (1.15), applying the log to the inequality

$$N \geq \log \left(\frac{T_0}{H_0} \right) - \log \left(\frac{T_f}{H_I} \right) \approx 67 + \log \left(\frac{H_I}{T_f} \right) \quad (1.17)$$

Flatness problem

Unlike the matter and radiation-dominated regimes, the parameter $|\Omega - 1|$ will be inversely proportional to the scale factor, i.e. it will shrink in time instead of growing. This can be seen through (1.6) with a constant Hubble parameter H_I

$$1 - \Omega \propto \frac{1}{a^2} \quad (1.18)$$

In the de Sitter regime, this will exponentially decrease in time. The ratio between this parameter at the beginning and at the end of inflation is given by

$$\frac{|1 - \Omega|_{t_f}}{|1 - \Omega|_{t_i}} = \left(\frac{a_i}{a_f} \right)^2 = e^{-2N} \quad (1.19)$$

Comparing it with (1.8) and (1.9) we obtain the same value for the necessary e-folds $N \approx 70$. This way, instead of a fine-tuning of order 10^{60} we just require several e-folds of order 10^1 , which is a sensible requirement. Under this condition $|1 - \Omega|$ is allowed to be of order unity today, even if it is big when inflation starts and considering that it grows during matter and radiation domination. In other words, inflation guarantees an almost flat universe nowadays.

Primordial perturbations and other issues

All HBB model problems related to the monopole density, massive fundamental particles, topological defects, etc., are solved by the exponential expansion of the universe. Such an expansion would drastically reduce their densities by an order of e^{3N} or more (since the production of such objects could predate the time when cosmological scales leave the horizon).

The entropy problem is solved by the reheating phase of inflation, as previously mentioned. Both of these problems, as well as the existence of primordial density fluctuations, are issues whose solutions lie in the fluid that dominates and originates inflation. As we detail in full during the Cosmological Perturbations chapter, the density fluctuations, and inflation itself, in the standard inflationary scenario are produced by a scalar field, the so-called inflaton.

1.2.2 The Inflaton

The understanding of the nature of the dominating fluid during inflation has changed through the years. Gliner (see [1] and references therein), even before the development of inflationary models to solve the HBB model problems, suggested a de Sitter phase governed by a super dense matter. Guth, on the other hand, made use of a super-cooled vacuum state to achieve a de Sitter regime. Such a vacuum would then reduce the universe's temperature. A subsequent phase transition would be responsible for the reheating (in a different manner from current standard inflation), whose own issues would lead to the waiver of this model.

Finally, scalar fields started being used to realize inflation, through its minimal coupling to gravity. The first models of the so-called new inflationary paradigm, which were then followed by chaotic models, were precursors in the use of this kind of field. Works by Linde [21, 22, 23] lead the way in advancing both scenarios. The general property of these models is the need that the potential of this field $V(\varphi)$ dominates relative to its kinetic energy $\dot{\varphi}$. The scalar field responsible for inflation was then named the inflaton.

The new inflationary paradigm was dominated by the use of fields of the Coleman-Weinberg type 1.20, associated with symmetry breaking in grand unification theories. However, in this scenario phase transitions were still being used, so that cooler temperatures were still necessary as in the previous Guth model. The scalar field potential for a

Coleman-Weinberg model is written below,

$$V(\varphi) = V_0 \left[\left(\frac{\varphi}{\mu} \right)^4 \left(\log \left(\frac{\varphi}{\mu} \right) - \frac{1}{4} \right) + \frac{1}{4} \right] \quad (1.20)$$

Chaotic inflation [22] marked the start of the modern-like construction of inflationary models. The need for low temperature imposed on the inflaton potential $V(\varphi)$ no longer existed. That allowed for inflationary models to move to a near Planck scale regime, and for inflation to take place without any need of cooling. In chaotic inflation models the potentials are generally exponential or power-law in the field φ 1.21. They are also called large-field models. We detail some other quirks of the chaotic models in section 2.4.5. An example of a chaotic inflationary model potential is shown below

$$V(\varphi) = \frac{\lambda \varphi^n}{n M_{\text{Pl}}^{n-4}}. \quad (1.21)$$

Following the classification of inflationary models, according to the required energy scale, the new inflationary paradigm models are called small field models. Alternatively, we also have models classified as hybrid [23], common to supersymmetry theories. In those cases, some additional fields are necessary, which in turn are more closely related to the small field class. There are other ways to realize inflation, either making use of multiple fields [24], non-minimal coupling to gravity [25], axions [26], non-canonical kinetic term [27], and many others. In the string theory scenario, inflation is the leading candidate for explaining the early universe, despite some recent works on the swampland and the trans-Planckian conjecture [28]. More on models with many fields in 1.2.5.

In addition, modified gravity proposals can also produce inflation, such as the previously mentioned Starobinsky model, which is one of the most successful inflationary scenarios, with respect to fitting current observations [29]. There are comprehensive reviews of inflationary models in the literature, such as [30, 31], that go into detail about many models proposed over the years. We shall focus mainly on the Starobinsky proposal, alongside the Curvaton scenario of inflation, throughout the thesis.

1.2.3 Inflaton dynamics

It remains to explain how the different scalar field types mentioned above could originate an inflationary phase. As it has been previously anticipated, the necessary condition for that to happen is the scalar field to have an equation of state $\rho \approx -p$, which means $V \gg \dot{\varphi}^2$. From the minimally coupled inflaton action, we have

$$S = \int d^4x \sqrt{-g} \left[\frac{1}{2} R + \frac{1}{2} \partial^\mu \varphi \partial_\mu \varphi - V(\varphi) \right] \quad (1.22)$$

From the varying of the action, we find the equation of motion for a scalar field in an FLRW spacetime,

$$\ddot{\varphi} + 3H\dot{\varphi} + V_{,\varphi} = 0, \quad (1.23)$$

where the subscript in $X_{,\varphi}$ means derivative of the function X with respect to φ .

From the energy-momentum tensor obtained from the action (1.22) it is possible to extract the expressions for energy density and pressure for the field

$$\rho = \frac{\dot{\varphi}^2}{2} + V(\varphi) \quad (1.24)$$

$$p = \frac{\dot{\varphi}^2}{2} - V(\varphi) \quad (1.25)$$

As detailed, for the inflaton we need $p \approx -\rho$. Therefore, it needs to satisfy

$$\frac{\dot{\varphi}^2}{2} \ll V(\varphi) \quad (1.26)$$

The expression (1.26) is known as the slow-roll condition. The potential energy should dominate over the kinetic energy of the field, that is why *slow-rolling*: the field will evolve slowly through its potential, rolling down little by little. Another reason explaining the slow-roll behavior comes from the equation of motion (1.23): the second term in the LHS represents a friction term when the universe expands, as we see from its dependence on H . The faster the expansion and the velocity of the field, the larger the friction is. In turn, such friction impedes the field to gain speed in the first place. Hence, a slow-roll

down its potential.

When the slow-roll condition is no longer respected inflation ends. The field perturbations do not affect the background dynamics so that we can express the equation of motion and the Friedmann equations as

$$\ddot{\varphi} + 3H\dot{\varphi} + V_{,\varphi} = 0 \quad (1.27)$$

$$H^2 = \frac{1}{3} \left(\frac{\dot{\varphi}^2}{2} + V(\varphi) \right) \quad (1.28)$$

Applying the slow-roll conditions in the above equations allow for the construction of a scenario suitable for the treatment of inflation, that we work on next.

The different potentials allowed for inflaton candidates to realize the slow-roll conditions in a different manner. Chaotic type fields start in a large value of the potential, of the Planck mass M_{Pl} order, and slowly roll down its potential thanks to the friction term. Small field models have a different kind of potential, that usually leads to a small variation of the field, in what we classify as almost flat or plateau-type potentials, see Figure 1.1.

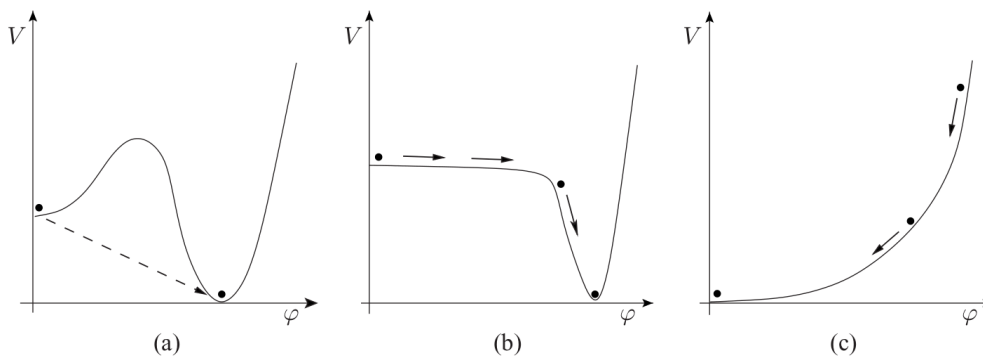


Figure 1.1: Types of inflationary potentials: (a) Old Inflation, (b) New Inflation (hybrid of small field), and (c) Chaotic inflation (large field).

In both cases, inflation should take at least around $60 \sim 70$ e-folds, hence all HBB model problems are solved.

1.2.4 Inflation Phenomenology

The inflationary regime phenomenology focuses on the cosmological perturbations observed in the CMB. Quantities like the spectral index, the amplitude of the perturbations,

among others, are determinants to the evaluation of different inflation candidates.

As will be briefly hinted in the Cosmological Perturbations chapter, the CMB power spectrum is gently scale-dependent (red-tilted), thanks to inflation not being an exact de Sitter expansion. We can express such deviation through defining new parameters, the so-called slow-roll parameters [32]. These will also be present in the description of cosmological observables.

Before defining those parameters, it is interesting to establish the duration of the inflationary regime. The precise definition of the number of e-folds during inflation is

$$dN = H dt \tag{1.29}$$

$$N = \int_{t_i}^{t_f} H dt = \log \left(\frac{a_f}{a_i} \right) \tag{1.30}$$

The number of e-folds is a quantity essential for the phenomenology approach to inflation. All the following slow-roll parameters will be expressed in terms of the number of e-folds in the standard inflationary models. As a consequence, the expected range for the number of e-folds, between $60 \sim 70$, will allow for an assessment of the observables predicted for every model.

The Hubble slow-roll parameters (HSRP) are exactly defined using background values. The first of the parameters is ϵ_1 , defined from the deviation of the Hubble parameters from an exact de Sitter regime

$$\epsilon_1 = -\frac{\dot{H}}{H^2} \tag{1.31}$$

The parameter ϵ_1 , in conjunction with the Friedmann equations, results in

$$\epsilon_1 = \frac{3}{2}(\omega + 1) = \frac{1}{2} \frac{\dot{\varphi}^2}{H^2} \tag{1.32}$$

$$\frac{\ddot{a}}{a} = H^2(1 + \epsilon_1) \tag{1.33}$$

In the exact de Sitter limit, $\epsilon_1 \rightarrow 0$, which corresponds to H being a constant in (1.31). In addition, in this limit, $\omega = -1$, as seen from (1.32).

Inflation needs to take enough time, and that implies a constraint to (1.27): the second derivative of the field must be inexpressive in comparison to the other terms, as friction and potential derivative. We then reach one more slow-roll condition, which is mathematically expressed as the second HSRP η_H

$$\eta_H = -\frac{\ddot{\varphi}}{H\dot{\varphi}} = \frac{d \log |\dot{\varphi}|}{dN} \quad (1.34)$$

The use of the number of e-folds can be used to re-express ϵ_1 and η_H

$$\epsilon_1 = -\frac{d \log H}{dN} \quad (1.35)$$

$$\eta_H = \epsilon_1 - \frac{1}{2\epsilon_1} \frac{d\epsilon_1}{dN} \quad (1.36)$$

In terms of the HSRP, we can sum up the slow-roll approximation as $\epsilon_1 \ll 1$, $|\eta_H| \ll 1$. Only under these conditions that slow-roll inflation can take place. Additionally, $\epsilon_1 = 1$ can be defined as the end of inflation.

We need to solve the system of equations (1.27)-(1.28) that gives the background evolution in order to make full use of the HSRP. It is possible to simplify these equations using the slow-roll conditions. That will lead us to the so-called Potential Slow-Roll Parameters (PSRP), that receive such a name thanks to being completely defined by the inflaton potential.

Simplifying (1.27)-(1.28) leads us to

$$H^2 \simeq \frac{1}{3}V(\varphi) \quad (1.37)$$

$$3H\dot{\varphi} = -V_{,\varphi} \quad (1.38)$$

The conditions (1.26) and $|\ddot{\varphi}| \ll |3H\dot{\varphi}|$, together with the above expressions, lead to

$$\dot{\varphi}^2 \ll V(\varphi) \Rightarrow \left(\frac{V_{,\varphi}}{V}\right)^2 \ll 1 \quad (1.39)$$

$$|\ddot{\varphi}| \ll |3H\dot{\varphi}| \Rightarrow \frac{V_{,\varphi\varphi}}{V} \ll 1 \quad (1.40)$$

From (1.39) and (1.40) we define the PSRP

$$\epsilon_v = \frac{M_{\text{Pl}}^2}{2} \left(\frac{V_{,\varphi}}{V} \right)^2 \quad (1.41)$$

$$\eta_v = M_{\text{Pl}}^2 \frac{V_{,\varphi\varphi}}{V} \quad (1.42)$$

$$\epsilon_v, |\eta_v| \ll 1 \quad (1.43)$$

Both types of slow-roll parameters, HSRP and PSRP, can be expressed in terms of each other, which will be valid throughout the slow-roll regime

$$\epsilon_1 \simeq \epsilon_v \quad (1.44)$$

$$\eta_H \simeq \eta_v - \epsilon_v \quad (1.45)$$

1.2.5 Multi-Field Inflation

In the previous sections, I have presented the inflationary scenario in its single-field regime, where there is only one inflaton field responsible for the background expansion. That scenario is referred to as Single Field Inflation (SFI). However, in many formulations for the early universe, the presence of other scalar fields must be taken into account. The scenario of multi-field inflation [24], where multiple fields dominate the background evolution, which can lead to many inflationary expansions, is then a straightforward extension of the SFI case.

The first models of multi-field inflation were constructed in the late '80s and early '90s, in the context of double inflation [33, 34, 35, 36]. That led to the subsequent works on a hybrid model of inflation heavily inspired by the presence of an axion during the early universe [37, 38, 23]. Many other attempts have been developed over the last decades

There are some advantages of the multi-field models in comparison to the single-field prescriptions. In recent years, theoretical arguments indicate that the (cold) single field scenario might be not in the string theory landscape but in its swampland [39, 40, 41, 42]. That indicates that for inflation to happen in the string theory landscape [28] either many fields must be responsible for the regime or a warm inflation is needed [43, 44, 45].

In addition, SFI is not suitable to address the CMB anomalies or observation of primordial non-Gaussianities. The CMB anomalies manifested on the Planck data [18] still have a low statistical significance of 3σ . Nevertheless, the fact that they were measured by two different surveys, namely WMAP and then the Planck collaboration, suggests that these anomalies might not be just a systematic error or foreground contamination, and if they exist, the statistical anomalies indicate a violation of the cosmological principle [46, 47]. Therefore, there is phenomenology that cannot be explained by the single field models.

In the second part of this thesis (Chapter 4), we will analyze just one type of multi-field model, the curvaton scenario of inflation [48]. In curvaton models, the inflaton remains the scalar field responsible for the background quasi-de Sitter expansion (and subsequent reheating). However, the cosmological perturbations are produced by the non-adiabatic fluctuations from another scalar field, the so-called curvaton [49].

Curvaton models are favored in our analysis due to their simplicity and rich phenomenology. Contrary to other multi-field inflationary models, in the curvaton scenario there is only one inflationary regime. The curvaton field does not change the background dynamics. Inflation takes place just like in SFI models: the inflaton slow-rolls down its potential, then, after coherent oscillations around its minimum, decays during reheating. In the meantime, the curvaton field also rolls-down its potential, decaying after the inflaton has decayed as well ⁵. In addition, the power spectrum of density perturbations is still red-tilted following the quasi-de Sitter background expansion. The curvaton field contribution to the spectral index is of second order when η_σ is small enough. Therefore, most of what has been already established for SFI models, both at background and perturbation level, is still valid.

However, thanks to the nature of the cosmological perturbations in the curvaton scenario, these models allow for crucial differences with respect to SFI. First, the energy-scale of inflation can be taken to be lower, because the amplitude of density perturbations – as detected by WMAP, Planck – do not constrain the inflaton field. It is the curvaton field fluctuations that need to match the scalar cosmological perturbations we detect. When the energy scale of inflation is lower, the amplitude of tensor perturbations is lower as well. Therefore, the tensor-to-scalar ratio for curvaton models is a lot smaller than in SFI.

⁵The exact details of the relative time between the decays of both fields are better mentioned on Chapter 4.

That allows for a small tensor-to-scalar ratio to be predicted even for chaotic inflation-like inflaton fields used in the curvaton scenario. In addition, curvaton models also allow for the presence of scale-dependent non-Gaussianity [50, 51]. The latest Planck results cannot rule out this type of non-Gaussianity [52], as the scale-dependence can be such that for CMB-scales the non-Gaussianity is negligible. Moreover, the aforementioned CMB anomalies might be explained by a scale-dependent non-Gaussian coupling [53], something that SFI models cannot explain, but that curvaton models can easily accommodate [54].

One additional peculiarity of the curvaton scenario is that, thanks to the suppressed tensor-to-scalar ratio and the fact that scalar and tensor spectral indexes are the same, curvaton models are dual to the types of bouncing cosmologies we construct in Chapter 3. Once again, we connect inflationary to bouncing cosmologies, and highlight the need to further works in both scenarios.

The interested reader can learn more about the phenomenology of other multi-field models in the references [24, 55].

1.3 Bouncing Cosmologies

There are many alternate scenarios to the inflationary proposal to the early universe [56, 57]. Inflationary models present solutions to the HBB puzzles, but they are not free of conceptual problems of their own [58]. From the difficulties we have previously listed, we have seen that the cosmic singularity is not tackled by usual inflationary models [59]. That is one of the reasons why many non-singular universe models have been proposed since the beginning of modern cosmology. How one avoids a singularity, however, will be left for section 1.3.3.

The CMB homogeneity can be solved through the dynamics of the universe in the case the universe is eternal or pre-existing. The solution to such a problem lies in the guarantee that regions inside the current particle horizon – i.e. the regions covered by the CMB – were inside the same horizon in the distant past. If we consider that the universe already existed and is made of the same matter components as today, we conclude that this condition is satisfied. Given enough time for causal contact (any mechanism) to homogenize the necessary region, physical scales that are on the current horizon will have

their homogeneity justified. However, it is necessary that the region connecting the times where these scales existed the horizon to our current time has not ruined the previous homogeneity of the universe.

For the current flatness of the universe, we look for the same behavior as an inflationary cosmology: a phase in which $|1 - \Omega|$ decreases, reducing the contribution from the curvature. In a universe that only expands, given the present matter components (radiation, matter, cosmological constant), the only solution is an inflationary one.

If the universe presents a contracting phase before the current FLRW expansion, then it is possible to have $|1 - \Omega|$ decrease as wanted. That can be achieved in two distinct manners. Either via multiple phases of contraction and expansion in a cyclic manner, or through a single contracting phase followed by a bounce, that would lead to the current expansion of the universe. The latter leads to the construction of the so-called non-singular bouncing models [60], which do as good as inflation to explain the HBB puzzles, but do not solve all problems. Additionally, non-singular bouncing cosmologies try to solve the presence of a cosmic singularity – either via quantum gravity or generalizations/extensions/classical modifications of GR.

1.3.1 Bouncing Scenario

In the bouncing scenario of primordial universe physics, it is possible to construct a model in which the background dynamics follows the usual Friedmann equations, up until the proximity of the bounce. That allows for the construction of a universe model which is homogeneous, isotropic, and whose mechanism for originating the bounce is left for a fundamental theory of some sort. The origin of bounce separates different types of models because the previous contracting universe must respect observational constraints on cosmological perturbation (See Section 1.3.3). The origins and nature of these perturbations can also vary, as curvaton-like models are possible [61, 62].

Without a cosmological constant or any other exotic fluid, a pre-existing universe would follow FLRW evolution. First, pressureless dust-like matter (effective equation of state $\omega \approx 0$) would dominate the contraction. As it will be worked on next, matter domination is essential for the predictions coming from bouncing models to match recent observational results. Wands' duality, which we analyze in detail in the next section, will connect the predictions from universes expanding in a de Sitter phase to the ones

contracting thanks to dust [63].

As in the case of inflation, which is not an exact de Sitter expansion, we do not expect a behavior that is precisely like pressureless dust. The construction of such universe model will not be realized by an exact zero equation of state parameter, but close to it [8, 64].

Homogeneity before the bounce is a point of debate between the different proposals of the early universe, something that adherents of the inflationary scenario argue that bouncing models need to better explain it [65, 66]. In the inflationary scenario, we have that the region that comprehends the whole observable universe today – as previously mentioned, in causal contact – was incredibly small before the start of inflation. This infinitesimal size would justify today’s homogeneity, as this region was approximately Minkowski flat spacetime. For the bouncing scenario, the solution to this problem comes from the opposite argument. We can postulate that the homogeneity comes as an initial condition, because the far past early universe was incredibly large, flat and low-energy, which would allow for such a setting. In an inflationary universe, such conditions are posed in a high-temperature and energy setting, which might mean that we have less control over initial conditions than in bouncing universes. New phenomena might be important.

Notwithstanding, the bouncing scenario is not immune to critics [67]; there is a long-standing discussion over if anisotropies could ruin the predictions [65]. An ekpyrotic phase could then prove to be necessary, as it would smooth the anisotropies [68, 69]. We leave the analysis of those issues to the references.

Hot big-bang model problems

The homogeneity problem, as we mentioned, can be mathematically formulated. In a contracting universe, dominated by a perfect fluid with an equation of state parameter ω , the particle horizon is given by

$$R_H = \frac{3(1+\omega)}{1+3\omega} t_f \left[1 - \left(\frac{t_i}{t_f} \right)^{\frac{1+3\omega}{3(1+\omega)}} \right], \quad (1.46)$$

where t_i and $t_f < 0$ mark the beginning and end of contraction. Given that $|t_i| \gg |t_f|$, any fluids with $\omega > -1/3$ leads to contraction dotted with an initial horizon arbitrarily large. Therefore, causal contact between the CMB regions would have been established

[65].

The flatness problem is solved similarly to inflation, in the sense that we get a stage where $|1 - \Omega|$ decreases. Taking the time derivative of this parameter, (1.6),

$$\frac{d|1 - \Omega|}{dt} = -2|k| \frac{\ddot{a}}{a^3} \quad (1.47)$$

The derivative will be negative during contraction in case $\ddot{a} < 0$ and $\dot{a} < 0$. Therefore, during this stage, $|1 - \Omega|$ will get close to 0 even if we start from order unity. One difference from inflation comes from the fact that the curvature becomes important at small scale factor values, as it scales as a^{-2} . For the curvature today to be close to 0, we need a contraction phase that lasted even longer than our current expansion branch. Then, the curvature today would not have grown back to its initial value. Relative to the beginning of the contraction, we are still close to the bounce phase, far from the initial value of the size of the universe.

Bouncing cosmologies propose solutions to the puzzle of the origin of cosmological perturbations as well. In this case, they are originated in the contracting regime of the universe, in the really far past. It happens when they reside inside the Hubble scale, just like inflation, leaving the horizon at some point during matter domination. One advantage of such a scenario is that there is no need to resort to Planck scales for the creation of the perturbations – since it happened when the universe was extremely large. It is, however, important to guarantee that the bounce phase will preserve the needed characteristics for the perturbations, such as scale dependence, and will not lead to inconsistencies. Hence, high energy physics issues are related to the bounce mechanism itself and how cosmological perturbations survive the crossing, instead of being related to the production of the perturbations, as it happens for inflationary models [6, 70, 71, 72, 73, 74].

Contracting universes also need to explain how particle production took place, which generally takes place during the bounce. Without such development, it is impossible to conclude if the problems related to grand unification and thermal relics are solved. Recent papers have tackled such issue, see [75, 76]. An inherent difference in particle production between inflationary and bouncing scenarios may help distinguish these types of models. No concrete evidence for such difference has been found.

1.3.2 Matter Bounce Scenario

Before the development of inflationary scenarios, other early universe proposals besides the HBB model had already been proposed. The first cosmological models that presented bouncing phases were the cyclic universes from Lemaitre [77]. From the Friedmann equations to a closed universe, the existence of a Big Crunch is natural, so that one needed only some mechanism to make it expand once again. Proposals have been constructed since then, such as recent tries including ekpyrotic phases in the brane-world context, such as [10, 69, 78, 79, 80].

The development of singularity theorems in GR made non-singular bouncing proposals lose importance for a while. However, new findings, such as fields that could violate the null energy condition (see ref. 1.3.3) rescued the field of research.

We must note that a pre-bounce universe, in general, possesses only matter (dust, dark matter) and radiation, besides residual curvature. Some proposals also include dark energy [81]. The previously mentioned Wands duality has renewed the interest in such scenario. As we explain in the next chapter, the duality shows that a symmetry in the Mukhanov-Sasaki equations that maps solutions in the (quasi-)de Sitter regime to solutions in the (quasi-) matter-dominated universes. It leads to the eventual construction of many bouncing models that predict the correct power spectrum for the CMB fluctuations [64, 9].

It is a common strategy, as we will do in this work, to use a scalar field – expressed as φ – to describe the matter component in such a contracting universe. Its interpretation can be done either as a true scalar field driving the background dynamics or as a phenomenological description of matter.

Therefore, can use action (1.22), and equations (1.27) and (1.28). This time, however, the imposed conditions are not slow-roll ones. As we need matter domination, $p \ll \rho$, so from the definition (1.24) e (1.25) we get

$$\dot{\varphi}^2 \simeq 2V \Rightarrow \ddot{\varphi} \simeq V_{,\varphi} \tag{1.48}$$

These are named as the quasi-matter domination conditions. We can re-write equations (1.27) and (1.28) as

$$H^2 \simeq \frac{2}{3}V \quad (1.49)$$

$$3H\dot{\varphi} + 2V_{,\varphi} \simeq 0 \quad (1.50)$$

The scalar field that produces exact matter domination has potential $V(\varphi) = e^{-\sqrt{3}|\varphi|}$. Scalar fields with similar φ dependence will lead to an equation of state similar to that of matter.

The theory of cosmological perturbations can be used, unequivocally, for either inflation or matter-dominated regimes. The same behavior obtained for scales in and outside the Hubble scale will be recovered in the present scenario as well. Additionally, as the Wands duality proves, the solution to the Mukhanov-Sasaki equations will also be the same and will induce a quasi-scale invariant spectrum of perturbations.

However, it is important to note some other differences between inflation and bouncing models. In the contracting universe, the dominant perturbations mode will be different, and it grows during this branch [8]. That will not lead to problems on the scale dependence of the universe [64], thanks to the mixing of modes in the expanding branch of the universe in this scenario. Sometimes it is also argued that the contracting phase could lead to divergent perturbations during the non-singular bounce, but it has been proven that is not the case. Issues also arise with the correct gauge we need to use during the bounce phase, but that has also been shown to not be a problem. See references [82, 83, 6].

1.3.3 Realizing the bounce

In order to avoid the cosmic singularity, bouncing models need to have at least one of the two conditions: a modification to General Relativity or a fluid that violates the Null Energy Condition (NEC). In other words, it is needed to violate the conditions on the singularity theorems of Hawking and Penrose.

The NEC is the GR condition that states that $T_{\mu\nu}n^\mu n^\nu \geq 0$, where n^μ is a null vector. In cosmological context, where we work with perfect fluids, the NEC implies that $\rho + P \geq 0$. If the NEC is preserved, then it is impossible for the Hubble parameter first derivative to change its sign from negative to positive,

$$\dot{H} = -\frac{1}{2}(\rho + P). \quad (1.51)$$

Hence, during contraction, the Hubble parameter would diverge to negative values as it reaches a singularity. If the NEC is violated, it is possible to halt the contraction and realize a bounce. During the bounce phase, when $\dot{H} > 0$, the Hubble parameter changes sign, going from large negative values to large positive values. Away from the bounce, when the NEC is recovered, the Hubble parameter slows down, as \dot{H} negative once again.

The NEC violation is usually attached to the presence fields with negative kinetic energy, i.e. ghosts. However, some proposals include less-orthodox fields, such as Galileons [65] to avoid such issues. There are even string theory-motivated scenarios, such as the Dirac-Born-Infeld models [84].

Resorting to quantum cosmology, either via Wheeler-deWitt quantization [85, 86] or Loop Quantum Cosmology [14, 87, 88], has been a deeply explored field in recent years, reaching good results [57, 89]. That is the approach we take in chapter 3, where we build a bouncing cosmology using the Loop Quantum Cosmology (LQC) setting. In chapter 5, we resort to the Wheeler-de Witt quantization in the de Broglie-Bohm (dBB) quantum cosmology [86].

References [60, 65] analyze lots of different proposals, how they produce the bounce, and what could be their downside.

1.4 Inflation vs. Bounce

Inflationary and bouncing cosmologies, despite offering possible solutions to the HBB problems, are not guaranteed to succeed in this effort. Both of these scenarios have their own set of problems, inconsistencies, or ill-defined properties that are a topic of research until today.

Inflationary models are the most accepted early universe setting, but, if they are not constructed based of a quantum theory of gravity, they are not capable of explaining events from Planck-scale times. The cosmological singularity, in this case, remains a mystery to be solved. Consequently, all-things related to the initial conditions of inflation are beyond the reach of a model. That is most relevant for the issue of the necessary

homogeneity in the space-time patch that inflates and becomes the observed universe.

As we have mentioned in prior sections, in the inflationary paradigm justifies the homogeneity of CMB fluctuations with the fact that the original inflating patch was homogeneous as well. In turn, the reasoning behind said homogeneity is that any small patch in the universe by that time was locally homogeneous. However, such a statement has been prone to critiques, which are based on the fact that the required homogeneity scale is at Planck length, and therefore could only be explained by a full quantum theory. In other words, all inflationary predictions on scales that were smaller than Planck length on the onset of inflation are inconsistent – and such scales are precisely those present in the CMB. That has also been named the Trans-Planckian Problem [90, 42].

Bouncing cosmologies have their own issues. In the same way that the inflationary scenario cannot satisfactorily explain the initial condition for the onset of inflation, no bounce model can explain the initial conditions for the contracting universe prior to the bounce. The notion of initial conditions to an eternal universe is, in itself, already troublesome.

An extremely large universe, doted only with pressureless dust and radiation, is expected to be highly homogeneous. In addition, the infinite time to the far past allows for the regions seen at the CMB to be in thermal equilibrium. That supports the case for a bouncing universe to explain the homogeneity puzzle. However, some argue that the contraction phase produces anisotropies that make the bounce unfeasible [68, 69]. Such a problem would require an additional phase prior to the bounce, the so-called Ekpyrotic phase of contraction [68], that dilutes the anisotropies and allow the bounce to safely occur.

In this thesis we will not address neither the inflationary nor the bouncing scenario conceptual issues. These problems are, however, motivation to continue to work on both types of models; we remark once again that no scenario is strongly favored by current cosmological observations. In the future, we hope that data will offer, under the correct analysis, a concrete indication that one of these scenarios is the correct description of the early universe. Meanwhile, our research focus on finding clues that help disentangle inflationary and bouncing models: understanding their degeneracies in order to find distinctions between the scenarios.

Chapter 2

Cosmological Perturbations

Over the last decades, international collaborations such as WMAP [91] and Planck [92] promoted a great advancement in observational cosmology. New data allowed for tight constraints on cosmological parameters [19] and the power spectrum of CMB anisotropies [93], inaugurating the age of high precision data cosmology. It is mainly through the analysis of cosmological perturbations that data meets theory and we can distinguish new models for the early and late-time universe.

The theory of cosmological perturbations [94] is present in every type of early-universe cosmology, be it inflationary [95, 96], pre-big-bang [97, 98], bouncing [8, 99], ekpyrotic [68, 100, 101, 70], among others. The precise mechanism for the generation of cosmological perturbations change to different models. The type of perturbation produced will also change, as the allowed amplitude of scalar, vector, tensor modes and the ratio between them. It is necessary to study cosmological perturbations outside the classical GR regime when dealing with early universe models where quantum effects are present, as LQC [102, 103] or de Broglie Bohm Quantum cosmology [5, 6].

The production and evolution of cosmological perturbations throughout the history of the universe extend to different energy and length scales. At high energy scales (during inflation or during the bounce phase), both the space-time metric and the matter fields fluctuate at the quantum level. Only near Planck scales is that metric fluctuations are large [104]. In the inflationary scenario, the short-wavelength fluctuations associated to those scales are stretched to a classical regime and become the seeds of cosmological structure. In bouncing cosmologies, the growth in amplitude of cosmological fluctuations happens mainly during the crossing of the bounce, once again a regime near Planck scales.

Consequently, both scenarios need a framework to deal with quantum perturbations. When the cosmological perturbations are classical, we resort to the GR approach to gravitational instabilities (or the modified gravity theory in the model).

In this chapter, we first introduce the linear cosmological perturbation formalism in the context of General Relativity. We also display the case for single and multi-field scalar fluctuations, where we reconsider the analysis of adiabatic and non-adiabatic perturbations. Next, cosmological perturbations in the context of $f(R)$ theories are introduced. Lastly, we showcase the connection between theory and observations. We start from the two-point functions, then present the case of higher-order correlation functions and non-Gaussianities. The chapter concludes with the presentation of the δN -formalism, and we demonstrate how it facilitates the analysis of inflationary and bouncing models.

2.1 Newtonian Perturbations

The description of cosmological perturbations at classical level includes both Newtonian gravity and General Relativity. The Newtonian theory is applied to the evolution of density perturbations at an expanding (or contracting) background at sub-Hubble scales, in particular in the context of galaxy and clusters¹. In other words, the Newtonian theory is valid to study how the primordial cosmic seeds evolved to become large-scale structures. General Relativity is, on the other hand, the correct framework for the analyze of cosmological perturbations at super-Hubble scales.

Small inhomogeneities, like density fluctuations, are amplified by simple gravitational instability. Matter attracts matter, fluctuations grow and heterogeneous structures such as galaxies are formed. The first description of structure formation was made by Sir James Jeans, which brings the name to this mechanism, the so-called Jeans instability. The kind of perturbations responsible for those structures are Adiabatic Perturbations. We shall present both Adiabatic and non-Adiabatic perturbations throughout this section.

Some conclusions can be reached in the Newtonian context, concerning the evolution of structure. Adiabatic perturbations present in matter (especially in the dark matter fraction of it) will grow in case they have wave-length greater than the Jeans scale, whose wave-number is given by

¹In the context of modified gravity the regime may be better described by non-Newtonian physics, due to mechanisms such as screening [105, 106].

$$k_J = \left(\frac{4\pi G \rho_0}{c_s^2} \right)^{1/2}. \quad (2.1)$$

The Jeans length indicates the scale to which hydrodynamic pressure effects can react to changes in the gravitational potential and dominate the dynamics of the system [107]. Gravitation dominates for wavelengths greater than the Jeans wavelength and the perturbations grow.

For the radiation domination epoch, $\lambda_J \approx H_p$, while for the matter domination $\lambda_J \rightarrow 0$. Therefore density fluctuations that have $\lambda \ll H_p$ will grow only during matter domination. The amplitude of the perturbations grows only proportionally to the scale factor. The damping of the perturbations due to this behavior in radiation domination is called the Meszaros effect.

Conclusions about the importance of dark matter to the evolution of the universe are readily obtained.

The existence of dark matter is important to the evolution of the universe as we see it. Baryons and photons are coupled until recombination, and therefore baryon fluctuations do not have time enough to grow and be responsible for all the structures we observe today. We need a matter field that starts growing before recombination and that pushes the matter-radiation equality to an earlier time, allowing for a longer period of matter domination without spoiling Big-Bang Nucleosynthesis constraints. That is allowed if the dark matter component consists of approximately 30% of the energy density today.

As previously mentioned, the Newtonian regime is valid only for sub-Hubble scales. Beyond that, it is needed to make use of GR, because the perturbation equations are dominated by metric perturbations. That shall be the focus of the next sections.

2.2 Cosmological Perturbations in GR

To understand the origin of the perturbations mentioned in the previous section we need to study the quantum regime. Despite having no quantum description of gravity, we should start with metric perturbations. After that, we shall study how scalar field fluctuations are detailed, given that they are the fields responsible of inflationary and bouncing models in our work.

Both scalar field and metric perturbations are stretched beyond Hubble scales in the

early universe models – for inflation, it happens due to the exponential growth of the scale factor, while for bouncing models it happens during contraction of the horizon scale. The amplitude of adiabatic perturbations during inflation freeze beyond Hubble scales, i.e. they do not evolve and preserve their characteristics. The observation of these perturbations nowadays offers a window to the primordial universe. During contraction before the bounce (under the same adiabatic condition), the amplitude of the perturbations grows, without spoiling other details such as their scale-dependence. When we study those early-universe models in the next chapter, we demonstrate and solve the perturbations equations of motion. Our work on the scenario in which only non-adiabatic pressure is present, both for inflationary and bouncing universes.

Metric and matter perturbations are intimately linked. Perturbations in the field induce perturbations on the metric – a modification in the source term from the Einstein equations – while conversely, the metric perturbations modify the Klein-Gordon equation, which guides the matter (field) content.

Since we are dealing with covariant theories, there is no preferential reference system for the perturbations. The gauge freedom can produce fictional perturbations for certain coordinate systems. Therefore we work using a gauge-invariant approach and the longitudinal gauge (as we know how to deal to gauge-dependent effects on it).

Throughout this section, we define the scale in which the perturbations cross the particle horizon as $k_* = aH$. The formalism developed is used for both inflationary and bouncing models².

2.2.1 Linear Metric Perturbations

The perturbed FLRW metric can be decomposed according to the $SO(3)$ group. The 6 physical degrees of freedom of the metric can be separated into scalars (spin 0, with 2 d.o.f.), a vector (spin 1, with 2 d.o.f.), and a tensor (spin 2, with 2 d.o.f.). Vector perturbations will not be treated because we do not deal with fields with rotational velocity (for both inflationary and bouncing models), which is needed for their production. Therefore they would rapidly decay during expansion (either after inflation or post-bounce). Tensor perturbations are the gravitational waves. They are separated into two types. Primordial

²The details in regards to dominant modes during the dynamics will be highlighted throughout the chapter.

gravitational waves are produced thanks to the early universe physics – during inflation or during the contraction/bounce. The stochastic gravitational wave background (SGWB), on the other hand, is produced thanks to second-order effects. We do not work with SGWB production in our models. Scalar perturbations are the seeds of density fluctuations. We first present the linear regime, where all components evolve independently and will be studied separately. Later we present the higher-order regime for scalar perturbations only, and therefore we will not deal with second-order gravitational waves³.

Scalar Perturbations

Perturbing the FLRW metric in its scalar degrees of freedom, we obtain

$$ds^2 = a^2 \left[(1 + 2\phi) d\eta^2 + 2B_{,i} d\eta dx^i - ((1 - 2\psi) \delta_{ij} - 2E_{,ij}) dx^i dx^j \right]. \quad (2.2)$$

The four functions used above, ϕ , B , ψ , and E account for 4 dynamical degrees of freedom. Due to coordinate transformations, we can reduce this number to the previous count of 2. We set the remaining two d.o.f. to be the Bardeen potentials.

A general coordinate transformation $x^\alpha \rightarrow \tilde{x}^\alpha = x^\alpha + \xi^\alpha$, where ξ^α are infinitesimal functions. Under such transformation the scalars from (2.2) transform as:

$$\phi \rightarrow \tilde{\phi} = \phi - \frac{1}{a} (a\xi^0) \quad , \quad (2.3)$$

$$\psi \rightarrow \tilde{\psi} = \psi + \frac{a'}{a} \xi^0 \quad , \quad (2.4)$$

$$B \rightarrow \tilde{B} = B + \bar{\xi}' - \xi^0 \quad , \quad (2.5)$$

$$E \rightarrow \tilde{E} = E + \bar{\xi} \quad , \quad (2.6)$$

where $\xi^\alpha = (\xi^0, \xi^i) = (\xi^0, \xi_\perp^i + \bar{\xi}^i)$, $\bar{\xi}$ is a scalar and ξ_\perp^i is a divergence-free vector. We can make the reduction from 4 to 2 functions because only $\bar{\xi}$ and ξ^0 have a role in the transformations (2.3)-(2.6). Using the four previous scalars, we define the Bardeen Potentials as

³This kind of GW can be produced thanks to the second-order effects coming from scalars.

$$\Phi \equiv \phi - \frac{1}{a} [a(B - E')]', \quad (2.7)$$

$$\Psi \equiv \psi + \frac{a'}{a} (B - E') \quad (2.8)$$

In a flat universe and at hypersurfaces with constant conformal time η , the intrinsic spacial curvature is given by:

$${}^{(3)}R = \frac{4}{a^2} \nabla^2 \psi. \quad (2.9)$$

Due to the above expression, ψ is known as the curvature perturbations. All relevant quantities will be derived from it. It is not a gauge-invariant scalar, differently from the Bardeen potential Ψ .

Tensor Perturbations

The line element for the tensor component is given by

$$ds^2 = a^2 \left[d\eta^2 - (\delta_{ij} - h_{ij}) dx^i dx^j \right] \quad (2.10)$$

No tensor d.o.f. is present in coordinate transformations, which means that tensor perturbations are gauge invariant. They already have only 2 degrees of freedom, because h_{ij} is trace-free and transverse, which reduces its d.o.f. from 6 to 2. The remaining d.o.f. are the polarization modes from gravitational waves.

2.2.2 Perturbation in the Matter Content

The dominant contribution to the energy-momentum tensor during the universe in the models being studied is given by a scalar field. It provides density and pressure (from the scalar d.o.f.) and anisotropic stress (from tensor d.o.f.). As previously stated, the fluctuations from these quantities will induce the formation of metric perturbations through the Einstein equations.

Minimally coupled scalar fields lead to vanishing anisotropic stress, as it will be the case for the models of inflation and bouncing cosmologies we work with. It also implies that vector perturbations will not be sourced, which further explains their absence from the aforementioned models. The tensor perturbations' equation of motion will not be sourced as well⁴, although they are produced during the early universe.

2.2.3 Gauge Invariance

Except for tensor components and the Bardeen potentials, all the perturbations mentioned in the previous sections are dependent on the chosen gauge. Different slicing leads to different definitions of gauge-invariant quantities.

At the comoving slicing, where observers do not measure energy flux – the field φ is constant in space – the curvature perturbations transform according to the change in slicing. By construction, its result is gauge-invariant and is named as conformal curvature perturbation \mathcal{R} ⁵

$$\psi \rightarrow \psi_{\text{com.}} = \psi + \mathcal{H} \delta\eta = \psi + \mathcal{H} \frac{\delta\varphi}{\varphi'} \quad (2.11)$$

$$\mathcal{R} = \psi + \mathcal{H} \frac{\delta\varphi}{\varphi'} = \psi|_{\delta\varphi=0}. \quad (2.12)$$

\mathcal{R} is interpreted as the gravitational potential on the comoving slicing.

Another important slicing is that in which there are no density perturbations, $\delta\rho = 0$. Just as it happens in the comoving slicing, in the so-called slices of uniform energy density the curvature perturbation transformation will lead to a gauge-invariant quantity, ζ , defined as

$$\zeta = \psi + \frac{\delta\rho}{\rho'} = \psi|_{\delta\rho=0}. \quad (2.13)$$

ζ represents the gravitational potential in the uniform energy density slicing. It plays a similar role to \mathcal{R} in its respective slicing.

⁴In some other non-standard early universe scenarios it is possible to source GW thanks to mechanisms that allow for anisotropic stress to be present of some sort.

⁵In (2.11) $\delta\eta$ is the temporal displacement that leads from a general slicing to the comoving one.

Lastly, we can also define the flat slicing, where $\psi \equiv 0$. The gauge-invariant function will be the scalar field perturbation at the flat slicing

$$Q = \delta\varphi + \frac{\varphi'}{\mathcal{H}}\psi \quad (2.14)$$

In the case of super-horizon scales, $\mathcal{R} = \zeta$. We prove such a result using the linearized Einstein equations, which relate them by

$$-\zeta = \mathcal{R} + \left(\frac{k}{aH}\right)^2 \frac{2\rho}{3(\rho+p)}\Psi \quad (2.15)$$

Therefore, at super-horizon scales ($k \ll aH$)

$$\mathcal{R} = -\zeta \quad \text{for } k \ll aH \quad (2.16)$$

During inflation, after horizon exit, $k \ll aH$ is satisfied, therefore the equivalence (2.16) holds.

No non-adiabatic pressure is present in single-field inflation, hence both ζ and \mathcal{R} are conserved on super-horizon scales⁶. Therefore, after the perturbations cross the horizon they freeze and conserve their amplitude.

It is only after re-entry, at radiation or matter domination, that perturbations grow again. Hence, we can compute the evolution of perturbations from the moment they re-enter the horizon, as it acts as the initial conditions for the post re-entry evolution.

At the time of horizon re-entry, that we define as t_* , the perturbations have frequency $k_* = a(t_*)H(t_*)$. The $*$ subscript indicates the horizon re-entry time for each individual wavelength. It does not represent a single time value.

2.2.4 Adiabatic and Non-Adiabatic Perturbations

In this section we compute the production of cosmological perturbations, both in the adiabatic and non-adiabatic regime. For the single fluid (matter or field) case, only the

⁶We prove this on section 2.2.4, (2.44), when we analyze the multi-fluid case.

adiabatic regime is important. When there are more than two fluids or scalar fields in the system, it is possible to produce non-adiabatic fluctuations, also called entropy perturbations. As we have mentioned before, this channel of production of perturbations is central to the curvaton scenario of inflation.

First, we analyze the simplest case, of only one fluid. We deduce the Mukhanov-Sasaki equation and study the initial conditions for the production of (almost) scale-independent fluctuations. Then we study the two fluid case, followed by the case of two scalar fields.

Our work in this thesis present of all of those cases. In our first work, present on Chapter 3, we make use of just one scalar field. In our next work, see Chapter 4, we analyze two-field case of the curvaton scenario. Lastly, on Chapter 5, we analyze a system with one perfect fluid and one scalar field, but conclude that no entropy perturbations are produced [108].

One Field

Matter fields fluctuate. For single-field inflation, such field will be the inflaton, while for a matter-bounce it will be the scalar field that drives the background contraction. The Klein-Gordon equation for cosmology is, in cosmic time,

$$\ddot{\varphi} + 3H\dot{\varphi} - \frac{\nabla^2\varphi}{a^2} + V_{,\varphi} = 0 \quad (2.17)$$

The field fluctuations can be expanded in Fourier modes,

$$\delta\varphi(\mathbf{x}) = \int \frac{d^3\mathbf{k}}{(2\pi)^{3/2}} e^{i\mathbf{k}\cdot\mathbf{x}} \delta\varphi_{\mathbf{k}}(t), \quad (2.18)$$

that will also obey the Klein-Gordon equation

$$\delta\ddot{\varphi} + 3H\delta\dot{\varphi} + \frac{k^2\delta\varphi}{a^2} + V_{,\varphi} = 0 \quad (2.19)$$

We can also perturb the Klein-Gordon equation itself, just like we perturbed the metric. Using the conformal time, it leads us to

$$\delta\varphi'' + 2\frac{a'}{a}\delta\varphi' - \partial_i\partial^i\delta\varphi - \phi'\varphi' - 3\psi'\phi' - \partial_i\partial^i B\varphi' = -\delta\varphi\frac{\partial^2 V}{\partial\varphi^2}a^2 - 2\varphi\frac{\partial V}{\partial\varphi} \quad (2.20)$$

The analysis of cosmological scalar perturbations is mainly done in the comoving gauge. Tensor perturbations are gauge-independent, and therefore can be directly analyzed. Hence, for the scalar component, we substitute (2.11) in (2.2) and we neglect the perturbations B and ϕ because they are only related to \mathcal{R} via constraint equations. We then expand the GR action with a minimally coupled scalar field to second order in \mathcal{R} ,

$$S = \frac{1}{2} \int d^4x \sqrt{-g} [R - g^{\mu\nu} \partial_\mu\varphi \partial_\nu\varphi - 2V(\varphi)] \quad (2.21)$$

$$S_{(2)} = \frac{1}{2} \int d^4x a^3 \frac{\dot{\varphi}^2}{H^2} \left[\dot{\mathcal{R}}^2 - \frac{(\partial_i\mathcal{R})^2}{a^2} \right] \quad (2.22)$$

We then define the Mukhanov variable v and the pump-field function z_s as

$$v = z_s \mathcal{R} \quad (2.23)$$

$$z_s = a \frac{\dot{\varphi}}{H} \quad (2.24)$$

Applying these two variables in (2.22) and using the conformal time, we get

$$S_{(2)} = \frac{1}{2} \int d\eta d^3x \left[v'^2 + (\partial_i v)^2 + \frac{z_s''}{z_s} v^2 \right] \quad (2.25)$$

Using the Fourier expansion of v above, we vary the action and obtain the Mukhanov-Sasaki equation

$$v_{\mathbf{k}}'' + \left(k^2 - \frac{z_s''}{z_s} \right) v_{\mathbf{k}} = 0 \quad (2.26)$$

Equation (2.26) is similar to that of a parametric harmonic oscillator, because z_s (2.24) depends on the background dynamics, therefore it also depends on time. We can mass term

$$M_{MS-s} = \frac{z''_s}{z_s}, \quad (2.27)$$

The Wands' duality [63], that we present in chapter 3, is centered on a symmetry of the mass term (2.27).

The pump function z will be generalized in section 2.3, since (2.24) is valid only for a scalar field minimally coupled to gravity. To quantize v we use the canonical quantization procedure. The operator \hat{v} is defined as

$$\hat{v} = \int \frac{d\mathbf{k}^3}{(2\pi)^3} \left[v_{\mathbf{k}}(\eta) \hat{a}_{\mathbf{k}} \exp^{i\mathbf{k}\cdot\mathbf{x}} + v_{\mathbf{k}}^*(\eta) \hat{a}_{\mathbf{k}}^\dagger \exp^{-i\mathbf{k}\cdot\mathbf{x}} \right] \quad (2.28)$$

It is necessary to set the boundary conditions for the system. We use the normalization of the modes ⁷

$$\langle v_{\mathbf{k}}, v'_{\mathbf{k}'} \rangle = \frac{i}{\hbar} \left(v_{\mathbf{k}}^* v'_{\mathbf{k}'} - v_{\mathbf{k}'}^* v_{\mathbf{k}} \right) = 1 \quad (2.29)$$

We must also choose the vacuum initial conditions. For scalar fields in an inflationary background, the k^2 term in (2.26) dominates over the mass term. For a bouncing cosmology, it is necessary that the mass term (2.27) decreases to the far past of the contracting branch [109], so that k^2 term dominates the Mukhanov-Sasaki equations as well ⁸.

Under those circumstances, the Mukhanov-Sasaki equation is

$$v_{\mathbf{k}}'' + k^2 v_{\mathbf{k}} = 0. \quad (2.30)$$

In this limit, the solution of (2.30) sets the Bunch-Davies vacuum [110] as

$$\lim_{\eta \rightarrow -\infty} v_{\mathbf{k}} \propto \frac{\exp^{-ik\eta}}{\sqrt{2k}} \quad (2.31)$$

For inflation, in the de Sitter background limit, $z''/z = a''/a$ and therefore

$$v_{\mathbf{k}}'' + \left(k^2 - \frac{2}{\eta^2} \right) v_{\mathbf{k}} = 0 \quad (2.32)$$

The solution, under the boundary conditions (2.29) and (2.31), is

⁷The creation and annihilation operators satisfy the canonical commutation relations thanks to the normalization.

⁸We shall see in 5 that there are cases in which the k^2 term might not dominate over the other terms, which leads to a different vacuum for the cosmological perturbations.

$$v_k = \frac{\exp^{-ik\eta}}{\sqrt{2k}} \left(1 - \frac{i}{k\eta} \right) \quad (2.33)$$

For the tensor perturbations, h_{ij} , the second order expansion of (2.21) leads to

$$S_{(2)} = \frac{M_{\text{Pl}}^2}{8} \int d\eta dx^3 a^2 \left[(h'_{ij})^2 - (\partial_l h_{ij})^2 \right] \quad (2.34)$$

The two degrees of freedom for tensor perturbations are the polarization modes defined by

$$h_{ij} = h_+ e_{ij}^+ + h_\times e_{ij}^\times, \quad (2.35)$$

where e^+ and e^\times are polarization tensors.

The Fourier expansion for the polarization modes, $h_{\mathbf{k}}^s$, $s = (+, \times)$, and the definition of the Mukhanov variable $v_{\mathbf{k}}^s = aM_{\text{Pl}}h_{\mathbf{k}}^s/2$ results in

$$S_{(2)} = \sum_s \frac{1}{2} \int d\eta d^3x \left[(v_{\mathbf{k}}^{s'})^2 - \left(k^2 - \frac{a''}{a} \right) (v_{\mathbf{k}}^s)^2 \right] \quad (2.36)$$

The Mukhanov-Sasaki equation for each polarization mode and the mass term for them are

$$v_{\mathbf{k}}^{s''} + \left(k^2 - \frac{a''}{a} \right) v_{\mathbf{k}}^s = 0 \quad (2.37)$$

$$M_{MS-t} = \frac{a''}{a} \quad (2.38)$$

Once again we note that the above mass term is valid only for GR and will change, for instance, for the $f(R)$ gravity case. For a de Sitter background, we have that both scalar and tensor perturbations have the same mass terms, and therefore the modes follow the same equations. Hence the result (2.33) is valid for each polarization.

Two Fluids

Adiabatic or Curvature perturbations are defined as the cosmological perturbations that evolve following the same background trajectory, so that, for any quantities X and Y we

have

$$\frac{\delta X}{\dot{X}} = \frac{\delta Y}{\dot{Y}}, \quad (2.39)$$

whereas, for non-adiabatic or isocurvature perturbations the above relation does not hold.

When dealing with adiabatic perturbations, equation 2.39 is true for density and pressure, so that

$$\frac{\delta \rho}{\dot{\rho}} = \frac{\delta p}{\dot{p}}. \quad (2.40)$$

Therefore, for a general pressure perturbation, we can decompose it in its adiabatic and non-adiabatic perturbations

$$\delta p = \delta p_{ad} + \delta p_{nad}. \quad (2.41)$$

$$= \frac{\dot{p}}{\dot{\rho}} \delta \rho + \delta p_{nad}. \quad (2.42)$$

Conservation of energy [111] tells us that density perturbations, at super-horizon scales, evolve as

$$\dot{\delta \rho} = -3H(\delta \rho + \delta p) - 3\dot{\psi}(\rho + p) \quad (2.43)$$

In the uniform-density gauge, $\delta \rho = 0$, which implies that $\delta p = \delta p_{nad}$. Additionally, we have that $\psi = \zeta$, and, therefore, for the evolution of the curvature perturbations at super-horizon scales follows

$$\dot{\zeta} = -\frac{H}{p + \rho} \delta p_{nad}. \quad (2.44)$$

This means that, in the presence of non-adiabatic pressure, curvature perturbations

are not frozen at super-horizon scales. During single-field inflation, there is no source of such pressure, therefore the perturbations are conserved. That is not what happens for the curvaton scenario.

The isocurvature perturbation, also known as entropy perturbation, between two fluids is written as

$$\mathcal{S}_{ij} = H \left(\frac{\delta\rho_i}{\dot{\rho}_i} - \frac{\delta\rho_j}{\dot{\rho}_j} \right). \quad (2.45)$$

Two Fields

In this work, we shall limit the analysis of perturbations for the case of two scalar fields. The case for N-fields is straightforward to evaluate and we refer to [49].

In the general relativity regime, the action for of two massive scalar fields φ and χ minimally coupled to gravity is given by

$$S = \int d^4\mathbf{x} \sqrt{-g} \left[\frac{R}{2} - \frac{1}{2} (\partial\varphi)^2 - \frac{1}{2} (\partial\chi)^2 - V(\varphi, \chi) \right], \quad (2.46)$$

where in the non-interacting case we have $V(\varphi, \chi) = V(\varphi) + V(\chi) \equiv V$, where the last definition is given for simplicity. In a homogeneous and isotropic background given by the FLRW metric, each scalar field obey the Klein-Gordon equation (for $\phi_I = (\varphi, \chi)$)

$$\ddot{\phi}_I + 3H\dot{\phi}_I + V_{\phi_I} = 0, \quad (2.47)$$

where H is the Hubble parameter given by

$$H^2 = \frac{1}{3} \left[\sum_I \frac{1}{2} \dot{\phi}_I^2 + V(\phi_I) \right]. \quad (2.48)$$

We decompose the field $\phi_I(t, \mathbf{x})$ in its homogeneous and perturbed part as $\phi_I(t, \mathbf{x}) = \phi_I(t) + \delta\phi_I(t, \mathbf{x})$. We shall work in the flat gauge⁹, $\psi_{flat} = 0$, where the field fluctuations

⁹The flat gauge is defined as the slicing where there is no spatial curvature, $\psi = 0$

are equal to the Mukhanov-Sasaki variables

$$Q_I \equiv \delta\phi_I + \frac{\dot{\phi}_I}{H}\psi_{flat} = \delta\phi_I. \quad (2.49)$$

For a comoving wavenumber $k = 2\pi a/\lambda$ in Fourier space, working in terms of the Mukhanov-Sasaki variables, the equation of motion for the field fluctuations are

$$\ddot{Q}_I + 3H\dot{Q}_I + \frac{k^2}{a^2}Q_I + \sum_J \left[V_{\phi_I\phi_J} - \frac{1}{a^3} \frac{d}{dt} \left(\frac{a^3}{H} \dot{\phi}_I \dot{\phi}_J \right) \right] Q_J = 0. \quad (2.50)$$

A definition of new field variables allows for a better analysis and distinction of adiabatic and non-adiabatic (entropy) perturbations. In the field space of (φ, χ) , we define the angle θ between the tangent of the background trajectory and the φ -axis such as

$$\cos\theta = \frac{\dot{\varphi}}{\sqrt{\dot{\varphi}^2 + \dot{\chi}^2}}; \quad \sin\theta = \frac{\dot{\chi}}{\sqrt{\dot{\varphi}^2 + \dot{\chi}^2}} \quad (2.51)$$

See Figure 2.1, adapted from [49], where we show the decomposition of the entropy perturbation following Eq. (2.51).

We can then define the adiabatic field σ and the non-adiabatic field s via their velocities, and their respective fluctuations

$$\dot{\sigma} = (\cos\theta)\dot{\varphi} + (\sin\theta)\dot{\chi}; \quad \delta\sigma = (\cos\theta)\delta\varphi + (\sin\theta)\delta\chi \quad (2.52)$$

$$\dot{s} = -(\sin\theta)\dot{\varphi} + (\cos\theta)\dot{\chi}; \quad \delta s = -(\sin\theta)\delta\varphi + (\cos\theta)\delta\chi \quad (2.53)$$

The adiabatic field is tangent to the background trajectory in field space, while the entropy field is orthogonal to it.

The same decomposition can be applied to the derivatives of the scalar potential V , which appear in the equations of motion later in this section,

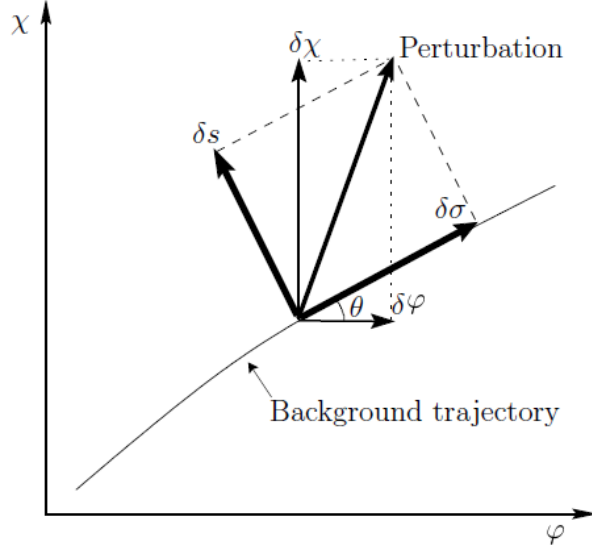


Figure 2.1: Decomposition of the entropy perturbation.

$$V_\sigma = (\cos \theta) V_\varphi + (\sin \theta) V_\chi \quad (2.54)$$

$$V_s = -(\sin \theta) V_\varphi + (\cos \theta) V_\chi \quad (2.55)$$

$$V_{\sigma\sigma} = (\sin^2 \theta) V_{\chi\chi} + (\sin 2\theta) V_{\varphi\chi} + (\cos^2 \theta) V_{\varphi\varphi} \quad (2.56)$$

$$V_{ss} = (\sin^2 \theta) V_{\varphi\varphi} - (\sin 2\theta) V_{\varphi\chi} + (\cos^2 \theta) V_{\chi\chi} \quad (2.57)$$

We can then write the comoving curvature perturbation in the flat gauge simply as

$$\mathcal{R} = \frac{H}{\dot{\sigma}} \delta\sigma_{flat} \quad (2.58)$$

We note that $\delta\sigma$ is gauge-dependent, while δs is gauge-independent¹⁰.

For the total entropy perturbation, which is also gauge-independent, we have

$$\mathcal{S} = H \left(\frac{\delta p}{\dot{p}} - \frac{\delta \rho}{\dot{\rho}} \right). \quad (2.59)$$

The above equation can be rewritten for the two fields φ and χ using the definition for pressure and density, which can, in turn, be transformed and rewritten in terms of the

¹⁰From the definition of \dot{s} one can see that for the classical trajectory $s = const.$ and therefore s is gauge-independent

adiabatic and entropy fields as

$$\mathcal{S} = -\frac{4}{3} \frac{V_\sigma}{\dot{\sigma} (3H\dot{\sigma} + 2V_\sigma)} \left(\frac{k^2}{a^2} \Psi \right) - \frac{2}{3} \frac{\dot{\theta}}{\dot{\sigma}} \delta s, \quad (2.60)$$

where

$$\dot{\theta} = \frac{V_s}{\dot{\sigma}}, \quad (2.61)$$

and Ψ is once again the curvature perturbation (i.e. the Bardeen potential).

From Eq. (2.60) we see that the total entropy perturbation at large scales is proportional to the entropy field fluctuation δs , which justifies its nomenclature.

In the presence of entropy fluctuations, as anticipated, the comoving entropy perturbation can vary in time according to

$$\dot{\mathcal{R}} = \frac{H}{\dot{H}} \frac{k^2}{a^2} \Psi + 2H \frac{\dot{\theta}}{\dot{\sigma}} \delta s \quad (2.62)$$

This result differs from the single field case, where the conservation of \mathcal{R} at large scales is sometimes referred to as the Weinberg theorem.

As long as the entropy fluctuation is nonzero and the angle θ varies, we have that the comoving curvature perturbation evolves even at super-horizon scales.

The entropic mechanism is defined as achieving cosmically relevant \mathcal{R} mainly by the enhancement of it via its coupling to entropy perturbations.

The variation of θ implies that for the entropic mechanism to happen the background trajectory in field space needs to turn; i.e. it must have a period of enhanced importance of χ to the background evolution.

To find out if those conditions are satisfied, we need to solve the equations for the adiabatic and entropy perturbations. We shall write $\delta\sigma_{flat}$ simply as $\delta\sigma$ for convenience.

$$\ddot{\delta\sigma} + 3H\dot{\delta\sigma} + \left[\frac{k^2}{a^2} + V_{\sigma\sigma} - \dot{\theta}^2 - \frac{1}{a^3} \frac{d}{dt} \left(\frac{a^3 \dot{\sigma}^2}{H} \right) \right] \delta\sigma = 2 \frac{d}{dt} (\dot{\theta} \delta s) - 2 \left(\frac{V_\sigma}{\dot{\sigma}} + \frac{\dot{H}}{H} \right) \dot{\theta} \delta s \quad (2.63)$$

The equation for $\delta\sigma$, in this case, is the same as that for the Mukhanov-Sasaki variable, similarly to what happens for ϕ_I . We see that it is coupled to the entropy fluctuation δs , as expected due to the coupling present on \mathcal{R} .

For the entropy fluctuation, though, the equation of motion will be decoupled from the adiabatic mode

$$\ddot{\delta s} + 3H\dot{\delta s} + \left[\frac{k^2}{a^2} + V_{\sigma\sigma} + 3\dot{\theta}^2 \right] \delta s = 4 \frac{\dot{\theta}}{\dot{\sigma}} \frac{k^2}{a^2} \Psi \quad (2.64)$$

As long as the entropy fluctuation is nonzero, it evolves even at large scales. As a consequence, it enhances the magnitude of the curvature perturbations.

2.2.5 Entropic Mechanism

In the context of multi-field cosmology, one cannot ignore the presence of non-adiabatic fluctuations, which, as we presented above, may lead to entropy perturbations and the enhancement of curvature modes. There are lots of early universe models that make use of the production of the curvature perturbations due to non-adiabatic pressure, in the so-called entropic mechanism – like the curvaton model mentioned on Sec. 1.2.5.

The main challenge of early universe models that use the entropic mechanism is to devise a way in which $\dot{\theta} \neq 0$ somewhere along the evolution.

The original curvaton scenario uses the decaying phase of the curvaton field to produce the curvature perturbations. During decay, the field oscillates harmonically around its minimum and behaves as non-relativistic matter. By that time, the universe is filled with a photon fluid (from the inflaton decay). The mixture between matter (the field) and photons provides a relative non-adiabatic pressure between the two fluids. Therefore, as seen in (2.44), the curvature perturbation grows. It then achieves the amplitude as seen on the CMB.

Bouncing models can also use the entropic mechanism. Generally speaking, the non-

adiabatic fluctuations will be produced during contraction, acquiring an almost scale-invariant dependence. The passage from entropy to adiabatic perturbations will vary between models.

Ekpyrotic models [112, 113, 114, 115] generally make use of a turning in the trajectory near the bounce point. For a short time, the scalar potential for the lightest field (in our notation, χ) turns on a large contribution to the total scalar potential, dominating the dynamics. During this short domination, the background evolution becomes more dependent on $\dot{\chi}$ – i.e., its trajectory in field space turns, leading to $\dot{\theta} \neq 0$.

Curvaton-like mechanisms in the matter bounce scenario are also possible [61, 116]. As the models of ekpyrotic contraction, there will be a light field – the curvaton – responsible for the entropy perturbations, while the matter domination is due to the other(s) field(s). Once again, it is during the bounce phase in which the entropic mechanism happens, thanks to a time when the curvaton field dominates the background. No ekpyrotic phase takes place, but at least one of the fields should be responsible for the breaking of the Null Energy Condition, to realize the bounce.

An interesting feature found in these kinds of models [61] is the kinetic amplification of entropy perturbations in the bounce phase due to an effective tachyonic mass for the fluctuations of the curvaton. Therefore, the entropy perturbations will enhance the curvature perturbations via the entropic mechanism at the same time that they amplify their amplitude. This process helps explain the low tensor-to-scalar ratio because the tensor perturbations do not suffer the same amplification as their scalar counterparts.

2.3 Perturbation Theory for $f(R)$ Gravity

$f(R)$ theories have an extra scalar degree of freedom in comparison to GR, with no additional vector or tensor modes [117]. Through its scalar-tensor theory equivalence, we know that this degree of freedom is massless and propagates with the speed of light. Despite such difference, it is just at the perturbation level that its effect is highlighted. For the background dynamic, it is possible to adjust the model in order to match the Λ CDM behavior.

The line element for an FLRW universe is still valid in this case. The additional degree of freedom is not present in the metric. A general action that included $f(R)$ theories is

[117, 118]

$$S = \int d^4x \sqrt{-g} \left[\frac{1}{2\kappa^2} f(R, \varphi) - \frac{1}{2} \omega(\varphi) \partial^\mu \varphi \partial_\mu \varphi - V(\varphi) \right] . \quad (2.65)$$

When $f(R, \varphi) = f(R)$ e $\varphi = 0$, $\omega = 1$ we recover $f(R)$ theories without a minimally coupled scalar field, as it is the case for the Starobinsky model [2]. We shall deal with this case throughout this section.

The extra degree of freedom is $F = \partial f / \partial R$. It can be separated in its background value \bar{F} and perturbation δF , $F = \bar{F} + \delta F$.

All gauge-invariant quantities described in 2.2.3 are still valid, and in addition, we have the variation of F and another gauge-invariant quantity associated with it

$$\delta F = F - \dot{F} \xi^0 \quad (2.66)$$

$$\mathcal{R}_{\delta F} = \psi - \frac{H}{\bar{F}} \delta F \quad (2.67)$$

Repeating the previous procedure, it is possible to choose a gauge in which $\delta F = 0$. This choice fixes the gauge, therefore there are no extra degrees of freedom. For our work, $\mathcal{R} = \mathcal{R}_{\delta F}$.

The perturbed Einstein equations at first order are not necessary for this section, and therefore we refer to References [117, 119, 120].

2.3.1 Quantum Perturbations in $f(R)$

The perturbed second-order action is given by

$$S_{(2)} = \int dt d^3x a^3 Q_s \left[\dot{\mathcal{R}}^2 - \frac{(\partial_i \mathcal{R})^2}{a^2} \right] \quad (2.68)$$

$$Q_s = \frac{3\dot{F}^2 / 2\kappa^2 F}{\left[H + \left(\frac{\dot{F}}{2F} \right) \right]^2} \quad (2.69)$$

Revisiting the action 2.22 we note that the function z_s is multiplying the term inside square brackets in the same way as the function Q_s . Therefore it is not surprising that varying action 2.68, we get

$$u_{\mathbf{k}}'' + \left(k^2 - \frac{z_f''}{z_f} \right) u_{\mathbf{k}} = 0 \quad (2.70)$$

$$u_{\mathbf{k}} = z_f \mathcal{R}_{\mathbf{k}} \quad (2.71)$$

$$z_f = a\sqrt{Q_s} \quad (2.72)$$

The method to identify the pump function z_s is similar to that of the GR scenario. In GR, however, we have $F = 1$ e $Q_s = \dot{\phi}^2/H^2$. We identify the e new mass term from the Mukhanov-Sasaki equation as

$$M_{MS-f} = \frac{z_f''}{z_f} \quad (2.73)$$

Once again, this term will depend on the background dynamics.

The quantization procedure for u is identical to that on [2.2.4](#) so that we have the same asymptotic limits and the same vacuum, the Bunch-Davies initial conditions. The solution for the de Sitter case will be similar, given the difference being the function Q_s , as it is a generalization of the previous result. Therefore, we can compute the scalar power spectrum and check that it is dependent on Q_s :

$$\mathcal{P}_{\mathcal{R}} = \frac{k^3}{2\pi^2} |\mathcal{R}|^2 = \frac{k^3}{2\pi^2} \left| \frac{u}{z_f} \right|^2 \quad (2.74)$$

$$= \frac{1}{Q_s} \left(\frac{H}{2\pi} \right)^2 \quad (2.75)$$

For the tensor perturbations, the computations are analogous. There are no extra degrees of freedom for this case, so we have the same definitions for the polarization as in [2.2.4](#). As in the scalar case, we get an additional term from the perturbed $f(R)$ action, which results in a new definition for u_λ :

$$S_{(2)} = 2.M_{\text{Pl}}^2 \int d\eta dx^3 \frac{a^2}{4} F \left[(h'_{ij})^2 - (\partial_l h_{ij})^2 \right] \quad (2.76)$$

$$u''_\lambda + \left(k^2 - \frac{z_t''}{z_t} \right) u_\lambda = 0 \quad (2.77)$$

$$u_\lambda = M_{\text{Pl}} z_t h_\lambda \quad (2.78)$$

$$z_t = a\sqrt{F} \quad (2.79)$$

Once again we get a different mass term in comparison to GR

2.4 Observations

2.4.1 Cosmological Perturbations Statistics

The connection between the cosmological perturbation theory and CMB observations is given mainly by its correlation functions. For inflationary and bouncing cosmologies in general the most important statistical measure is the power spectrum, from both \mathcal{R} and tensor perturbations. The power spectrum $\mathcal{P}_{\mathcal{R}}$ is computed from the two-point correlation function. In addition, higher-order correlation functions, such as the three and four-point, are also important to fully distinguish between models. For them, there are other relevant functions, as the non-linearity parameters f_{NL} , g_{NL} and τ_{NL} , that we present in section [2.4.2](#).

In our notation, for the two-point correlation function, we have

$$\langle \mathcal{R}_{\mathbf{k}} \mathcal{R}_{\mathbf{k}'} \rangle = \delta^3(\mathbf{k} - \mathbf{k}') \frac{2\pi^2}{k^3} \mathcal{P}_{\mathcal{R}} = \delta^3(\mathbf{k} - \mathbf{k}') 2\pi^2 P_{\mathcal{R}} \quad (2.80)$$

$$\rightarrow \langle |\mathcal{R}|^2 \rangle = \int \frac{d^3k}{2\pi^3} |\mathcal{R}_{\mathbf{k}}|^2 = \int \frac{dk}{k} \frac{k^3}{2\pi^2} |\mathcal{R}_{\mathbf{k}}|^2 \quad (2.81)$$

$$\mathcal{P}_{\mathcal{R}} = \frac{k^3}{2\pi^2} |\mathcal{R}|^2 \quad (2.82)$$

Using the results from the previous section we can obtain the power spectrum for an inflationary universe. For an exact de Sitter regime the power spectrum is scale-invariant, i. e. it is independent of k . However inflation corresponds to a quasi-de Sitter regime,

which results in $\mathcal{P}_{\mathcal{R}}$ that depends on scale thanks to the different times the modes k leave the horizon. Since all values we compute correspond to horizon crossing, those quantities will evolve according to the evolution of aH through the different values of k . The expression for the comoving curvature power spectrum is then

$$\langle \hat{\mathcal{R}}_{\mathbf{k}} \hat{\mathcal{R}}_{\mathbf{k}'} \rangle = \frac{H^2}{\dot{\varphi}^2} \langle \hat{v}_{\mathbf{k}} \hat{v}_{\mathbf{k}'} \rangle = \delta(\mathbf{k} - \mathbf{k}') \frac{H^2}{\dot{\varphi}^2} \frac{H^2}{2k^3} (1 + k^2 \eta^2) \quad (2.83)$$

$$\langle |\mathcal{R}|^2 \rangle = \frac{H^2}{2k^3} \frac{H^2}{\dot{\varphi}^2}, \quad (2.84)$$

where we used the fact that on super-horizon scales $|k\eta| \ll 1$ and the de Sitter scale factor $a = -1/H\eta$. Therefore we get, using 2.82,

$$\mathcal{P}_{\mathcal{R}}(k) = \left(\frac{H}{2\pi} \right)^2 \frac{H^2}{\dot{\varphi}^2} \quad (2.85)$$

Throughout the thesis, we focus on phenomenological aspects of the models, so that the computation of the power spectrum is not of utmost importance. We must compute the relevant observational quantities, such as the spectral index (both scalar and tensor), and also the non-Gaussianity parameters f_{NL} and g_{NL} . For the scalar spectral index, we obtain the power-spectrum dependence on the frequency k

$$n_{\mathcal{R}} - 1 = \frac{d \log \mathcal{P}_{\mathcal{R}}}{d \log k} \quad (2.86)$$

$$\rightarrow \mathcal{P}_{\mathcal{R}} = A_s \left(\frac{k}{k_*} \right)^{n_s - 1} \quad (2.87)$$

For the tensor perturbations, we get it directly from the polarization modes

$$\mathcal{P}_T(k) = \frac{k^3}{2\pi^2} \sum_{\lambda} |h_{\mathbf{k}}|^2 = 8 \frac{k^3}{2\pi^2} |v_{\mathbf{k}}|^2 = \frac{8}{M_{\text{Pl}}^2} \left(\frac{H}{2\pi} \right)^2 \quad (2.88)$$

$$n_T = \frac{d \log \mathcal{P}_T}{d \log k} \quad (2.89)$$

$$\rightarrow \mathcal{P}_T = A_T \left(\frac{k}{k_*} \right)^{n_T} \quad (2.90)$$

However, it shall be more relevant to compute the ratio between the tensor-to-scalar

perturbations in order to study the tensor perturbations. Such ratio is simply given by

$$r = \mathcal{P}_T/\mathcal{P}_R \tag{2.91}$$

As we shall detail in the next chapter, for inflationary models it is possible to rewrite those functions in terms of the so-called Slow-Roll Parameters (SRP). Therefore, the values of the spectral index and ratio r follow easily after one computes the SRPs in single-field inflation models.

Cosmic Microwave Background Radiation

After the theoretical introduction to cosmological perturbations, we need to understand how such quantities can be evaluated and put to test using observations.

Involuntarily discovered by Penzias and Wilson [121], the Cosmic Microwave Background Radiation(CMB-R) is the current most direct source for observation of cosmological perturbations. Formed during the last stages of recombination, resulting in the so-called Last Scattering Surface (LSS), the CMB peaks on the frequency of microwaves (hence its name), and follows a blackbody radiation spectra, at $2.72K$. That temperature is not completely homogeneous throughout the whole angular extension of the CMB. The temperature anisotropies are sourced by matter distribution during recombination, the cosmic seeds originated by the curvature perturbations induced by the primordial universe (inflation, bouncing cosmology, or any other mechanism)

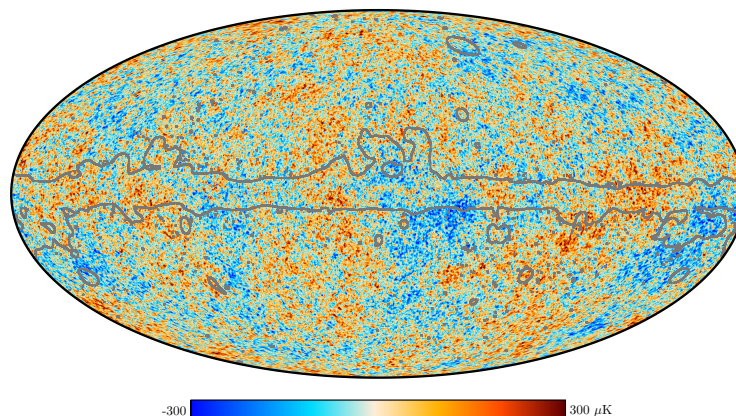


Figure 2.2: CMB temperature Fluctuations using the SMICA method.

The cosmological perturbations responsible for the temperature fluctuations in the CMB re-entered the horizon during the transition between radiation and matter-dominated

epochs. As we have previously mentioned, at super-Hubble scales the perturbations were frozen and did not evolve. After re-entry, they evolved following the Einstein equations.

The earlier the re-entry, the smaller are the scales correspondent to the modes, such that, for example, modes that re-entry during radiation domination are responsible for the smallest scales anisotropies. They modify the original primordial spectrum because they evolved until CMB formation. In the CMB power-spectrum Fig. 2.3, they correspond to multipoles $\ell > 30$.

On the other hand, perturbation modes that made re-entry after recombination and around last-scattering kept intact their properties as generated in the early universe. They correspond to multipoles $\ell < 30$ in Fig. 2.3. That is why the power spectrum at low multipoles has an almost scale-independent behavior.

To compute how the CMB looks, starting from the primordial spectra, we must take into account all the effects that take place from the moment the perturbations re-enter the horizon until the moment we observe the CMB photons. For that, it is necessary to solve the Einstein and the Boltzmann equations responsible for the matter and photon perturbations. In the following, we present the Sachs-Wolfe effect, the main source of the photon temperature fluctuations observed in the CMB. We leave the precise details of the computations for references [104, 122].

Sachs-Wolfe Effect

The Sachs-Wolfe effect can be understood as the dominant production mechanism of the CMB fluctuations. From the Boltzmann equations for the temperature fluctuations, we obtain

$$\frac{\delta T}{T} + \Phi = cte. \quad (2.92)$$

Neglecting the monopole term in the l^i direction (as it is pure gauge), we have that the fractional temperature fluctuation observed today is decomposed as

$$\frac{\delta T}{T} = \left(\frac{\delta T}{T} \right)_{LS} + \Phi_{LS} \quad (2.93)$$

The fluctuations at the last scattering surface (the first term in the RHS) can be obtained as a function of the photon energy density fluctuations δ_γ . After some algebraism

to obtain δ_γ (by comparing the hydro-dynamical and kinetic energy-momentum tensors), the Fourier expansion of 2.93 is

$$\frac{\delta T}{T} = \int \left[\left(\Phi + \frac{\delta_\gamma}{4} \right)_{\mathbf{k}} - \frac{3\delta_\gamma'}{4k^2} \frac{\partial}{\partial \eta_0} \right]_{LS} \exp^{i\mathbf{k}(\mathbf{x}_0 + \mathbf{l}(\eta_{LS} - \eta_0))} \frac{d^3k}{(2\pi)^{3/2}} \quad (2.94)$$

In turn, δ_γ can also be written in terms of the gravitational potential

$$\delta_\gamma \simeq -\frac{8}{3}\Phi_k \ ; \ \delta_\gamma' = 0 \quad (2.95)$$

$$\Rightarrow \frac{\delta T}{T} \simeq \frac{1}{3}\Phi_{LS} = \frac{1}{5}\mathcal{R}_{LS} \quad (2.96)$$

Therefore, 2.96 is the expression that relates the CMB temperature fluctuations to the curvature perturbations. We did not consider the integrated Sachs-Wolfe effect or the influence of the photon energy density on the curvature.

Angular Power Spectrum

The CMB temperature fluctuations can be expressed in terms of multipole moments. From this angular power spectrum 2.3 it is possible to compute amplitude and spectral index of scalar perturbations, A_s and n_s . Its precise shape, plotted in 2.3, depends of course on A_s and n_s , and also on the other cosmological parameters (as Ω_Λ , etc.) due to the evolution of the perturbations once inside the particle horizon from re-entry to observation.

It is possible to re-express the temperature anisotropies in terms of spherical harmonics as

$$\frac{\delta T(\theta, \phi)}{T} = \sum_{l,m} a_{l,m} Y_{l,m}(\theta, \phi) \quad (2.97)$$

$$\langle a_{l'm'}^* a_{lm} \rangle = \delta_{ll'} \delta_{mm'} C_l^{TT} \Leftrightarrow C_l^{TT} = \frac{1}{2l+1} \langle a_{lm}^* a_{lm} \rangle \quad (2.98)$$

$$l(l+1)C_l^{TT} \propto \left(\frac{\delta T(\theta, \phi)}{T} \right)^2 \quad (2.99)$$

For large angular scales, $\ell \ll 200$, a scale invariant spectrum A_s ($n_s = 1$) has a plateau

$$l(l+1)C_l^{TT} \simeq \frac{9A_s}{100\pi} \quad (2.100)$$

Despite the power spectrum not being exactly scale invariant, as explicit on Section 2.4.1, the above result can be observed on Figure 2.3 ¹¹

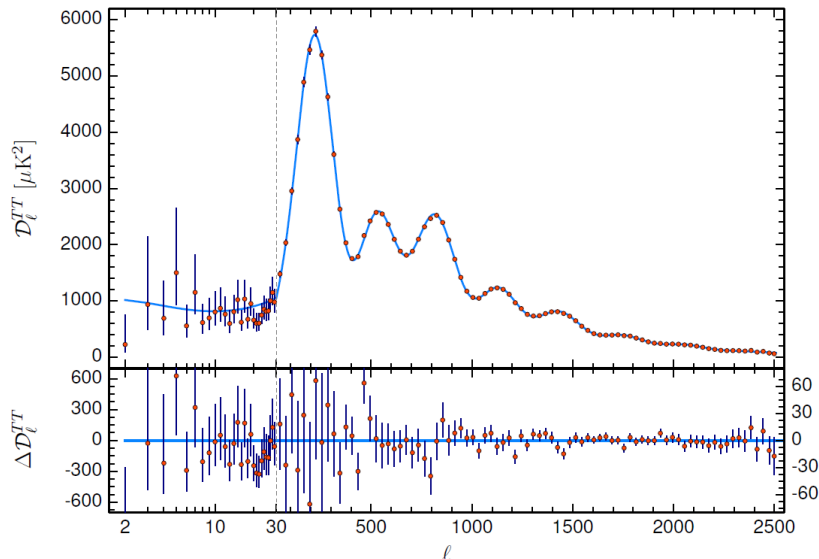


Figure 2.3: CMB angular power spectrum (top) and its residual (bottom).

For small angular scales, as the perturbations evolve, the computation of its multipole moments C_ℓ is a lot more troublesome, and we must resort to the computation of the transfer functions [123, 104], that, as the name suggests, will transport the functional form of the power spectrum from re-entry to observation today. Making such computations, we note the presence of peaks in $\ell(\ell+1)C_\ell$, the so-called acoustic peaks. As previously mentioned, the determination of cosmological parameters is possible from the analysis of these acoustic peaks. For example, the determination of the spectral index n_s makes use of the ratio between the heights of peaks number 3 (in ℓ_3) and number 1 (ℓ_1), $q \equiv h_3/h_1$:

$$\frac{\Delta q}{q} \approx 1 - \left(\frac{l_3}{l_1}\right)^{1-n_s} \approx (n_s - 1) \log\left(\frac{l_3}{l_1}\right) \quad (2.101)$$

Above, we considered only the scalar density fluctuation. However, tensor perturbations can leave their imprints on the CMB as well, otherwise, it would not be possible to determine some of the previously mentioned observables, such as r and n_T .

¹¹The function $\ell(\ell+1)C_\ell$ is of order square of temperature fluctuations

Primordial Gravitational Waves

Tensor perturbations are a lot harder to detect on the CMB power spectrum. Their influence on the temperature fluctuations is a lot dimmer than the scalar contribution, and in addition, they rapidly decrease with ℓ , therefore being hard to separate from other cosmological effects. The most likely first detection of primordial gravitational waves is the detection of primordial B-mode polarization in the CMB, despite recent advancements in stochastic gravitational wave detection theory.

The CMB has two modes of polarization, E and B , generated by Thomson scattering. The scalar perturbations do not generate B modes, while tensor perturbations do. Foreground gravitational lensing from the LSS can generate B modes from E ones, and therefore such an effect has to be completely taken into account in the de-lensing of the CMB (when the lensing effects are removed from the data). As the only source left for CMB polarization would come from recombination events, the detection of B modes would provide evidence of primordial gravitational waves.

Unfortunately, the polarization signal is weak (about 1% of the temperature fluctuations at large angular scales). In addition, the B modes represent only a small fraction of this signal to most of the inflationary and bouncing models. Other obstacles to observations come from the process of filtering the signal, identifying the background (as the failed detection by BICEP2 in 2014), and any other effects.

Due to the lack of detection of B modes that surveys like Planck can only establish upper limits to the values of the tensor-related observables r e n_T . After the filtering of the data, and having its statistics determined, we can compute what would be the highest possible value for r so that no signal from B modes could have been detected.

2.4.2 Non-Gaussianities

In our work, we have considered that every field and its fluctuations are Gaussian in nature. Any non-Gaussianity arises from a non-linear relationship between the field fluctuations and the curvature perturbation production. Therefore, it is not necessary to go to second order in the metric fluctuations in (2.2). The full analysis of higher-order perturbation theory can be found in Ref. [124]. In this section we summarize the main results, that are necessary for our work.

The non-Gaussianities in the CMB anisotropies are described by higher-order correlation functions. Contrary to Gaussian distributions, which in cosmology are completely described only by their variance, non-Gaussian distributions can be defined by an arbitrary number of free parameters.

All primordial universe models and scenarios predict deviation from Gaussianity for cosmological perturbations. The predictions can range from small values, as in single-field slow-inflation [125], to larger results, as in most multi-field and other less orthodox models. The measure of non-Gaussianities is of particular interest if the early universe physics result in a small and undetectable primordial gravitational waves signal. That is common for low energy scale models, as the curvaton scenario 4.3.1. Contrary to GW, the amplitude of non-Gaussianities does not reduce with scale. Hence, the search for non-Gaussianities is crucial for the study of the early universe.

The Bispectrum

Moving beyond the two-point correlation function and its associated power spectrum, the bispectrum B_ζ is the lowest order statistical function that distinguishes Gaussian and non-Gaussian distributions. It is defined the Fourier transform of the three-point correlation function, as ¹²

$$\langle \hat{\zeta}_{\mathbf{k}_1} \hat{\zeta}_{\mathbf{k}_2} \hat{\zeta}_{\mathbf{k}_3} \rangle = (2\pi)^3 \delta^3(\mathbf{k}_1 + \mathbf{k}_2 + \mathbf{k}_3) B_\zeta(k_1, k_2, k_3), \quad (2.102)$$

where we have assumed statistical homogeneity and isotropy. The bispectrum depends only on the magnitudes of the \vec{k}_i wave-vectors due to rotational invariance (statistical isotropy). Besides its amplitude, the bispectrum provides information about the relationship between the wave-vectors. That is commonly represented by the shape $S(k_1, k_2, k_3)$, a dimensionless function,

$$B_\zeta(k_1, k_2, k_3) \equiv \frac{S(k_1, k_2, k_3)}{(k_1 k_2 k_3)^2} \mathcal{P}_\zeta \quad (2.103)$$

Taking k_1 as reference, and keeping the total momentum $K = \frac{1}{3}(k_1 + k_2 + k_3)$ fixed, the

¹²In this section we work with ζ , the curvature perturbation on uniform density slices, which equals \mathcal{R} are super-horizon scales.

relationship between ratios $x_2 = k_2/k_1$ and $x_3 = k_3/k_1$ gives the type of the bispectrum shape. When $x_2 \gg x_3$, the bispectrum is in the squeezed shape. For $x_2 \approx x_3 \approx 1$ the bispectrum is in the Equilateral Shape. The orthogonal shape, as suggested by its name, has been designed to be orthogonal to the equilateral. These three types of shape are the most common to be analyzed, as they have been by the Planck collaboration [52]. In addition, there exists the so-called Folded configuration, when $x_2 \approx x_3 < 1$.

The most important shape for early universe physics is the squeezed one. As it was shown by Creminelli and Zaldarriaga [125], single-field slow-roll inflation predicts a small squeezed non-Gaussian signal, suppressed by the spectral index. Thus, if observations show any order unity value for the squeezed signal, then single-field inflation as we understand is ruled out. Other types of inflationary models predict different shapes for the non-Gaussianities, and measurement of high values for those shapes would too rule out single-field slow-roll models.

Local Non-Gaussianity

In real space, using the Bardeen potential Φ and its Gaussian component Φ_g , the first-ever parametrization of non-Gaussianity [126] is

$$\Phi(\vec{x}) = \Phi_g(\vec{x}) + f_{\text{NL}}^{\text{local}} \left[\Phi_g(\vec{x})^2 - \langle \Phi_g(\vec{x})^2 \rangle \right] \quad (2.104)$$

As this definition is local in real space, this has been called the local non-Gaussianity. The local non-linearity parameter $f_{\text{NL}}^{\text{local}}$ provides the amplitude of the non-Gaussianity. In terms of the curvature perturbation ζ , related to Φ during matter domination via $\Phi = \frac{3}{5}\zeta$ we have

$$\zeta(\vec{x}) = \zeta_g(\vec{x}) + \frac{3}{5} f_{\text{NL}}^{\text{local}} \left[\zeta_g(\vec{x})^2 - \langle \zeta_g(\vec{x})^2 \rangle \right] \quad (2.105)$$

The variance is constant and is only added in order for the expectation value of ζ to be zero. It is irrelevant for all modes besides $k = 0$, hence it is neglected in most cases, as in the present work. It also applies for the higher-order correlation functions.

For the local shape of the bispectrum, we have

$$B_{\zeta}(k_1, k_2, k_3) = \frac{6}{5} f_{\text{NL}}^{\text{local}} \frac{\mathcal{P}_{\zeta}}{(k_1 k_2 k_3)^3} \left(\frac{k_1^2}{k_2 k_3} + \frac{k_2^2}{k_1 k_3} + \frac{k_3^2}{k_1 k_2} \right) \quad (2.106)$$

$$= \frac{6}{5} f_{\text{NL}}^{\text{local}} [P_{\zeta}(k_1)P_{\zeta}(k_2) + P_{\zeta}(k_2)P_{\zeta}(k_3) + P_{\zeta}(k_1)P_{\zeta}(k_3)] \quad (2.107)$$

We will show that the δN formalism, presented in the next section, allows for quick computation of the nonlinearity parameter $f_{\text{NL}}^{\text{local}}$. In our work, we only local non-Gaussianity in the squeezed shape. That is the shape with the largest amplitude in the curvaton scenario of inflation. Therefore, for simplicity, we define $f_{\text{NL}}^{\text{local}} \equiv f_{\text{NL}}$. Another advantage of the local shape is that gravitational interactions during structure formation do not generate a squeezed signal. Therefore, the measurement of local f_{NL} indicates primordial origin. The other bispectrum shapes are not analyzed in our work.

We recommend the references [123, 124, 127] for a didactic demonstration of the properties of other non-Gaussianity shapes, and references [128, 129, 130, 131] for future observational perspectives.

The Trispectrum

Similarly to what has been developed for the three-point correlation function, the four-point correlation function can be described by its power spectrum, this time called the trispectrum

$$\langle \hat{\zeta}_{\mathbf{k}_2} \hat{\zeta}_{\mathbf{k}_2} \hat{\zeta}_{\mathbf{k}_3} \hat{\zeta}_{\mathbf{k}_4} \rangle_c = (2\pi)^3 \delta^3(\mathbf{k}_1 + \mathbf{k}_2 + \mathbf{k}_3 + \mathbf{k}_4) T_{\zeta}(k_1, k_2, k_3, k_4), \quad (2.108)$$

where the subscript 'c' indicates that we are dealing with the connected part¹³ of the four-point function.

When we expand the curvature perturbation up to third order, we make use of the g_{NL} parameter

¹³The connected part of a correlation function is defined as the part that cannot be re-expressed as a product of lower order expectation values. In regards to the trispectrum, the connected part of the four-point correlation function is the only part which cannot be expressed as a product of two-point correlation functions [124].

$$\zeta(\vec{x}) = \zeta_g + \frac{3}{5}f_{\text{NL}}\zeta_g^2 + \frac{9}{25}g_{\text{NL}}\zeta_g^3 + \dots \quad (2.109)$$

Then, computing the trispectrum as a function of f_{NL} and g_{NL} ,

$$T_\zeta(k_1, k_2, k_3, k_4) = \tau_{\text{NL}} [P_\zeta(|\mathbf{k}_1 + \mathbf{k}_3|) P_\zeta(k_3) P_\zeta(k_4) + 11 \text{ perms.}] + \frac{54}{25}g_{\text{NL}} [P(k_2)P(k_3)P(k_4) + 3 \text{ perms.}] \quad (2.110)$$

$$\tau_{\text{NL}} \equiv \frac{36}{25}f_{\text{NL}}^2 \quad (2.111)$$

where in the last line we defined the τ_{NL} parameter for the single-source case ¹⁴.

2.4.3 δN formalism

The δN formalism was first developed by Starobinsky [133] and Salopek & Bond [134], and later reintroduced by Sasaki & Stewart in Ref. [135]. It generalizes the derivation of the curvature perturbations during inflation for any number of dynamical degrees of freedom. Hence, it is a useful tool for multi-field models. As we show below, it allows for the computation of the curvature perturbation using only the background value of inflationary fields. It also simplifies the computation of higher-order correlations of functions, such as the non-linearity parameters mentioned in the previous section.

The rate of expansion $\tilde{\theta}$ with respect to coordinate time is defined, at super-horizon scales (where $k^2 \ll 1$), as

$$\frac{1}{3}\tilde{\theta} = H + \dot{\psi} \quad (2.112)$$

For an integral curve $\gamma(\tau)$ connecting two hypersurfaces $\Sigma(t_1)$ and $\Sigma(t_2)$, we define \mathcal{N} as

¹⁴In case more than one field contributes to the curvature perturbations, it is possible that τ_{NL} breaks the Suyama-Yamaguchi inequality [132] so that (2.111) no longer holds.

$$\mathcal{N} = \int_{\gamma(\tau)} \frac{1}{3} \tilde{\theta} \quad (2.113)$$

Hence, integrating (2.112) along $\gamma(\tau)$ results in

$$\Delta\psi = \mathcal{N} - N = \delta N \quad (2.114)$$

For inflation, we take the initial time t_1 to be the horizon crossing time of the wave-number k , and the time t_2 the given time t we want to compute the curvature perturbation, still at super-horizon scales. In case we take the initial hypersurface at t_1 to be flat, and at t_2 to be comoving, it means that

$$\psi_{com.} = \mathcal{R} = \delta N \quad (2.115)$$

The function \mathcal{N} can be regarded as dependent on the values of the fields at the first hypersurface $\Sigma(t_1)$ and on the time t_2 , as we can simply evolve the fields from t_1 to t_2 using their equations of motion.

Therefore, we can write the curvature perturbation as

$$\mathcal{R} = \delta N = \frac{\partial N}{\partial \phi^a} \delta \phi_{flat}^a(t_1, \mathbf{x}) \quad (2.116)$$

where ϕ_{flat}^a is the a^{th} field background value at the flat hypersurface in t_1 . An alternative derivation of this result can be found in [111], where they present for the first time the Separate Universe Approach to the computation of cosmological perturbations.

In [136], eq. (2.116) is generalized for higher-order perturbations by simply adding quadratic terms on $\delta\phi^a$, under the condition that the fields' perturbations are sufficiently Gaussian. That was later extended to any order, as in a Taylor expansion [137],

$$\mathcal{R} = N_a \delta \phi^a + \frac{1}{2} N_{ab} \phi^a \phi^b + \frac{1}{6} N_{abc} \phi^a \phi^b \phi^c + \dots \quad (2.117)$$

where N_i denotes the derivative of N with respect to ϕ^i , N_{ij} denotes the derivative of N with respect to ϕ^i and ϕ^j , and so on. From now on, we will extrapolate Einstein's summation convention, such that every repeated roman letter works means a sum, even when they are both subscripts.

For the power spectrum at horizon crossing, assuming almost Gaussian fluctuations for the light fields ϕ^i in a quasi de Sitter ¹⁵, we have

$$\mathcal{P}_{\delta\phi_i} = \left(\frac{H_*}{2\pi} \right)^2 \quad (2.118)$$

Using the δN expansion, we can then compute the total curvature power spectrum as

$$\mathcal{P}_{\mathcal{R}} = \left(\frac{H_*}{2\pi} \right)^2 N_a^2 \quad (2.119)$$

For higher order perturbations and the non-linearity parameters, for any number of fields, the use of (2.117) leads to [136, 127]

$$B_\zeta(k_1, k_2, k_3) = \frac{N_{ab} N_a N_b}{(N_c N_c)^2} [P(k_1)P(k_2) + 2 \text{ perms.}] \quad (2.120)$$

$$\begin{aligned} T_\zeta(k_1, k_2, k_3, k_4) &= \frac{N_b N_c N_{ab} N_{ac}}{(N_d N_d N_d)^3} [P_\zeta(|\mathbf{k}_1 + \mathbf{k}_3|) P_\zeta(k_3) P_\zeta(k_4) + 11 \text{ perms.}] + \\ &+ \frac{N_a N_b N_c N_{abc}}{(N_d N_d N_d)^3} [P(k_2)P(k_3)P(k_4) + 2 \text{ perms.}] \end{aligned} \quad (2.121)$$

Consequently, we have

¹⁵Or quasi-matter dominated contracting universe, as both of these types of expansion lead to an almost-flat spectrum

$$f_{\text{NL}} = \frac{5 N_a N_b N_{ab}}{6 (N_c N_c)^2} \quad (2.122)$$

$$g_{\text{NL}} = \frac{25 N_a N_b N_c N_{abc}}{54 (N_d N_d N_d)^3} \quad (2.123)$$

$$\tau_{\text{NL}} = \frac{N_b N_c N_{ab} N_{ac}}{(N_d N_d N_d)^3} \quad (2.124)$$

The δN formalism is an extremely powerful tool for computing curvature perturbations in a multi-field model. To be possible to make such a computation knowing only the background value of the fields greatly simplifies the calculations. In 4.4.3, we see that the formalism, when applied to the Curvaton model, allows us to compute all relevant quantities with respect to the curvaton field value at the onset of its oscillations.

2.4.4 Current Observational Results

The latest Planck results [92, 19, 29], in combination with other probes, strengthens the case for the Λ CDM model and provide accurate information on the cosmological parameters. The 6 parameters that define the Λ CDM model, alongside model-dependent cosmological quantities, have been measured by collaboration and are listed on the Table 2.1 below,

It is worth noting that there are reasonable discrepancies concerning the values of H_0 and σ_8 between the early-times CMB observations by the Planck satellite and the late-times probes by H0LiCOW [138], SH0es [139], KiDS [140] teams. The so-called H_0 -tension has been extensively analyzed over the decade [141, 142, 143], but it escapes the scope of the present thesis. The same goes for the σ_8 -tension [144, 145].

In regards to cosmological perturbations, the combined observations from Planck result in a spectral index of $n_s = 0.9649 \pm 0.0042$. The tensor-to-scalar ratio has an upper limit of $r < 0.101$ for Planck only observations, but when combined with BICEP2/Keck Array BK14 data such a limit is tightened to $r < 0.064$ [29].

It has been observed that the primordial density perturbations are consistent with Gaussian curvature perturbations. Primordial non-Gaussianities have not yet been detected, but there are constraints for all types of shapes. Most importantly, the local shape is constrained to be $f_{\text{NL}}^{\text{local}} = -0.9 \pm 5.1$ to 68% confidence level [52]. For other relevant

Table 2.1: First, the measured confidence limits for the 6 parameters from the Λ CDM model. The second section of the table contains derived quantities, such as the Hubble parameter today, H_0 . Taken from [19].

| Parameter | Planck alone | Planck + BAO |
|--|-------------------------|-------------------------|
| $\Omega_b h^2$ | 0.02237 ± 0.00015 | 0.02242 ± 0.00014 |
| $\Omega_c h^2$ | 0.1200 ± 0.0012 | 0.11933 ± 0.00091 |
| $100\theta_{\text{MC}}$ | 1.04092 ± 0.00031 | 1.04101 ± 0.00029 |
| τ | 0.0544 ± 0.0073 | 0.0561 ± 0.0071 |
| $\ln(10^{10} A_s)$ | 3.044 ± 0.014 | 3.047 ± 0.014 |
| n_s | 0.9649 ± 0.0042 | 0.9665 ± 0.0038 |
| H_0 | 67.36 ± 0.54 | 67.66 ± 0.42 |
| Ω_Λ | 0.6847 ± 0.0073 | 0.6889 ± 0.0056 |
| Ω_m | 0.3153 ± 0.0073 | 0.3111 ± 0.0056 |
| $\Omega_m h^2$ | 0.1430 ± 0.0011 | 0.14240 ± 0.00087 |
| $\Omega_m h^3$ | 0.09633 ± 0.00030 | 0.09635 ± 0.00030 |
| σ_8 | 0.8111 ± 0.0060 | 0.8102 ± 0.0060 |
| $\sigma_8(\Omega_m/0.3)^{0.5}$ | 0.832 ± 0.013 | 0.825 ± 0.011 |
| z_{re} | 7.67 ± 0.73 | 7.82 ± 0.71 |
| Age[Gyr] | 13.797 ± 0.023 | 13.787 ± 0.020 |
| r_* [Mpc] | 144.43 ± 0.26 | 144.57 ± 0.22 |
| $100\theta_*$ | 1.04110 ± 0.00031 | 1.04119 ± 0.00029 |
| r_{drag} [Mpc] | 147.09 ± 0.26 | 147.57 ± 0.22 |
| z_{eq} | 3402 ± 26 | 3387 ± 21 |
| k_{eq} [Mpc $^{-1}$] | 0.010384 ± 0.000081 | 0.010339 ± 0.000063 |
| Ω_K | -0.0096 ± 0.0061 | 0.0007 ± 0.0019 |
| Σm_ν [eV] | < 0.241 | < 0.120 |
| N_{eff} | $2.89^{+0.36}_{-0.38}$ | $2.99^{+0.34}_{-0.33}$ |
| $r_{0.002}$ | < 0.101 | < 0.106 |

shapes, the Planck collaboration was consistent with Gaussian statistics too, but the error bars are still large due to the difficulty to clean the data, non-linearity due to structure formation, etc. The value for the equilateral shape is $f_{\text{NL}}^{\text{equil.}} = -26 \pm 47$, while for the orthogonal shape it is $f_{\text{NL}}^{\text{ortho.}} = -30 \pm 24$, to 68% CL too. As for the trispectrum, the Planck results for the g_{NL} parameter was $g_{\text{NL}} = (-5.8 \pm 6.5) \times 10^4$ (68% CL). For more information about the data collection, cleaning and analysis, we recommend the original Planck team paper [52].

2.4.5 Cosmological Perturbations for Inflation

The slow-roll parameters can be used to rewrite the cosmological observables and how they depend on the number of e-folds ¹⁶. All quantities are being computed at horizon crossing, $k = k_* = aH$. From (1.32), (2.85) and (2.88):

$$\mathcal{P}_{\mathcal{R}} = \frac{1}{8\pi^2} \frac{H^2}{M_{\text{Pl}}^2} \frac{1}{\epsilon_1} \quad (2.125)$$

$$\mathcal{P}_T = \frac{2}{\pi^2} \frac{H^2}{M_{\text{Pl}}^2} \quad (2.126)$$

It is straightforward to obtain the tensor-to-scalar ratio in terms of the HSRP,

$$r = \frac{\mathcal{P}_T}{\mathcal{P}_{\mathcal{R}}} = 16\epsilon_1 \quad (2.127)$$

To the spectral indexes, we start from (2.86) and (2.89), then we apply the above results (2.125) and (2.126).

¹⁶The full derivation of these expressions, in special the use of the Hubble Slow-Roll Parameters can be found in [95, 123].

$$n_{\mathcal{R}} - 1 = \frac{d \log \mathcal{P}_{\mathcal{R}}}{d \log k} = \frac{d \log \mathcal{P}_{\mathcal{R}}}{dN} \frac{dN}{d \log k} \quad (2.128)$$

$$= (-2\epsilon_1 - 2(\epsilon_1 - \eta_H))(1 + \epsilon_1) \quad (2.129)$$

$$\simeq 2\eta_H - 4\epsilon_1 \quad (2.130)$$

$$n_T = \frac{d \log \mathcal{P}_T}{d \log k} = \frac{d \log \mathcal{P}_T}{dN} \frac{dN}{d \log k} \quad (2.131)$$

$$= -2\epsilon_1(1 + \epsilon_1) \quad (2.132)$$

$$\simeq -2\epsilon_1 \quad (2.133)$$

Similarly, one can express these observables in terms of the Potential Slow-Roll Parameters. Thanks to these expressions, we only need the inflaton potential in order to obtain the observational predictions from the respective inflationary model.

$$n_{\mathcal{R}} - 1 = 2\eta_v - 6\epsilon_v \quad (2.134)$$

$$n_T = -2\epsilon_v \quad (2.135)$$

$$r = 16\epsilon_v \quad (2.136)$$

As it should be, in the de Sitter limit the slow-roll parameters are null and the spectral indexes show scale invariance.

Example: $m^2\varphi^2$ inflation

The first developed chaotic inflationary model was the quadratic potential $V(\varphi) = m^2\varphi^2/2$. Its PSRP and number of e-folds are

$$\epsilon_v(\varphi) = \eta_v(\varphi) = 2 \left(\frac{M_{\text{Pl}}^2}{\varphi} \right)^2 \quad (2.137)$$

$$N(\varphi) = \frac{\varphi^2}{4M_{\text{Pl}}^2} - \frac{1}{2} \quad (2.138)$$

The number of e-folds related to the production of the largest scales in the CMB is around $N_{\text{CMB}} \approx 60$. In this case, the inflaton field value is approximately $15M_{\text{Pl}}$. Hence,

its PSRPs and predicted value for observables can be written as

$$\epsilon_v = \eta_v = \frac{1}{2N} \quad (2.139)$$

$$n_R = 1 - \frac{2}{N} \quad (2.140)$$

$$r = \frac{8}{N} \quad (2.141)$$

Once again using $N_{CMB} \approx 60$, we obtain $n_R \simeq 0.96$ for the spectral index and $r \simeq 0.1$ for the tensor-to-scalar ratio. Despite the spectral index being close to the value obtained by the Planck collaboration [29], the prediction for the gravitational waves surpasses the upper value for r . Chaotic inflationary models are disfavored with respect to current observations at 95% confidence value [146]. See 2.4 below, taken from [29].

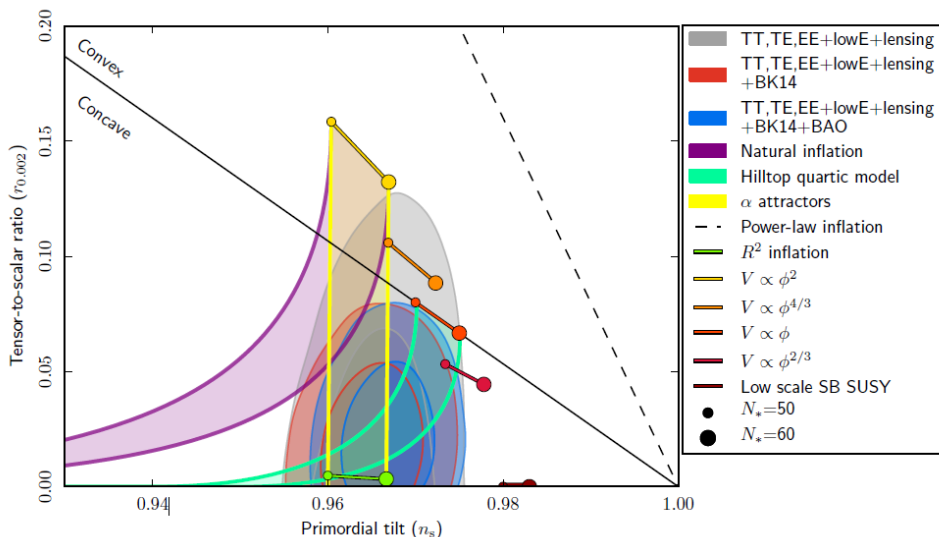


Figure 2.4: 68% and 95% confidence levels for n_s and r from the combination of Planck, BICEP2/Keck Array and BAO results, in comparison to theoretical predictions from different inflationary models.

2.4.6 Cosmological Perturbations for Bouncing Cosmologies

Cosmological perturbations in bouncing cosmologies depend more on the background evolution than in the inflationary scenario. The reasons are various. As we explain in the end of this section, the background contraction is required to be dominated by dust-like matter ($\omega \approx 0$). In this case, one mode of the perturbations grows – according to a

function that depends on the background scale factor – while the other mode is constant. Then, during the bounce, the modes mix, and the mixing depends on the background evolution too. Not only that, but the amplitude of both modes also drastically increase during contraction and during the bounce phase. Hence, the dynamics of the bounce phase contribute to the perturbations as well. After the bounce, the dominant mode has the same scale-dependence as the previous constant mode. However, its amplitude carries contributions from both modes due to the mixing. During inflation there is no mode mixing. One of the modes decays, while the dominant mode is constant. We elaborate on these subtleties in Sec. 3.6, in particular when analyzing the bounce in the Loop Quantum Cosmology scenario, while in Sec. 5.2 we will present the de Broglie-Bohm quantum cosmology case.

However, there are some general features, such as the spectral index of the perturbations for both scalar and tensor modes. For the cosmologically relevant wave-lengths, the horizon exit and horizon re-entry happen during a completely classical regime, where GR is valid. These modes do not leave the horizon during the bounce phase, where quantum gravity effects are relevant.

A background evolution with equation of state $p = \omega\rho$ leads to a power-law contraction in the far past

$$a(t) \propto t^{\frac{2}{3(1+\omega)}} \quad (2.142)$$

In de Broglie-Bohm Cosmology, computing the modified Mukhanov-Sasaki equations leads to both scalar and tensor perturbations to have the same spectral index

$$n_s - 1 = n_T = \frac{12\omega}{1 + 3\omega} \quad (2.143)$$

The same happens for a classical contraction dominated by a matter-like field, albeit without a ω dependence on the denominator [64]. As we are going to further elaborate in Section 3.3, this means that a quasi-matter-dominated contraction, which has $\omega \approx 0$, leads to an almost scale-invariant spectrum just like an quasi-de Sitter inflationary expansion. However, it is important to note that the red-tilt of the scalar perturbations do now allow

baryonic or dark matter to dominate the background contraction, as they do not allow $\omega \leq 0$, a required condition for negative spectral index – i.e. a red-tilted spectrum. Other pre-big-bang cosmologies predict different spectra, such as some string-related cosmologies [16, 147]. Concerning the computation of the tensor-to-scalar ratio, as it represents the ratio between amplitudes, one needs further knowledge about the origin of perturbations and the background evolution until horizon entry at CMB scales.

Chapter 3

Starobinsky-like Bouncing Model

This chapter aims to construct a bounce equivalent to the Starobinsky model of inflation. First, we introduce the model and highlight its strengths. Next, we revise the Wands' duality. We then re-parametrize the Starobinsky inflationary model and apply the Wands' duality to it. Then, the resulting contracting universe is constructed, followed by a bouncing connecting it to an expanding phase. Finally, we compute the scalar and tensor perturbations throughout the whole evolution, including across the bounce. The chapter is based on our work Ref. [148].

3.1 Introduction

$f(R)$ theories have many applications in cosmology [149]. In the years that followed the publication of General Relativity, many shortcomings of the theory were discovered, as the existence of curvature singularities. There are also more recent developments, such as cosmic acceleration, the existence of Dark Matter, and the modeling of early universe physics – be it with an inflationary or bouncing scenario. Despite the success of the Λ CDM model, that year by year improves its matching to observations [92], there are still alternate models to explain the previously mentioned phenomena.

Dark Matter [150], Dark Energy and current cosmic acceleration [151, 152] can be discussed in the context of $f(R)$ theories. It is worth noting that $f(R)$ gravity is equivalent to Brans-Dicke theories, which are scalar-tensor theories¹. Both make part of the so-called Horndeski theories, that generalize many of the possible GR extensions – it comprehends

¹This makes it clear that there is an additional scalar degree of freedom to $f(R)$ theories, as previously mentioned.

all models that are second-order in the equations of motion [153, 154].

However, it is in the inflationary paradigm that $f(R)$ theories find their great success, in the form of the Starobinsky inflation [2]. The non-singular cosmological setting, desired by Starobinsky, was not obtained, but the de Sitter-type universe used for it proved to be useful. The resulting inflationary phase from the $f(R)$ Starobinsky model is currently the best-fit model to cosmological perturbations in the CMB [31]. That is why we decided to use such a model to analyze single-field inflation.

In case an inflationary model fits well to observations, does it make it the unique model to explain such results? Could there be a primordial universe model that not only solves the HBB problems but predicts the same observational results as such an inflationary model? It is for such inquiries that the Wands' duality becomes important [63]. Thanks to a symmetry in the equations of motion for cosmological perturbations, as we demonstrate next, it is possible to show the observational equivalence between inflationary and quasi-matter domination contraction models.

This chapter presents the procedure we developed to obtain a contracting universe from the Starobinsky model of inflation. An extra modification of the Starobinsky model is necessary, and we explain its phenomenological reasoning and construction. We revise Wands duality and make brief comments about the mapping between primordial universe models. Using the duality and the Loop Quantum Cosmology scenario, a Starobinsky-like bouncing model is built. Finally, we compute the scalar and tensor perturbations for such a model and compare them with the original Starobinsky inflation.

3.2 Starobinsky Inflation

The generalized action for $f(R)$ theories, with no coupled scalar field, can be written as

$$S = \frac{1}{2\kappa^2} \int d^4x \sqrt{-g} f(R) + \int d^4x \mathcal{L}_M(g_{\mu\nu}, \Psi_M), \quad (3.1)$$

where the second term represents the matter content, which depends on the metric and the matter fields. From the trace of the equation of motion obtained from the varying of (3.1) with respect to the metric, we get

$$F(R)R_{\mu\nu} - \frac{1}{2}f(R) - \nabla_\mu \nabla_\nu F(R) + g_{\mu\nu} \square F(R) = \kappa^2 T_{\mu\nu} \quad (3.2)$$

$$3\square F(R) + F(R)R - 2f(R) = \kappa T, \quad (3.3)$$

where $F(R) = \partial f(R)/\partial R$.

There is a the Sitter solution exists for the vacuum ($T = 0$) and constant R . Therefore, equation (3.3) becomes

$$F(R)R - 2f(R) = 0 \quad (3.4)$$

Justifying the above, $f(R) = \alpha R^2$ satisfies equation (3.4), and it is its solution (beyond that one, there is the trivial one $R = 0$). From the equations of motion ² we conclude that, for an exact de Sitter solution to exist, with no matter, it is necessary that $f(R) = \alpha R^2$ [117].

As previously explained, the exact de Sitter solution is not the best for inflation, as it does not allow for a transition to the current FLRW universe – a so-called graceful exit. That is not a problem for the Starobinsky model, since the linear term on R , which describes GR, is not absent from the model. Such term dominates for smaller values of R , leading to the end of the inflationary regime, such that a graceful exit is present by default.

However, the model has not been built in an attempt to describe inflation and its graceful exit. The primary objective of the work was to study General Relativity modifications thanks to one-loop corrections in the matter fields, and check if such a universe could be non-singular [2]. The conclusion was that the singularity could not be evaded, but the de Sitter regime being used was confirmed to be possible to exist, given the previously established modifications.

Therefore, we transfer the role of modifying the Einstein equations from the matter fields to the functional form of the Einstein-Hilbert action, obtaining the already mentioned term αR^2 . For the Starobinsky inflation, we then have

²The equations of motion are obtained in the metric formalism, which differs from the Palatini approach.

$$f(R) = R + \frac{R^2}{6M^2} \quad (3.5)$$

In order to obtain the relevant cosmological quantities, such as the evolution of the scale factor, the Hubble function, and so on, we leave the necessary computations to the references [94, 2].

It is necessary to mention that the Starobinsky inflation can be described both in the Jordan and Einstein frames. In the former, the theory is described by the action (3.1), while for the latter inflation can be understood as being realized by a scalar field minimally coupled to gravity. Reference [94] solves the background through the Einstein frame, due to the possibility of treating every single scalar field model in a general manner. In this work, though, we focus on the Jordan frame approach ³.

Therefore, for the scale factor we have

$$a(t)_{R^2} = a_0 (t_s - t)^{1/2} \exp \left[-\frac{M^2}{12} (t_s - t)^2 \right] \quad (3.6)$$

where t_s defines the inflationary scale – the end of inflation on time $t \sim t_s$ – and $(t_s - t)$ is big, because $t_s \gg t$ [155]. The a_0 parameter is a constant of integration related to the size of the universe during inflation. The scale factor 3.6 makes it clear that inflation takes place in a quasi-de Sitter regime, as the exact case would consist of a purely exponential function.

Other relevant quantities, that will be used later for the phenomenology of cosmological perturbations in Starobinsky inflation, are the Hubble function and its temporal derivative

$$H_{R^2} = \frac{-3 + M^2 (t_s - t)^2}{6 (t_s - t)} \quad (3.7)$$

$$\dot{H}_{R^2} = \frac{1}{2 (t_s - t)^2} - \frac{M^2}{6} \quad (3.8)$$

The above quantities allow for the calculus of the first slow-roll parameter, ϵ_1 ,

³Inflation can be treated in both frames due to the preservation of the curvature invariants [104], despite the fact that physical quantities are only well defined in the Jordan frame [117]. The discussion about the reference frames is extensive in the literature, see [155].

$$\epsilon_{h,R^2} = \frac{6 \left(3 + M^2 (t_s - t)^2 \right)}{\left(3 - M^2 (t_s - t)^2 \right)^2} \quad (3.9)$$

$$\simeq \frac{M^2}{6H^2} \quad (3.10)$$

During inflation we need $\epsilon_1 \ll 1$, therefore we conclude that for the regime to start we need $H^2 \gg M^2$.

It is also possible to obtain the equation that describes the temporal evolution of the curvature R ,

$$\ddot{R} + 3H\dot{R} + M^2R = 0 \quad (3.11)$$

$$R \simeq 12H^2 - M^2 \quad (3.12)$$

We remind once again that R^2 does not dominate the action when inflation ends. Using the previous result, that $H^2 \gg M^2$ for the start of inflation, we can approximate that $R \simeq 12H^2$. For the initial values above we can also approximate that

$$H_{R^2} \simeq \frac{M^2}{6} (t_s - t) \quad (3.13)$$

$$\dot{H}_{R^2} \simeq -\frac{M^2}{6} \quad (3.14)$$

When one goes beyond leading order in the slow-roll approximation, as done in Ref. [156], the solution for evolution for the inflationary background changes. The observational differences between the above and the below results will be negligible, as we later prove. Hence,

$$a(t)_{BSR} = a_0 (t_s - t)^{-1/6} \exp \left[-\frac{M^2}{12} (t_s - t)^2 \right] \quad (3.15)$$

$$H_{BSR} = \frac{1 + M^2 (t_s - t)^2}{6 (t_s - t)} \quad (3.16)$$

$$\dot{H}_{BSR} = \frac{1}{6 (t_s - t)^2} - \frac{M^2}{6} \quad (3.17)$$

where the subscript *BSR* indicates the quantities in the beyond-slow-roll approximation.

We note the same behavior for the beginning of the inflationary regime in both models: the exponential is dominant in such case, and for the scale factors of both the exponent is the same. The only difference between them is the polynomial multiplying the exponential, which lightly modifies the dynamics. Thanks to that the regime is of quasi-de Sitter. The same reasoning will allow us to modify the power of the polynomial, a requirement for our reconstruction procedure later in this chapter.

For completeness, we also present the inflationary background evolution in the Einstein Frame. Given the correct conformal transformation, we can also obtain the potential for the scalar field – the "inflaton" for the Einstein frame. It is of 'plateau'-type, as inflation takes place when the inflaton evolves along the extremely flat plateau in its potential.

$$V(\varphi) = \frac{3M^2}{4\kappa^2} \left(1 - e^{-\sqrt{2/3}\kappa\varphi} \right)^2 \quad (3.18)$$

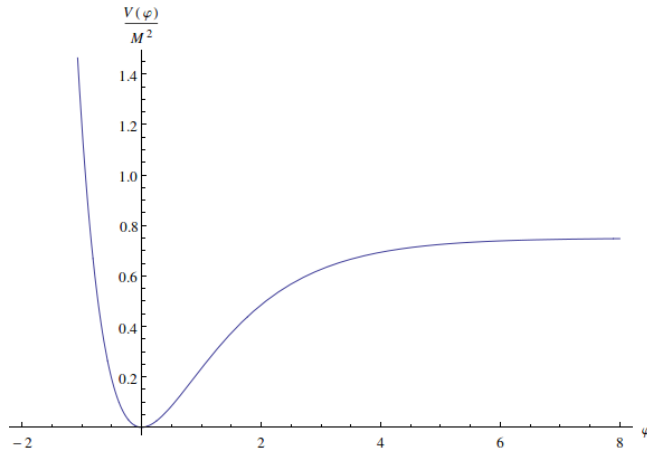


Figure 3.1: Scalar field potential for the Starobinsky inflation in the Einstein frame.

After the Starobinsky inflationary regime, there is a reheating phase, as present in other inflation models. In terms of the Einstein frame, it can be understood as a phase in which the scalar field φ oscillates around the minimum of its potential. For small field values, the Starobinsky potential (3.18) can be approximated by a quadratic term, $V = \varphi^2$.

It is interesting to note that during reheating the differences between using the Jordan and the Einstein frames are stark. The equivalence between them during inflation was valid because of the negligible difference between scalars, such as the Ricci R . However, when we compare its evolution on both frames we note a difference in how R decays with time. Details can be found in section 7.2 of the reference [94].

On the Einstein frame, we have that Starobinsky inflation is equivalent to Higgs inflation [157, 146]. Therefore, it is also favored by Planck results [158, 31]. This model, as the name suggests, uses the Standard Model Higgs as the inflaton. However, Higgs inflation does not take place when the Higgs boson is non-minimally coupled to gravity [25].

Perturbations and Phenomenology

Access to the evolution of the cosmos during inflation is made possible by observing the effects of the primordial cosmological perturbations. For an inflating universe doted with a minimally coupled scalar field, we have already detailed the perturbation theory in terms of the slow-roll parameters. However, for the case of the Starobinsky model in the Jordan frame, we need some modifications. We need to detail some additional parameters, in special due to the nonexistence of an inflaton in this gauge.

The HSRP are the same as the ones described in 2. However, we can define two more parameters, following [117],

$$\epsilon_3 = \frac{\dot{F}}{2HF} \tag{3.19}$$

$$\epsilon_4 = \frac{E}{2HE} \tag{3.20}$$

$$E = F \left[\omega + \frac{3\dot{F}^2}{2\kappa\dot{\varphi}^2 F} \right] \tag{3.21}$$

For a quasi-de Sitter regime, the spectral index can be rewritten in terms of the HSRP as [117]

$$n_{\mathcal{R}} - 1 \simeq -4\epsilon_1 - 2\eta_H + 2\epsilon_3 - 2\epsilon_4. \quad (3.22)$$

Starobinsky inflation happens for a universe without an inflaton, i. e., without any other background fluids. Thanks to that, for the beginning of inflation we have

$$F = 1 + \frac{R}{3M^2} \simeq \frac{4H^2}{M^2} \quad (3.23)$$

In the literature, it is common to rewrite the observables in terms of the number of e-folds. For the current Starobinsky inflationary background evolution (3.6), we have that

$$N_{R^2} = \int_{t_i}^{t_s} H dt = \int_{t_i}^{t_s} \frac{3 - M^2 (t_s - t)^2}{6 (t_s - t)} dt \quad (3.24)$$

$$\simeq \frac{M^2}{12} (t_s - t_i)^2 \quad (3.25)$$

For the first Hubble slow-roll parameter, ϵ_1 , we get

$$\epsilon_{R^2} = \frac{6 (3 + M^2 (t_s - t)^2)}{(3 - M^2 (t_s - t)^2)^2} \quad (3.26)$$

$$= \frac{1}{2 (t_s - t)^2 H^2} + \frac{M^2}{6H^2} \quad (3.27)$$

$$\simeq \frac{6}{M^2 (t_s - t)^2} = \frac{M^2}{6H^2} \quad (3.28)$$

Finally, applying the expressions for the Hubble slow-roll parameters above to the definition of the new ones, we get $\epsilon_3 \simeq \epsilon_4$. Additionally, $\eta_H = 0$ because there is no scalar field in this frame. Therefore we simplify the spectral index to

$$n_{\mathcal{R}} - 1 \simeq -4\epsilon_1 = -\frac{2}{N} \quad (3.29)$$

The same can be done to the tensor-to-scalar ratio

$$r \simeq 48\epsilon_3 \simeq 48\epsilon_1^2 \simeq \frac{12}{N^2} \quad (3.30)$$

For the number of e-folds required for solving the HBB model problems, $N \approx 55 \sim 60$, the spectral index matches with the most recent CMB results [158, 159], and the same is valid for the ratio r given by 3.30. The way that both quantities vary with the number of e-folds is typical for Starobinsky inflation, and it is also found for the Einstein Frame.

The equivalence between the evolution 3.15 and 3.6⁴ can also be seen from the relation between their ϵ_1 parameters.

$$\epsilon_{BSR} = \frac{6 \left(-1 + M^2 (t_s - t)^2 \right)}{\left(1 + M^2 (t_s - t)^2 \right)^2} \quad (3.31)$$

$$= \frac{-1}{6 (t_s - t)^2 H^2} + \frac{M^2}{6H^2} \quad (3.32)$$

$$\simeq \frac{M^2}{6H^2} = \epsilon_{R^2} \quad (3.33)$$

On the other hand, in the Einstein Frame the Starobinsky inflation we can use the potential slow-roll parameters from chapter 2, such that from the potential 3.18 we get

$$\epsilon_v \simeq \frac{4}{3} \left(e^{-\sqrt{2/3}\kappa\varphi} - 1 \right)^{-2} \quad (3.34)$$

$$\eta_v \simeq -\frac{4}{3} e^{-\sqrt{2/3}\kappa\varphi} \left(1 - 2e^{-\sqrt{2/3}\kappa\varphi} \right) \quad (3.35)$$

Rewriting them in terms of the number of e-folds N ,

$$N \simeq \kappa^2 \int_{\varphi_f}^{\varphi_i} \frac{V}{V_{,\varphi}} d\varphi \simeq \frac{3}{4} e^{\sqrt{2/3}\kappa\varphi} \quad (3.36)$$

$$\Rightarrow \epsilon_v \simeq \frac{3}{4N^2} \quad (3.37)$$

$$\Rightarrow \eta_v \simeq -\frac{1}{N} \quad (3.38)$$

⁴To be more precise, the equivalence under the correct approximation for the observational predictions of both expressions.

When we apply the above to the spectral index and tensor-to-scalar ratio we get

$$n_{\mathcal{R}} - 1 \simeq 2\eta_H - 6\epsilon_1 \simeq -\frac{2}{N} \quad (3.39)$$

$$r \simeq 16\epsilon_1 \simeq \frac{12}{N^2} \quad (3.40)$$

As mentioned, 3.39 is identical to 3.29, while 3.30 equals 3.40.

From the power spectrum amplitude, we can also extract the order of magnitude of M for Starobinsky inflation, which results in

$$\mathcal{P}_{\mathcal{R}} \simeq \frac{N^2}{3\pi} \left(\frac{M^2}{M_{\text{Pl}}} \right)^2 \quad (3.41)$$

$$M \simeq 15 \times 10^{-6} M_{\text{Pl}} \quad (3.42)$$

The Planck 2018 release [29] gives a spectral index of $n_{\mathcal{R}} = 0.9649 \pm 0.0042$ at 68% confidence level. This implies that $50 < N < 65$. We can recast the spectral index and the tensor-to-scalar ratio as

$$n_{\mathcal{R}} - 1 \approx -3,51 \times 10^{-2} \left(\frac{N}{57} \right)^{-1}, \quad (3.43)$$

$$r \approx 3,69 \times 10^{-3} \left(\frac{N}{57} \right)^{-2}. \quad (3.44)$$

The Planck 95% confidence level upper limit on the tensor-to-scalar ratio is $r_{0.002} < 0.10$. This value is tightened by a combining analysis with the BICEP2/Keck Array BK14 data that brings the tensor-to-scalar value down to $r_{0.002} < 0.064$. The predicted value for the Starobinsky inflation Eq. (3.44) is safely within the observational measurements.

3.3 Wands Duality

The ambiguity in regards to the origin of the cosmological perturbations power spectrum was explored by Wands and others [63, 160] at the turn of the century, and has become of great importance to the research on early universe models. Given a sensible

model-building, the quasi-matter domination scenario can be mapped into the standard inflationary models. That is the main motivation of this section of the thesis.

We can understand the Wands' duality simply as the symmetry present in the Mukhanov-Sasaki equations for cosmological perturbations. For the field fluctuations (the treatment is the same for curvature perturbations), we get

$$u_{\mathbf{k}}'' + (k^2 - \mu^2) u_{\mathbf{k}} = 0 \quad (3.45)$$

$$\mu^2 \equiv -\frac{a''}{a}, \quad (3.46)$$

where the initial conditions from chapter 2 are valid.

Generically, a universe dominated by an adiabatic perfect fluid with an equation of state given by $p = \omega \rho$ (with constant ω) has a scale factor with a power law in cosmic time of the form $a(t) \propto t^{2/3(1+\omega)}$. In terms of conformal time, the scale factor evolves as

$$a(\eta) \propto \eta^{\frac{1}{2}-\nu} \quad (3.47)$$

$$\nu = \frac{3}{2} - \frac{3(1+\omega)}{1+3\omega} \quad (3.48)$$

$$\Rightarrow \mu^2 = \frac{\nu^2 - 1/4}{\eta^2} \quad (3.49)$$

A radiation fluid has zero mass term since $a \propto \eta$ and there is no possible duality to be performed. For all other fluids, the power spectrum associated with this evolution is given by

$$\mathcal{P}_u = \frac{C^2(|\nu|)k^2(-k\eta)^{1-2|\nu|}}{4\pi^2}, \quad (3.50)$$

where $C^2(|\nu|)$ is a numerical coefficient.

Note that the above power spectrum is invariant under $\nu \rightarrow -\nu$, which can be translated into a transformation of the fluid's equation of state as

$$\omega \rightarrow \tilde{\omega} = \frac{1 + \omega}{-1 + 3\omega} \quad . \quad (3.51)$$

This transformation has two fixed points at $\omega = -\frac{1}{3}$ and 1. For these fixed points, the evolution of the linear perturbations is unequivocally determined by the background dynamics. For any other value, there are two background dynamics associated with the same perturbed dynamics. Indeed, it is straightforward to verify that two subsequent transformations return to the same equation of state, i.e. $\tilde{\tilde{\omega}} = \omega$. Therefore, in general, there is a pair of adiabatic perfect fluid background dynamics associated with the same evolution for the linear perturbations. Even though de Sitter evolution is not a power law for the scale factor, its duality transformation is still described by Eq. (3.51). As already mentioned before, a de Sitter universe, which has $\omega = -1$ is mapped into a dust-dominated universe $\omega = 0$.

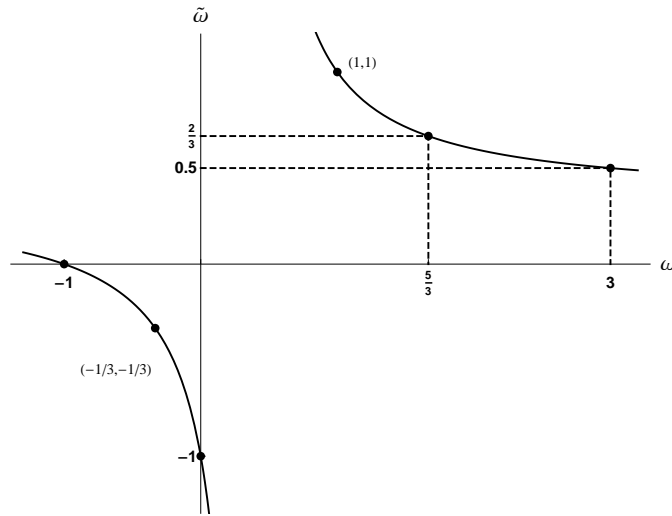


Figure 3.2: Wands' duality maps an equation of state ω into $\tilde{\omega}$. There are only two fixed points that mapped into itself given by $\omega = -\frac{1}{3}$ and 1. The solid lines represent the map according to Eq. (3.51). The dots mark conventional equation of states in cosmology such as $\omega = -1, -\frac{1}{3}, 0, 1$.

For inflation and the matter-dominated universe, this happens because the mass term in both cases is the same, $\mu^2 = 2/\eta^2$. Coincidentally that is also the mass term required for exact scale-independence for the perturbations. Therefore results in the same spectra (3.45), modulo initial conditions. For the metric, this symmetry results in

$$a(\eta) \rightarrow \tilde{a}(\eta) \equiv a_B(\eta) = Ca(\eta) \int_{\eta_*}^{\eta} \frac{d\eta'}{a^2(\eta')} \quad (3.52)$$

Therefore, the same power spectra will be found for a family of solutions to two parameters. The constant C just re-scales the metric, with no observational influence, while η_* defines a family of solutions to one parameter.

For the curvature perturbations, following the Mukhanov-Sasaki equation (2.26), the same symmetry is present

$$z(\eta) \rightarrow \tilde{z}(\eta) \equiv z_B(\eta) = Cz(\eta) \int_{\eta_*}^{\eta} \frac{d\eta'}{z^2(\eta')} \quad (3.53)$$

Therefore, for a single-field inflationary universe which has pump-field function $z(\eta)$ will be indistinguishable from a contracting universe with pump-field $z_B(\eta)$ in terms of scalar perturbations.

For tensor perturbations, the same reasoning follows, given that the Mukhanov-Sasaki equations are the same. However, it is not guaranteed that universes doted with the same scalar spectrum will present the same tensor spectrum. For the tensor perturbations, the symmetry in the Mukhanov-Sasaki equation is

$$z_t(\eta) \rightarrow \tilde{z}_t(\eta) \equiv z_{B-t}(\eta) = Cz_t(\eta) \int_{\eta_*}^{\eta} \frac{d\eta'}{z_t^2(\eta')} \quad (3.54)$$

For a single minimally coupled scalar field, $z_s(\eta) \propto a(\eta)$ e $z_t(\eta) = a(\eta)$ [63]. That is not the case for Starobinsky inflation and $f(R)$ theories in general. Therefore we shall use the functions presented on 2.3. It means that, for the latter scenarios, scalar and tensor perturbations can differ in scale-dependence. For the former, both spectral indexes will be the same.

We should also note that the symmetry does not indicate how the scalar perturbations in a quasi-matter-dominated contracting universe are produced. Only the function form of $z_{s,t}(\eta)$ is defined, but the production and evolution of scalar perturbations happens differently from the inflationary scenario. We demonstrate that in the last sections of this

3.4 Starobinsky Inflation Parametrization

As the duality is present in the Mukhanov-Sasaki equation in conformal time, we need to re-express the scale factor for the Starobinsky model. However the transformation from the cosmic time t to the conformal time $d\eta = a^{-1}(t)dt$ for (3.6) is not analytically possible. That comes from the impossibility of integrating $x^p \exp[ax + bx^2]$, with $b > 0$, $p < 0$. We must then solve the integral

$$\eta = \int \frac{dt}{a(t)} \quad (3.55)$$

in some other form. We have chosen to change (3.6), in such a manner that the main observables of the theory did not change. In other words, we must obtain approximately the same slow-roll parameters, at least equal to first order.

As demonstrated in the previous sections, the modification of the polynomial attached to the exponential in (3.6) is of small relevance for the slow-roll parameter ϵ_1 . That means that both Starobinsky inflation models, (3.6) and (3.15), have the same predictions to first order in slow-roll. Inspired by this fact, our Starobinsky-like scale factor for inflation will have the exponential factor from (3.6) – especially because it is where the model-related parameter M^2 is situated – but with a changed polynomial function attached to it. We have chosen the polynomial to analytically solve the integral (3.55). Other choices were possible but required higher-order polynomials.

Our choice for the scale factor is

$$a(t) = a_0 (t_s - t)^{-1} \exp \left[-\frac{M^2}{12} (t_s - t)^2 \right] \quad (3.56)$$

For the coordinate change, to the conformal time, we thus have

$$\eta = \int \frac{1}{a_0} (t_s - t) \exp \left[\frac{M^2}{12} (t_s - t)^2 \right] dt \quad (3.57)$$

$$= \frac{-6}{a_0 M^2} \exp \left[\frac{M^2}{12} (t_s - t)^2 \right] \quad (3.58)$$

$$= \frac{-6}{M^2} \frac{a(t)^{-1}}{(t_s - t)} \quad (3.59)$$

$$\Rightarrow a(\eta) = \frac{\sqrt{3}}{M} \left[\eta^2 \log \left(\frac{-a_0 M^2 \eta}{6} \right) \right]^{-1/2} = \frac{\sqrt{3}}{M} \left[\eta^2 \log(\bar{\eta}) \right]^{-1/2} \quad (3.60)$$

where we defined $\bar{\eta} \equiv \frac{-a_0 M^2 \eta}{6}$ in order to simplify the expressions.

We confirm that the new scale factor (3.56) does, indeed, reproduce the same observational results as the previous versions (3.6) and (3.15). We compute the Hubble parameter and the HSRP ϵ_1

$$H = \frac{6 + M^2 (t_s - t)^2}{6 (t_s - t)} \quad (3.61)$$

$$\epsilon_1 = \frac{6 \left(-6 + M^2 (t_s - t)^2 \right)}{\left(6 + M^2 (t_s - t)^2 \right)^2} \quad (3.62)$$

$$\simeq \frac{6}{M^2 (t_s - t)^2} \quad (3.63)$$

As expected, we obtain to first order the same expression for the first slow-roll parameter ϵ_1 as before.

Throughout the chapter it will be useful to compute all quantities in conformal time,

$$\mathcal{H}(\eta) = -\frac{1}{\eta} - \frac{1}{2\eta \ln(\bar{\eta})} \quad (3.64)$$

$$H(\eta) = \frac{\mathcal{H}(\eta)}{a(\eta)} \quad (3.65)$$

$$= \frac{M}{\sqrt{3}} [\ln(\bar{\eta})]^{1/2} + \frac{M}{2\sqrt{3}} [\ln(\bar{\eta})]^{-1/2} \quad (3.66)$$

$$\epsilon_1 = -\epsilon_3 = -\epsilon_4 = \frac{1}{2 \ln(\bar{\eta})} \left[1 + \mathcal{O} \left(\frac{1}{\ln(\bar{\eta})} \right) \right] \quad (3.67)$$

We point out that the Hubble function $H(\eta)$ differs a bit from the exact de Sitter case.

Also, that η has negative values during inflation, while $\bar{\eta}$ is positive.

3.5 Starobinsky-like bounce

The new scale factor for the Starobinsky-like inflationary model 3.56 allow for the computation of the function $z_s(\eta)$. We can then use the Wands' duality to find the equivalent contracting universe, that predicts the same scalar perturbations as our inflationary model

For $f(R)$ theories we have

$$z_s(t) \equiv a(t) \sqrt{Q_s} \quad (3.68)$$

$$= a(t) \left(\frac{3\dot{F}^2/2\kappa^2 F}{\left[H + \left(\frac{\dot{F}}{2F} \right) \right]^2} \right)^{1/2} \quad (3.69)$$

$$z_s(\eta) = a(\eta) \left(\frac{3F'^2/2a(\eta)^2\kappa^2 F}{\left[H(\eta) + \left(\frac{F'}{2a(\eta)F} \right) \right]^2} \right)^{1/2} \quad (3.70)$$

where from the second to the third line we changed the derivatives from cosmic to conformal time, using $ad\eta = dt$.

For the F function we use the approximated version from last section, $F(\eta) \cong 4H(\eta)^2/M^2$, where $H(\eta) = \mathcal{H}(\eta)/a(\eta)$. Thus we can compute the function $z_s(\eta)$, by virtue of (3.70),

$$z_s(\eta) = a(\eta) \left(\frac{\left[3(4H(\eta)^2/M^2)^2 \right] / \left[2a(\eta)^2\kappa^2 4H(\eta)^2/M^2 \right]}{\left[H(\eta) + \left(\frac{(4H(\eta)^2/M^2)'}{2a(\eta)4H(\eta)^2/M^2} \right) \right]^2} \right)^{1/2} \quad (3.71)$$

However, it is still necessary to approximate the F function, not only to simplify the next computations but also in order to the integration present in the Wands' duality to be analytically possible. In the large $\bar{\eta}$ limit,

$$F \approx \frac{4H(\eta)^2}{M^2} \quad (3.72)$$

$$= \frac{4}{M^2} \left[\frac{M}{\sqrt{3}} [\ln(\bar{\eta})]^{1/2} + \frac{M}{2\sqrt{3}} [\ln(\bar{\eta})]^{-1/2} \right]^2 \quad (3.73)$$

$$= \frac{4}{3} [\ln(\bar{\eta})]^{-1} \left[\ln(\bar{\eta}) + \frac{1}{2} \right]^2 \quad (3.74)$$

$$\simeq \frac{4}{3} [\ln(\bar{\eta})] \quad (3.75)$$

Therefore, using (3.56), (B.9) and also the computations from the Appendix A, we get for $z_s(\eta)$

$$z_s(\eta) = a(\eta) \left[\frac{\frac{2M^2}{3\kappa^2}}{\frac{M^2}{3} \ln(\bar{\eta})} \right]^{1/2} \quad (3.76)$$

$$= \frac{-1}{\eta} \sqrt{3} [\ln(\bar{\eta})]^{-1/2} \frac{\sqrt{2}}{\kappa} [\ln(\bar{\eta})]^{-1/2} \quad (3.77)$$

$$= \frac{-\sqrt{6}}{\kappa} [\eta \ln(\bar{\eta})]^{-1} \quad (3.78)$$

We can then compute $z_s''(\eta)$ and the total mass term for our model

$$z_s''(\eta) = \frac{d^2 z_s(\eta)}{d\eta^2} \quad (3.79)$$

$$= -\frac{\sqrt{6} (2 \log^2(\bar{\eta}) + 3 \log(\bar{\eta}) + 2)}{\kappa \eta^3 \log^3(\bar{\eta})} \quad (3.80)$$

$$\Rightarrow \frac{z_s''(\eta)}{z_s(\eta)} = \frac{2 \log^2(\bar{\eta}) + 3 \log(\bar{\eta}) + 2}{\eta^2 \log^2(\bar{\eta})} \quad (3.81)$$

$$\simeq \frac{2}{\eta^2} \left[1 + \frac{3}{2} \frac{1}{\ln(\bar{\eta})} + \frac{1}{\ln(\bar{\eta})^2} \right] \quad (3.82)$$

Next, we use the Wands' duality to obtain z_s^B , where the B superscript means that this function belongs to a contracting universe that has a bounce connecting it to the current FLRW expansion. Choosing $\eta^* = 0$, we get

$$\begin{aligned}
z_s^B(\eta) &= c_0 \cdot z_s(\eta) \int_{\eta_*}^{\eta} \frac{d\eta'}{z_s(\eta')^2} \\
&= \frac{c_0}{3\sqrt{6}} \eta^2 \ln(\bar{\eta}) \left[1 - \frac{2}{3 \ln(\bar{\eta})} + \frac{2}{9 \ln^2(\bar{\eta})} \right] + C(\eta_*) \\
&= C_1 \eta^2 \ln(\bar{\eta}) \left[1 + \mathcal{O}\left(\frac{1}{\ln(\bar{\eta})}\right) \right], \tag{3.83}
\end{aligned}$$

The first term is the dominant one for large η , which guarantees that $z_s^B(\eta)$ is positive. For the mass term,

$$\frac{z_s^{B''}}{z_s^B} = \frac{4 \ln(\bar{\eta})^4 - 6 \ln(\bar{\eta})^3 + 18 \ln(\bar{\eta})^2 - 27 \ln(\bar{\eta}) + 18}{\eta^2 \ln(\bar{\eta})^2 (2 \ln(\bar{\eta})^2 - 6 \ln(\bar{\eta}) + 9)} \tag{3.84}$$

$$\simeq \frac{2}{\eta^2} \left[1 + \frac{3}{2} \frac{\ln(\bar{\eta})^3}{(\ln(\bar{\eta})^4 - 3 \ln(\bar{\eta})^3 + \frac{9}{2} \ln(\bar{\eta})^2)} + \mathcal{O}(\ln(\bar{\eta})^{-3}) \right] \tag{3.85}$$

where C_1 is an arbitrary constant. It is straightforward to check that z_s^B and z_s produce the same mass term μ_s up to $\mathcal{O}(\ln^{-1}(\bar{\eta}))$. This result strengthens the approximations we have done so far.

Once we have the function z_s^B , we must specify within which scenario the universe is evolving. This extra step is necessary to associate z_s^B with specific background dynamics. For the present analysis, we choose to immerse this function in a GR contracting solution with the matter content described by a minimally coupled scalar field, hence we have $z_s^B = a_B \dot{\varphi}/H$. The bounce phase will later be detailed, but we have chosen the Loop Quantum Cosmology setting.

For the scalar field case, we use the fact that since a de Sitter model is mapped into an exact matter-dominated universe, the Wands' duality will then map a quasi-de Sitter universe in a quasi-matter dominated universe. See Plot. 3.2.

Matter domination means that the effect equation of state is $p = 0$. For a scalar field, according to (1.25), the kinetic energy must equal the potential energy

$$\dot{\varphi} \simeq \sqrt{2} V^{1/2}. \tag{3.86}$$

When we apply such conditions to the Friedmann equations, we have

$$H \simeq \frac{\sqrt{2}}{3M_{\text{Pl}}} V^{1/2} \quad (3.87)$$

$$\frac{\dot{\varphi}}{M_{\text{Pl}}} \simeq \sqrt{3}H \quad . \quad (3.88)$$

Since the $z_s(\eta)$ function – from a universe whose background is dominated by a minimally coupled scalar field – is proportional to the ratio between $\dot{\varphi}$ and H , it means that it is also proportional to the scale factor

$$z_s(\eta) = a(\eta) \frac{\dot{\varphi}}{H} \quad (3.89)$$

$$z_s(\eta) = 3a(\eta) \quad (3.90)$$

$$\Rightarrow a^B(\eta) = \frac{z_s^B(\eta)}{3} \quad (3.91)$$

Therefore, a quasi-matter dominated universe that produces the same scalar perturbations as our Starobinsky-like inflation has the scale factor below

$$a_B(\eta) = a_{B0} \eta^2 \ln(\bar{\eta}) \left[1 - \frac{2}{3 \ln(\bar{\eta})} + \mathcal{O}\left(\frac{1}{\ln^2(\bar{\eta})}\right) \right] \quad , \quad (3.92)$$

$$\mathcal{H} = \frac{2}{\eta} \left[1 + \frac{1}{2 \ln(\bar{\eta})} + \mathcal{O}\left(\frac{1}{\ln^2(\bar{\eta})}\right) \right] \quad . \quad (3.93)$$

In order to find the time dependence of the scalar field and its potential, we can use the exact expression

$$\varphi'^2 = 2 \left(\mathcal{H}^2 - \mathcal{H}' \right) \quad , \quad (3.94)$$

$$V = \frac{(2\mathcal{H}^2 + \mathcal{H}')}{a^2} \quad . \quad (3.95)$$

which is valid for a scalar field with arbitrary potential V . The approximation Eq. (3.88) is sufficient to argue that $\dot{\varphi}/H$ is constant, while Eq. (3.94) gives the correct numerical factor for φ' . Using Eq.s (3.94) and (3.95), the time dependence of the

potential and of the scalar field read

$$V(\eta) = \frac{6}{a_{B0}^2} \frac{1}{\eta^6 \log^2(\bar{\eta})} \left[1 + \frac{15}{6 \ln(\bar{\eta})} + \mathcal{O}\left(\frac{1}{\ln^2(\bar{\eta})}\right) \right] \quad , \quad (3.96)$$

$$\varphi = -\sqrt{12} \ln \left[\bar{\eta} \ln^{5/12}(\bar{\eta}) \right] + \mathcal{O}\left(\frac{1}{\ln(\bar{\eta})}\right) \quad . \quad (3.97)$$

As a consistency check we can calculate the effective equation of state given by the ratio of pressure and energy density, i.e. $\omega \equiv p/\rho$. Using the above equations we find

$$\omega = \frac{\varphi'^2 - 2a^2 V}{\varphi'^2 + 2a^2 V} = -\frac{1}{6 \ln(\bar{\eta})} + \mathcal{O}\left(\frac{1}{\ln^2(\bar{\eta})}\right) \quad . \quad (3.98)$$

For $\bar{\eta} \gtrsim 10^4$, the equation of state is close to zero with less than 2%. Recall that $\bar{\eta} = -a_0 M^2 \eta / 6$ and the mass parameter is expected to be very large, hence relatively small values of conformal time should already satisfy this condition. It is worth noticing that $\omega \lesssim 0$. This is a crucial property to guarantee a slight redshift in the almost scale-invariant power spectrum. A positive equation of state would produce a blueshift that contradicts current observations.

Finally, we can combine the above equations to find the potential in terms of the scalar field $V(\varphi)$. After some simple algebra, we find

$$V(\varphi) = V_0 \sqrt{1 - \varphi/\varphi_*} e^{\sqrt{3}\varphi} \quad , \quad (3.99)$$

with V_0 and φ_* two constant parameters that completely specify the potential. A dust fluid can be described by a scalar field with potential $\exp[\sqrt{3}\varphi]$, hence it is not surprising that $V(\varphi)$ has this kind of exponential dependence. The novelty is the square root correction, which is intrinsically related to the polynomial correction in the scale factor of Starobinsky inflation. We can again check our construction plotting the phase portrait associated with the potential Eq. (3.99). Fig. 3.3 shows the trajectories of the scalar field in the $(\varphi, \dot{\varphi})$ plane. For relatively large values of φ the velocity $\dot{\varphi}$ rapidly goes to zero, which is consistent with a dust fluid given the exponential dependence of the potential $V(\varphi)$.

For a universe under matter domination, the $\log k$ dependence on conformal time is the

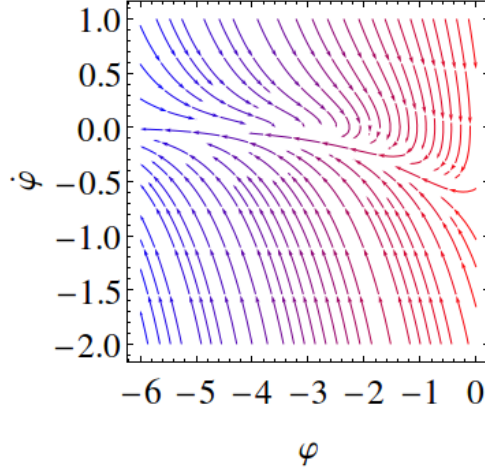


Figure 3.3: Phase portrait of $\dot{\varphi}$ versus φ for the potential Eq. (3.99) using the values $V_0 = \varphi_* = 1$. One can see that the dynamics generated by this reconstructed potential are very similar to the exact dust ($p = 0$) potential showing that the square root deformation of the exponential potential works as a small correction.

same as that of an inflationary universe. The mass term in the Mukhanov-Sasaki equations is also the same, hence the solutions have the same power spectra and dependence on k [64]. Therefore, we have built a model that predicts the same scalar perturbations as the Starobinsky-like inflationary model we parametrized.

3.5.1 Scalar Duality vs. Tensor Duality

The whole process above was done when considering the scalar perturbations. Therefore only the quantities related to such perturbations will be the same in both the scenarios. However, it was also possible to construct a bouncing cosmology that resulted in the same spectral index of tensor perturbations as predicted by the Starobinsky model of inflation.

We repeat the same process we have used for the scalar perturbations, using the same parametrization as before and also the same approximations to F ,

$$z_t(\eta) = a(\eta)\sqrt{F} \simeq \frac{2}{M}\mathcal{H}(\eta) \quad (3.100)$$

$$= \frac{2}{M} \left[-\frac{1}{\eta} - \frac{1}{\eta \ln(\bar{\eta})} \right] \quad (3.101)$$

where the subscript t indicates that the quantity is computed for the cosmology with the same tensor perturbations as in Starobinsky inflation.

We can then use Wands duality ⁵:

$$z_t^B(\eta) = C \cdot z_t(\eta) \int_{\eta^*}^{\eta} \frac{d\eta'}{z_t(\eta')^2} \quad (3.102)$$

$$\simeq \frac{M}{2} \left[-\frac{1}{\eta} - \frac{1}{\eta \ln(\bar{\eta})} \right] \left[\frac{1}{3} \eta^3 - \frac{\eta^3}{1 + \log(\bar{\eta})} \right] \quad (3.103)$$

$$= l_1 \eta^2 - l_2 \frac{\eta^2}{\ln(\bar{\eta})}, \quad (3.104)$$

where $l_1 = M/6$ and $l_2 = -M/3$.

We are dealing with the tensor perturbations of a scalar field, so that $a_B^t = z_t^B$ and hence

$$\Rightarrow a_t^B = l_1 \eta^2 - l_2 \frac{\eta^2}{\ln(\bar{\eta})}. \quad (3.105)$$

We see that the behavior of such a universe is close to exact matter domination, signaling that we have achieved almost scale-invariance as desired. However, it differs from the scalar duality case (3.92).

The mass term from the Mukhanov-Sasaki equations for the tensor perturbations of this new model is

$$\frac{a_t''}{a_t} = \frac{2 \left(\ln(\bar{\eta})^3 - 2 \ln(\bar{\eta})^2 + 3 \ln(\bar{\eta}) - 2 \right)}{\eta^2 (\ln(\bar{\eta}) - 2) \ln(\bar{\eta})^2} \quad (3.106)$$

$$\simeq \frac{2}{\eta^2} \left[1 + \frac{3}{\ln(\bar{\eta})} \frac{1}{(-2 + \ln(\bar{\eta}))} - \frac{1}{\ln(\bar{\eta})^2} \frac{2}{(-2 + \ln(\bar{\eta}))} \right] \quad (3.107)$$

Therefore, we expect that this contracting universe will produce the same tensor perturbations as the Starobinsky-like inflationary model.

In section 3.5 we have constructed a model from the scalar duality, through its scalar pump-field function $z(\eta)$. For a scalar field dominated universe, this function is proportional to the scale factor $z(\eta) \propto a(\eta)$, therefore the mass term for tensor perturbations in the scalar reconstructed universe is the same as before, (3.85)

⁵In order to avoid a Exponential Integral we have made some approximations

$$\frac{a_s''}{a_s} = \frac{4 \ln(\bar{\eta})^4 - 6 \ln(\bar{\eta})^3 + 18 \ln(\bar{\eta})^2 - 27 \ln(\bar{\eta}) + 18}{\eta^2 \ln(\bar{\eta})^2 (2 \ln(\bar{\eta})^2 - 6 \ln(\bar{\eta}) + 9)} \quad (3.108)$$

$$\simeq \frac{2}{\eta^2} \left[1 + \frac{3}{2} \frac{\ln(\bar{\eta})^3}{(\ln(\bar{\eta})^4 - 3 \ln(\bar{\eta})^3 + \frac{9}{2} \ln(\bar{\eta})^2)} + O(\ln(\bar{\eta})^{-3}) \right] \quad (3.109)$$

Therefore, we see that both mass terms for the tensor perturbations differ. It demonstrates that the reconstructed universe using the scalar duality does not reproduce the same tensor perturbations as the original Starobinsky-like inflationary model.

3.6 Cosmological Perturbations

3.6.1 Crossing the Bounce

Bounce models are a subclass of non-singular models that commonly have a single contracting phase followed by an expanding phase. By construction, the contracting phase is smoothly connected to the expanding phase, hence the universe is eternal and free of spacetime singularities. However, this does not mean that one should oppose bounce and inflationary models. Even though a pure inflationary mechanism cannot avoid the initial singularity [161, 162], a non-singular model can accommodate an inflationary phase [59, 5]. However, bounce models are frequently understood as alternatives to inflation.

There are viable bounce models that are consistent with almost scale-invariant power spectrum and small tensor-to-scalar ratio [163, 57, 164, 87, 165, 166, 167]. In these models, the dynamic through the bounce influences the observable effects. For instance, the mode mixing of scalar perturbations across the bounce is responsible for producing the almost scale-invariant power spectrum. Therefore, it seems reasonable that in order to consider bounce models as a physically viable scenario for the primordial universe, one should recognize them as alternatives to inflation and not just as a complementary phase prior to it. Bounce-inflation models [168, 169, 170, 171] are beyond the scope of this thesis.

Bounce and inflation have completely distinct background dynamics. Besides the differences concerning the singularity problem, at the background level, inflation and bounce models have different shortcomings and theoretical challenges of their own [172, 90, 65, 56]. Notwithstanding, at first-order perturbation, bounce and inflation are formally

very similar. Indeed, Wands' duality described in section 3.3 is one manifestation of the mathematical similarity between these two scenarios.

Generically, the dynamics of linear perturbations $\nu_{\mathbf{k}}$ are described by a parametric oscillator equation like Eq. (2.27) where the time-dependent mass term μ_{α} encodes the background dynamics. In each case, we have a specific definition for $\nu_{\mathbf{k}}$ and μ_{α} but the framework is almost identical. Let us compare some of their features.

In both scenarios, even though for different physical reasons, the initial conditions are set in the most (possible) remote past and have a quantum vacuum fluctuation origin. In inflationary models, we have a quasi-de Sitter expansion, which makes the physical length of interest for present cosmology much smaller than the curvature scale. As a consequence, the perturbations are not influenced by the expansion, and the initial state is set as a Bunch-Davies vacuum state. In a bounce model, there are different approaches to setting the the initial conditions. We chose the semi-classical approach, where the conditions are given in the far past much before the bounce phase. The universe is immense and with negligible curvature, hence, the initial state is a Minkowski vacuum (rather similar to the Bunch-Davies case).

As the universe evolves the relation between the physical length and the Hubble length changes. In both scenarios the ratio between these two lengths increases. In terms of the perturbed dynamic equation, this means that with the background evolution, the mass term increases compared to the wavenumber until they become comparable in magnitude. This moment specifies the crossing from outside to inside the potential for the perturbations. The mass term continues to grow until it reaches a maximum that typically locates the bounce or the reheating period for inflationary models. Then the potential starts to decrease until its value becomes again comparable to the wavenumber characterizing the crossing outside the potential (inside the Hubble length)⁶. Thereupon, both scenarios are connected to the FLRW radiation epoch and the dynamics follow the standard model.

It is evident from the above description that the violent quasi-de Sitter expansion phase is related to the long contracting phase of bounce models. Moreover, the reheating phase of inflation should be compared to the physical processes during the bounce phase. Thus, it is not surprising that the reheating and the bounce are the two most speculative

⁶Note that the description in terms of the potential for the perturbation (the time-dependent mass term) is the opposite as compared to the relative size of the physical and Hubble lengths. Crossing outside the Hubble length means going inside the potential and vice-versa.

periods of evolution.

Inflationary models often overlook the details of the reheating processes. In a certain sense, this is due to the assumption that whatever physical process taking place in this period should only transfer energy into the matter fields and not significantly modify the other physical quantities such as the almost scale-invariant power spectrum or the tensor-to-scalar ratio⁷. This idea has support on Weinberg's theorem [173] that states that, in the large wavelength limit, the field equations for the cosmological perturbations in the Newtonian gauge always have an adiabatic solution with \mathcal{R} constant and nonzero in all eras.

In contrast, bounce models cannot avoid examining the bounce phase since one must define the physical mechanism that produces the bounce. In addition, the physics of the bounce remains encoded in the spectrum of primordial perturbations. As we will show in the following, the relation between the scalar spectral index and the tensor-to-scalar ratio depends on the physics of the bounce. The observational data available are not yet sensitive enough to discriminate between different bounce mechanisms but as in the case of non-Gaussianities, future experiments might allow us to probe the physics of the bounce [128].

In order to connect the contracting phase of the model constructed in the last section to the CMB observables, in the following sections we shall describe the bounce as a quantum gravity effect using the Loop Quantum Cosmology (LQC) framework [14, 174]. There are other appealing frameworks such as Wheeler-DeWitt [7, 85, 175, 176, 177, 178] or string cosmology [179]. However, LQC has analytical bounce solutions for a scalar field mimicking a perfect fluid, hence, from a technical point of view, it is the most direct description to accommodate a previous Starobinsky-like contracting phase.

Loop quantum gravity (LQG) is a non-perturbative, background-independent quantum theory of gravity. It is based on a reformulation of GR in terms of the Ashtekar-Barbero variables. The classical variables promoted to operators are the holonomies of the Ashtekar connection and the fluxes of the densitized triads. One important kinematical result of this quantization procedure is the discretization of spacetime, which in turn establishes a minimum of length, area, and volume. LQC relies on using loop quantization techniques to quantize the holonomies and the fluxes of homogeneous and

⁷It is worth mentioning that non-Gaussianities encoded in the bispectrum are much more sensitive to reheating.

isotropic universes. It is not a full quantum gravity theory but an effective approach that hopefully captures the essential features of LQG in a cosmological scenario (for further details see [180, 181, 182, 164]). The cosmological dynamics can be described by a phenomenological Hamiltonian. Given a flat FLRW metric, the dynamics with respect to cosmic time reads

$$H^2 = \frac{M_{\text{Pl}}^{-2}}{3} \rho \left(1 - \frac{\rho}{\rho_c} \right) \quad , \quad (3.110)$$

$$\dot{H} = -\frac{M_{\text{Pl}}^{-2}}{6} (\rho + p) \left(1 - \frac{2\rho}{\rho_c} \right) \quad , \quad (3.111)$$

$$\dot{\rho} + 3H(\rho + p) = 0 \quad , \quad (3.112)$$

where ρ_c is a critical energy density that establishes the energy scale where quantum corrections are important⁸. This dynamic system has analytical bounce solutions for perfect fluids $p = \omega\rho$ with constant ω [14, 109, 103]. Furthermore, we can use a scalar field with exponential potentials to model the perfect fluid with constant ω . Indeed, using the fact that

$$\rho = \frac{1}{2}\dot{\varphi}^2 + V(\varphi) \quad , \quad p = \frac{1}{2}\dot{\varphi}^2 - V(\varphi) \quad ,$$

one can show [109] that there is an exact solution

$$\rho = \rho_c \left(\frac{a_B}{a} \right)^{3(1+\omega)} \quad , \quad (3.113)$$

$$a(t) = a_B \left(1 + \alpha^2 (t - t_B)^2 \right)^{1/3(1+\omega)} \quad , \quad (3.114)$$

$$\varphi(t) - \varphi_B = \frac{\sqrt{\rho_c(1+\omega)}}{\alpha} \operatorname{arcsinh} \left(\alpha(t - t_B) \right) \quad , \quad (3.115)$$

where $\alpha = \sqrt{3\rho_c}(1+\omega)/2M_{\text{Pl}}$ for constant ω . That is only valid for exponential potentials that try to mimic the constant equation of state we desire. The parameters t_B and a_B are respectively the values of the cosmic time and the scale factor at the bounce. Note that the energy density reaches its maximum value at the bounce Eq. (3.113). This is a characteristic feature of symmetric bounces. The scalar field potential for this solution

⁸We have used the conservation of energy-momentum as our third dynamic equation but we could instead have used the Klein-Gordon equation for the scalar field. The two systems of equations are equivalent.

is given by

$$V = \frac{\rho_c(1-\omega)}{2} \operatorname{sech}^2 \left[\frac{\alpha(\varphi - \varphi_B)}{\sqrt{\rho_c(1+\omega)}} \right] , \quad (3.116)$$

where φ_B is an arbitrary constant. This solution has two parameters a_B and φ_B in addition to the energy density scale ρ_c of LQC. The classical limit is approached when $\rho_c \rightarrow \infty$. In this limit, Eq. (3.116) tends to $V \sim \exp\left(\sqrt{3(1+\omega)}\varphi/M_{\text{Pl}}\right)$, which corresponds to the scalar field potential that describes a perfect fluid with equation of state ω in GR.

3.6.2 Scalar Perturbations in Bounce Models

Quantum cosmology is an attempt to include quantum effects in the evolution of the universe. In this manner, we must necessarily consider modifications in the GR equations of motion. However, bounce models generically assume that far from the bounce region we recover the GR dynamics. Therefore, long before and after the bounce the scalar perturbations are described by

$$v'' + (k^2 - \mu_s^2)v = 0 , \quad \text{with} \quad \mu_s^2 = \frac{z_s''}{z_s} , \quad (3.117)$$

$$v \equiv z_s \mathcal{R} \quad , \quad z_s \equiv \frac{a}{H} \sqrt{\rho + p} = a \frac{\dot{\varphi}}{H} . \quad (3.118)$$

Using the quasi-matter dynamics of last section Eq. (3.83), we find that the classical contracting phase has

$$v^{in}(\eta) = \sqrt{\frac{-\pi\eta}{4}} \text{H}_\gamma^{(1)}(-k\eta) \quad , \quad (3.119)$$

$$\gamma = \frac{3}{2} + \epsilon_c = \frac{3}{2} + \frac{1}{\ln(\bar{\eta})} + \frac{2}{3} \frac{1}{\ln(\bar{\eta})^2} \quad , \quad (3.120)$$

where $\text{H}_\gamma^{(1)}$ is the Hankel function of the first kind and we have defined in the last expression $\epsilon_c \equiv \gamma - \frac{3}{2}$. The ϵ_c will play a role analogous to a slow-roll parameter, which differs from the matter bounce parameter [64] by being a small quantity $|\epsilon_c| \ll 1$. Indeed, during the period of validity of the above solution, this term is very small compared to unit, hence, we can consider series expansion in its powers. Our task now is to describe the bounce and use matching conditions to connect this contracting phase with the expanding

phase of the standard model.

There are different approaches to analyze cosmological perturbations in LQC. In the closed algebra [183], dressed metric [184, 185] and hybrid [186] approaches, the perturbations need to be computed in the quantum regime, as they are produced during an inflationary expansion after a bounce. In the Separate Universe framework [103], however, we can treat the perturbations semi-classically, as we deal with a pure bouncing cosmology, such that there is no inflationary regime. That is the approach we use in our work.

The LQC perturbed equations have two modifications with respect to GR. The Mukhanov-Sasaki equation now reads [187, 14]

$$v'' + \left[\left(1 - \frac{2\rho}{\rho_c} \right) k^2 - \frac{z''}{z} \right] v = 0 \quad , \quad (3.121)$$

where the z function is defined as

$$z = \frac{a\sqrt{\rho + P}}{H} = M_{\text{Pl}} \sqrt{\frac{3(1 + \omega)}{1 - \rho/\rho_c}} a \quad . \quad (3.122)$$

Far away from the bounce, the energy density is much less than the critical density, i.e. $\rho/\rho_c \ll 1$ and we recover the classical definitions. Thus, during the contracting phase far away from the bounce, we have Eq. (3.119). We need to match this solution with a solution valid during the bounce. Eq. (3.121) can be transformed into an integral equation given by

$$\begin{aligned} v(\eta) = & B_1 z + B_2 z \int^\eta \frac{d\bar{\eta}}{z^2} - k^2 \int^\eta \frac{d\bar{\eta}}{z^2} \int^{\bar{\eta}} d\bar{\bar{\eta}} z v \\ & + \frac{2k^2}{\rho_c} z \int^\eta \frac{d\bar{\eta}}{z^2} \int^{\bar{\eta}} d\bar{\bar{\eta}} z v \quad . \end{aligned} \quad (3.123)$$

Close to the bounce, it is the mass term that dominates hence we can series expand the solution in powers of the wavenumber. The solution Eq.s (3.114) and (3.115) are given in cosmic time. We can interpret the conformal time of the above expression as a function of cosmic time. Using the LQC background solution we find at leading order

$$v(t) = B_1 z(t) + B_2 z(t) \left(\frac{a_B^{-3} M_{\text{Pl}}^{-2}}{3(1+\omega)} \right) \times \quad (3.124)$$

$$\times \left[\frac{\alpha^2 t^3}{3} {}_2F_1 \left[\frac{3}{2}, \frac{2+\omega}{1+\omega}, \frac{5}{2}, -\alpha^2 t^2 \right] + c_2 \right],$$

where ${}_2F_1[a, b, c, z]$ is the hypergeometric function and c_2 is an integration constant that can be chosen conveniently to simplify the matching at the contracting phase. The function $x^3 {}_2F_1 \left[\frac{3}{2}, \frac{2+\omega}{1+\omega}, \frac{5}{2}, -x^2 \right]$ goes to a constant in the limit $x \rightarrow \pm\infty$, hence we can choose c_2 to cancel this constant term in the far past. Consequently, we will have $2c_2$ in the far future after the bounce. Taking the limit $\alpha t \rightarrow -\infty$ we find that $c_2 = \frac{\pi}{4\alpha}$. The coefficient B_1 represents the decreasing mode during Hubble crossing in the contracting phase. We can immediately see from the above expression that due to the behavior of the hypergeometric function the bounce produces a mode mixing transferring the coefficient B_2 to the dominant mode after the bounce.

The validity of the contracting solution Eq. (3.119) relies on ϵ_c being almost constant in time and small $\epsilon_c \ll 1$. Thus, we can perform the matching between the contracting phase and the bounce solution well inside the potential for the perturbation but still very far from the bounce. This means that we should take the limit $k\eta \rightarrow 0$ in Eq. (3.119) and the limit $t \ll -1/\alpha$ in Eq. (3.124). In addition, our contracting phase has equation of state given by Eq. (3.98), hence we must identify $\omega = -\frac{1}{6}\epsilon_c$. In this limit, we can write the scale factor and the cosmic time in terms of the conformal time, i.e.

$$a(\eta) = a_B \left[\frac{\alpha(1-\epsilon_c/3)}{3} a_B \eta \right]^{2+\epsilon_c}, \quad (3.125)$$

$$\alpha t(\eta) = \left[\alpha \left(\frac{1-\epsilon_c/3}{3} \right) a_B \eta \right]^{3+\epsilon_c}, \quad (3.126)$$

where we have used $\epsilon_c \ll 1$ and kept only the leading order terms. Using Eq.'s (3.122)-(3.124) we find

$$z(\eta) = a_B^{3+\epsilon_c} \left(1 - \frac{13\epsilon_c}{12}\right) \frac{\sqrt{\rho_c}}{2} \left(\frac{\rho_c}{12M_{\text{Pl}}^2}\right)^{(1+\epsilon_c)/2} \eta^{2+\epsilon_c} , \quad (3.127)$$

$$v(\eta) = B_1 a_B^{3+\epsilon_c} \left(1 - \frac{13\epsilon_c}{12}\right) \frac{\sqrt{\rho_c}}{2} \left(\frac{\rho_c}{12M_{\text{Pl}}^2}\right)^{(1+\epsilon_c)/2} \eta^{2+\epsilon_c} \\ - \frac{4B_2 a_B^{-3-\epsilon_c}}{\sqrt{3} \sqrt{\rho_c}} \left(1 + \frac{5\epsilon_c}{12}\right) \left(\frac{M_{\text{Pl}}^2}{\rho_c}\right)^{(1+\epsilon_c)/2} \eta^{-1-\epsilon_c} . \quad (3.128)$$

This solution has to be matched with the contracting solution Eq. (3.119) in the limit $k\eta \ll 1$, namely

$$v^{in}(\eta) = \frac{1}{3\sqrt{2}} k^{3/2+\epsilon_c} \eta^{2+\epsilon_c} + \frac{i}{\sqrt{2}} k^{-3/2-\epsilon_c} \eta^{-1-\epsilon_c} . \quad (3.129)$$

A straightforward comparison shows that

$$B_1 = \frac{\sqrt{2} a_B^{-3-\epsilon_c}}{3\sqrt{\rho_c}} \left(1 + \frac{13\epsilon_c}{12}\right) \left(\frac{\rho_c}{12M_{\text{Pl}}^2}\right)^{-(1+\epsilon_c)/2} k^{3/2+\epsilon_c} , \quad (3.130)$$

$$B_2 = -i \frac{\sqrt{3}}{4\sqrt{2}} \frac{\sqrt{\rho_c}}{a_B^{-3-\epsilon_c}} \left(1 - \frac{5\epsilon_c}{12}\right) \left(\frac{\rho_c}{M_{\text{Pl}}^2}\right)^{(1+\epsilon_c)/2} k^{-3/2-\epsilon_c} . \quad (3.131)$$

The solution Eq.(3.124) is valid across the bounce. Having defined the coefficients B_1 and B_2 we can find the solution after the bounce. The expanding phase solution is described by taking the limit $t \gg 1/\alpha$ in Eq.(3.124), i.e.

$$v^{out}(\eta) = \left[B_1 + B_2 \left(\frac{\pi a_B^{-3}(1 + \epsilon_c/3)}{3\sqrt{3}\rho_c M_{\text{Pl}}} \right) \right] z(\eta) \quad (3.132) \\ = \left[\frac{k^{3/2+\epsilon_c}}{3\sqrt{2}} - i \frac{\pi \left(1 - \frac{7\epsilon_c}{6}\right)}{48\sqrt{6}} \left(\frac{a_B^2 \rho_c}{M_{\text{Pl}}^2}\right)^{3/2+\epsilon_c} k^{-3/2-\epsilon_c} \right] \eta^{2+\epsilon_c} .$$

In cosmological perturbations we are interested in the small wavenumber limit, hence for very small wavenumbers, it is the $k^{-3/2}$ that dominates. However, this is true only if the numerical factors are of order one. The parameter ρ_c is expected to be smaller but comparable in at least a few order of magnitude of the Planck energy density, i.e. $\rho_c = 10^{-n} \rho_{\text{Pl}}$, with $1 < n < 10$. The value of the scale factor at the bounce must be at least a few orders of magnitude higher than the Planck mass, otherwise, we could not

rely on our quantum cosmology effective scenario, i.e. $a_B = 10^m l_{\text{Pl}}$ with $5 > m > 2$. The ratio between the two terms above is

$$\approx 14.28 \times 10^{3(m-n/2)} l_{\text{Pl}}^{-3} k^{-3} \gg 1 \quad . \quad (3.133)$$

Therefore, it is indeed the $k^{-3/2}$ the dominant coefficient for all values of interest of wavenumber in cosmology and the scalar perturbation is

$$\mathcal{R} = \frac{v}{z} \approx \frac{\pi}{12\sqrt{2}} \sqrt{\frac{\rho_c}{M_{\text{Pl}}^4}} k^{-\frac{3}{2}-\epsilon_c} \approx 0.185 \sqrt{\frac{\rho_c}{M_{\text{Pl}}^4}} k^{-\frac{3}{2}-\epsilon_c} \quad , \quad (3.134)$$

with spectral index given by

$$n_s - 1 = -2\epsilon_c \quad . \quad (3.135)$$

As expected, the power spectrum is almost scale invariant but with a small redshift. Using the Planck 2018 release $n_s = 0.9649 \pm 0.0042$ (see Ref. [29]), we have $0.0196 < \epsilon_c < 0.0155$.

3.6.3 Tensor Perturbations

Similar to the scalar perturbations, the dynamic equation for tensor perturbations in LQC has quantum corrections proportional to ρ/ρ_c . The Mukhanov-Sasaki variable is defined in terms of the tensor perturbations $h = 2v/z_T M_{\text{Pl}}$, where function z_T is also modified due to quantum corrections. The Mukhanov-Sasaki equation reads

$$v'' + \left[\left(1 - \frac{2\rho}{\rho_c} \right) k^2 - \frac{z_T''}{z_T} \right] v = 0 \quad , \quad (3.136)$$

where the function z_T is given by

$$z_T = \frac{a}{\sqrt{1 - 2\rho/\rho_c}} \quad . \quad (3.137)$$

The tensor perturbations in the contracting phase have the same solution as the scalar perturbations, namely

$$v^{in}(\eta) = \sqrt{\frac{-\pi\eta}{4}} \text{H}_\gamma^{(1)}(-k\eta) \quad , \quad (3.138)$$

where again $\gamma = 3/2 + \epsilon_c$. Following the same procedure as before, we can transform the differential equation into an integral equation for μ similar to Eq. (3.123). The solution across the bounce can be obtained by a series expansion on powers of the wavenumber. At leading order in k , the formal solution to its integral form is

$$v(t) = D_1 z_T(t) + D_2 z_T(t) \int^{\bar{\eta}} \frac{d\eta}{z_T(\eta)^2} \quad , \quad (3.139)$$

where D_1 and D_2 are two constants of integration. By virtue of Eq. (3.137), the formal solution is

$$v(t) = D_1 z_T(t) + \frac{D_2}{a_B^3} z_T(t) \left[\frac{\alpha^2 t^3}{3} {}_2F_1 \left(\frac{3}{2}, \frac{2+\omega}{1+\omega}, \frac{5}{2}, -\alpha^2 t^2 \right) + \right. \\ \left. -t \times {}_2F_1 \left(\frac{1}{2}, \frac{2+\omega}{1+\omega}, \frac{3}{2}, -\alpha^2 t^2 \right) + C \right] \quad . \quad (3.140)$$

As before, we chose the constant C conveniently to cancel the constant term in the far past. As a result we have $C = -\frac{\pi\omega}{2\alpha}$. Recall that $\alpha = \sqrt{3\rho_c}(1+\omega)/2M_{\text{Pl}}$ and $\omega = -\frac{1}{6}\epsilon_c$. In order to match this solution with the contracting phase, we must take the limit $t \ll -1/\alpha$ that gives

$$v(t) = \frac{D_1(1-\epsilon_c)}{a_B^{-3-\epsilon_c}} \left(\frac{\rho_c}{12M_{\text{Pl}}^2} \right)^{1+\epsilon_c/2} \eta^{2+\epsilon_c} + \frac{D_2}{3a_B^3} \left(1 + \frac{2\epsilon_c}{3} \right) \left(\frac{12M_{\text{Pl}}^2}{\rho_c} \right)^{1+\epsilon_c/2} \eta^{-1-\epsilon_c} \quad . \quad (3.141)$$

This expression has to be matched with the limit $k\eta \ll 1$ for the classical solution (3.119), namely

$$v^{in}(\eta) = \frac{1}{3\sqrt{2}} k^{\frac{3}{2}+\epsilon_c} \eta^{2+\epsilon_c} - i \frac{1}{\sqrt{2}} k^{-\frac{3}{2}-\epsilon_c} \eta^{-1-\epsilon_c} . \quad (3.142)$$

Thus, we identify

$$D_1 = \frac{(1+\epsilon_c)}{3\sqrt{2}a_B^{3+\epsilon_c}} \left(\frac{12M_{\text{Pl}}^2}{\rho_c} \right)^{1+\epsilon_c/2} k^{\frac{3}{2}+\epsilon_c} , \quad (3.143)$$

$$D_2 = -i \frac{3a_B^3}{\sqrt{2}} \left(1 - \frac{2\epsilon_c}{3} \right) \left(\frac{\rho_c}{12M_{\text{Pl}}^2} \right)^{1+\epsilon_c/2} k^{-\frac{3}{2}-\epsilon_c} . \quad (3.144)$$

The expanding phase is given by taking the limit $t \gg 1/\alpha$. Thus, we have

$$v^{out}(\eta) = \left[D_1 - \frac{D_2}{a_B^3} \frac{\pi M_{\text{Pl}}}{3\sqrt{3}\rho_c} \epsilon_c \right] z_T^c(\eta) , \quad (3.145)$$

where D_1 and D_2 are given by Eq.s (3.143) and (3.144). It is worth noting that the term proportional to D_2 is linear in ϵ_c , hence the mode mixing in the tensor perturbation depends on how small is the slow-roll parameter. To leading order in wavenumber, the tensor perturbation reads

$$\begin{aligned} h &= \frac{2v}{z_T M_{\text{Pl}}} = \frac{2}{M_{\text{Pl}}} \left[D_1 - \frac{D_2}{a_B^3} \frac{\pi M_{\text{Pl}}}{3\sqrt{3}\rho_c} \epsilon_c \right] \\ &\approx \frac{i\pi}{6\sqrt{6}} \epsilon_c \sqrt{\frac{\rho_c}{M_{\text{Pl}}^4}} k^{-\frac{3}{2}-\epsilon_c} \approx 0.214 i \epsilon_c \sqrt{\frac{\rho_c}{M_{\text{Pl}}^4}} k^{-\frac{3}{2}-\epsilon_c} . \end{aligned} \quad (3.146)$$

Thus, the tensor spectral index is $n_t = -2\epsilon_c = n_s - 1$. Finally, using Eq.s (3.134) and (3.146), we find the tensor-to-scalar ratio

$$r = \frac{\mathcal{P}_T}{\mathcal{P}_R} = 2 \frac{|h|^2}{|\mathcal{R}|^2} = \frac{8}{3} \epsilon_c^2 = \frac{2}{3} (n_s - 1)^2 . \quad (3.147)$$

Note that we succeed in obtaining the same relation between $n_s - 1$ and r as in the Starobinsky inflation. However, even though with the correct power of the slow-roll parameter ϵ_c^2 , there is a numerical factor difference of order unit. Eqs. (3.39) and (3.40)

show that Starobinsky inflation has a relation between the scalar spectral index and the tensor-to-scalar ratio given by

$$r = 3(n_s - 1)^2 \quad , \quad (3.148)$$

hence our model is a factor $2/9$ smaller. This difference is a convolution of two contributions coming from the ratio z_s/z_T but they have a completely distinct physical origin.

First, in inflationary models, the ratio $(z_s/z_T)^2$ is $2\epsilon_c^{-2}$ larger than its value in bouncing models. Indeed, one can check that in the Starobinsky model we have $(z_s/z_T)^2 = Q_s/F \approx \frac{3}{2}M_{\text{Pl}}^2\epsilon_c^2$, while for a matter bounce model we have $(z_s/z_T)^2 = 3M_{\text{Pl}}^2$. The simple fact that the horizon crossing happens in two different background dynamics (quasi-de Sitter for inflation and quasi-matter for bounce) changes the tensor-to-scalar ratio by a factor $2\epsilon_c^{-2}$. The factor $\epsilon_c^2/9$ has a completely different physical origin. It comes from the dynamics across the bounce.

Inflationary models with adiabatic perturbations have a decreasing and a constant mode. With the quasi-exponential expansion, it is the constant mode that dominates and gives the almost scale-invariant power spectrum. In contrast, bounce models have a constant and an increasing mode before the bounce. The bounce dynamics make the latter the dominant mode after the bounce (there is a mode mixing), which has an integral contribution of z^{-2} (see Eq. (3.139)). This term carries information across the bounce and depends on the dynamics chosen to describe the bounce. In our case, we get a $\epsilon_c^2/9$ contribution from the time integral across the LQC bounce. Another quantum bounce like dBB should give a different numerical factor but the same ϵ_c^2 contribution. We note that classical bounces do not follow such behavior.

In summary, there is a crucial difference in how inflation and bounce models obtain a small tensor-to-scalar ratio. Both dynamics start with the same vacuum state but, in comparison to our model, the inflationary dynamics amplify⁹ the scalar perturbations more than the quasi-matter contraction does, by a factor $2\epsilon_c^{-2}$. On the other hand, the evolution across the bounce suppresses the tensor perturbations by a factor $\epsilon_c^2/9$. The net result is the $2/9$ difference factor between the two tensor-to-scalar ratios given by Eq.s

⁹Note that this amplification difference appears only for the tensor-to-scalar ratio and it is irrelevant for the amplitude of the scalar perturbations since one can always adjust the free parameter ρ_c in order to accommodate this difference. This is not the case for r since the scalar and tensor perturbations have the same dependence on ρ_c hence it drops out (see Eq.s (3.134) and (3.146)).

(3.147)-(3.148).

3.7 Results on the reconstruction of bouncing cosmologies from inflationary models

In the near future, we expect to have decisive new observational data of the very early universe. The 21 cm redshift surveys together with measurements of the CMB B-mode polarization, non-Gaussianities, and primordial gravitational waves will enable us to discriminate between different primordial universe scenarios. Therefore, it is pressing to identify signatures of each type of primordial universe scenario that would allow us to make testable predictions.

We have used Wands' duality to construct a quasi-matter bounce that mimics the Starobinsky inflation. This map allows us to identify the correct contracting phase dynamics that give the same time-dependent mass term in the Mukhanov-Sasaki equation. The adequate scalar field potential $V(\varphi)$, given by Eq. (3.99), is a deformation of the exponential potential known to describe a pressureless dust fluid. This result agrees with the fact that a quasi-de Sitter phase should be mapped into a quasi-matter-dominated contracting universe. After the linear perturbations cross the horizon, the system must go through a bounce phase. We chose to describe the bounce using LQC inasmuch it is the easiest quantum bounce if the matter field is described by a scalar field.

Our constructive method enables us to discriminate the contribution of each dynamical phase in the primordial power spectrum. In particular, we showed that mapping the Starobinsky inflation into a quasi-matter bounce gives the correct relation between the scalar spectral index $n_s - 1$ and the tensor-to-scalar ratio r but it appears a factor $2/9$ of difference. The crucial point is to understand the origin of this numerical factor. It comes from the ratio z_s/z_T and it is a convolution of two distinct contributions. The comparison between this ratio from an inflationary expansion to a quasi-matter contraction gives a factor $2\epsilon_c^{-2}$, while the dynamics through the LQC bounce results in an additional factor $\epsilon_c^2/9$.

An interesting feature of our analysis is to show that the bounce leaves a signature in the primordial power spectrum. The scalar and tensor spectral indexes depend on the background dynamics during the horizon crossing. But the amplitudes of the scalar

and tensor power spectrum, hence the tensor-to-scalar ratio, carry information from the dynamics across the bounce.

We note that curvaton models which use a Starobinsky-like inflaton field will also be dual to the bouncing cosmology we have constructed. As we present in the next chapter, [4](#), the spectral index of scalar perturbations in the curvaton scenario is the same as in the single-field inflationary model which uses the same inflaton field. Not only that, but curvaton models have a suppressed tensor-to-scalar ratio, which makes them even more degenerate with our reconstructed bouncing cosmology.

Chapter 4

Reconstructed Self-Interacting Curvaton

This chapter begins with an introduction to the statistical anomalies present in the CMB, and how they could be connected to primordial universe physics. Then, we present the self-interacting curvaton case and how we compute the non-Gaussianities for this scenario. Next, we demonstrate, in order to create a curvaton model from a f_{NL} parameter, how we have built our reconstruction procedure. A concrete example follows. Finally we show the connection between the produced f_{NL} signal and the CMB anomalies. The chapter is based on our work Ref. [188].

4.1 Introduction

Inflation is generally chosen as the mechanism to explain the existence of the primordial cosmological perturbations. The most simple scenario is that of single-field inflation (SFI), see 1.2, where a scalar field follows a slow-roll dynamics and is simultaneously responsible for driving the almost exponential expansion of the Universe and its density perturbations work as seeds for the CMB [96]. Thus, a slow-roll SFI model provides the observed Gaussian and almost scale-independent temperature fluctuations [125]. However, throughout this thesis I have already highlighted a few motivations to consider alternatives to SFI. It is important to note that SFI is not the unique successful scenario of the early Universe. There are two main alternative classes of models.

One route is to work with bouncing models, the focus of Section 1.3 and chapters

3 and 5. Another route is to preserve an inflationary phase, albeit not in a single-field slow-roll setting. Multi-field Inflation (MFI) models [24], as presented in 1.2.5, in which there is more than one scalar field ruling the inflationary regime, could be a requirement for inflation to happen in the string theory landscape [28], while warm inflation provides alternative routes around the issues [43, 44].

Among the MFI models, curvaton models, as first mentioned in 1.2.5, are simple extensions of SFI with the addition of only one extra scalar field. In this scenario, the background dynamics is still driven by the inflaton but the cosmological perturbations now come from the density fluctuations of the curvaton field. A distinct feature of these models is that the curvaton produces isocurvature perturbations instead of the common inflaton adiabatic perturbations. Only after the decay into radiation, the curvaton isocurvature modes turn into adiabatic ones, which then seed the CMB. This scenario alleviates the constraints on the inflaton field [189] while still producing the observed almost scale-invariant spectrum and the negligible amplitude of the primordial gravitational waves. Another advantage of this scenario is that it allows for large non-Gaussianities, much higher than in SFI.

Are there any observational consequences from curvaton models that could help its case against SFI? Could we use the fact that curvaton models predict stronger non-Gaussianity to make them more suitable than the standard inflationary models? Could the phenomenology of multi-field inflation break the degeneracy between inflationary and bouncing models?

In this chapter, we motivate the search of curvaton models by virtue of the presence of statistical anomalies in the CMB perturbations and their connection to non-Gaussianities. In particular, we show how to construct viable curvaton models from the properties of the f_{NL} parameter. In order to do so, we have developed a reconstruction procedure based on the curvaton slow-roll equation and some assumptions regarding the field potential. We build an example following a reasonable *ansatz* for the behavior of f_{NL} . In particular, due to a change of sign in the parameter, we manage to have a f_{NL} close to zero at the observable scales but still have large non-Gaussianities away from the pivot scale. Finally, we connect the recovered f_{NL} parameter and its k -dependence to the dipolar modulation of the CMB.

4.2 CMB Anomalies

Deviations from isotropy were first measured by WMAP [91], and have been reinforced by Planck [18]. These CMB anomalies have a low statistical significance, of order approximately 3σ . However, the fact that they were found by different satellites, in addition to studies on systematical errors and the cosmological foreground, suggests that they might have primordial origin.

The presence of anomalies [46, 47] violates the cosmological principle, and is difficult to be produced in the single-field inflationary paradigm [190]. This amplifies the debate [191] in regards to which scenario best describes the primordial universe, an inflationary or a bouncing scenario. Among the anomalies with greater statistical support are the hemispherical asymmetry (also known as the dipolar modulation) and the lack of power at lower multipoles. Inflationary models are generally unable to justify the presence of anomalies because they predict the statistical independence of the CMB multipoles. Therefore, there is a need to introduce new mechanisms, inside or outside of the inflationary context, to explain the anomalies.

Concerning the dipolar modulation of the CMB, many attempts to explain it have been made in the literature. It can be described by a function $f(\hat{\mathbf{n}})$, which modulates the isotropic fluctuations [192]

$$\hat{\Theta}(\hat{\mathbf{n}}) = [1 + f(\hat{\mathbf{n}})] \Theta(\hat{\mathbf{n}}), \quad (4.1)$$

where $\hat{\Theta}(\hat{\mathbf{n}})$ represents the observed non-isotropic fluctuations and the modulation function $f(\hat{\mathbf{n}})$ is direction-dependent, of expressive magnitude only for the dipole component, and modulates the isotropic temperature field $\Theta(\hat{\mathbf{n}})$. The direction of this asymmetry is measured in galactic coordinates, $(l, b) = (227, -17)$ [18]. The dipolar modulation is constrained by different observations, from its values at low CMB multipoles to its limits obtained from the quasar database [193] at higher multipoles. The result of these analysis [194, 195] shows that the dipolar modulation is highly scale-dependent, providing an asymmetry between hemispheres of order $A < 0.0153$ at high values of l , while for low multipoles ($l \leq 64$) its value is $A = 0.07 \pm 0.02$ [18]. This scale-dependence can be expressed in terms of another parametrization [196], providing, in terms of the power spectrum $P(k)$,

$$\mathcal{P}_{obs} \approx \frac{k^3 P(k)}{2\pi^2} (1 + 2A(k)\hat{\mathbf{p}} \cdot \hat{\mathbf{n}} + \dots), \quad (4.2)$$

where the amplitude of the asymmetry is given by $A(k)$, where the scale-dependence is obtained in $k \sim 0.5$, $\hat{\mathbf{p}}$ is the direction of the modulation and $\hat{\mathbf{n}}$ is the Earth's line-of-sight. Different parametrizations [54] can be made, resulting in different ways to express the scale-dependence of the dipolar modulation.

An asymmetry between CMB hemispheres signals a privileged direction, a direct violation of the isotropy principle. Motivated by this fact, Ericksek, Kamionkowski e Carroll [197] postulated the existence of a large scale cosmological perturbation mode, above the Hubble scale. This perturbation would be reminiscent of the inflationary stage, and its wave vector, k_D , would be the responsible for the existence of a privileged direction.

The proposed mechanism (named EKC, given the authors names) uses the amplitude of the super-horizon perturbation¹ to modify the value of the background inflationary field. This value is intimately linked to the amplitude of the fluctuations present at the CMB, therefore a modification could imply in the production of the asymmetry. However, as demonstrated in the original paper, the super-horizon perturbation cannot have its origin in the inflaton [197]. The existence of such perturbation would imply the break down not only of the isotropy, but also the homogeneity of the universe. Measurements of the homogeneity of the CMB constrains the possible values of a perturbation amplitude beyond the Hubble scale. To accomplish the asymmetry, the EKC mechanism through the inflaton would need to violate those limits, therefore being inconsistent with observations.

Thus, for the realization of EKC-like mechanisms it is necessary to make use of alternate scenarios, such as multi-field inflation. In the original paper [197] it was demonstrated that the aforementioned curvaton scenarios [198] could present a super-horizon perturbation without violating the homogeneity constraints observed in the universe. However, they would present a certain degree of non-gaussianities that could trespass the observed limits. Ensuing results [18, ?] indicate that the original EKC mechanism in the curvaton scenario cannot explain the anomalies without the existence of non-gaussianities above the observed magnitude.

Since then, different EKC-like mechanisms have been built [199, 200]. Owing to the

¹The Hubble scale is commonly called Hubble horizon. Therefore perturbations at a scale above the Hubble one are called super-horizon.

originally obtained results by EKC, those models are generally inside a multi-field set-up, either with different fields responsible for inflation or through curvaton-like fields.

EKC and related mechanisms are not the only ways to produce a dipolar modulation in the CMB. In particular, mechanisms that make use of a non-gaussianity-driven coupling between cosmological perturbations have been built in the context of different scenarios. This development was first established in [53], where the coupling due to the presence of non-gaussianities is fulfilled between modes of short and large wavelengths. The latter, as before, means super-horizon scales. The advantage of this type of model is that it does not need to modify the energy density of the universe, avoiding the violation of homogeneity constraints. As those modes are at super-horizon scales, another advantage is to escape from the current CMB non-gaussianity constraints, as they are determined for the modes inside the horizon, which requires a scale-dependent non-gaussianity. However there are some setbacks to be considered. The model from reference [53] does not produce a scale-dependent dipolar modulation, going against the previously mentioned constraints, which require a low value for the asymmetry at large values of l . Once again, we have an inconsistency between model and observations. There are other limitations to these models, such as the fact that the non-linearity parameter f_{NL} , cannot exceed the previously detailed limits, of order unity $\mathcal{O}(1)$.

For both types of models, solutions to these setbacks are present in the literature. The chosen route to avoid these problems is two-fold: the use of highly scale-dependent non-gaussianities [54] or the four (or more) point correlation function [201, 202]. Scenarios which present non-gaussianities of such nature are common [170, 203, 204], but once again they deviate from the usual single-field inflation models.

The scenario we choose is that of the curvaton, as anticipated earlier. In contrast to single-field models, obtaining expressive non-gaussianity for super-horizon modes is easy in the curvaton scenario, especially when dealing with self-interacting curvaton models [205, 206, 51]. In these cases, the self-interaction of the curvaton is responsible for the production of non-gaussianities, and there is a direct relation between the intensity of this interaction and the amplitude of the bispectrum. It is the self-interaction that will also allow the scale-dependence of non-gaussianities, either from the three (the bispectrum) or four (trispectrum) point functions.

A major part of the advancements on the non-gaussian modulation proposal is based

on a phenomenological approach, predominantly in the inflationary paradigm, in generic form. Models are built without the inclusion of the micro-physics behind them, i.e., modulation forms are proposed without the full primordial universe context that explains them. The same is done for EKC-like mechanisms. It is thus necessary to construct primordial universe models that result in the already made phenomenological proposals. Only then a complete panorama on the formation of the CMB anomalies, in special the ones mentioned, can be finalized. Therefore, the study of CMB anomalies adds one more probe to primordial universe models, which could contribute to break the degeneracies between different scenarios and models.

4.3 Curvaton Scenario

The curvaton scenario goes beyond SFI by the addition of a second scalar field dubbed the curvaton. Usually, this extra scalar field is minimally coupled to gravity and does not interact with the inflaton. The latter drives the background dynamics while the curvaton produces the observed cosmological perturbations. There are also interactive models [207, 208] where the potential has a cross term coupling the curvaton with the inflaton. These interactive models satisfy the observational constraints but at the cost of increasing the number of free parameters of the model. Here, we shall consider only self-interacting curvaton models, which have scale-dependent non-Gaussianity [54], such that the Lagrangian reads

$$\mathcal{L}(\varphi, \sigma) = \bar{K}(\varphi) + K(\sigma) + \bar{V}(\varphi) + V(\sigma) , \quad (4.3)$$

where $\bar{K}(\varphi)$ and $\bar{V}(\varphi)$ denote the kinetic and potential terms of the inflaton field, while $K(\sigma)$ and $V(\sigma)$ denote those quantities for the curvaton field. In contrast to SFI models, in the curvaton scenario, the inflaton has a negligible contribution to the cosmological perturbations due to a lower inflaton mass m_φ as compared to the SFI models [209]². As a consequence, the magnitude of tensor perturbations is likewise negligible as compared to the SFI. Notwithstanding, the energy density of the curvaton is always subdominant and does not contribute to the background dynamics. It is the inflaton slow-roll regime

²The scenario allows for both fields to contribute to cosmological perturbations [207, 208].

that drives the almost exponential expansion of the Universe, while the curvaton follows its evolution, which does not need to be frozen – it can be a slow-roll evolution different from the inflaton dynamics, or even a non-slow-roll regime.

As usual, reheating takes place at the end of the inflaton slow-roll regime, when it oscillates around the minimum of the potential with an equation of state $p = \omega\rho$ with $\omega \approx 0$. During this process, the inflaton decays into radiation. After decay, we are left with a radiation-dominated universe.

In our scenario, the curvaton field follows a similar decay regime, albeit delayed in time. Thus, we consider potentials for the curvaton with a local minimum, that can be approximated by a quadratic potential, and where the coherent oscillations make the curvaton decay as pressureless dust.³ In addition, we assume the sudden decay approximation in which the curvaton instantaneously decays into radiation when its decay rate equals the Hubble parameter⁴ i.e., $\Gamma_\sigma = H$.

4.3.1 Linear Cosmological Perturbations

During the inflationary phase, the curvaton produces only isocurvature perturbations. Due to thermal and chemical equilibrium, after the curvaton decay, they are then converted into adiabatic perturbations. This conversion process was first proposed by Mollerach [212] and later applied to the curvaton scenario in Refs. [198, 213]. The transfer of isocurvature perturbation into curvature perturbation can be described as [198]

$$\zeta \sim r_{\text{dec}}\delta, \quad (4.4)$$

where r_{dec} and δ are the curvaton's fractional energy density and the isocurvature perturbation, respectively, and ζ is the final adiabatic perturbation. The fractional energy density gives the curvaton contribution to the total energy density and reads

$$r_{\text{dec}} = \left. \frac{3\rho_\sigma}{3\rho_\sigma + 4\rho_\gamma} \right|_{\text{dec}} \sim \frac{V(\sigma_{\text{dec}})}{3\Gamma^2}, \quad (4.5)$$

³There are models in which the behavior of the potential at small values of the field is not quadratic, see Ref. [210] and references therein.

⁴It can be shown that the sudden decay is a good approximation for the exact gradual decay. Moreover, it has no impact on the primordial observables [211].

where ρ_σ and ρ_γ are the curvaton and the radiation density, respectively, at the time of the curvaton decay. During its reheating, the curvaton redshifts more slowly than radiation, since it behaves as dust; hence, if the curvaton decays long after the inflaton, the curvaton dominates the energy density of the Universe and $r_{\text{dec}} \sim 1$. On the other hand, if the decay happens shortly after the inflaton's decay, then $r_{\text{dec}} \ll 1$, which means a large non-Gaussianity [see discussion after Eq. (4.17)]. Therefore, we assume that the curvaton decays not long after the inflaton and hence $r_{\text{dec}} \sim 10^{-2}$.

The curvaton fluctuations are decoupled from the inflaton's, and therefore their equations of motion for the wavenumber k are [198]

$$\delta\ddot{\sigma}_{\mathbf{k}} + 3H\delta\dot{\sigma}_{\mathbf{k}} + \left[\frac{k^2}{a^2} + V_{\sigma\sigma} \right] \delta\sigma_{\mathbf{k}} = 0 \quad (4.6)$$

Assuming an almost flat curvaton potential ($V_{\sigma\sigma} \ll H^2$) during inflation, the above equation describes the quantum fluctuations of a massive scalar field during a quasi-de Sitter stage. We can rewrite equation (4.6) in conformal time, for a quasi-de Sitter stage where $\dot{H} = -\epsilon_H H^2$,

$$\delta\sigma_{\mathbf{k}}'' + \left[k^2 - \frac{a''}{a} + V_{\sigma\sigma} a^2(\eta) \right] \delta\sigma_{\mathbf{k}} = 0 \quad (4.7)$$

where

$$\frac{a''}{a} \approx \frac{1}{\eta^2} (2 + 3\epsilon_H) \quad (4.8)$$

Recasting (4.7) using $\nu_\sigma \simeq \frac{3}{2} + \epsilon_H - \eta_\sigma$, one finds the solution for $\mathcal{P}_{\delta\sigma}$ that is proportional to $k^{3-2\nu_\sigma}$. One also computes [198, 213] the power spectrum to be

$$\mathcal{P}_\zeta = \frac{r_{\text{dec}}^2}{16} \frac{H_k^2}{\pi^2 \sigma_k^2} \quad (4.9)$$

Hence, the spectral index reads

$$n_s - 1 = \frac{d \ln \mathcal{P}_\zeta}{d \ln k} = 3 - 2\nu_\sigma \quad (4.10)$$

Using the definition of ν_σ , we therefore have for the spectral index of the curvaton

$$n_s - 1 \approx -2\epsilon_H + 2\eta_\sigma \approx 2\frac{\dot{H}_k^2}{H_k^2} + 2\frac{V_{,\sigma\sigma}}{3H_k^2} \quad , \quad (4.11)$$

Notwithstanding, the inflaton still gives important contributions, since it dominates the background dynamics. In the above equation, we define the slow-roll parameters as usual – namely,

$$\epsilon_H \equiv \frac{\dot{H}_k^2}{H_k^2} \quad , \quad \eta_\sigma \equiv \frac{V_{,\sigma\sigma}(t_k)}{3H_k^2} \quad (4.12)$$

Even though the curvaton does not interact with the inflaton, the scalar perturbations and spectral index have contributions from both fields. The spectral index [Eq. (4.11)] has a leading contribution ϵ_H , the inflaton slow-roll parameter. The curvaton η_σ , if positive, must be subleading and of order 10^{-2} or lower so that the spectrum is red and quasi-scale-invariant.⁵ The tensor-to-scalar ratio r is largely suppressed in the curvaton scenario as compared to SFI,

$$r = 16\epsilon_H \frac{\mathcal{P}_\varphi}{\mathcal{P}_\zeta} \approx 0 \ll r_{SFI} \quad , \quad (4.13)$$

where again we are dealing with the fact that the inflaton does not contribute to the perturbations $\mathcal{P}_\zeta \gg \mathcal{P}_\varphi$. One of the advantages of the curvaton scenario is to evade the need for $\epsilon_H \propto 1/N^2$ (for N around 60 e-folds) in order to fit the current observational sensibility, $r < 10^{-2}$ [189]. Indeed, SFI models that lead to $\epsilon_H \propto 1/N$, such as chaotic inflation [214, 96], can now be used as the inflaton component of the curvaton scenario,

⁵Models with a negative spectral index would be preferred because of the requirement of a red spectrum, and would alleviate some conditions imposed on the inflaton, via ϵ_H

since they satisfy both constraints on r and $n_s - 1$.

4.3.2 Non-Gaussianities

In order to quantify the amount of non-Gaussianity in the model, we make use of the non-linearity parameters f_{NL} and g_{NL} as we defined in 2.4.2. Repeating the Taylor expansion for the curvature perturbation $\zeta(k)$ in terms of its Gaussian component ζ_G ,

$$\zeta = \zeta_G + \frac{3}{5}f_{\text{NL}}\zeta_G^2 + \frac{9}{25}g_{\text{NL}}\zeta_G^3 + \mathcal{O}(\zeta_G^4). \quad (4.14)$$

By definition, the nonlinearity parameters f_{NL} and g_{NL} encode the non-Gaussianity from the second and third-order terms, respectively. During the phase of coherent oscillations around the minimum of the potential, the energy density of the curvaton field for a mode k can be approximated by $\rho_\sigma = m_\sigma^2 \sigma_{\text{osc}}^2 / 2$. Using the expansion to third order in the δN formalism [137], we have

$$\begin{aligned} \zeta(k) &= \frac{2r_{\text{dec}}}{3} \frac{\sigma'_{\text{osc}}}{\sigma_{\text{osc}}} \delta\sigma_k(t_k) \\ &+ \frac{1}{9} \left[3r_{\text{dec}} \left(1 + \frac{\sigma_{\text{osc}} \sigma''_{\text{osc}}}{\sigma_{\text{osc}}^2} \right) - 4r_{\text{dec}}^2 - 2r_{\text{dec}}^2 \right] \left(\frac{\sigma'_{\text{osc}}}{\sigma_{\text{osc}}} \right)^2 \delta\sigma_k^2(t_k) \\ &+ \frac{4}{81} \left[10r_{\text{dec}}^4 + 3r_{\text{dec}}^5 + \frac{9r_{\text{dec}}}{4} \left(\frac{\sigma_{\text{osc}}^2 \sigma'''_{\text{osc}}}{\sigma_{\text{osc}}^3} + 3 \frac{\sigma''_{\text{osc}} \sigma_{\text{osc}}}{\sigma_{\text{osc}}^2} \right) \right. \\ &\quad \left. - 9r_{\text{dec}}^2 \left(1 + \frac{\sigma_{\text{osc}} \sigma''_{\text{osc}}}{\sigma_{\text{osc}}^2} \right) \right] \left(\frac{\sigma'_{\text{osc}}}{\sigma_{\text{osc}}} \right)^3 \delta\sigma_k^3(t_k) + \mathcal{O}(\delta\sigma_k^4) \end{aligned} \quad (4.15)$$

Note that the nonlinearity parameters f_{NL} and g_{NL} are scale-dependent. In order to have a scale-independent parameter one needs $\sigma_{\text{osc}}(\sigma_k)$ not to depend on σ_k . Straightforward comparison of Eqs. (4.14) and (4.15) gives

$$\begin{aligned} f_{\text{NL}} &= \frac{5}{4} \frac{f_{\text{osc}}}{r_{\text{dec}}} - \frac{5}{3} - \frac{5}{6} r_{\text{dec}} \quad , \\ g_{\text{NL}} &= \frac{25}{24} \frac{g_{\text{osc}}}{r_{\text{dec}}^2} - \frac{25}{6} \frac{f_{\text{osc}}}{r_{\text{dec}}} - \frac{25}{12} \left(f_{\text{osc}} - \frac{10}{9} \right) + \frac{125}{27} r_{\text{dec}} + \frac{25}{18} r_{\text{dec}}^2 \quad , \end{aligned} \quad (4.16)$$

where

$$f_{\text{osc}} \equiv 1 + \frac{\sigma_{\text{osc}} \sigma_{\text{osc}}''}{\sigma_{\text{osc}}'^2}, \quad g_{\text{osc}} \equiv \frac{\sigma_{\text{osc}}^2 \sigma_{\text{osc}}'''}{\sigma_{\text{osc}}'^3} + 3 \frac{\sigma_{\text{osc}}'' \sigma_{\text{osc}}}{\sigma_{\text{osc}}'^2}. \quad (4.17)$$

A prime in the above equations indicates derivatives with respect to σ_k . The terms proportional to r_{dec}^{-1} show that the faster the curvaton decays, the larger are the non-Gaussianities. In addition, the lower the cross-section Γ , the longer it takes for the system to reach the sudden decay condition $H \sim \Gamma$. Note that to lower the value of the cross-section means to reduce the magnitude of the curvaton interactions, and consequently also their fluctuations. Thus, higher r_{dec} values produce smaller magnitudes of fluctuation and smaller non-Gaussianities.

The curvaton dynamics are characterized by two distinct regimes. The first is the slow-roll regime of the curvaton, given by

$$3H\dot{\sigma} + m_\sigma^2 \sigma + V_{,\sigma}^{\text{SI}}(\sigma) \approx 0, \quad (4.18)$$

where $V^{\text{SI}}(\sigma)$ is the self-interacting part of the potential.

The solution for the slow-roll regime σ_{SR} is a nonlinear function of σ_k . We assume that it is valid until the time t_q when the curvaton reaches its second regime. There, the curvaton oscillates around its quadratic minimum and the self-interactions are no longer important. This is known as a coherent oscillating phase, whose dynamics reads

$$\ddot{\sigma} + 3H\dot{\sigma} + m_\sigma^2 \sigma \approx 0. \quad (4.19)$$

The solution for this stage is of the form $\sigma(t) = \sigma_{\text{osc}} f_{\text{inf}}(t)$, where f_{inf} is a function dependent only on the background dynamic given by the inflaton; see Refs. [54, 215]. We suppose an instantaneous transition between the slow-roll and the coherent oscillation regimes and match the respective solutions, which allows us to write $\sigma_{\text{osc}} = \beta \sigma_{\text{SR}}(t_q)$, where β is a constant parameter. Therefore, σ_{osc} is proved to be dependent on σ_k as well.

We are interested in a particular set of self-interaction curvaton models, where the σ_k dependence on σ_{osc} is chosen to better fit observational results. In the next section, we show how recent observations suggest the behavior needed for f_{NL} , and, consequently, $\sigma_{\text{osc}}(\sigma_k)$.

4.4 Curvaton Reconstruction Procedure

The Planck Collaboration [19] showed that the strength of the non-Gaussian signal for f_{NL} does not go beyond order unity, indicating that primordial non-Gaussianities are seemingly very small. A way out of this constraint is to consider scale-dependent non-Gaussianity models, in order to have large values of f_{NL} away from the observed scales (in particular, away from the pivot scale used for the CMB maps). Models with a change of sign in f_{NL} , so that it remains close to zero over a limited range of wavenumbers, can be adjusted to satisfy the present observational constraints. Such a range of wave numbers must be identified with the CMB scales which constrain the free parameters of the models. This procedure allows us to study how much fine-tuning is required to fit the observational data. The scale-dependent models are particularly interesting when one needs high values of non-Gaussianities, for instance, to account for the CMB anomalies [54, 190, 203]. In the following, we analyze how to construct models with a change of sign in the f_{NL} parameter and the effect it has on the dynamics of the curvaton field.

4.4.1 Crossing f_{NL} parameter

In the literature, the non-Gaussianity parameter f_{NL} is typically parametrized as a power law given by

$$f_{\text{NL}}(k) = f_{\text{NL}}^0 \left(\frac{k}{k_0} \right)^{n_{f_{\text{NL}}}} \quad (4.20)$$

where f_{NL}^0 is the amplitude at a given pivot scale k_0 , and the index $n_{f_{\text{NL}}}$ is a constant [216, 50]. However, this parametrization is no longer valid if f_{NL} crosses the zero – namely, if it changes sign [54]. As we present in Sec. 4.5, a better-suited parametrization allows for multiple changes in sign.

We can find the value of σ_{osc} in terms of σ_k where the change of sign happens. The RHS of Eq. (4.17) shows that

$$f_{\text{osc}} = \frac{(\sigma_{\text{osc}}^2)''}{2\sigma_{\text{osc}}'^2} = 0 \quad \Rightarrow \quad (\sigma_{\text{osc}}^2)'' = 0. \quad (4.21)$$

The conditions for f_{osc} and f_{NL} to cross zero are different. Nevertheless, for $r_{\text{dec}} \sim 0.05$,

the values of the last two terms on the RHS of Eq. (4.16) are of order unity. The crossing is still guaranteed as long as the scale dependence of f_{NL} is strong enough. Thus, instead of the crossing of f_{NL} , we consider the condition for $f_{\text{osc}} = 0$. Equation (4.21) implies that the crossing is an extremal point for

$$\left(\sigma_{\text{osc}}^2\right)' = 2\sigma_{\text{osc}}\sigma'_{\text{osc}}. \quad (4.22)$$

The function σ_{osc} is assumed to be a monotonic function of σ_k and the derivative σ'_{osc} must not cross zero; otherwise f_{osc} diverges. Moreover, the value of k at the crossing of f_{osc} differs from the extreme of σ'_{osc} due to the factor σ_{osc} . As a fact, at the extremal of σ'_{osc} we have $\sigma''_{\text{osc}} = 0$, which means $f_{\text{osc}} = 1$ instead of 0. Notwithstanding, it suffices that σ'_{osc} has one extremal point for Eq. (4.21) to be satisfied and, given the scale-dependence of the system, we expect that the values of k for these two conditions should be close.

In summary, the function σ_{osc} is monotonic and σ'_{osc} has an extremal point but it is never zero, hence it is always positive or negative. The function σ''_{osc} does change sign at least once and must vary enough to guarantee that f_{NL} also changes sign. There are different ways in which one can implement these features. In the next section, we show one way to construct the curvaton potential in order to have exactly this kind of behavior. We study the parameter space of the model by combining the observational data with the conditions on σ_{osc} and its derivatives.

4.4.2 Constructing the curvaton potential

The non-Gaussianity parameters depend basically on the relation $\sigma_{\text{osc}}(\sigma_k)$ – i.e., on how σ_{osc} is written in terms of σ_k . And to find $\sigma_{\text{osc}}(\sigma_k)$, we need to solve the two regimes in Eqs. (4.18) and (4.19), hence different curvaton potentials result in different relations. Our goal is to be able, given a functional form $\sigma_{\text{osc}}(\sigma_k)$, to specify the potential that after solving the dynamical equations will produce the desired $\sigma_{\text{osc}}(\sigma_k)$.

We start by separating the slow-roll regime of the curvaton into two steps. We assume that when the value of the curvaton field is close to σ_{osc} , the potential is close to quadratic and remains so until the minimum of the potential at the origin $\sigma = 0$. This guarantees the validity of the results from the conventional self-interaction curvaton scenario.

Recall that $\sigma_q \equiv \sigma(t_q) \propto \sigma_{\text{osc}}$, and away from σ_q , we need to consider the full expression

of the potential, in particular, for the evolution around the observable scales σ_k . Solving the slow-roll equation for these two regimes gives

$$\int_{\sigma_k}^{\sigma_q} \frac{d\sigma}{\bar{V}_{,\sigma}} \sim \int_{\sigma_k}^{\sigma_*} \frac{d\sigma_q}{\bar{V}_{,\sigma}} + \int_{\sigma_*}^{\sigma_q} \frac{d\sigma}{\sigma} = -\bar{\eta}_\sigma \mathcal{I}(t_q, t_k), \quad (4.23)$$

where $\bar{V} \equiv V/m_\sigma^2$, and σ_* is the field value where we apply the matching condition to connect the slow-roll dynamics to the quadratic local minimum regime. Note that σ_* cancels from the final expression, since it is evaluated where both solutions are equal, and hence is irrelevant. Following Ref. [54], in Eq. (4.23), we have defined

$$\mathcal{I}(t_q, t_k) \equiv H_k^2 \int_{t_k}^{t_q} \frac{dt}{H(t)} \quad , \quad \bar{\eta}_\sigma = \frac{m_\sigma^2}{3H_k^2}. \quad (4.24)$$

Given an appropriate choice of t_q , the integral during the curvaton slow-roll regime gives $\mathcal{I}(t_q, t) \approx 1/\bar{\eta}_\sigma$. Thus, for values of $t \ll t_q$, the rhs of Eq. (4.23) equals $-\bar{\eta}_\sigma \mathcal{I} \approx -1$ and we can consider this term independent of σ_k . Close to σ_q we have

$$\int \frac{d\sigma}{\bar{V}_{,\sigma}} = \log[\sigma] \quad (4.25)$$

Now we assume that the potential is such that the integral containing $\bar{V}_{,\sigma}^{-1}$ admits a primitive function $G(\sigma)$, namely

$$\int_{\sigma_k}^{\sigma_q} \frac{d\sigma}{\bar{V}_{,\sigma}} \sim G(\sigma_q) - G(\sigma_k), \quad (4.26)$$

and Eq. (4.23) can be recast as

$$G(\sigma) = \log[\sigma_{\text{osc}}(\sigma)] + \text{terms independent of } \sigma_k. \quad (4.27)$$

To find the potential, we can invert Eq. (4.26) and write

$$V(\sigma) = m_\sigma^2 \int d\sigma \frac{\sigma_{\text{osc}}}{\sigma'_{\text{osc}}}, \quad (4.28)$$

where σ_{osc} should be understood as the function $\sigma_{\text{osc}}(\sigma)$ with the same functional form as $\sigma_{\text{osc}}(\sigma_k)$. Given a physically motivated ansatz $\sigma_{\text{osc}}(\sigma_k)$, integration of Eq. (4.28) gives

the potential satisfying the slow-roll dynamics that produces the desired non-Gaussianity encoded in $\sigma_{\text{osc}}(\sigma_k)$. By construction, the slow-roll solution is approximately $G(\sigma)$. This allows us to compute the curvaton slow-roll parameters and compare them with the observation of the primordial power spectrum. Moreover, using Eq. (4.16), we can also compute the non-Gaussianity parameters f_{NL} and g_{NL} of the model.

4.4.3 Observables from the reconstruction

Similar to what we have done for f_{NL} , we can write the derivatives of the potential, namely the slow-roll parameters, in terms of σ_{osc} and its derivatives. Using (Eq. 4.28), we have

$$V_{,\sigma} = m_\sigma^2 \frac{\sigma_{\text{osc}}}{\sigma'_{\text{osc}}}, \quad (4.29)$$

$$V_{,\sigma\sigma} = m_\sigma^2 \left(1 - \frac{\sigma_{\text{osc}} \sigma''_{\text{osc}}}{\sigma'^2_{\text{osc}}} \right). \quad (4.30)$$

Comparing the above expression with the definition of f_{osc} , (4.17), one immediately sees that

$$f_{\text{osc}} + \frac{V_{,\sigma\sigma}}{m_\sigma^2} = 2. \quad (4.31)$$

It is worth remarking that the above expression is independent of the solution σ_{osc} . Since $f_{\text{osc}} = 1$ for $\sigma''_{\text{osc}} = 0$, Eq. (4.31) shows that $V_{,\sigma\sigma} = m_\sigma^2$ at this point as well. We also conclude that

$$\eta_\sigma = \frac{m_\sigma^2 (2 - f_{\text{osc}})}{3H_k^2} = 2\bar{\eta}_\sigma - \frac{4r_{\text{dec}} \bar{\eta}_\sigma}{5} \left(f_{\text{NL}} + \frac{5}{3} + \frac{5r_{\text{dec}}}{6} \right), \quad (4.32)$$

hence, for any model from our procedure, the parameter η_σ can be written in terms of $\bar{\eta}_\sigma$ and f_{NL} . Equation (4.32) generalizes the relation presented in Ref. [217], since it is still valid for large values f_{NL} and η_σ . We see that in our scenario, there is an additional expression relating f_{NL} , η_σ and H_k . Note also that we can recover the condition $\eta_\sigma = 2\bar{\eta}_\sigma$ from Ref. [54], if $f_{\text{NL}}(k_0) = -5/3 - 5r_{\text{dec}}/6$.

In Sec. 4.4.1 we associated the change of sign in f_{osc} with the second derivative of σ''_{osc} being zero somewhere along the curvaton trajectory. Now, using Eq. (4.31), we conclude that the potential must also have an inflection point – i.e., $V_{,\sigma\sigma} = 0$. The inflection point, like for f_{osc} , is not located where $\sigma''_{\text{osc}} = 0$.

4.4.4 Reconstructing a polynomial potential

The quartic and higher-power polynomial models have been studied in the literature [215, 206, 51, 54]. Despite producing scale-dependent non-Gaussianities, these models predict high values of η_σ over the region of low f_{NL} . Therefore such models are not favored by the Planck satellite results. Our goal here is to use them only as an example to show how our procedure works. In the next section, we shall deal with fitting the model to observations. For a polynomial potential of the form $V(\sigma) = \frac{1}{2}m^2\sigma^2 + \lambda\sigma^n$ with $n > 2$, the curvaton slow-roll solution is given by

$$\sigma_{\text{osc}}(\sigma_{\text{k}}) = \frac{\sigma_{\text{k}}}{\left[e^{n-2} + (ne^{n-2} - n)\lambda\sigma_{\text{k}}^{n-2}\right]^{1/(n-2)}}. \quad (4.33)$$

Using Eq. (4.33) as the ansatz for the procedure of Sec. 4.4.2, we obtain a potential given by

$$V(\sigma) = \frac{1}{2}m^2\sigma^2 + \lambda_{\text{eff}}\sigma^n \quad \text{with } \lambda_{\text{eff}} = \lambda(1 - e^{-n+2}). \quad (4.34)$$

We see that the reconstruction gives a lower value for the coupling constant. The worst case is for $n = 3$, where $\lambda_{\text{eff}} \approx 0.6321\lambda$ but already increases to $\lambda_{\text{eff}} \approx 0.865\lambda$ for $n = 4$. The higher the power of the self-interaction, the more precise is the reconstruction. This kind of shift in our reconstruction procedure does not change the qualitative behavior of our model but it can change some observational scales such as the pivot value at which the non-Gaussianity parameter f_{NL} changes sign. The important point is that any feature in the ansatz will also be present in the solutions derived by using the reconstructed potential; hence, the consistency of the procedure is guaranteed.

4.5 Reconstructed Curvaton Model

In Sec. 4.4.1, we described the main features that a solution $\sigma_{\text{osc}}(\sigma_k)$ must have to produce a viable curvaton model with a change of sign in f_{NL} . A possible realization of these conditions is for $\sigma_{\text{osc}}''(\sigma_k)$ to be a linear function of σ_k . Therefore, we consider an ansatz of the form

$$\sigma_{\text{osc}} = a\sigma + \frac{1}{2}b\sigma^2 + \frac{1}{6}c\sigma^3 \quad , \quad (4.35)$$

where a , b and c are the free parameters of the solution. Applying the construction procedure of the last section, we arrive at the potential

$$\frac{V(\sigma)}{m^2} = V_0 + \frac{b}{3c}\sigma + \frac{\sigma^2}{6} - V_{\text{lg}} \log(2a + 2b\sigma + c\sigma^2) + V_{\text{arc}} \arctan\left(\frac{b + c\sigma}{\sqrt{-b^2 + 2ac}}\right) \quad , \quad (4.36)$$

where the two coefficients V_{lg} and V_{arc} are given in terms of the free parameters as

$$V_{\text{lg}} = \frac{b^2 - 2ac}{3c^2} \quad , \quad V_{\text{arc}} = \frac{4b(b^2 - 3ac)}{6c^2\sqrt{2ac - b^2}} \quad . \quad (4.37)$$

The argument of the arctan has the same structure as the ansatz acceleration – i.e., $\sigma_{\text{osc}}'' = (b + c\sigma)$. Therefore, the inflection point for this term happens where the acceleration is zero, $\sigma_z = -b/c$. However, for the total potential [Eq. (4.36)], the inflection point is shifted away from σ_z due to the presence of the other (subleading) terms.

To reduce the number of free parameters – and simplify the analysis of the parameter space, we shall fix $a = 1/e$, which gives the quadratic curvaton solution in the limit $b = c = 0$. Note also that we have implicitly assumed $\sigma_{\text{osc}}(0) = 0$. The ansatz is constructed to facilitate the study of the curvaton slow-roll solution and its resulting f_{NL} parameter. Therefore, it is convenient to discuss the model parameter space in terms of b and c and not in terms of the coefficients of the potential, because the former are directly connected to the non-Gaussianity parameters f_{NL} and g_{NL} .

The first constraint on b and c comes from the change of sign of $\sigma_q''(\sigma_k)$, which should

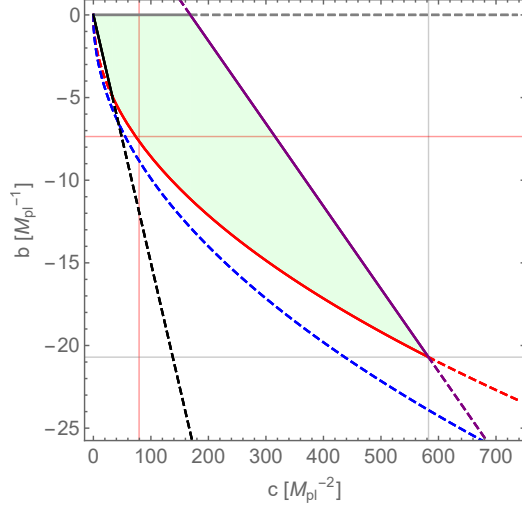


Figure 4.1: Final allowed region for b in green, when $\sigma_{\max} = 0.15$, $c > 0$, including all constraints. The red grid lines indicate the point $(b, c) = (-20/e, 216/e)$ for the model in Sec. 4.5.1.

happen during the curvaton slow roll. Therefore, the point $\sigma = -b/c$ should be smaller than the initial value of the field $\sigma_{ini.} \equiv \sigma_{\max}$. That is represented by the black dotted lines in Fig. 4.1. This also implies that b and c must have opposite signs, since $\sigma > 0$ during the slow roll.

The derivative σ'_q should not vanish anywhere; otherwise, both f_{NL} and g_{NL} diverge. Therefore, the models have a positive minimum for σ'_q – i.e., we must have $b > -\sqrt{2c/e}$ – that gives the red dashed line a constraint in Fig. 4.1. Note that this condition also avoid divergences in the potential [Eq. (4.36)]. Also, σ_q is a monotonically increasing function of σ_k , since its derivative is always positive.

In addition, the \log term of Eq. (4.36) has an argument proportional to σ'_{osc} ; hence we must also avoid $\sigma'_q = 0$. As a consequence, we must exclude negative values of c – i.e., $c > 0$.

The curvaton field should always be positive during the slow roll, therefore $\sigma_q > 0$, resulting in the blue dotted line in Fig. 4.1. This condition is, however, less strict and does not contribute since it is always below the red line.

The last constraint comes from the condition on the curvaton evolution. We want the field to move towards the minimum of the potential at $\sigma = 0$, hence σ_q should never be greater than σ_k , which gives the purple dash-dotted curve in Fig. 4.1. To sum up, the system of constraints reads

$$\begin{aligned}
&\text{if } 0 < c < \frac{2}{\sigma_{\max}^2} \quad , \quad -c\sigma_{\max} < b < 0 \\
&\text{if } \frac{2}{\sigma_{\max}^2} < c < \frac{6e-6}{\sigma_{\max}^2} \quad , \quad -\sqrt{2c} < b < 0 \\
&\text{if } \frac{6e-6}{\sigma_{\max}^2} < c < c_{\max} \quad , \quad -\sqrt{2c} < b < \frac{2e-2}{\sigma_{\max}} - \frac{1}{3}c\sigma_{\max} \\
&\text{where } c_{\max} \equiv \frac{3}{\sigma_{\max}^2} \left(1 + 2e + \sqrt{12e-3}\right) .
\end{aligned} \tag{4.38}$$

As a result, we conclude that the higher the value of σ_{\max} , the smaller the allowed parameter region for (b, c) . In other words, low values of σ_{\max} alleviate the possible fine-tuning of models.

4.5.1 Example A: $b = -20/e$, $c = 216/e$

In order to show the behavior of the non-Gaussianities parameter, in this section we study a concrete example by fixing $b = -20/e$ and $c = 216/e$. These values are well within the allowed parameter region (see Fig. 4.1), and they make the difference between the value $\sigma_q'' = 0$ for the ansatz and that for the reconstructed solution small. Notice that these values of b and c extrapolate the current observational limits of f_{NL} and g_{NL} (see Ref. [52] and Fig. 4.6). However, they are suitable for studying the main features of the model. In Sec. 4.7 we discuss the observational constraints of b and c . Let us first compute the curvaton potential [Eq.(4.36)]. To determine the value of V_0 , we require that $V(0) = 0$ – i.e.,

$$V_0 \equiv \frac{2b(3c-b^2)}{3c^2\sqrt{2c-b^2}} \tan^{-1} \left(\frac{b}{\sqrt{2c-b^2}} \right) - \frac{\log 2}{3c^2} (2c-b^2) \tag{4.39}$$

which gives $V_0 \sim 0.016$ for the chosen values of the parameters. The Taylor expansion of the potential (4.36) at $\sigma = 0$ reads

$$V(\sigma) = \frac{m^2\sigma^2}{2} - b \frac{m^2\sigma^3}{6} + \mathcal{O}(\sigma^4) \quad , \tag{4.40}$$

confirming that indeed the potential can be approximated by a quadratic potential close to the origin. In Fig. 4.2 we show the results of our procedure. The top panel of Fig. 4.2 displays the potential constructed from the ansatz [Eq. (4.35)], while in

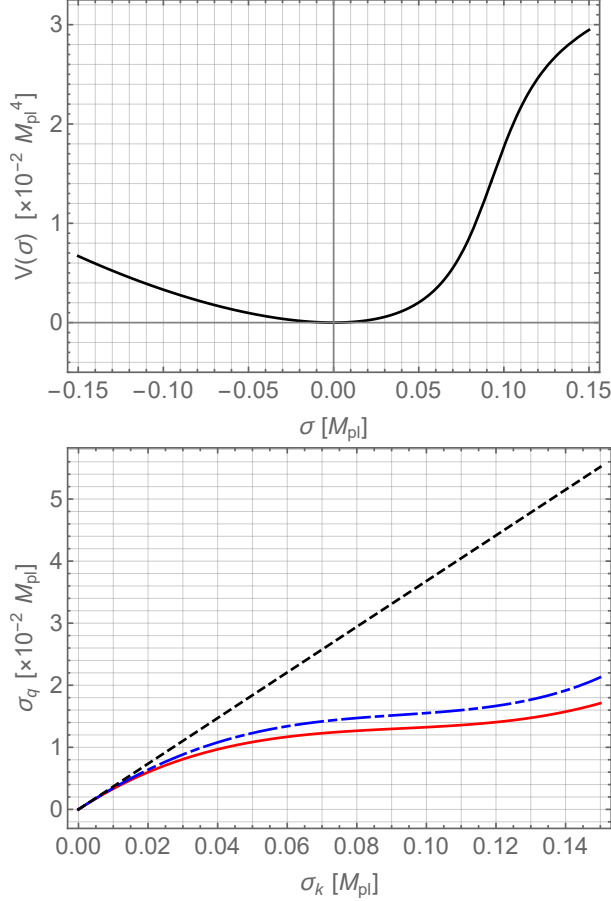


Figure 4.2: Top: curvaton potential $V(\sigma)$ for example A, where $b = -20/e$, $c = 216/e$. The inflection point is located at $V_{\sigma\sigma} = 0$. Bottom: reconstructed (blue dash-dotted line), ansatz (red solid line), and quadratic potential (black dashed line) solutions for the curvaton slow-roll equation results in terms of σ_k .

the bottom panel we compare three solutions: the one coming from the reconstructed potential, the original ansatz, and the solution for the quadratic potential $V(\sigma) = m^2\sigma^2/2$.

Note that the field solution has no maximum or minimum, which guarantees that its velocity is never zero as constructed. The non-Gaussianity parameter f_{NL} is computed in the top panel of Fig. 4.3, top panel. The shape of the original ansatz and the reconstructed solution agree, but with a small difference in the amplitude. Therefore, we managed to recreate the behavior for f_{NL} as desired. The agreement between the two results grows⁶ the closer the choice of parameters is to $b = -\sqrt{2}c$; see Fig. 4.4. However, such a choice also implies stronger non-Gaussianity and running $n_{f_{\text{NL}}}$, beyond the allowed values given by recent observations.

Figure 4.3 also shows the behavior of the g_{NL} parameter in the bottom panel. It has

⁶The results become more alike as the point of their change of sign tends toward $-b/c$.

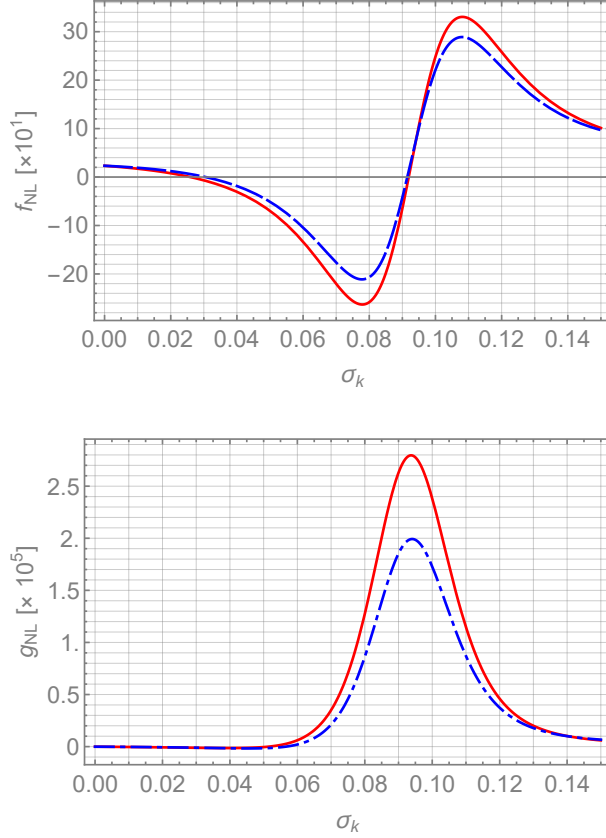


Figure 4.3: Top: reconstructed f_{NL} (dash-dotted) parameter for example A in comparison to the ansatz (solid) with $b = -20/e$ and $c = 216/e$. Bottom: the same for g_{NL} .

an extreme at $\sigma_{\text{osc}}'' = 0$, and since the first term of Eq. (4.17) dominates, it has σ_{osc}''' constant at the extreme. Note that with our choice of parameters, the magnitude of the g_{NL} is close to the current observational limit, which is $g_{\text{NL}} \approx 5 \times 10^5$.

The authors of Ref. [217] analyze the relationship between the features in the curvaton potential and a large running of the scalar spectral index. However, they make no explicit connection between features and the change of sign of f_{NL} and η_σ , as in Sec. 4.4.3. For our model, recalling Eq. (4.32), we have

$$\eta_\sigma = \frac{2m_\sigma^2}{3H_\kappa^2} - \frac{4r_{\text{dec}}}{5} \bar{\eta}_\sigma \left(f_{\text{NL}} + \frac{5}{3} + \frac{5r_{\text{dec}}}{6} \right) \quad (4.41)$$

The CMB constrains η_σ to be of order 10^{-2} where f_{NL} changes sign, but the former also depends on the inflationary scale. In turn, to constrain the value of H_k we need to evaluate the spectral index and the amplitude of the perturbations, eq. 4.9. In fact, we should also include the physics of the reheating [210]. Therefore, in the present analysis

we will not fix H_k . To circumvent this issue, we plot f_{NL} together to $V_{,\sigma\sigma}$. As argued in Sec. 4.4.3 and also in Ref. [217], for large values of f_{NL} we have $f_{\text{NL}} \propto -\eta_\sigma$.

We show that a feature on $V(\sigma)$ induces a change of sign in σ'' – i.e., a feature on the solution $\sigma_q(\sigma_k)$. The converse is also true: if we start with an ansatz in which $\sigma'' = 0$ somewhere, there will be a change of sign in the reconstructed $V_{,\sigma\sigma}$. The same goes for f_{NL} . We conclude that features are shared by these different observables.

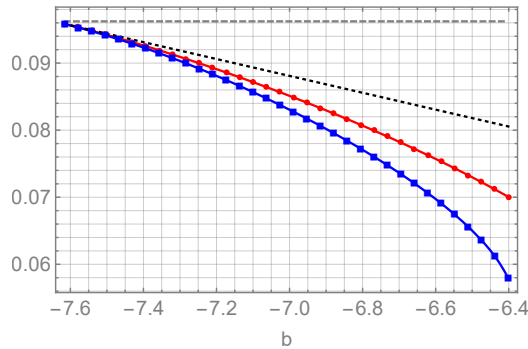


Figure 4.4: Numerically computed zeros of f_{osc} , as a function of b , from ansatz (red, circle) and reconstructed (blue, square) solutions. The ratio $-b/c$ is the black dotted line, while the ratio $b = -\sqrt{2c/e}$ is the gray dashed line. $c = 216/e$.

We have also already demonstrated that the change of sign for the ansatz f_{osc} and $V_{,\sigma\sigma}$ happens in different scales. In Fig. 4.5 we show that, even for the reconstructed f_{osc} , the zeroes of those functions are symmetric around the point where $f_{\text{osc}} = V_{,\sigma\sigma}$. For f_{osc} the zero is located before $\sigma = -b/c$, while for the second derivative of the potential it happens after this value. We can also see what is indicated in Eq. (4.32): when we choose the pivot scale to be where $f_{\text{NL}} = 0$, we have $\eta > 0$.

4.6 Producing the CMB Anomalies

The scale dependence of f_{NL} can be explicitly written by expanding the integral $\mathcal{I}(t_q, t_k)$ [see Eq. 4.24] in terms of $\log(k/k_0)$. The pivot scale k_0 is defined as the value at which $f_{\text{NL}} = 0$. Near the pivot scale, we have

$$\mathcal{I} = \log(k/k_0) [1 + \epsilon_0 \log(k/k_0)] \quad , \quad (4.42)$$

where ϵ_0 is the inflationary first slow-roll parameter at the pivot scale. Note that this

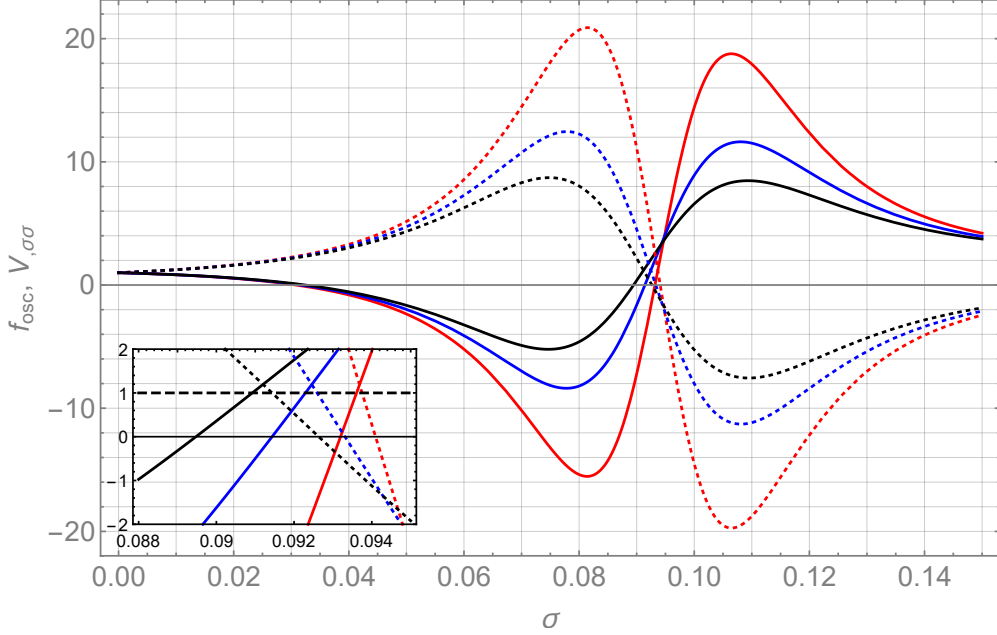


Figure 4.5: Reconstructed f_{osc} (solid lines) and $V_{\sigma\sigma}$ (dotted lines) for varying b , $a = 1/e$, and $c = 216/e$. Their magnitudes grow with $|b|$. The distance between the crossing position decreases with growing $|b|$ for the chosen parameter range. In the highlight, we show the point where both are equal, which happens for a value a bit above $V_{\sigma\sigma} = 1$.

modification makes f_{NL} depend on $\bar{\eta}_\sigma$ as well. The reconstructed solution for f_{NL} and g_{NL} can then be written in terms of $\log(k/k_0)$; see Fig. 4.6 below. Differently from Eq. (4.20), around the pivot scale for our model the f_{NL} parameter is best described by a log parametrization; see Ref. [54].

As we vary the parameters b and c , we see that the scale dependence of both nonlinear parameters changes. Higher values of $|b|$ enhance the non-Gaussianities of the scalar perturbations. On the other hand, higher values of c result in lower values for f_{NL} and g_{NL} . We illustrate the behavior for variations on b in Fig. 4.6

As is known, models with scale-dependent non-Gaussianities can account for the CMB anomalies as, for instance, the dipolar modulation [53, 54, 190, 204, 201]. Indeed, the model analyzed in Refs. [53, 204] uses the non-Gaussianities to couple short- and long-scale modes to produce the hemispherical asymmetry. The presence of long (super-Hubble) modes of wavenumber k_l can modulate the Bardeen power spectrum on short scales (inside the horizon). In such a model, the Universe remains isotropic, since the dependence on k appears only due to the mode coupling. These models have the advantage, compared to Ref. [203], that there is no need for a large amplitude of the super-Hubble perturbations [204].

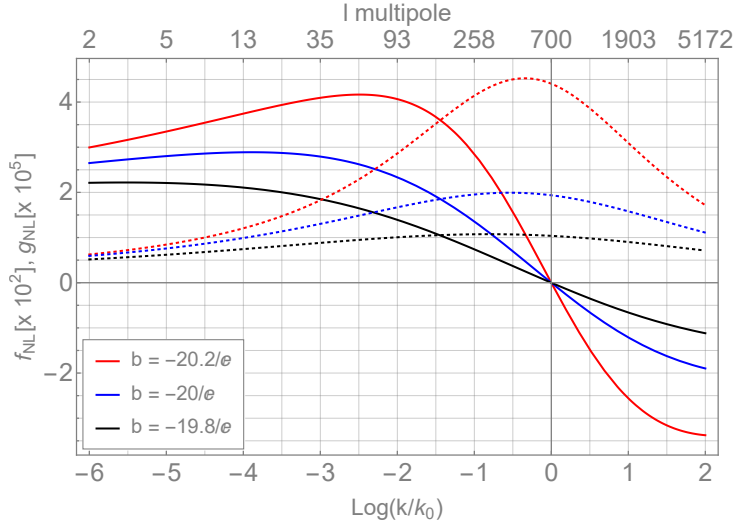


Figure 4.6: Non-Gaussianity parameters f_{NL} (solid lines) and g_{NL} (dotted lines) for the model example A. We vary b by $\pm 10\%$. The slow-roll parameters were chosen as $\epsilon_0 = 1/128$ and $\bar{\eta}_\sigma = 0.01$. k_0 is the pivot scale 0.05Mpc^{-1} , defined as the scale at which $f_{\text{NL}} = 0$.

The scale dependence of the dipolar modulation roughly follows that of f_{NL} [204]. Thus, we expect f_{NL} to peak at $\ell < 64$. This provides a new source of observational constraint, which helps in constraining the parameters of non-Gaussian models. In Fig. 4.6, we show the behavior of f_{NL} for different values of b and c . Varying the parameters b and c changes the position of the peak of f_{NL} . Most recent observational results indicate the hemispherical asymmetry to be $A \approx 0.072$ for $\ell < 64$ [18, 47]. For shorter scales it reduces to $A < 0.0045$, for $\ell > 600$ [194, 218]. The region of the parameter space which provides a peak for larger scales is preferred; otherwise, the asymmetry would be too high for smaller scales. That is particularly relevant for the quadrupole asymmetry [193, 219, 220]. It is also important to note that the spectral index is modulated in scenarios in the case that the non-Gaussianity is scale-dependent [204], which presents another probe for f_{NL} and its effects.

Scale-dependent non-Gaussianity can also lead to bias in the cosmological parameter estimation based on the CMB, especially in the presence of scale-dependent trispectrum [201]. Depending on the magnitude and scale dependence of the trispectrum, the bias on the spectral index n_s can reach the order of 10^{-2} , which is of the same order as the expected value of η_σ . Therefore, in different scenarios for non-Gaussian modulation, it is necessary to take into account all effects arising from the scale dependence from both the bispectrum and trispectrum, to rightly access the constraints on the system's parameter

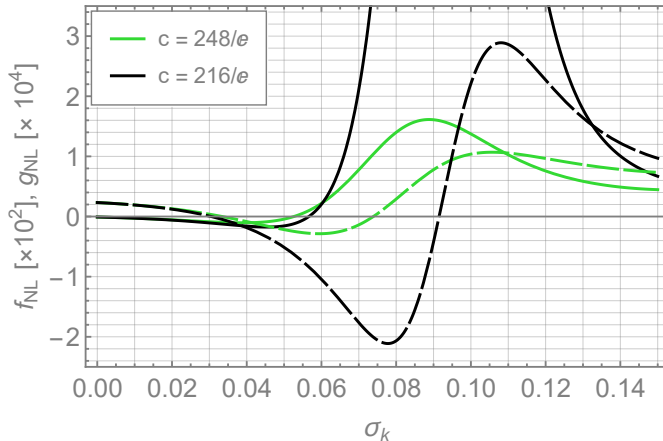


Figure 4.7: Non-Gaussianity parameters f_{NL} (dashed lines) and g_{NL} (solid lines) for $b = -20/e$ and different values of c . Note that a change in c causes g_{NL} to drop below the observational constraints – i.e., $g_{\text{NL}} = (-5.8 \pm 6.5) \times 10^4$.

space.

So far we have focused on building models in which the reconstruction procedure detailed in Sec. 4.4.2 is well behaved, meaning that the point where f_{NL} changes sign is the closest possible between the ansatz and reconstructed solution. However, discordance between the two solutions does not mean the choice of parameters is wrong. Such models may not agree with Eq. (4.35), but they still provide a scale dependence and magnitude for f_{NL} that fits observational constraints. Therefore, the theoretical predictions from the whole parameter space in Fig. 4.1 should be tested in comparison to observations.

4.7 Results on the non-Gaussianities and CMB anomalies in curvaton models

We have presented a procedure to reconstruct the curvaton potential from the non-Gaussianity parameter f_{NL} . Assuming a slow-roll dynamic for the curvaton field, our procedure gives the curvaton potential that produces the desired f_{NL} [more precisely the σ_{osc} , hence f_{NL} see Eq. (4.16)].

Planck’s latest results indicate that cosmological perturbations at the pivot scale are highly Gaussian, $f_{\text{NL}}^{\text{local}} = -0.9 \pm 5.1$ [52]. That can be true for truly Gaussian fluctuations or scale-dependent f_{NL} . The latter satisfies the observational constraints if f_{NL} crosses zero close to the pivot scale but allows for higher values of non-Gaussianity for other scales.

We exemplified our method by devising a curvaton model that results in a scale-dependent f_{NL} that changes sign twice and is bounded from above and below. In this manner, the non-Gaussianities have the desired features at the CMB pivot scale and avoid issues with the large scales probed by LSS surveys.

Scale-dependent non-Gaussianities are also known to be able to produce the hemispherical asymmetry observed in the CMB, in particular via non-Gaussian coupling between scalar modes [53]. Using the fact that our model predicts a peak in the f_{NL} parameter for scales larger than the pivot scale, we showed that it is possible to constrain the model using the asymmetry. If the peak is located towards higher values of ℓ , constraints on the asymmetry are violated, which shows that the model should not predict a peak for f_{NL} located at $\ell > 64$. Note that our reconstructed model has the correct scale dependence for f_{NL} – i.e., it grows towards larger scales/lower ℓ . That is an advantage with respect to other curvaton models in the literature that commonly have the opposite scale dependence.

In Sec. 4.5.1 we used $b = -20/e$ and $c = 216/e$ for the two parameters of the model in Eq. (4.35). As already mentioned, these values produce f_{NL} and g_{NL} larger than the latest Planck observational constraint, $f_{\text{NL}} = -0.9 \pm 5.1$, $g_{\text{NL}} = (-5.8 \pm 6.5) \times 10^4$. However, as Fig. 4.7 shows a small increase in c already drops f_{NL} and g_{NL} below the observational constraints (and this applies similarly to the parameter b). Therefore the model on Fig. 4.7, with parameters $b = -20/e$ and $c = 248/e$, satisfies the Planck constraints [52]. It is worth noting that the Planck bounds for the nonlinearity parameters f_{NL} and g_{NL} are constructed considering a f_{NL} parameter that satisfies a power law [Eq. 4.20] and a scale-independent g_{NL} . That is not true for our model, so the available constraints for both parameters may not be directly applied.

In order to adequately fit the parameters of the model with the observations we need to consider additional effects present beyond first- and second-order scalar perturbations. In addition to the amplitude of perturbations and its spectral index (and subsequent running), in our scale-dependent curvaton scenario, the observational constraints also apply to the reheating scale (which is present in r_{dec} , since it depends on Γ , which for the sudden decay approximation will have the same value as $H_{\text{reh.}}$). Thus, we have five free parameters: two from inflation H_k and $H_{\text{reh.}}$, and three from the parametrization, a , b , and c . The value of H_k is especially important, since it enters in the computation of $\bar{\eta}_\sigma$.

A numerical analysis is needed to precisely constrain the parameter space of the model. Our analytical computations do not consider the reheating process, which can slightly change scales for the crossings, as well as the amplitude of the nonlinearity parameters. It will be interesting to compute all these effects and by-products such as a modulation on the spectral index and a bias on cosmological parameter estimation.

Chapter 5

Bouncing Curvaton Scenario

In this chapter we construct a bouncing cosmology where the universe consists of a matter-like fluid plus a curvaton-like scalar field. First, we introduce the de Broglie-Bohm quantum cosmology. We analyze a matter-dominated contracting universe, its background evolution and cosmological perturbations for both fluid and a generic scalar field. Then, we analyze the predictions for two different scalar fields; first a negative Mexican hat scalar field potential, and then a modified version of it. Finally, we summarize the preliminary results of this work in progress.

5.1 Introduction

Multi-field inflationary models help to alleviate constraints on the inflaton field, as we have seen in the case of the curvaton scenario on Chapter 4. Chaotic inflation fields, such as those with $\bar{V} \propto \varphi^2$, do not respect the most recent observations if inflation is single field. However, in the curvaton scenario, those fields can play the role of the inflaton while the system still respect the latest Planck results [29], thanks to the curvaton field. The presence of an additional field has physical effects, as the presence of (scale-dependent) non-Gaussianities, that would help explain the existence of the CMB anomalies. Combining such advantages could make multi-field inflationary models favored by most recent data, in comparison to single-field models.

Curvaton models make use of the entropic mechanism. Multi-field scenarios must take into account the production of perturbations through this phenomenon [24]. The main challenge of early universe models that use the entropic mechanism is to devise a way in

which the entropy perturbations transform into or induce adiabatic modes. That requires large entropy perturbations and the presence of non-adiabatic pressure [49].

As we have presented in 4.3.1, the curvaton scenario of inflation generates a non-adiabatic pressure during the curvaton field decay. Ekpyrotic models [112, 113, 114, 115, 221, 222] generally make use of a turning in the trajectory near the bounce point. During this period, the background evolution has a larger contribution from $\dot{\sigma}$ – i.e., its trajectory in field space turns, leading to $\dot{\theta} \neq 0$. That implies in the growth of \mathcal{R} , see (2.62).

Likewise, multi-component scenarios could alleviate the conditions on the matter-like fluid, or scalar field, responsible for the quasi-matter domination on bouncing cosmologies (such as in the model presented in Chapter 3). In addition, they could present richer phenomenology, including once again (scale-dependent) non-Gaussianities and the prediction of CMB anomalies.

Curvaton-like mechanisms in the matter bounce scenario have been developed [61, 116]. As the models of ekpyrotic contraction, there will be a light field – the curvaton – responsible for the entropy perturbations, while the matter domination is due to the other(s) component(s). An interesting feature found in those kinds of models [61] is the kinetic amplification of entropy perturbations in the bounce phase, that only affects the scalar perturbations. It justifies a low tensor-to-scalar ratio, as the tensor perturbations do not suffer the same amplification as their scalar counterparts.

Contrary to the case of two or more fields, fluid and field perturbations do not mix [108]. Therefore, a natural question arises. Is it possible to construct a curvaton-like bouncing scenario without resorting to the entropic mechanism by using a matter fluid? A scenario like this would be analogous to the mixed inflaton-curvaton scenario [207, 208, 223], where both fields contribute to the scalar perturbations, differently from the single-source curvaton models previously mentioned. Furthermore, can this scenario present more advantages than the simplest matter bounce models or the multi-field case? Can it explain the existence of CMB anomalies as well?

This chapter presents the preliminary work on the construction of a mixed fluid-field bouncing cosmology. It is a first step to analyze the phenomenology of multi-component models. We have chosen the de Broglie-Bohm bouncing cosmology, dominated by a matter fluid, as the background of our model. First, we present the solutions for background and fluid perturbations. Then, we compute the scalar perturbations for a scalar field

in a bouncing cosmology. We make the assumption that the scalar field rolls-down its potential in a slow-roll, in order to preserve the condition that $\eta_\sigma \ll 1$. The vacuum initial conditions are an important topic, that we cover in detail. Then, we present the results for the total mixed power spectrum and spectral index. Finally, we analyze the cases of a particular scalar field and one modification of it. They have been chosen to make the spectral index red-tilted, and we analyze what are the conditions for that to happen. We conclude with our preliminary results for the mixed fluid-field bouncing cosmology.

5.2 de Broglie-Bohm Scenario

The de Broglie-Bohm scenario of quantum cosmology [7] has been developed over the last few years with great success [177, 224, 5, 76, 86]. There, the classical background contraction can be given by a fluid, such as dust and radiation, or a scalar field. However, after the universe contracts enough, quantum effects start to kick in. The Wheeler-deWitt approach can be used for the computations, however it is necessary to resort to a different interpretation of quantum mechanics, as the Copenhagen interpretation is not valid for quantum cosmology. By using the de Broglie-Bohm interpretation of quantum mechanics [225, 226, 227], one makes use of the well-defined Bohmian trajectories, which allow for the computation of the evolution of the scale factor in quantum scales. By doing so, a non-singular bounce is found.

Many works have been developed in the area, which analyzed how different fluids and fields lead to bouncing cosmologies in the de Broglie-Bohm context [175]. In our work, we analyze a background with a perfect fluid modeled by a scalar field, as it was done in the Sec. 2.2 of Ref. [86], plus a generic scalar field, which is decoupled to the fluid. Therefore, we can compute their perturbations separately.

5.2.1 Background Evolution

The canonical quantization of the mini-superspace model describes a contracting universe that possesses a non-singular bounce (the proof can be seen in [86]).

The solution of the Bohmian trajectories results in the following scale factor

$$a(T) = a_b \left[1 + \left(\frac{T}{T_b} \right)^2 \right]^{\frac{1}{3(1-\omega)}} \quad (5.1)$$

where the time variable T is related to the cosmic and conformal time by $dT = a(t)^{-3\omega} dt = a(\eta)^{-3\omega+1} d\eta$. The subscript b represents the variables at the bounce, where T_b represents the time scale of the bounce (and it is related to the width of the Gaussian wave-function of the universe) and a_b is the value of the scale factor.

The Friedmann equation for this fluid-dominated universe, in the classical regime, is

$$H^2 = \frac{1}{3} \rho_f. \quad (5.2)$$

Away from the bounce, we consider the limit $T \gg T_b$, which results in the expected evolution of a classical universe dominated by a matter-like fluid with equation of state ω . That is valid for both before and after the bounce.

5.2.2 Cosmological Perturbations

The computation of cosmological perturbations for a dBB quantum cosmology is rather similar to the classical case. We instruct the reader to read Ref. [86] for a thorough derivation of the Mukhanov-Sasaki equations for both fluids and fields in dBB cosmology. In this section, we present and analyze the final expressions for them, and, to conclude, show their results for the scalar perturbations.

For a perfect fluid with equation of state ω , the Mukhanov-Sasaki equations for the variable $v_k(\eta) = a\delta\varphi$ is

$$v_k'' + \left(\omega k^2 - \frac{a''}{a} \right) v_k = 0 \quad (5.3)$$

For the relevant cases we study, we leave the computations for Appendix C. For the perfect fluid case, computed in C.1, the power spectrum and its spectral index are (C.34) and (C.36), repeated below,

$$\mathcal{P} = \frac{\bar{k}^3}{2\pi^2} |\zeta|^2 = A^2 k^{3-\frac{3(1-\omega)}{1+3\omega}} \quad (5.4)$$

$$n_F - 1 = \frac{12\omega}{(1+3\omega)} \approx 12\omega > 0. \quad (5.5)$$

As for the scalar field, we need its full evolution in order to compute the amplitude of the perturbations. However, the spectral index can be computed, resulting in (C.37),

$$n_\sigma - 1 = 3 - 2\nu_\sigma = 3 - 2\sqrt{\nu_F^2 - \frac{12\eta_\sigma}{(3\omega + 1)^2}} \quad (5.6)$$

The amplitude of the perturbations can only be numerically computed model by model, as we need the whole evolution of the field, from the contracting to the expanding phase, including the solution across the bounce.

5.2.3 Initial Conditions for the Perturbations of Massive Fields

We now discuss whether the massive curvaton fields, in the far past, have dominant or subdominant mass terms in the Mukhanov-Sasaki equation.

Following the results in the dBB context, from [5], but including the scalar field potential in the equations of motion, we have

$$v_k'' + \left(k^2 - \frac{a''}{a} + m_\sigma^2 a^2 \right) v_k = 0 \quad (5.7)$$

where $m_\sigma^2 = V_{\sigma\sigma}$. In the far past limit, we have

$$v_k'' + \left(k^2 + \frac{1}{\eta^2} \frac{2(3\omega - 1)}{(3\omega + 1)^2} + \frac{1}{\eta^2} \frac{12\eta_\sigma}{(3\omega + 1)^2} \right) v_k = 0 \quad (5.8)$$

where $\eta_\sigma = V_{\sigma\sigma}/3H^2$.

In order to solve this equation, we need to consider its different regimes, including the nature of the vacuum of curvaton perturbations. If η_σ is small enough throughout the whole evolution, as a typical slow-roll regime requires, we can solve the equation of

motion for the perturbations just as for the curvaton during inflation. In this case, every mode is inside the horizon, and the k^2 term dominates in the far past. Therefore the vacuum state of the perturbations is just the Bunch-Davies vacuum.

However, even if $|\eta_\sigma| \gg 1$, it is still possible to have a Bunch-Davies vacuum. The condition is that η_σ/η^2 should decrease as we go to the far past, where the initial conditions are set. In this case, once again the k^2 term dominates and, therefore, a Bunch-Davies vacuum is present. That is the case of our working model 5.4.

An analogous situation happens in [61], where the η_σ parameter is constant. This is possible because η_σ is proportional to the square of the ratio between their main field ϕ and the Hubble parameter, which is itself proportional to ϕ , giving a constant η_σ . Their result is similar to inflationary models thanks to this behavior of the curvaton mass.

However, when $V_{\sigma\sigma}a^2$ is non-zero and dominant in the far past, the situation changes. In such a case, the vacuum is no longer a Bunch-Davies state. The WKB approximation is needed, such that an adiabatic vacuum still exists. The adiabatic initial conditions are defined for the effective frequency $w_k^2 = k^2 + V_{\sigma\sigma}a^2$. As it has been shown in the matter bounce curvaton scenario using two fields [116], the adiabaticity condition is satisfied, $|w'_k/w_k^2| \ll 1$, so that the perturbation has an asymptotic solution at the far past that rapidly oscillates with frequency w_k . That changes the scale-dependence of perturbations in comparison to the usual Bunch-Davies case, and one needs to resort to numerical computation of the vacuum initial conditions.

In addition, it might be the case that k^2 dominates in the far past, but the perturbations are not squeezed, because the mass term dominates over a''/a . We do not desire such situations, because then the amplitude of the perturbations is highly damped given its oscillatory behavior – the mass term is positive so that the Mukhanov-Sasaki equation will be analogous to that of a harmonic oscillator.

5.3 Mixed Fluid-Curvaton Bouncing Scenario

5.3.1 Background Evolution

The system we study is constituted of a perfect fluid and a classical scalar field. For the perfect fluid, the equation of state $p = \omega\rho$ is satisfied, where ω is a constant. The scalar field is considered to be subdominant in the background throughout the whole dynamics.

The background solution follows that of Section 5.2.1, equation (5.1).

5.3.2 Mixed Fluid-Field Perturbations

In a system with a fluid and a scalar field, the perturbations could, in principle, be adiabatic or non-adiabatic. It all depends on the equation of state from both matter contents. As stated for the curvaton field during inflation, non-adiabatic pressure appears only when the curvaton behaves like matter, while the inflaton has already decayed into radiation.

Following the results of [108], we conclude that there is no entropy component when the fluid behaves as pressureless dust ($\omega_F \approx 0$) and the scalar field is in a slow-roll evolution ($\omega_\phi \approx -1$).

Then, we need to sum the contributions to the total curvature perturbation from each component. From [228], for a non-interacting mixture of fluid and scalar field we get

$$\zeta_T = \sum_{\alpha} \frac{\dot{\rho}_{\alpha}}{\dot{\rho}} \zeta_{\alpha}, \quad (5.9)$$

$$\mathcal{R}_T = \sum_I \frac{\rho_I + P_I}{\rho + P} \mathcal{R}_I. \quad (5.10)$$

Therefore, it is straightforward to compute the total curvature perturbations, following the individual results for each component.

5.3.3 Mixed Perturbations

The amplitude of perturbations is presented on C.1. We assume the scalar field follows a slow-roll throughout the whole background evolution. Any scalar field potential we use must result in a slow-roll evolution during contraction and through the bounce as well. It is of interest to generalize this result in future works.

We directly quote the results from the Appendix C.1 below. First, for the power spectrum,

$$\mathcal{P}_{\mathcal{R}} \approx W^2 \omega^{-\nu_F} \left[\frac{3(1+\omega)}{2\omega} \right] k^{3-2\nu_F} + \frac{W^2}{9} \left[\frac{\dot{\sigma}^2}{H^2} \right] \left[\frac{3(1+\omega)}{2\omega} \right]^2 k^{3-2\nu_{\sigma}} \quad (5.11)$$

Then we show that the spectral index is

$$n_{\mathcal{R}} - 1 = G(n_F - 1) + (1 - G)(n_\sigma - 1) \quad (5.12)$$

$$G = \frac{\omega^{-\nu_F}}{\omega^{-\nu_F} + \frac{1}{9} \left[\frac{\dot{\sigma}^2}{H^2} \right] \left[\frac{3(1+\omega)}{2\omega} \right]} \quad (5.13)$$

This result is valid for any scalar field whose vacuum initial conditions is Bunch-Davies, and whose evolution follows a slow-roll.

5.4 Negative Mexican Hat Potential Model

5.4.1 Background

In this section, we analyze a curvaton field potential of the form

$$V(\sigma) = -\frac{\lambda}{m}\sigma^m + \frac{\beta}{2m}\sigma^{2m} \quad (5.14)$$

where $m > 2$, $\lambda, \beta > 0$. Scalar potentials like that have a local maximum at $\sigma = 0$. We consider the case that the field starts exactly at this local maximum, and therefore we can approximate the potential as only the first term in (5.14).

Under these circumstances, for a contracting universe whose background is dominated by a perfect fluid with an equation of state $p_F = \omega\rho_F$, we have

$$\ddot{\sigma} + \frac{2}{1+\omega} \frac{\dot{\sigma}}{t} - \lambda\sigma^{m-1} = 0 \quad (5.15)$$

This equation allows for an analytical solution,

$$\sigma = \frac{D}{t^{\frac{2}{m-2}}}, \quad (5.16)$$

$$\lambda = \frac{D^{2-m}}{(m-2)^2} \left[\frac{2m(1+\omega) - 4(m-2)}{1+\omega} \right] \quad (5.17)$$

In such a case, we can compute the η_σ parameter as

$$\eta_\sigma = \frac{V_{\sigma\sigma}}{3H^2} = \frac{3(m-1)(1+\omega)}{4(m-2)^2} [4(m-2) - 2m(1+\omega)] \quad (5.18)$$

We note that the above η_σ parameter is constant in time, and will be so for every $m > 2$. We note that the exact case $m = 2$ results in a divergent η_σ .

5.4.2 Scalar Field Cosmological Perturbations

Let us now analyze the mass term $V_{\sigma\sigma}a^2$. During matter domination, $t^{2/3} \propto \eta^2$, and therefore $a(\eta)^2 \propto \eta^4$. Following the solution (5.16), we can write the evolution $V_{\sigma\sigma}$ for any polynomial potential as

$$\begin{aligned} V_{\sigma\sigma} &= -\lambda(m-1) \left(\frac{D}{t^{\frac{2}{m-2}}} \right)^{m-2} \\ &= \lambda(m-1) D^{m-2} \eta^{-6} \end{aligned} \quad (5.19)$$

Hence the mass term behaves as

$$V_{\sigma\sigma}a^2 \propto \eta^{-2}. \quad (5.20)$$

Therefore, for every polynomial potential in which $m > 2$, we have that the mass term decays with η^{-2} , just like the horizon term for matter domination. It means that, in the far past, the k term dominates the Mukhanov-Sasaki equation, and the initial conditions for the cosmological perturbations are the Bunch-Davis vacuum, as we have detailed in 5.2.3. We note that this could have been noted when we analyzed η_σ , (5.18). As previously mentioned, since this term is constant in time, we can use the results of section C.1.1.

Therefore, we can define the parameter B as the sum horizon and mass terms and write the Mukhanov-Sasaki equations as

$$v_\sigma'' + \left(k^2 - \frac{B}{\eta^2}\right)v_\sigma = 0 \quad (5.21)$$

The value of B for the present model is

$$\begin{aligned} B &= \frac{a''}{a} - V_{\sigma\sigma}a^2 \\ &= 2 \frac{m^2(-8 - 3 + 9\omega^2) + m(41 + 48\omega - 9\omega^2) - 48\omega - 32}{(m-2)^2(1+3\omega)^2} \end{aligned} \quad (5.22)$$

In order to find a scale-invariant spectrum for the curvaton, we must have $B = 2$, which is the trivial case where no curvaton field is present (which contradicts the finding that η_σ diverges). It also happens for $m = 4$ when $\omega = 0$, as the coupling parameter in (5.17) will also be null, $\lambda = 0$.

For a red-tilted power spectrum, by comparing (5.21) with (C.5) and (C.37), we conclude that $B > 2$. That is possible when the mass term is sufficiently negative, so that the second term in the RHS of (C.37) dominates over the first – which is positive, given that $0 < \omega \ll 1$ for a dust dominated contracting universe.

5.4.3 Cosmological Perturbations: Fluid + Field

The total cosmological perturbations for a universe constituted by a fluid and a scalar field is given by (5.9) and (C.52). Due to the fluid's perturbation equations being dependent on the fluid sound velocity c_s^2 , the modes will leave the horizon much sooner than the perturbations from the curvaton field. Therefore, the fluid perturbations' amplitude is amplified, in contrast to the curvaton perturbations. That can be seen using (C.57): the constant G is extremely close to 1 in the studied universe, where $\omega \ll 1$, $\nu_F \approx 3/2$, $\rho_F \gg \rho_\sigma$. Hence, we expect the final power spectrum to be closely related to the fluid, so that the spectral index will be blue-tilted just like the fluid perturbations, see (C.56).

This situation indicates that, for the total power spectrum to be red-tilted, we have two options. One it to use a scalar field with larger magnitude, which would violate the conditions we pose for the contraction universe – we suppose that the field is subdominant in comparison to the fluid. The other option is to have a field power spectrum that is

strongly red-tilted, counterbalancing (C.56) in such a way that the final result is lightly red-tilted as we observe in the CMB.

Such a strongly red-tilted power spectrum can be obtained once we consider $\eta_\sigma \ll 0$. That is possible for $m = 2 + \epsilon$, where $\epsilon \ll 1$. We analyze this case in the next section.

5.5 Revisiting the Negative Mexican Hat Model: Corrections to the case $m = 2$

We now reconsider the negative Mexican hat potentials for the case where $m = 2 + \epsilon$, where $\epsilon \ll 1$. For this choice of m , both η_σ and B are well-behaved.

When we expand the potential $V = -\frac{\lambda}{2+\epsilon}\sigma^{2+\epsilon}$ for small values of ϵ , we get

$$V \approx -\frac{\lambda}{2}\sigma^2 \left(1 - \frac{\epsilon}{2} + \epsilon \log \sigma\right). \quad (5.23)$$

The form of such potential reminds us of Coleman-Weinberg corrections [229] to scalar fields, which happens in some early universe models such as Higgs Inflation [230, 231, 232], but is mainly a feature of the Coleman-Weinberg inflationary universes [233, 234, 235]. This correction entails the change in the coupling constant given quantum effects and is generally proportional to $\log(V_{\chi\chi}/\mu)$, where χ is a scalar field and μ is the renormalization scale.

In [236], the authors chose a model-independent approach to the corrections of λ , which result in an expansion on powers of $\log(\chi)$. That is the closest we have found to the expansion of the $m = 2 + \epsilon$ model, and suggests that the correction we use is well-motivated.

Following equations (C.56) and (5.18), we conclude that such a correction is responsible for the large value of the red-tilt for a curvaton field.

5.5.1 Background

According to the previous results, for $m = 2 + \epsilon$ the λ coupling function will be given by

$$\begin{aligned}
\lambda &= \frac{2(2+\epsilon)(1+\omega) - 4\epsilon}{\epsilon^2(1+\omega)} D^\epsilon \\
&\approx \frac{4+4\omega-2\epsilon}{\epsilon^2(1+\omega)} D^\epsilon \\
&\approx \frac{4}{\epsilon^2} D^\epsilon \\
&\approx \frac{4}{\epsilon^2} + \frac{4}{\epsilon} \log D,
\end{aligned} \tag{5.24}$$

where, in the above computation, we used the fact that both $\omega, \epsilon \ll 1$, at different passages.

In addition, using the solution for σ , (5.16), we have that

$$\sigma = \frac{D}{t^{2/\epsilon}} \tag{5.25}$$

Using both results, we can compute the potential $V(\sigma(t))$ and its evolution on time

$$V = \frac{\lambda}{2+\epsilon} \sigma^{2+\epsilon} \tag{5.26}$$

$$\approx 2 \frac{D^\epsilon}{\epsilon^2} \left(\frac{D}{t^{2/\epsilon}} \right)^{2+\epsilon} \tag{5.27}$$

$$\approx 2 \frac{D^2}{\epsilon^2} \frac{1}{t^{4/\epsilon}} \tag{5.28}$$

We see that, for the remote past, the curvaton potential is extremely small, which guarantees that it will be subdominant with respect to the dust-like perfect fluid.

The η_σ parameter can also be computed for the present case, leading to

$$\begin{aligned}
\eta_\sigma &= -\frac{3}{4}(1+\omega)(1+\epsilon) \frac{1}{\epsilon^2} [(4+2\epsilon)(1+\omega) - 4\epsilon] \\
&\approx \frac{-3(1+\epsilon+\omega)}{\epsilon^2} \\
&\approx -\frac{3}{\epsilon^2}
\end{aligned} \tag{5.29}$$

In the limit that $\epsilon \ll 1$, we have $|\eta_\sigma| \gg 1$. That was the behavior we anticipated in

the previous section. Such a curvaton field has an extremely red-tilted spectrum ¹

The effective equation-of-state parameter for this field is computed as

$$\omega_\sigma = \frac{\frac{1}{2}\dot{\sigma}^2 - V}{\frac{1}{2}\dot{\sigma}^2 + V} \quad (5.30)$$

$$= \frac{1 - t^2}{1 + t^2} \quad (5.31)$$

This field behaves like a cosmological constant, but it does not dominate the background for the remote past, because both pressure and density decay fast going back in time – to the power of $t^{-4/\epsilon}$, which is a lot faster than how the fluid evolves, t^{-2} .

5.5.2 Cosmological Perturbations

Given the expression for the final spectral index, (C.37), and the expression for B , we can compute the dependence of the spectral index on ω , ϵ , and other background values.

First, let us reconsider the curvaton spectral index, $n_\sigma - 1$. Using (C.37) and (5.22), we know that for quasi-matter domination ²

$$\begin{aligned} n_\sigma - 1 &= 3 - 2\nu = 3 - 2\sqrt{B + \frac{1}{4}} \\ &\approx 3 - 3\sqrt{\frac{16}{\epsilon^2}} \\ &\approx -\frac{12}{\epsilon} \end{aligned} \quad (5.32)$$

As expected, we find the same result when we sum a''/a with $3\eta_\sigma \mathcal{H}^2$ using the η_σ value from (5.29),

$$-\frac{a''}{a} + 3\eta_\sigma \mathcal{H}^2 = -\frac{2}{\eta^2} (1 - 9\omega) + \frac{12}{\eta^2} \left(\frac{-3}{\epsilon^2}\right) (1 - 6\omega) \quad (5.33)$$

$$\Rightarrow -\frac{B}{\eta^2} \approx -\frac{36}{\eta^2 \epsilon^2} \quad (5.34)$$

¹We note once again that we do not expect a high magnitude of η_σ to be a problem, as it appears divided by η^2 in the Mukhanov-Sasaki equations. Therefore, the vacuum initial conditions are not an issue, so that the Bunch-Davies vacuum is valid as anticipated.

²We are considering $\omega \approx 0$ for the quasi-matter contraction scenario.

Therefore

$$\nu^2 - \frac{1}{4} = \frac{36}{\epsilon^2} \quad (5.35)$$

$$n_\sigma - 1 \approx 3 - 2\sqrt{\frac{36}{\epsilon^2}} \approx -\frac{12}{\epsilon}, \quad (5.36)$$

The results match because η_σ is constant in time, and therefore the approximations made in C are valid.

5.5.3 Total Spectral Index

Now, we can rewrite C.56 using $G = 1 - g$, where g will be small and is identified as the contribution from the field, and apply the result for $n_\sigma - 1$,

$$n_{\mathcal{R}} - 1 = (1 - g)(n_F - 1) + (g)(n_\sigma - 1) \quad (5.37)$$

$$= 12\omega - 12\omega g - 12\frac{g}{\epsilon} \quad (5.38)$$

At first, we can study the simplest approximation, by taking $\omega, g, \epsilon \ll 1$, which makes the first two terms in the RHS of (5.38) negligible. Therefore, we can re-express ϵ in terms of g and the spectral index,

$$n_{\mathcal{R}} - 1 \approx -12\frac{g}{\epsilon} \quad (5.39)$$

$$\epsilon \approx -12\frac{g}{(n_{\mathcal{R}} - 1)} \quad (5.40)$$

Using the definition of G , (C.57), approximating $\nu_F \approx 3/2$ and $(1 + \omega)/\omega \approx \omega^{-1}$,

$$\epsilon = \frac{-12}{(n_{\mathcal{R}} - 1)} \left[1 - \frac{\omega^{-3/2}}{\omega^{-3/2} + \frac{1}{6}R\omega^{-1}} \right] \quad (5.41)$$

$$\epsilon = \frac{-12}{(n_{\mathcal{R}} - 1)} \left[\frac{(R/6)\omega^{-1}}{\omega^{-3/2} + (R/6)\omega^{-1}} \right] \quad (5.42)$$

$$\Rightarrow \epsilon \approx -\frac{2R\omega^{1/2}}{(n_{\mathcal{R}} - 1)} \quad (5.43)$$

where we defined $R = \dot{\sigma}^2/H^2$, and that for our scenario $R \ll 1$. Therefore, we have found an expression relating ϵ , ω , $n_{\mathcal{R}} - 1$ and R .

For a scenario in which the perfect fluid tries to mimic dark matter, then $\omega \leq 10^{-3}$. We also expect that $R \leq 10^{-4}$ for the background to be dominated by the fluid. For a spectral index $n_{\mathcal{R}} - 1 = -0.03$, we then expect that

$$\epsilon \leq 0.67 \times 10^{-5} \quad (5.44)$$

Applying this result in the expression for λ , we approximately get

$$\lambda \approx 9 \times 10^6 + 6 \times 10^3 \log D \quad (5.45)$$

For the η_σ parameter, we have

$$\eta_\sigma \approx -4.5 \times 10^{10}, \quad (5.46)$$

while the curvaton spectral index equals

$$n_\sigma - 1 \approx -1.8 \times 10^6 \quad (5.47)$$

That is the required red-tilt for the curvaton field fluctuations to turn the total power spectrum from blue- to red-tilted, given the dominance of the fluid on the background and perturbations.

5.5.4 The issue of the field initial conditions

The results show an extremely small value for V in the far past, almost 0, as it evolves a lot faster than the perfect fluid. If we want V to be nonzero, D must have an extremely large value, otherwise, the curvaton potential is completely negligible in the remote past.

In section III.B from [203], the authors comment on the initial conditions of the field

in a plateau potential. They argue that the field must have its classical rolling to be larger than its quantum fluctuations. For their curvaton model, that is a problem. Hence, we must also check if the quantum fluctuations of our field are larger than the rolling down the potential. As σ evolves really slowly, thanks to a really small ϵ present on (5.25), we might have the same issue as [203].

Roughly speaking, in a contracting universe, the condition on the evolution of the field is

$$\frac{d\sigma}{dN} \gg \left| \frac{v}{a} \right| \quad (5.48)$$

To the far past, the dominant mode in (C.12) is actually the decaying mode – it decays towards the bounce, consequently it grows going back in time. The value of A_1 can be computed by identifying the decaying mode of (C.7). Using the results (C.17) and (C.18), we have

$$\frac{d\sigma}{dN} \gg (k\eta)^{\nu_\sigma} \eta^{-7/2} \quad (5.49)$$

In our model, $a(t) \approx t^{2/3}$ ³, and therefore

$$\eta^{-7/2} = H^{7/6} \quad (5.50)$$

and also

$$\log(a) = N = \frac{2}{3} \log(t) \quad (5.51)$$

$$t = \exp^{\frac{3N}{2}} \quad (5.52)$$

The horizon crossing in our model is defined when $k^2 = 2/B^2$, therefore,

³For now we loosely write t instead of $|t|$

$$k\eta \approx \sqrt{B} \approx \frac{1}{\epsilon^2} \quad (5.53)$$

Using equations (5.35), (5.49), (5.51), and (5.53) we have

$$\sigma(N) = D e^{\frac{-3N}{\epsilon}} \quad (5.54)$$

$$\frac{d\sigma}{dN} = -\frac{3D}{\epsilon} e^{\frac{-3N}{\epsilon}} \gg \frac{H_*^{7/6}}{\epsilon^{1/\epsilon^2}} = e^{\frac{7N}{4}} \left(\frac{1}{\epsilon}\right)^{\frac{1}{\epsilon^2}} \quad (5.55)$$

Given the extremely small value for ϵ , (5.44), in addition to $N \gg 0$, we see that quantum fluctuations might be a serious problem for this model. We shall address this issue in future work.

5.6 Preliminary results for the mixed fluid-field dBB bounce cosmology

Our research on the construction of a successful mixed fluid-field dBB bouncing model is still ongoing. In this chapter, we have motivated the search for bouncing models with more than one component, as well as presented some examples from the literature. Similarly to the curvaton scenario of inflation, most multi-component bouncing models deal with two scalar fields, and therefore make use of the entropic mechanism for the production of curvature perturbations.

In the analyzed scenario, the perturbations from fluid and field are decoupled. The perfect fluid has equation of state parameter $\omega \simeq 0$, which represents a quasi-matter dominated contraction. The field is chosen to have a constant η_σ parameter, so that Bunch-Davies vacuum initial conditions are used. We have also detailed the general requirements for allowing the Bunch-Davies vacuum to be used for scalar fields in a contracting background. The perturbations from both components, under the specified conditions, are well known from previous works.

Then, we computed the total curvature perturbation, that has contribution from both components. It allowed us to compute the final spectral index (5.12), for any scalar field

that respects the aforementioned conditions. This spectral index is analogous to the mixed inflaton-curvaton spectral index, as detailed in C.2.2, eq. (C.63).

We then applied these results for a set of scalar field models that satisfy the conditions on η_σ and that might provide a red-tilt for the curvature perturbations. For the so-called negative Mexican hat potential, when $m = 2$, we solve the Klein-Gordon equation and certify that its η_σ parameter is constant. However, for this choice of m , the value of the B function diverges.

The second choice of m for the scalar field, $m = 2 + \epsilon$, results in a strong red-tilt for the field fluctuations, while keeping η_σ and the B function well-behaved. Such a red-tilt suggested that the correct total spectral index – when one considers the fluid perturbations, (5.12) – could be red-tilted as well. We obtained the conditions on ϵ for the final spectral index to be found inside the most recent constraints. However, if our preliminary analysis on the initial conditions on the field can be trusted, this regime is not allowed. The scalar field is required to be rolling down its potential so slowly that, actually, quantum diffusion would be dominant under those circumstances. We intend to keep working on this subject, as it is not clear if the diffusion regime in a contracting universe is analogous to the same regime in an inflationary setting.

Chapter 6

Conclusion

The true nature of the beginning of universe has been the object of study of philosophers and scientists from the earliest human civilizations. Thanks to the development of general relativity and the aid of the foremost advanced satellites and telescopes, modern cosmology has gotten closer to find out how the universe began. However, the degeneracy between inflationary and bouncing models presents one of the hardest challenges to solve in this endeavor.

The most recent results from the Planck collaboration [29] are not enough to settle if the early universe had an inflationary phase, or if it started large, contracted, and underwent a bouncing phase that connected it to the expanding phase we live in.

In Chapter 3, we analyzed the degeneracy between these early universe scenarios with respect to scalar perturbations at first order. The source of this degeneracy is a symmetry that is present in the Mukhanov-Sasaki equation [63]. The mass function z''/z is the same for a pair of pump field $z(\eta)$ functions. For the early universe, this symmetry connects a (quasi-) de Sitter stage, as in inflation, to a (quasi-) matter dominated contraction, as in bouncing cosmologies. This feature is present in the MS equations for both scalar and tensor perturbations.

We then developed a procedure to build a contracting universe whose scalar perturbations were the same as a particular inflationary model. In our work [148], we decided to mirror the Starobinsky model of inflation, as it is considered one of the most favored inflationary models by Planck results [29]. We then obtained a bouncing model that predicted the same spectra of scalar perturbations as the Starobinsky model. In addition, as we built our model in the context of Loop Quantum Cosmology, the predicted tensor-to-

scalar ratio was found to be extremely small, as it is predicted by Starobinsky inflation and as it is favored by the most recent data. Moreover, scalar and tensor perturbations in our reconstructed bouncing model have the same red-tilt. That is the same behavior found in curvaton models. Therefore, our bouncing model is dual to general curvaton models that use Starobinsky-like inflaton field.

We conclude that first order perturbations are not enough to distinguish between single source inflationary (and consequently curvaton models) and bouncing cosmologies that respect the Planck constraints. Beyond the Planck results, the models may be distinguishable.

A straightforward alternative to first order perturbations is to analyze what early universe models predict for higher order correlation functions, i.e. non-Gaussianity. Single-field inflationary models predict small non-Gaussianity for their perturbations, with a magnitude which is proportional to the spectral index $n_s - 1$. Multi-field inflationary models and bouncing cosmologies, on the other hand, are expected to predict a larger signal of non-Gaussianity. In addition, the CMB dipolar modulation might be the result of scale-dependent non-Gaussianity, which is also the type of non-Gaussianity that dribbles the current Planck constraints on non-Gaussianity and the non-linearity parameters [52].

In Chapter 4 we investigated the production of the CMB dipolar modulation from the non-Gaussianity of curvaton models. A non-Gaussian coupling of large and small scale modes is responsible for the modulation. That also requires that the non-Gaussianity is scale dependent. That results in non-linearity parameters that are functions of the wavenumber k . If the scale-dependence is such that the f_{NL} parameter is close to 0 at the pivot scale, then the Planck constraints can be respected.

In our work [188], we analyzed what type of f_{NL} function form could present a change in sign. Using the curvaton equation of motion and assuming that the curvaton potential has a quadratic minimum, we developed a procedure to recover a curvaton potential from a non-linearity parameter f_{NL} . We then applied a scale-dependent ansatz for f_{NL} to the procedure and reconstructed a curvaton model. The model, as expected, presents a f_{NL} parameter that changes sign for some k , which is identified with the pivot scale. We computed both f_{NL} and g_{NL} , in terms of the CMB multipole ℓ for the model. The latest Planck results [52] are respected if the correct choice of parameters of the model is made. In addition, the scale-dependence of f_{NL} results in the correct behavior of the

CMB dipolar modulation.

We conclude that curvaton models can be built in order to present any desired f_{NL} parameter, which then leads to the CMB dipolar modulation that is observed. That represented two types of observations (f_{NL} , the modulation itself) that can be used to distinguish between curvaton inflationary models and bouncing cosmologies.

In order to find out if bouncing models could present scale-dependent non-Gaussianity, we decided to investigate the multi-component scenario. The motivation was to construct a bouncing model that made use of a curvaton-like scalar field, which eases the computation of non-Gaussianities. Another choice we made was to work in the de Broglie-Bohm scenario to realize the bounce. We do not expect significant change in comparison to a LQC bounce, but in the dBB scenario we know that entropy perturbations are well-behaved. To avoid the use of entropy perturbations overall, we decided to use a matter fluid to dominate the background during contraction/expansion, as its perturbations are uncoupled from the curvaton-like field's. That makes our scenario the simplest multi-component bouncing cosmology available.

We present our work in progress in the last chapter, Chapter 5. Before computing if the bouncing model predicts the correct non-Gaussianity, it must respect the Planck constraints for the two point correlation functions. The fluid and field perturbations are uncoupled, which eases the computation of their perturbations. Our result resembles mixed inflaton-curvaton models, in which inflaton perturbations are also produced. We conclude that for our model to respect the Planck constraints, the field perturbations are required to be extremely red-tilted (if the perfect fluid that dominates the background is dust-like, $\omega = 0$).

Finally, we investigated if two curvaton-like scalar fields predicted the correct spectral index for the perturbations. Our preliminary analysis points out that the Corrected Negative Mexican Hat potential, 5.5, results in large red-tilted fluctuations, which in turn result in a slightly red-tilted total curvature perturbation. However, it might be the case that the model is invalid, if quantum diffusion takes place in the remote past, preventing the slow-roll of the field. The investigation of this topic is left for the continuation of our work.

In conclusion, we have seen that bouncing and inflationary cosmologies are intimately linked. Their predictions are degenerate, such that it is imperative to analyze any available

roots in order to disentangle them. In terms of the first order perturbations and two point correlation functions, both scenarios are indistinguishable. It is possible to construct a bouncing model in an attempt to mimic an inflationary cosmology, and we expect the reverse to be possible as well. In terms of higher order correlation functions, we have seen that the presence of scale-dependent non-Gaussianities is an effect that might be useful to distinguish between the scenarios, in particular curvaton models and single-source bouncing cosmologies. It is still early to assert if the dipolar modulation could be used as well, as we have not yet concluded the construction of a bouncing model that provides such effect.

Appendix A

Introduction to Cosmology

The objective of this appendix is to introduce basic concepts of cosmology.

Classical relativistic cosmology results from the solving of Einstein field equations to the background Friedmann-Lemaitre-Robertson-Walker metric, FLRW. This metric describes a homogeneous and isotropic universe. For a flat universe, in Cartesian coordinates,

$$ds^2 = dt^2 - a^2(t)\delta_{ij}dx^i dx^j \quad (\text{A.1})$$

For a universe with curvature k , where $k = 1, -1, 0$

$$ds^2 = dt^2 - a^2(t) \left[\frac{dr^2}{1 - kr^2} + r^2 d(\theta^2 + \sin^2 \theta d\varphi^2) \right] \quad (\text{A.2})$$

The Einstein equations are

$$G_{\mu\nu} = 8\pi GT_{\mu\nu} = \kappa^2 T_{\mu\nu} \quad (\text{A.3})$$

For a perfect fluid, the energy-momentum tensor for a comoving observer can be decomposed as

$$T_{\mu\nu} = (\rho, -p, -p, -p), \quad (\text{A.4})$$

where ρ is the energy density and p is pressure.

The Einstein equations for a perfect fluid in FLRW are the so-called Friedmann equations

$$\left(\frac{\dot{a}}{a}\right)^2 = -\frac{k}{a^2} + \frac{8\pi G}{3}\rho \quad (\text{A.5})$$

$$\frac{\ddot{a}}{a} = -\frac{4\pi G}{3}(\rho + 3p) \quad (\text{A.6})$$

We can introduce the Hubble parameter H ,

$$H \equiv \frac{\dot{a}}{a}, \quad (\text{A.7})$$

and we can then write the Friedmann equations as

$$H^2 = \frac{8\pi G}{3}\rho - \frac{k}{a^2}. \quad (\text{A.8})$$

From the conservation of the energy-momentum tensor, we get

$$\dot{\rho} + 3H(\rho + p) = 0 \quad (\text{A.9})$$

From the equation of state $\rho = \omega p$, with constant ω , we can obtain the behavior of the energy density as a function of the scale factor

$$\rho(a) = \rho_0 a^{-3(1+\omega)}. \quad (\text{A.10})$$

Therefore, for radiation, which has $\omega = 1/3$

$$\rho(a)_r = \rho_{r,0} a^{-4}. \quad (\text{A.11})$$

For dust, $\omega = 0$, so

$$\rho(a)_m = \rho_{m,0} a^{-3}. \quad (\text{A.12})$$

For the cosmological constant Λ , $\omega = -1$

$$\rho(a)_\Lambda = \rho_{\Lambda,0}. \quad (\text{A.13})$$

From the definition of the critical density $\rho_{\text{crit},0} = 3H_0^2/8\pi G$, i.e., the necessary density for the universe to be flat ($k = 0$), we re-write the Friedmann equations [A.8](#) as

$$\frac{H^2}{H_0^2} = \frac{\Omega_{r,0}}{a^4} + \frac{\Omega_{m,0}}{a^3} + \Omega_{\Lambda,0} + \frac{1 - \Omega_0}{a^2} \quad (\text{A.14})$$

where $\Omega_{i,0} = \rho_{i,0}/\rho_{\text{crit},0}$.

In terms of cosmic time t , the Friedmann equations can be solved in terms of the equation of state. For $\omega \neq -1$:

$$a(t) \propto t^{\frac{2}{3(1+\omega)}} \quad (\text{A.15})$$

In the case of dust, we have that $a(t) \propto t^{2/3}$.

For the cosmological constant,

$$a(t) \propto e^{Ht} \quad (\text{A.16})$$

That is the so-called de Sitter solution, a universe that expands exponentially.

Using conformal time η , defined from $d\eta = dt/a(t)$, we re-write the Friedmann equations as

$$a'^2 + ka^2 = \frac{8\pi G}{3}\rho a^4, \quad (\text{A.17})$$

$$a'' + ka^2 = \frac{4\pi G}{3}(\rho - 3p)a^3, \quad (\text{A.18})$$

where the superscript $'$ means a derivative with respect to η . The Friedmann equations can be solved again for the different fluid: radiation, dust and the cosmological constant.

For dust, $p = 0$, therefore

$$a(\eta) \propto \eta^2, \quad (\text{A.19})$$

with $-\infty < \eta < \infty$. For a universe dominated by cosmological constant or any other fluid with $\omega = -1$, we have

$$a(\eta) \propto -\frac{1}{\eta}, \quad (\text{A.20})$$

where $-\infty < \eta < 0$.

Appendix B

Computation of $z(\eta)$

Throughout chapter 3 it was necessary to compute F , defined as the derivative of $f(R)$ with respect to R , for the Starobinsky-like model in analysis. From this value, we could finally compute $z(\eta)$. In order to do so, we needed the derivatives of F and some other computations. They are described below.

$$F = \frac{4}{3} [\ln(\bar{\eta})] \quad (\text{B.1})$$

$$F' = \frac{dF}{d\eta} \quad (\text{B.2})$$

$$= \frac{4}{3\eta} \quad (\text{B.3})$$

$$\rightarrow \frac{F'}{F} = [\eta \ln(\bar{\eta})]^{-1} \quad (\text{B.4})$$

$$\rightarrow \frac{F'^2}{F} = \frac{4}{3} [\eta^2 \ln(\bar{\eta})]^{-1} \quad (\text{B.5})$$

$$\Rightarrow \frac{F'}{aF} = [\eta \ln(\bar{\eta})]^{-1} \frac{M}{\sqrt{3}} [\eta^2 \log(\bar{\eta})]^{1/2} \quad (\text{B.6})$$

$$= \frac{-M}{\sqrt{3}} [\ln(\bar{\eta})]^{-1/2} \quad (\text{B.7})$$

$$\Rightarrow \frac{F'^2}{a^2 F} = \frac{4}{3} [\eta^2 \ln(\bar{\eta})]^{-1} \frac{M^2}{3} [\eta^2 \log(\bar{\eta})] \quad (\text{B.8})$$

$$= \frac{4M^2}{9} \quad (\text{B.9})$$

We have considered the large η regime for the computations above.

Appendix C

Fluid and field perturbations in the dBB quantum cosmology

In this appendix we compute explicitly the perturbations for a fluid and for a field in the dBB quantum cosmology model.

C.1 Mixed fluid-field scalar perturbations

In this section, we consider a perfect fluid component, that dominates the background contraction, doted with an equation of state ω and resulting in the scale factor (5.1). We also consider a curvaton-like scalar field σ , which is subdominant with respect to the fluid. Therefore the background scale factor is given by the evolution of the fluid.

The theoretical development of the results for the cosmological perturbations of perfect fluid and a scalar field in the context of dBB quantum cosmology is present in the references [237, 163, 224, 5, 238, 175, 178].

To compute the perturbations from fluid and curvaton field, we note that both respect the same equations of motion, apart from a different scale-dependence and other numerical pre-factors. We also consider that the field has subdominant and constant η_σ parameter so that the Bunch-Davies vacuum gives the initial conditions for the perturbations.

C.1.1 Mukhanov-Sasaki equations

First, we review the equations for the perfect fluid. In the dBB context, we find that the equation of motion for the variable $v = a\delta\varphi$ ¹, in Fourier space, is

$$v_k'' + \left(\omega k^2 - \frac{a''}{a} \right) v_k = 0 \quad (\text{C.1})$$

where we recognize the same structure as for a perfect fluid in classical GR. The difference lies in the scale factor $a(\eta)$ which now satisfies 5.1. In the far past limit, we have

$$v_k'' + \left(\omega k^2 - \frac{1}{\eta^2} \left(\nu_F^2 - \frac{1}{4} \right) \right) v_k = 0 \quad (\text{C.2})$$

$$\nu_F = \frac{3(1-\omega)}{2(1+3\omega)} \quad (\text{C.3})$$

For the field, the equations of motion are almost the same. In this case, $v = a\delta\sigma + a\frac{\sigma'\sigma}{4H}$, and consequently

$$v_k'' + \left(k^2 - \frac{1}{\eta^2} \left(\nu_\sigma^2 - \frac{1}{4} \right) \right) v_k = 0 \quad (\text{C.4})$$

$$\nu_\sigma = \sqrt{\nu_F^2 - \frac{12\eta_\sigma}{(3\omega+1)^2}} \quad (\text{C.5})$$

where $\eta_\sigma = V_{\sigma\sigma}/3H^2$.

We see that both will result in the same type of solution, where for the fluid we work in terms of $\bar{k} = \sqrt{\omega}k$. We can also check that ν_σ is different from ν_F from the fluid (C.3) by a term proportional to the mass of the field.

The matching procedure for the initial conditions for both will result in the same constants, as in both cases we have the Minkowski vacuum. Therefore, apart from their ν parameters and wavenumber k , we have

¹where φ is the fluid velocity field

$$v_F = \sqrt{|\eta|} \left[C_{1F}(k) H_{\nu_F}^{(1)}(\bar{k}|\eta|) + C_{2F}(k) H_{\nu_F}^{(2)}(\bar{k}|\eta|) \right] \quad (\text{C.6})$$

$$v_\sigma = \sqrt{|\eta|} \left[C_{1\sigma}(k) H_{\nu_\sigma}^{(1)}(k|\eta|) + C_{2\sigma}(k) H_{\nu_\sigma}^{(2)}(k|\eta|) \right] \quad (\text{C.7})$$

where

$$C_{1F} = C_{1\sigma} = 0; \quad C_{2F} \propto C_{2\sigma} \quad (\text{C.8})$$

$$C_{2F} = \frac{\sqrt{\pi}}{2} e^{i(\nu_F+1/2)\frac{\pi}{2}} \quad (\text{C.9})$$

$$C_{2\sigma} = \frac{\sqrt{\pi}}{2} e^{i(\nu_\sigma+1/2)\frac{\pi}{2}} \quad (\text{C.10})$$

The dependence on ν will vanish for those constants when we take the absolute value of the final solution for computing \mathcal{R} or ζ . Therefore we can treat them as equals.

For the matching procedure with the solution across the bounce, we have that for both cases we can expand the solution in powers of k^2 . For the fluid we have

$$\begin{aligned} \frac{v_{Fk}}{z} = & A_{1F}(k) \left[1 - \omega k^2 \int_0^\eta \frac{d\bar{\eta}}{\bar{z}^2} \int_0^{\bar{\eta}} d\bar{\eta} \bar{c}_s^{\bar{z}} \bar{z}^2 + \dots \right] + \\ & + A_{2F}(k) \left[\int_{\eta^*}^\eta \frac{d\bar{\eta}}{\bar{z}^2} - \omega k^2 \int_0^\eta \frac{d\bar{\eta}}{\bar{z}^2} \int_0^{\bar{\eta}} d\bar{\eta} \bar{c}_s^{\bar{z}} \bar{z}^2 \int_{\eta^*}^{\bar{\eta}} \frac{d\bar{\eta}}{\bar{z}^2} \dots \right] \end{aligned} \quad (\text{C.11})$$

For the field we have

$$\begin{aligned} \frac{v_{\sigma k}}{a} = & A_{1\sigma}(k) \left[1 - k^2 \int_0^\eta \frac{d\bar{\eta}}{\bar{a}^2} \int_0^{\bar{\eta}} d\bar{\eta} \bar{c}_s^{\bar{a}} \bar{a}^2 + \dots \right] + \\ & + A_{2\sigma}(k) \left[\int_{\eta^*}^\eta \frac{d\bar{\eta}}{\bar{a}^2} - k^2 \int_0^\eta \frac{d\bar{\eta}}{\bar{a}^2} \int_0^{\bar{\eta}} d\bar{\eta} \bar{c}_s^{\bar{a}} \bar{a}^2 \int_{\eta^*}^{\bar{\eta}} \frac{d\bar{\eta}}{\bar{a}^2} \dots \right] \end{aligned} \quad (\text{C.12})$$

From the expansion around the bounce, we detect a difference in the use of z , defined as

$$z = \sqrt{\frac{3(1+\omega)}{2\omega}} \quad (\text{C.13})$$

For A_1 , z comes in the denominator, while for A_2 we have it in the numerator (since we determine it using $z^2(v/z)'$). Additionally, in the limit of the matching, the solution v_F acquires a dependence on ω , thanks to \bar{k} . Therefore, apart from the C_X 's, in terms of amplitude, we have that

$$A_{1F} = \omega^{\nu_F/2} \sqrt{\frac{2\omega}{3(1+\omega)}} A_{1\sigma} \quad (\text{C.14})$$

$$A_{2F} = \omega^{-\nu_F/2} \sqrt{\frac{3(1+\omega)}{2\omega}} A_{2\sigma} \quad (\text{C.15})$$

while for the k -dependence, we have:

$$A_{1F} \propto k^{\nu_F}; \quad A_{2F} \propto k^{-\nu_F} \quad (\text{C.16})$$

$$A_{1\sigma} \propto k^{\nu_\sigma}; \quad A_{2\sigma} \propto k^{-\nu_\sigma} \quad (\text{C.17})$$

In addition, thanks to the Hankel function present inside v_F , there is a weak time-dependence on the A coefficients of σ .

$$A_{1\sigma}(\eta) = \eta^{\nu_\sigma + \frac{-3(1-\omega)}{2(1+3\omega)}} \quad (\text{C.18})$$

$$A_{2\sigma}(\eta) = \eta^{-\nu_\sigma + \frac{3(1-\omega)}{2(1+3\omega)}} \quad (\text{C.19})$$

where it is worth noting that we can approximate

$$\eta^{-\nu_\sigma} \eta^{\frac{3(1-\omega)}{2(1+3\omega)}} \approx 1 \quad (\text{C.20})$$

for $\nu_\sigma \approx 3/2$ and $\omega \approx 0$. In such case, all A_{iX} are constants in time.

We follow the analysis from [238] where the dominant mode after the bounce mixes

the modes A_1 and A_2 for both perturbations and A_2 dominates.

Then, all that is left is to compute the amplitude for A_{2X} . Using the matching in the contracting phase, we have for the fluid

$$A_{2F} = z^2 \left(\frac{v_F}{z} \right)' = \omega^{-\nu_F/2} \sqrt{\frac{3(1+\omega)}{2\omega}} a^2 \left(\frac{v_\sigma}{a} \right)' \quad (\text{C.21})$$

$$= \omega^{-\nu_F/2} \sqrt{\frac{3(1+\omega)}{2\omega}} A_{2\sigma}|_{\nu_\sigma=\nu_F} \quad (\text{C.22})$$

$$= a_B e^{i(\nu_F - \frac{1}{2})\frac{\pi}{2}} 2^{\nu_F-2} \omega^{-\nu_F/2} \sqrt{\frac{3(1+\omega)}{2\omega}} \left(\frac{-3(1-\omega)}{(1+3\omega)} \right) \frac{\Gamma(\nu_F)}{\Gamma(3/2)} k^{-\nu_F} \quad (\text{C.23})$$

$$= a_B e^{i(\nu_F - \frac{1}{2})\frac{\pi}{2}} 2^{\nu_F-2} \omega^{-\nu_F/2} \sqrt{\frac{3(1+\omega)}{2\omega}} (-2\nu_F) \frac{\Gamma(\nu_F)}{\Gamma(3/2)} k^{-\nu_F} \quad (\text{C.24})$$

while for the field

$$A_{2\sigma} = a^2 \left(\frac{v_\sigma}{a} \right)' \quad (\text{C.25})$$

$$= a_B \eta^{\frac{4}{1+3\omega}} \left[\eta^{\frac{-2}{1+3\omega}} \eta^{\frac{1}{2}} e^{i(\nu_\sigma - \frac{1}{2})\frac{\pi}{2}} 2^{\nu_\sigma-2} \frac{\Gamma(\nu_\sigma)}{\Gamma(2/3)} k^{-\nu_\sigma} \eta^{-\nu_\sigma} \right]' \quad (\text{C.26})$$

$$= a_B e^{i(\nu_\sigma - \frac{1}{2})\frac{\pi}{2}} 2^{\nu_\sigma-2} \left(\frac{3(-1+\omega)}{2(1+3\omega)} - \nu_\sigma \right) \frac{\Gamma(\nu_\sigma)}{\Gamma(3/2)} \eta^{-\nu_\sigma} \eta^{\frac{3(1-\omega)}{2(1+3\omega)}} k^{-\nu_\sigma} \quad (\text{C.27})$$

$$= a_B e^{i(\nu_\sigma - \frac{1}{2})\frac{\pi}{2}} 2^{\nu_\sigma-2} (-\nu_F - \nu_\sigma) \frac{\Gamma(\nu_\sigma)}{\Gamma(3/2)} \eta^{-\nu_\sigma} \eta^{\nu_F} k^{-\nu_\sigma} \quad (\text{C.28})$$

C.1.2 The power spectrum for each component

Following [238], the definition of the ζ curvature perturbation is

$$\zeta_F = -2\sqrt{\pi} l_p \frac{v_F}{z} \quad (\text{C.29})$$

$$\zeta_\sigma = -2\sqrt{\pi} l_p \frac{H}{\dot{\sigma}} \frac{v_\sigma}{a} \quad (\text{C.30})$$

So that the power spectrum at CMB time is

$$\mathcal{P}_{\zeta_F} = \frac{k^3}{2\pi^2} |\zeta_F|^2 = \frac{2}{\pi} l_p^2 k^3 |A_{2F} B|^2 \quad (\text{C.31})$$

$$\mathcal{P}_{\zeta_\sigma} = \frac{k^3}{2\pi^2} |\zeta_\sigma|^2 = \frac{2}{\pi} l_p^2 k^3 |A_{2\sigma} B|^2 \left[\frac{H}{\dot{\sigma}} \right]^2 \left[\frac{3(1+\omega)}{2\omega} \right]^2 \quad (\text{C.32})$$

where the last factor in the r.h.s of (C.32) comes from the difference between the first integral in square brackets for A_2 for (C.11) and (C.12), with B the approximate value of such integration

$$B \equiv \int_{-\infty}^{\infty} \frac{d\bar{\eta}}{z^2} = \frac{4\pi\omega}{9(1-\omega^2)\sqrt{\Omega_{\omega 0}}} \left[\frac{1}{a_B} \right]^{3(1-\omega)/2} \quad (\text{C.33})$$

Therefore, we have

$$\begin{aligned} \mathcal{P}_{\zeta_F} &= \frac{a_B^2 l_p^2 |B|^2 2^{2\nu_F}}{8\pi} \times \\ &\times \omega^{-\nu_F} \left[\frac{3(1+\omega)}{2\omega} \right] [2\nu_F]^2 \left[\frac{\Gamma(\nu_F)}{\Gamma(3/2)} \right]^2 k^{3-2\nu_F} \end{aligned} \quad (\text{C.34})$$

$$\begin{aligned} \mathcal{P}_{\zeta_\sigma} &= \frac{a_B^2 l_p^2 |B|^2 2^{2\nu_\sigma}}{8\pi} \times \\ &\times \left[\frac{H}{\dot{\sigma}} \right]^2 \left[\frac{3(1+\omega)}{2\omega} \right]^2 [\nu_F + \nu_\sigma]^2 \left[\frac{\Gamma(\nu_\sigma)}{\Gamma(3/2)} \right]^2 \left[\eta^{-\nu_\sigma + \nu_F} \right]^2 k^{3-2\nu_\sigma} \end{aligned} \quad (\text{C.35})$$

C.1.3 Spectral index

Consequently, for the spectrum index for each matter component, we have

$$n_F - 1 = \frac{12\omega}{(1+3\omega)} \approx 12\omega > 0. \quad (\text{C.36})$$

$$n_\sigma - 1 = 3 - 2\sqrt{\nu_F^2 - \frac{12\eta_\sigma}{(3\omega+1)^2}} \quad (\text{C.37})$$

From (C.37), we see that in case $\eta_\sigma < 0$ it is possible that the spectral index from the

field is red-tilted, as the term inside the square root becomes large. More precisely, the condition for that is

$$n_\sigma - 1 < 0 \Rightarrow \sqrt{v_F^2 - \frac{12\eta_\sigma}{(3\omega + 1)^2}} > \frac{3}{2} \quad (\text{C.38})$$

$$\frac{(3\omega - 3)^2}{4(3\omega + 1)} - \frac{12\eta_\sigma}{(3\omega + 1)^2} > \frac{9}{4} \quad (\text{C.39})$$

$$\eta_\sigma < -\frac{3}{2}(\omega - \omega^2) \quad (\text{C.40})$$

Therefore, for models in which η_σ is constant, it is straightforward to check that the spectral index can be made red if it is negative.

C.1.4 Total power spectrum

For the total power spectrum, we remind equations (5.9) and (5.10)

$$\zeta_T = \sum_\alpha \frac{\dot{\rho}_\alpha}{\dot{\rho}} \zeta_\alpha \quad (\text{C.41})$$

$$\mathcal{R}_T = \sum_I \frac{\rho_I + P_I}{\rho + P} \mathcal{R}_I \quad (\text{C.42})$$

Via our definition, we have

$$\zeta_\alpha = -2\sqrt{\pi}l_p \mathcal{R}_\alpha \quad (\text{C.43})$$

So, from now on, we will work with \mathcal{R} , so that

$$\mathcal{R}_F = |A_{2F}B| \quad (\text{C.44})$$

$$= \frac{a_B |B| 2^{\nu_F}}{4} \omega^{-\nu_F/2} \left[\frac{3(1+\omega)}{2\omega} \right]^{1/2} [2\nu_F] \left[\frac{\Gamma(\nu_F)}{\Gamma(3/2)} \right] k^{\frac{3}{2}-\nu_F} \quad (\text{C.45})$$

$$= W_F \omega^{-\nu_F/2} \left[\frac{3(1+\omega)}{2\omega} \right]^{1/2} k^{\frac{3}{2}-\nu_F} \quad (\text{C.46})$$

$$\mathcal{R}_\sigma = \frac{H}{\dot{\sigma}} \left[\frac{3(1+\omega)}{2\omega} \right] |A_{2\sigma}B| \quad (\text{C.47})$$

$$= \frac{a_B |B| 2^{\nu_F}}{4} \frac{H}{\dot{\sigma}} \left[\frac{3(1+\omega)}{2\omega} \right] [\nu_F + \nu_\sigma] \left[\frac{\Gamma(\nu_\sigma)}{\Gamma(3/2)} \right] [\eta^{-\nu_\sigma + \nu_F}] k^{\frac{3}{2}-\nu_\sigma} \quad (\text{C.48})$$

$$= W_\sigma \frac{H}{\dot{\sigma}} \left[\frac{3(1+\omega)}{2\omega} \right] k^{\frac{3}{2}-\nu_\sigma} \quad (\text{C.49})$$

where we defined

$$W_F = \frac{a_B |B| 2^{\nu_F}}{4} \frac{\Gamma(\nu_F)}{\Gamma(3/2)} 2\nu_F \quad (\text{C.50})$$

$$W_\sigma = \frac{a_B |B| 2^{\nu_F}}{4} \frac{\Gamma(\nu_\sigma)}{\Gamma(3/2)} (\nu_F + \nu_\sigma) \quad (\text{C.51})$$

We note that $W_F \approx W_\sigma \equiv W$, as both ν parameters differ only by the small factors ω and η_σ .

Using (5.10), we have that the total curvature perturbation is

$$\mathcal{R}_T \approx (1+\omega) \mathcal{R}_F + \frac{\dot{\sigma}^2}{3H^2} \mathcal{R}_\sigma \quad (\text{C.52})$$

$$\begin{aligned} &= (1+\omega) W \omega^{-\nu_F/2} \left[\frac{3(1+\omega)}{2\omega} \right]^{1/2} k^{\frac{3}{2}-\nu_F} + \\ &+ \frac{1}{3} \frac{\dot{\sigma}}{H} W \left[\frac{3(1+\omega)}{2\omega} \right] k^{\frac{3}{2}-\nu_\sigma} \end{aligned} \quad (\text{C.53})$$

Therefore, for the curvature perturbations from the fluid to dominate, we need

$$\omega^{\frac{1}{2}-\frac{\nu_F}{2}} \gg \frac{\dot{\sigma}}{H} \quad (\text{C.54})$$

That is an expected result, as we require that the fluid dominates the background, and, consequently, that $H^2 \gg \dot{\sigma}^2$.

For the power spectrum, we have

$$\mathcal{P}_{\mathcal{R}} \approx W^2 \omega^{-\nu_F} \left[\frac{3(1+\omega)}{2\omega} \right] k^{3-2\nu_F} + \frac{W^2}{9} \left[\frac{\dot{\sigma}^2}{H^2} \right] \left[\frac{3(1+\omega)}{2\omega} \right]^2 k^{3-2\nu_\sigma} \quad (\text{C.55})$$

The spectral index will be, therefore

$$n_{\mathcal{R}} - 1 = G(n_F - 1) + (1 - G)(n_\sigma - 1) \quad (\text{C.56})$$

where

$$G = \frac{\omega^{-\nu_F}}{\omega^{-\nu_F} + \frac{1}{9} \left[\frac{\dot{\sigma}^2}{H^2} \right] \left[\frac{3(1+\omega)}{2\omega} \right]} \quad (\text{C.57})$$

C.2 Additional details about the scalar perturbations

C.2.1 Field spectral index

From (C.37), we see that in case $\eta_\sigma < 0$ it is possible that the spectral index from the field is red-tilted, as the term inside the square root becomes large. The condition for that is

$$n_\sigma - 1 < 0 \Rightarrow \sqrt{\nu_F^2 - \frac{12\eta_\sigma}{(3\omega+1)^2}} > \frac{3}{2} \quad (\text{C.58})$$

$$\frac{(3\omega-3)^2}{4(3\omega+1)} - \frac{12\eta_\sigma}{(3\omega+1)^2} > \frac{9}{4} \quad (\text{C.59})$$

$$\eta_\sigma < -\frac{3}{2}(\omega - \omega^2) \quad (\text{C.60})$$

Therefore, for models in which η_σ is constant, it is straightforward to check that the spectral index can be made red if it is negative.

C.2.2 Revisiting the mixed inflaton-curvaton scenario

For the scalar field, we arrive in a different result than usual findings from [5, 238, 175, 178]. In the context of the cited works, the scalar field is responsible for the background evolution. That is not the case of the present system, where the curvaton-like scalar field is subdominant, and therefore its perturbations do not source perturbations on the metric.

That is analogous to the curvaton scenario in inflation, where the curvaton is subdominant during slow-roll and, consequently, its fluctuations respect the equations of motion of a massive scalar field in a de Sitter spacetime [95]. In this case, the curvaton fluctuations spectral index is

$$n_\sigma - 1 = 2\eta_\sigma - 2\epsilon \quad (\text{C.61})$$

where $\eta_x = V_{xx}/3H^2$ and $\epsilon = -\dot{H}/H^2$ is the first slow-roll parameter.

That is particularly important in the scenario analogous to ours, the mixed inflaton-curvaton scenario [223]. There, inflaton and curvaton contribute to the curvature perturbations, as both fluid and scalar field contribute to our model. However, since inflaton dominates the background and is responsible for its evolution, its fluctuations will source fluctuations of the metric. Therefore the final equation of motion for the inflaton perturbations will slightly differ from that of the curvaton. As a result, the spectral index for the inflaton fluctuations is

$$n_\phi - 1 = 2\eta_\phi - 6\epsilon \quad (\text{C.62})$$

We see that inflaton and curvaton fluctuations have different scale dependence. The final curvature perturbation spectral index differs from both and is, actually, a weighted average [223]

$$n_{\mathcal{R}} - 1 = w_\sigma (n_\sigma - 1) + (1 - w_\sigma) (n_\phi - 1) \quad (\text{C.63})$$

where w_σ is the weight of the curvaton perturbations on the final curvature perturbation.

We obtain a similar result in our scenario, see [C.1](#), where the final spectral index will differ from the usual dust-dominated regime, which is blue-tilted instead of having the desired red-tilt observed on the CMB.

Bibliography

- [1] LINDE, A. D. Particle physics and inflationary cosmology. *Contemp. Concepts Phys.*, v. 5, p. 1–362, 1990.
- [2] STAROBINSKY, A. A. A New Type of Isotropic Cosmological Models Without Singularity. *Phys. Lett.*, B91, p. 99–102, 1980.
- [3] GUTH, A. H. The Inflationary Universe: A Possible Solution to the Horizon and Flatness Problems. *Phys. Rev.*, D23, p. 347–356, 1981.
- [4] NOVELLO, M.; SALIM, J. M. NONLINEAR PHOTONS IN THE UNIVERSE. *Phys. Rev.*, D20, p. 377–383, 1979.
- [5] FALCIANO, F. T.; PINTO-NETO, N. Scalar Perturbations in Scalar Field Quantum Cosmology. *Phys. Rev.*, D79, p. 023507, 2009.
- [6] FALCIANO, F. T.; PINTO-NETO, N.; VITENTI, S. D. P. Perturbations Through a Quantum Bounce. In: *Proceedings, 13th Marcel Grossmann Meeting on Recent Developments in Theoretical and Experimental General Relativity, Astrophysics, and Relativistic Field Theories (MG13): Stockholm, Sweden, July 1-7, 2012*. [S.l.: s.n.], 2015. p. 1625–1627.
- [7] PINTO-NETO, N.; FABRIS, J. C. Quantum cosmology from the de Broglie-Bohm perspective. *Class. Quant. Grav.*, v. 30, p. 143001, 2013.
- [8] BRANDENBERGER, R. H. The Matter Bounce Alternative to Inflationary Cosmology. 2012.
- [9] HARO, J. de; CAI, Y.-F. An Extended Matter Bounce Scenario: current status and challenges. *Gen. Rel. Grav.*, v. 47, n. 8, p. 95, 2015.

- [10] MAIER, R.; PINTO-NETO, N.; SOARES, I. D. Bouncing Model in Brane World Theory. *Phys. Rev.*, D87, n. 4, p. 043528, 2013.
- [11] NOJIRI, S.; ODINTSOV, S. D.; OIKONOMOU, V. K. Bounce universe history from unimodular $F(R)$ gravity. *Phys. Rev.*, D93, n. 8, p. 084050, 2016.
- [12] BAMBHA, K. et al. Bounce cosmology from $F(R)$ gravity and $F(R)$ bigravity. *JCAP*, v. 1401, p. 008, 2014.
- [13] BANERJEE, S.; SARIDAKIS, E. N. Bounce and cyclic cosmology in weakly broken galileon theories. 2016.
- [14] WILSON-EWING, E. The Matter Bounce Scenario in Loop Quantum Cosmology. *JCAP*, v. 1303, p. 026, 2013.
- [15] BRANDENBERGER, R. Matter Bounce in Horava-Lifshitz Cosmology. *Phys. Rev.*, D80, p. 043516, 2009.
- [16] BISWAS, T.; MAZUMDAR, A.; SIEGEL, W. Bouncing universes in string-inspired gravity. *JCAP*, v. 0603, p. 009, 2006.
- [17] LANGLOIS, D.; NARUKO, A. Bouncing cosmologies in massive gravity on de Sitter. *Class. Quant. Grav.*, v. 30, p. 205012, 2013.
- [18] ADE, P. A. R. et al. Planck 2015 results - XVI. Isotropy and statistics of the CMB. *A&A*, v. 594, p. A16, 2016. Disponível em: <<https://doi.org/10.1051/0004-6361/201526681>>.
- [19] Planck Collaboration; Aghanim, N. et al. Planck 2018 results - vi. cosmological parameters. *A&A*, v. 641, p. A6, 2020. Disponível em: <<https://doi.org/10.1051/0004-6361/201833910>>.
- [20] SAKHAROV, A. D. Violation of CP Invariance, c Asymmetry, and Baryon Asymmetry of the Universe. *Pisma Zh. Eksp. Teor. Fiz.*, v. 5, p. 32–35, 1967. [*Usp. Fiz. Nauk*161,61(1991)].
- [21] LINDE, A. A new inflationary universe scenario: A possible solution of the horizon, flatness, homogeneity, isotropy and primordial monopole problems. *Physics*

- Letters B*, v. 108, n. 6, p. 389 – 393, 1982. ISSN 0370-2693. Disponible em: <<http://www.sciencedirect.com/science/article/pii/0370269382912199>>.
- [22] LINDE, A. D. Chaotic Inflation. *Phys. Lett.*, B129, p. 177–181, 1983.
- [23] LINDE, A. D. Hybrid inflation. *Phys. Rev.*, D49, p. 748–754, 1994.
- [24] WANDS, D. Multiple field inflation. In: _____. *Inflationary cosmology*. 738. ed. [S.l.]: Springer, 2007. (Lecture notes in physics, 738), p. 275–304. ISBN 9783540743538.
- [25] BEZRUKOV, F. L.; SHAPOSHNIKOV, M. The Standard Model Higgs boson as the inflaton. *Phys. Lett.*, B659, p. 703–706, 2008.
- [26] LINDE, A. D. Axions in inflationary cosmology. *Phys. Lett.*, B259, p. 38–47, 1991.
- [27] ARMENDARIZ-PICON, C.; DAMOUR, T.; MUKHANOV, V. F. k - inflation. *Phys. Lett.*, B458, p. 209–218, 1999.
- [28] ACHÚCARRO, A.; PALMA, G. A. The string swampland constraints require multi-field inflation. *Journal of Cosmology and Astroparticle Physics*, IOP Publishing, v. 2019, n. 02, p. 041–041, Feb 2019. ISSN 1475-7516. Disponible em: <<http://dx.doi.org/10.1088/1475-7516/2019/02/041>>.
- [29] Planck Collaboration; Akrami, Y. et al. Planck 2018 results - x. constraints on inflation. *A&A*, v. 641, p. A10, 2020. Disponible em: <<https://doi.org/10.1051/0004-6361/201833887>>.
- [30] LYTH, D. H.; RIOTTO, A. Particle physics models of inflation and the cosmological density perturbation. *Phys. Rept.*, v. 314, p. 1–146, 1999.
- [31] MARTIN, J. et al. The Best Inflationary Models After Planck. *JCAP*, v. 1403, p. 039, 2014.
- [32] LIDDLE, A. R.; PARSONS, P.; BARROW, J. D. Formalizing the slow roll approximation in inflation. *Phys. Rev.*, D50, p. 7222–7232, 1994.
- [33] SILK, J.; TURNER, M. S. Double inflation. *Phys. Rev. D*, American Physical Society, v. 35, p. 419–428, Jan 1987. Disponible em: <<https://link.aps.org/doi/10.1103/PhysRevD.35.419>>.

- [34] MURPHY, P.; KIM, C. W. Solution of the horizon and flatness problems by multiple inflations. *Phys. Rev. D*, American Physical Society, v. 37, p. 2732–2742, May 1988. Disponível em: <<https://link.aps.org/doi/10.1103/PhysRevD.37.2732>>.
- [35] MULLER, V.; SCHMIDT, H.-J. The Origin of Double Inflation. *Gen. Rel. Grav.*, v. 21, p. 489–494, 1989.
- [36] OLIVE, K. A. Inflation. *Physics Reports*, v. 190, n. 6, p. 307–403, 1990. ISSN 0370-1573. Disponível em: <<https://www.sciencedirect.com/science/article/pii/037015739090144Q>>.
- [37] HODGES, H. M. et al. Nonstandard primordial fluctuations from a polynomial inflation potential. *Nuclear Physics B*, v. 335, n. 1, p. 197–220, 1990. ISSN 0550-3213. Disponível em: <<https://www.sciencedirect.com/science/article/pii/055032139090177F>>.
- [38] LINDE, A. Axions in inflationary cosmology. *Physics Letters B*, v. 259, n. 1, p. 38–47, 1991. ISSN 0370-2693. Disponível em: <<https://www.sciencedirect.com/science/article/pii/037026939190130I>>.
- [39] OBIED, G. et al. *De Sitter Space and the Swampland*. 2018.
- [40] AGRAWAL, P. et al. On the cosmological implications of the string swampland. *Physics Letters B*, Elsevier BV, v. 784, p. 271–276, Sep 2018. ISSN 0370-2693. Disponível em: <<http://dx.doi.org/10.1016/j.physletb.2018.07.040>>.
- [41] GARG, S. K.; KRISHNAN, C. Bounds on slow roll and the de sitter swampland. *Journal of High Energy Physics*, Springer Science and Business Media LLC, v. 2019, n. 11, Nov 2019. ISSN 1029-8479. Disponível em: <[http://dx.doi.org/10.1007/JHEP11\(2019\)075](http://dx.doi.org/10.1007/JHEP11(2019)075)>.
- [42] BEDROYA, A. et al. Trans-planckian censorship and inflationary cosmology. *Physical Review D*, American Physical Society (APS), v. 101, n. 10, May 2020. ISSN 2470-0029. Disponível em: <<http://dx.doi.org/10.1103/PhysRevD.101.103502>>.
- [43] MOTAHARFAR, M.; KAMALI, V.; RAMOS, R. O. Warm inflation as a way out of the swampland. *Physical Review D*, American Physical So-

- ciety (APS), v. 99, n. 6, Mar 2019. ISSN 2470-0029. Disponível em: <<http://dx.doi.org/10.1103/PhysRevD.99.063513>>.
- [44] DAS, S. Note on single-field inflation and the swampland criteria. *Physical Review D*, American Physical Society (APS), v. 99, n. 8, Apr 2019. ISSN 2470-0029. Disponível em: <<http://dx.doi.org/10.1103/PhysRevD.99.083510>>.
- [45] DAS, S.; RAMOS, R. O. Runaway potentials in warm inflation satisfying the swampland conjectures. *Phys. Rev. D*, American Physical Society, v. 102, p. 103522, Nov 2020. Disponível em: <<https://link.aps.org/doi/10.1103/PhysRevD.102.103522>>.
- [46] COPI, C. J. et al. Large angle anomalies in the CMB. *Adv. Astron.*, v. 2010, p. 847541, 2010.
- [47] SCHWARZ, D. J. et al. CMB anomalies after planck. *Classical and Quantum Gravity*, IOP Publishing, v. 33, n. 18, p. 184001, aug 2016.
- [48] LYTH, D. H.; WANDS, D. Generating the curvature perturbation without an inflaton. *Phys. Lett.*, B524, p. 5–14, 2002.
- [49] GORDON, C. et al. Adiabatic and entropy perturbations from inflation. *Phys. Rev. D*, American Physical Society, v. 63, p. 023506, Dec 2000. Disponível em: <<https://link.aps.org/doi/10.1103/PhysRevD.63.023506>>.
- [50] BYRNES, C. T. et al. Scale dependence of localfNL. *Journal of Cosmology and Astroparticle Physics*, IOP Publishing, v. 2010, n. 02, p. 034–034, feb 2010.
- [51] BYRNES, C. T. et al. Strongly scale-dependent polyspectra from curvaton self-interactions. *Journal of Cosmology and Astroparticle Physics*, IOP Publishing, v. 2011, n. 11, p. 011–011, nov 2011.
- [52] AKRAMI, Y. et al. Planck 2018 results. IX. Constraints on primordial non-Gaussianity. *arXiv 1905.05697*, 2019.
- [53] SCHMIDT, F.; HUI, L. Cosmic microwave background power asymmetry from non-gaussian modulation. *Phys. Rev. Lett.*, American Physical Society, v. 110, p. 011301, Jan 2013. Disponível em: <<https://link.aps.org/doi/10.1103/PhysRevLett.110.011301>>.

- [54] BYRNES, C. T.; TARRANT, E. R. Scale-dependent non-gaussianity and the CMB power asymmetry. *Journal of Cosmology and Astroparticle Physics*, IOP Publishing, v. 2015, n. 07, p. 007–007, jul 2015.
- [55] LANGLOIS, D.; RENAUX-PETEL, S. Perturbations in generalized multi-field inflation. IOP Publishing, v. 2008, n. 04, p. 017, apr 2008. Disponível em: <<https://doi.org/10.1088/1475-7516/2008/04/017>>.
- [56] BRANDENBERGER, R. H. Alternatives to the inflationary paradigm of structure formation. *Int. J. Mod. Phys. Conf. Ser.*, v. 01, p. 67–79, 2011.
- [57] PETER, P.; PINTO-NETO, N. Cosmology without inflation. *Phys. Rev. D*, v. 78, p. 063506, 2008.
- [58] BRANDENBERGER, R. Initial Conditions for Inflation - A Short Review. *Int. J. Mod. Phys.*, D26, n. 01, p. 1740002, 2016.
- [59] FALCIANO, F. T.; PINTO-NETO, N.; SANTINI, E. S. An Inflationary Non-singular Quantum Cosmological Model. *Phys. Rev.*, D76, p. 083521, 2007.
- [60] NOVELLO, M.; BERGLIAFFA, S. E. P. Bouncing Cosmologies. *Phys. Rept.*, v. 463, p. 127–213, 2008.
- [61] CAI, Y.-F.; BRANDENBERGER, R.; ZHANG, X. The matter bounce curvature scenario. *Journal of Cosmology and Astroparticle Physics*, IOP Publishing, v. 2011, n. 03, p. 003–003, mar 2011. Disponível em: <<https://doi.org/10.1088/1475-7516/2011/03/003>>.
- [62] CAI, Y.-F.; WILSON-EWING, E. Non-singular bounce scenarios in loop quantum cosmology and the effective field description. *Journal of Cosmology and Astroparticle Physics*, IOP Publishing, v. 2014, n. 03, p. 026–026, mar 2014. Disponível em: <<https://doi.org/10.1088/1475-7516/2014/03/026>>.
- [63] WANDS, D. Duality invariance of cosmological perturbation spectra. *Phys. Rev.*, D60, p. 023507, 1999.
- [64] ELIZALDE, E.; HARO, J.; ODINTSOV, S. D. Quasimatter domination parameters in bouncing cosmologies. *Phys. Rev.*, D91, n. 6, p. 063522, 2015.

- [65] BATTEFELD, D.; PETER, P. A Critical Review of Classical Bouncing Cosmologies. *Phys. Rept.*, v. 571, p. 1–66, 2015.
- [66] LEVY, A. M. Fine-tuning challenges for the matter bounce scenario. *Phys. Rev.*, D95, n. 2, p. 023522, 2017.
- [67] BRANDENBERGER, R.; PETER, P. Bouncing Cosmologies: Progress and Problems. *Found. Phys.*, v. 47, n. 6, p. 797–850, 2017.
- [68] KHOURY, J. et al. Density perturbations in the ekpyrotic scenario. *Phys. Rev.*, D66, p. 046005, 2002.
- [69] LINDE, A. D. Inflationary theory versus ekpyrotic / cyclic scenario. In: *Workshop on Conference on the Future of Theoretical Physics and Cosmology in Honor of Steven Hawking's 60th Birthday Cambridge, England, January 7-10, 2002*. [s.n.], 2002. p. 801–838. Disponível em: <<http://alice.cern.ch/format/showfull?sysnb=2312154>>.
- [70] MARTIN, J. et al. Passing through the bounce in the ekpyrotic models. *Phys. Rev.*, D65, p. 123513, 2002.
- [71] ALLEN, L. E.; WANDS, D. Cosmological perturbations through a simple bounce. *Phys. Rev.*, D70, p. 063515, 2004.
- [72] XUE, B. et al. Nonperturbative analysis of the evolution of cosmological perturbations through a nonsingular bounce. *Phys. Rev.*, D88, p. 083509, 2013.
- [73] QUINTIN, J. et al. Evolution of cosmological perturbations and the production of non-Gaussianities through a nonsingular bounce: Indications for a no-go theorem in single field matter bounce cosmologies. *Phys. Rev.*, D92, n. 6, p. 063532, 2015.
- [74] VITENTI, S. D. P. *Estudo das Perturbações em Universos com Ricochete*. 2011.
- [75] CELANI, D. C. F.; PINTO-NETO, N.; VITENTI, S. D. P. Particle Creation in Bouncing Cosmologies. *Phys. Rev.*, D95, n. 2, p. 023523, 2017.
- [76] SCARDUA, A. et al. Fermion production in bouncing cosmologies. *Phys. Rev. D*, American Physical Society, v. 98, p. 083505, Oct 2018. Disponível em: <<https://link.aps.org/doi/10.1103/PhysRevD.98.083505>>.

- [77] LEMAITRE, G. The expanding universe. *Gen. Rel. Grav.*, v. 29, p. 641–680, 1997. [Annales Soc. Sci. Brux. Ser. I Sci. Math. Astron. Phys.A53,51(1933)].
- [78] STEINHARDT, P. J.; TUROK, N. Cosmic evolution in a cyclic universe. *Phys. Rev.*, D65, p. 126003, 2002.
- [79] BRAX, P.; BRUCK, C. van de; DAVIS, A.-C. Brane world cosmology. *Rept. Prog. Phys.*, v. 67, p. 2183–2232, 2004.
- [80] LEHNERS, J.-L. Ekpyrotic and Cyclic Cosmology. *Phys. Rept.*, v. 465, p. 223–263, 2008.
- [81] BACALHAU, A. P.; PINTO-NETO, N.; VITENTI, S. D. P. Consistent scalar and tensor perturbation power spectra in single fluid matter bounce with dark energy era. *Phys. Rev. D*, American Physical Society, v. 97, p. 083517, Apr 2018. Disponível em: <<https://link.aps.org/doi/10.1103/PhysRevD.97.083517>>.
- [82] FALCIANO, F. T.; LILLEY, M.; PETER, P. A Classical bounce: Constraints and consequences. *Phys. Rev.*, D77, p. 083513, 2008.
- [83] VITENTI, S. D. P.; PINTO-NETO, N. Large Adiabatic Scalar Perturbations in a Regular Bouncing Universe. *Phys. Rev.*, D85, p. 023524, 2012.
- [84] ALISHAHIHA, M.; SILVERSTEIN, E.; TONG, D. DBI in the sky. *Phys. Rev.*, D70, p. 123505, 2004.
- [85] PINTO-NETO, N. et al. The Wheeler-DeWitt Quantization Can Solve the Singularity Problem. *Phys. Rev. D*, v. 86, p. 063504, 2012.
- [86] PINTO-NETO, N. Bouncing quantum cosmology. *Universe*, v. 7, n. 4, 2021. ISSN 2218-1997. Disponível em: <<https://www.mdpi.com/2218-1997/7/4/110>>.
- [87] CAI, Y.-F.; WILSON-EWING, E. Non-singular bounce scenarios in loop quantum cosmology and the effective field description. *JCAP*, v. 1403, p. 026, 2014.
- [88] CAI, Y.-F.; WILSON-EWING, E. A Λ CDM bounce scenario. *JCAP*, v. 1503, n. 03, p. 006, 2015.

- [89] PETER, P.; VITENTI, S. D. P. The simplest possible bouncing quantum cosmological model. *Mod. Phys. Lett.*, A31, n. 21, p. 1640006, 2016.
- [90] MARTIN, J.; BRANDENBERGER, R. H. Trans-planckian problem of inflationary cosmology. *Phys. Rev. D*, American Physical Society, v. 63, p. 123501, May 2001. Disponível em: <<https://link.aps.org/doi/10.1103/PhysRevD.63.123501>>.
- [91] BENNETT, C. L. et al. NINE-YEAR WILKINSON MICROWAVE ANISOTROPY PROBE(WMAP) OBSERVATIONS: FINAL MAPS AND RESULTS. *The Astrophysical Journal Supplement Series*, IOP Publishing, v. 208, n. 2, p. 20, sep 2013.
- [92] Planck Collaboration; Aghanim, N. et al. Planck 2018 results - i. overview and the cosmological legacy of planck. *A&A*, v. 641, p. A1, 2020. Disponível em: <<https://doi.org/10.1051/0004-6361/201833880>>.
- [93] Planck Collaboration; Aghanim, N. et al. Planck 2018 results - v. cmb power spectra and likelihoods. *A&A*, v. 641, p. A5, 2020. Disponível em: <<https://doi.org/10.1051/0004-6361/201936386>>.
- [94] MUKHANOV, V. F.; FELDMAN, H. A.; BRANDENBERGER, R. H. Theory of cosmological perturbations. Part 1. Classical perturbations. Part 2. Quantum theory of perturbations. Part 3. Extensions. *Phys. Rept.*, v. 215, p. 203–333, 1992.
- [95] RIOTTO, A. Inflation and the theory of cosmological perturbations. In: *Astroparticle physics and cosmology. Proceedings: Summer School, Trieste, Italy, Jun 17-Jul 5 2002*. [S.l.: s.n.], 2002. p. 317–413.
- [96] LYTH, D. H.; RIOTTO, A. Particle physics models of inflation and the cosmological density perturbation. *Phys. Rept.*, v. 314, p. 1–146, 1999.
- [97] DURRER, R.; VERNIZZI, F. Adiabatic perturbations in pre - big bang models: Matching conditions and scale invariance. *Phys. Rev.*, D66, p. 083503, 2002.
- [98] ENQVIST, K.; SLOTH, M. S. Adiabatic CMB perturbations in pre - big bang string cosmology. *Nucl. Phys.*, B626, p. 395–409, 2002.
- [99] PETER, P.; PINTO-NETO, N. Primordial perturbations in a non singular bouncing universe model. *Phys. Rev.*, D66, p. 063509, 2002.

- [100] LYTH, D. H. The Primordial curvature perturbation in the ekpyrotic universe. *Phys. Lett.*, B524, p. 1–4, 2002.
- [101] LEHNERS, J.-L. et al. Generating ekpyrotic curvature perturbations before the big bang. *Phys. Rev.*, D76, p. 103501, 2007.
- [102] LI, Y.; ZHU, J.-Y. Adiabatic and nonadiabatic perturbations for loop quantum cosmology. *Phys. Rev. D*, American Physical Society, v. 85, p. 023515, Jan 2012. Disponível em: <<https://link.aps.org/doi/10.1103/PhysRevD.85.023515>>.
- [103] WILSON-EWING, E. Separate universes in loop quantum cosmology: Framework and applications. *International Journal of Modern Physics D*, v. 25, n. 08, p. 1642002, 2016.
- [104] MUKHANOV, V. *Physical Foundations of Cosmology*. Oxford: Cambridge University Press, 2005. ISBN 0521563984, 9780521563987. Disponível em: <<http://www-spines.fnal.gov/spines/find/books/www?cl=QB981.M89::2005>>.
- [105] JOYCE, A. et al. Beyond the cosmological standard model. *Physics Reports*, v. 568, p. 1–98, 2015. ISSN 0370-1573. Beyond the cosmological standard model. Disponível em: <<https://www.sciencedirect.com/science/article/pii/S0370157314004487>>.
- [106] KOYAMA, K. Cosmological tests of modified gravity. *Reports on Progress in Physics*, IOP Publishing, v. 79, n. 4, p. 046902, mar 2016. Disponível em: <<https://doi.org/10.1088/0034-4885/79/4/046902>>.
- [107] Brandenberger, R. H. Lectures on the Theory of Cosmological Perturbations. In: _____. *The early universe and observational cosmology*, edited by N. Breton, J.L. Cervantes-Cota, and M. Salgado, *Lecture Notes in Physics*, vol. 646, 2004., p.127-167. [S.l.: s.n.], 2004. p. 127–167.
- [108] BARTOLO, N. et al. Perturbations in cosmologies with a scalar field and a perfect fluid. *Phys. Rev. D*, American Physical Society, v. 70, p. 043532, Aug 2004. Disponível em: <<https://link.aps.org/doi/10.1103/PhysRevD.70.043532>>.
- [109] MIELCZAREK, J. Multi-fluid potential in the loop cosmology. *Physics Letters B*, v. 675, n. 3, p. 273 – 278, 2009. ISSN 0370-2693. Disponível em: <<http://www.sciencedirect.com/science/article/pii/S0370269309004456>>.

- [110] BIRRELL, N. D.; DAVIES, P. C. W. *Quantum Fields in Curved Space*. Cambridge, UK: Cambridge Univ. Press, 1984. (Cambridge Monographs on Mathematical Physics). ISBN 0521278589, 9780521278584, 9780521278584. Disponível em: <<http://www.cambridge.org/mw/academic/subjects/physics/theoretical-physics-and-mathematical-physics/quantum-fields-curved-space?format=PB>>.
- [111] WANDS, D. et al. New approach to the evolution of cosmological perturbations on large scales. *Phys. Rev. D*, American Physical Society, v. 62, p. 043527, Jul 2000. Disponível em: <<https://link.aps.org/doi/10.1103/PhysRevD.62.043527>>.
- [112] KOYAMA, K.; WANDS, D. Ekpyrotic collapse with multiple fields. *Journal of Cosmology and Astroparticle Physics*, IOP Publishing, v. 2007, n. 04, p. 008–008, apr 2007. Disponível em: <<https://doi.org/10.1088/1475-7516/2007/04/008>>.
- [113] LEHNERS, J.-L.; STEINHARDT, P. J. Non-gaussian density fluctuations from entropically generated curvature perturbations in ekpyrotic models. *Phys. Rev. D*, American Physical Society, v. 77, p. 063533, Mar 2008. Disponível em: <<https://link.aps.org/doi/10.1103/PhysRevD.77.063533>>.
- [114] LEHNERS, J.-L.; STEINHARDT, P. J. Intuitive understanding of non-gaussianity in ekpyrotic and cyclic models. *Phys. Rev. D*, American Physical Society, v. 78, p. 023506, Jul 2008. Disponível em: <<https://link.aps.org/doi/10.1103/PhysRevD.78.023506>>.
- [115] LEHNERS, J.-L. Ekpyrotic Non-Gaussianity: A Review. *Adv. Astron.*, v. 2010, p. 903907, 2010.
- [116] CAI, Y.-F. et al. Two field matter bounce cosmology. *Journal of Cosmology and Astroparticle Physics*, IOP Publishing, v. 2013, n. 10, p. 024–024, oct 2013. Disponível em: <<https://doi.org/10.1088/1475-7516/2013/10/024>>.
- [117] FELICE, A. D.; TSUJIKAWA, S. $f(R)$ theories. *Living Rev. Rel.*, v. 13, p. 3, 2010.
- [118] SOTIRIOU, T. P.; FARAONI, V. $f(R)$ Theories Of Gravity. *Rev. Mod. Phys.*, v. 82, p. 451–497, 2010.
- [119] HWANG, J.-c. Quantum fluctuations of cosmological perturbations in generalized gravity. *Class. Quant. Grav.*, v. 14, p. 3327–3336, 1997.

- [120] HWANG, J.-c.; NOH, H. Cosmological perturbations in generalized gravity theories. *Phys. Rev.*, D54, p. 1460–1473, 1996.
- [121] PENZIAS, A. A.; WILSON, R. W. A Measurement of excess antenna temperature at 4080-Mc/s. *Astrophys. J.*, v. 142, p. 419–421, 1965.
- [122] DODELSON, S. *Modern Cosmology*. Amsterdam: Academic Press, 2003. ISBN 978-0-12-219141-1.
- [123] BAUMANN, D. The Physics of Inflation. PhD Lecture Notes, Cambridge University, Department of Applied Mathematics and Theoretical Physics. 2012.
- [124] BARTOLO, N. et al. Non-gaussianity from inflation: theory and observations. *Physics Reports*, v. 402, n. 3, p. 103–266, 2004. ISSN 0370-1573. Disponível em: <<https://www.sciencedirect.com/science/article/pii/S0370157304003151>>.
- [125] CREMINELLI, P.; ZALDARRIAGA, M. A single-field consistency relation for the three-point function. *Journal of Cosmology and Astroparticle Physics*, IOP Publishing, v. 2004, n. 10, p. 006–006, oct 2004.
- [126] KOMATSU, E.; SPERGEL, D. N. Acoustic signatures in the primary microwave background bispectrum. *Phys. Rev. D*, American Physical Society, v. 63, p. 063002, Feb 2001. Disponível em: <<https://link.aps.org/doi/10.1103/PhysRevD.63.063002>>.
- [127] BYRNES, C. T. Lecture notes on non-Gaussianity. *Astrophys. Space Sci. Proc.*, v. 45, p. 135–165, 2016.
- [128] MEERBURG, P. D. et al. Primordial Non-Gaussianity. 3 2019.
- [129] ANSARI, R. et al. Inflation and Early Dark Energy with a Stage II Hydrogen Intensity Mapping experiment. 10 2018.
- [130] ABAZAJIAN, K. N. et al. CMB-S4 Science Book, First Edition. 2016.
- [131] ABAZAJIAN, K. et al. CMB-S4 Science Case, Reference Design, and Project Plan. 7 2019.
- [132] SUYAMA, T.; YAMAGUCHI, M. Non-gaussianity in the modulated reheating scenario. *Phys. Rev. D*, American Physical Society, v. 77, p. 023505, Jan 2008. Disponível em: <<https://link.aps.org/doi/10.1103/PhysRevD.77.023505>>.

- [133] STAROBINSKY, A. A. Multicomponent de Sitter (Inflationary) Stages and the Generation of Perturbations. *JETP Lett.*, v. 42, p. 152–155, 1985.
- [134] SALOPEK, D. S.; BOND, J. R. Nonlinear evolution of long wavelength metric fluctuations in inflationary models. *Phys. Rev. D*, v. 42, p. 3936–3962, 1990.
- [135] SASAKI, M.; STEWART, E. D. A General analytic formula for the spectral index of the density perturbations produced during inflation. *Prog. Theor. Phys.*, v. 95, p. 71–78, 1996.
- [136] LYTH, D. H.; RODRÍGUEZ, Y. Inflationary prediction for primordial non-gaussianity. *Phys. Rev. Lett.*, American Physical Society, v. 95, p. 121302, Sep 2005. Disponível em: <<https://link.aps.org/doi/10.1103/PhysRevLett.95.121302>>.
- [137] SASAKI, M.; VÄLIVIITA, J.; WANDS, D. Non-gaussianity of the primordial perturbation in the curvaton model. *Phys. Rev. D*, American Physical Society, v. 74, p. 103003, Nov 2006. Disponível em: <<https://link.aps.org/doi/10.1103/PhysRevD.74.103003>>.
- [138] WONG, K. C. et al. H0LiCOW – XIII. A 2.4 per cent measurement of H0 from lensed quasars: 5.3 σ tension between early- and late-Universe probes. *Monthly Notices of the Royal Astronomical Society*, v. 498, n. 1, p. 1420–1439, 09 2019. ISSN 0035-8711. Disponível em: <<https://doi.org/10.1093/mnras/stz3094>>.
- [139] RIESS, A. G. et al. A Comprehensive Measurement of the Local Value of the Hubble Constant with 1 km/s/Mpc Uncertainty from the Hubble Space Telescope and the SH0ES Team. 12 2021.
- [140] Heymans, Catherine et al. Kids-1000 cosmology: Multi-probe weak gravitational lensing and spectroscopic galaxy clustering constraints. *A&A*, v. 646, p. A140, 2021. Disponível em: <<https://doi.org/10.1051/0004-6361/202039063>>.
- [141] VERDE, L.; TREU, T.; RIESS, A. G. Tensions between the Early and the Late Universe. *Nature Astron.*, v. 3, p. 891, 7 2019.
- [142] EFSTATHIOU, G. To H0 or not to H0? *Monthly Notices of the Royal Astronomical Society*, v. 505, n. 3, p. 3866–3872, 06 2021. ISSN 0035-8711. Disponível em: <<https://doi.org/10.1093/mnras/stab1588>>.

- [143] VALENTINO, E. D. et al. In the realm of the hubble tension - a review of solutions. *Classical and Quantum Gravity*, IOP Publishing, v. 38, n. 15, p. 153001, jul 2021. Disponível em: <<https://doi.org/10.1088/1361-6382/ac086d>>.
- [144] ANCHORDOQUI, L. A. et al. Dissecting the h_0 and s_8 tensions with planck + bao + supernova type ia in multi-parameter cosmologies. *Journal of High Energy Astrophysics*, v. 32, p. 28–64, 2021. ISSN 2214-4048. Disponível em: <<https://www.sciencedirect.com/science/article/pii/S2214404821000240>>.
- [145] Di Valentino, E. et al. Cosmology intertwined iii: $f\sigma_8$ and s_8 . *Astroparticle Physics*, v. 131, p. 102604, 2021. ISSN 0927-6505. Disponível em: <<https://www.sciencedirect.com/science/article/pii/S0927650521000487>>.
- [146] KEHAGIAS, A.; DIZGAH, A. M.; RIOTTO, A. Remarks on the Starobinsky model of inflation and its descendants. *Phys. Rev.*, D89, n. 4, p. 043527, 2014.
- [147] BRANDENBERGER, R. H. String Gas Cosmology: Progress and Problems. *Class. Quant. Grav.*, v. 28, p. 204005, 2011.
- [148] GUIMARÃES, L. F.; FALCIANO, F. T.; BRANDO, G. Quasimatter bounce equivalent to starobinsky inflation. *Phys. Rev. D*, American Physical Society, v. 99, p. 103515, May 2019. Disponível em: <<https://link.aps.org/doi/10.1103/PhysRevD.99.103515>>.
- [149] CLIFTON, T. et al. Modified Gravity and Cosmology. *Phys. Rept.*, v. 513, p. 1–189, 2012.
- [150] BOEHMER, C. G.; HARKO, T.; LOBO, F. S. N. Dark matter as a geometric effect in $f(R)$ gravity. *Astropart. Phys.*, v. 29, p. 386–392, 2008.
- [151] STAROBINSKY, A. A. Disappearing cosmological constant in $f(R)$ gravity. *JETP Lett.*, v. 86, p. 157–163, 2007.
- [152] NOJIRI, S.; ODINTSOV, S. D. Dark energy, inflation and dark matter from modified $F(R)$ gravity. *TSPU Bulletin*, N8(110), p. 7–19, 2011.
- [153] HORNDESKI, G. W. Second-order scalar-tensor field equations in a four-dimensional space. *Int. J. Theor. Phys.*, v. 10, p. 363–384, 1974.

- [154] GLEYZES, J. et al. Healthy theories beyond Horndeski. *Phys. Rev. Lett.*, v. 114, n. 21, p. 211101, 2015.
- [155] KAMENSHCHIK, A. Yu. et al. Transformations between Jordan and Einstein frames: Bounces, antigravity, and crossing singularities. *Phys. Rev.*, D94, n. 6, p. 063510, 2016.
- [156] KOSHELEV, A. S. et al. Occurrence of exact R^2 inflation in non-local UV-complete gravity. *JHEP*, v. 11, p. 067, 2016.
- [157] BEZRUKOV, F. L.; GORBUNOV, D. S. Distinguishing between R^2 -inflation and Higgs-inflation. *Phys. Lett.*, B713, p. 365–368, 2012.
- [158] MARTIN, J.; RINGEVAL, C.; VENNIN, V. Encyclopædia Inflationaris. *Phys. Dark Univ.*, v. 5-6, p. 75–235, 2014.
- [159] ADE, P. A. R. et al. Planck 2015 results. XX. Constraints on inflation. *Astron. Astrophys.*, v. 594, p. A20, 2016.
- [160] BRUSTEIN, R.; GASPERINI, M.; VENEZIANO, G. Duality in cosmological perturbation theory. *Phys. Lett.*, B431, p. 277–285, 1998.
- [161] BORDE, A.; VILENKIN, A. Eternal inflation and the initial singularity. *Phys. Rev. Lett.*, American Physical Society, v. 72, p. 3305–3308, May 1994. Disponível em: <<https://link.aps.org/doi/10.1103/PhysRevLett.72.3305>>.
- [162] BORDE, A.; VILENKIN, A. Singularities in inflationary cosmology: A review. *International Journal of Modern Physics D*, v. 05, n. 06, p. 813–824, 1996. Disponível em: <<https://doi.org/10.1142/S0218271896000497>>.
- [163] PETER, P.; PINHO, E. J. C.; PINTO-NETO, N. Noninflationary model with scale invariant cosmological perturbations. *Phys. Rev. D*, American Physical Society, v. 75, p. 023516, Jan 2007. Disponível em: <<https://link.aps.org/doi/10.1103/PhysRevD.75.023516>>.
- [164] BOJOWALD, M. Quantum cosmology: a review. *Reports on Progress in Physics*, v. 78, n. 2, p. 023901, 2015. Disponível em: <<http://stacks.iop.org/0034-4885/78/i=2/a=023901>>.

- [165] CRAIG, D. A.; SINGH, P. Consistent probabilities in loop quantum cosmology. *Classical and Quantum Gravity*, v. 30, n. 20, p. 205008, 2013. Disponible em: <http://stacks.iop.org/0264-9381/30/i=20/a=205008>.
- [166] ASHTEKAR, A.; PAWLOWSKI, T.; SINGH, P. Quantum nature of the big bang: Improved dynamics. *Phys. Rev. D*, American Physical Society, v. 74, p. 084003, Oct 2006. Disponible em: <https://link.aps.org/doi/10.1103/PhysRevD.74.084003>.
- [167] SINGH, P.; VANDERSLOOT, K.; VERESHCHAGIN, G. V. Non-singular bouncing universes in loop quantum cosmology. *Phys. Rev. D*, American Physical Society, v. 74, p. 043510, Aug 2006. Disponible em: <https://link.aps.org/doi/10.1103/PhysRevD.74.043510>.
- [168] ASHTEKAR, A.; SLOAN, D. Probability of Inflation in Loop Quantum Cosmology. *Gen. Rel. Grav.*, v. 43, p. 3619–3655, 2011.
- [169] BHARDWAJ, A.; COPELAND, E. J.; LOUKO, J. Inflation in loop quantum cosmology. *Phys. Rev. D*, American Physical Society, v. 99, p. 063520, Mar 2019. Disponible em: <https://link.aps.org/doi/10.1103/PhysRevD.99.063520>.
- [170] AGULLO, I. Loop quantum cosmology, non-gaussianity, and cmb power asymmetry. *Phys. Rev. D*, American Physical Society, v. 92, p. 064038, Sep 2015. Disponible em: <https://link.aps.org/doi/10.1103/PhysRevD.92.064038>.
- [171] BARBOZA, L. N.; GRAEF, L. L.; RAMOS, R. O. Warm bounce in loop quantum cosmology and the prediction for the duration of inflation. *Phys. Rev. D*, American Physical Society, v. 102, p. 103521, Nov 2020. Disponible em: <https://link.aps.org/doi/10.1103/PhysRevD.102.103521>.
- [172] BRANDENBERGER, R. H. A Status review of inflationary cosmology. In: *Proceedings, 10th Workshop on General Relativity and Gravitation in Japan (JGRG10): Osaka, Japan, September 10-14, 2000*. [S.l.: s.n.], 2000.
- [173] WEINBERG, S. Adiabatic modes in cosmology. *Phys. Rev.*, D67, p. 123504, 2003.
- [174] CAI, Y.-F.; WILSON-EWING, E. A lcdm bounce scenario. *Journal of Cosmology and Astroparticle Physics*, v. 2015, n. 03, p. 006, 2015. Disponible em: <http://stacks.iop.org/1475-7516/2015/i=03/a=006>.

- [175] VITENTI, S. D. P.; FALCIANO, F. T.; PINTO-NETO, N. Quantum Cosmological Perturbations of Generic Fluids in Quantum Universes. *Phys. Rev.*, D87, n. 10, p. 103503, 2013.
- [176] FALCIANO, F. T.; PINTO-NETO, N.; STRUYVE, W. Wheeler-dewitt quantization and singularities. *Phys. Rev. D*, American Physical Society, v. 91, p. 043524, Feb 2015. Disponível em: <<https://link.aps.org/doi/10.1103/PhysRevD.91.043524>>.
- [177] PINTO-NETO, N.; SANTINI, E. S.; FALCIANO, F. T. Quantization of Friedmann cosmological models with two fluids: Dust plus radiation. *Phys. Lett.*, A344, p. 131–143, 2005.
- [178] FALCIANO, F. T.; PINTO-NETO, N.; VITENTI, S. D. P. Scalar Field Perturbations with Arbitrary Potentials in Quantum Backgrounds. *Phys. Rev.*, D87, n. 10, p. 103514, 2013.
- [179] GASPERINI, M.; VENEZIANO, G. The Pre - big bang scenario in string cosmology. *Phys. Rept.*, v. 373, p. 1–212, 2003.
- [180] ASHTEKAR, A.; PAWLOWSKI, T.; SINGH, P. Quantum nature of the big bang: An analytical and numerical investigation. *Phys. Rev. D*, American Physical Society, v. 73, p. 124038, Jun 2006. Disponível em: <<https://link.aps.org/doi/10.1103/PhysRevD.73.124038>>.
- [181] ASHTEKAR, A.; SINGH, P. Loop quantum cosmology: a status report. *Classical and Quantum Gravity*, IOP Publishing, v. 28, n. 21, p. 213001, sep 2011. Disponível em: <<https://doi.org/10.1088/0264-9381/28/21/213001>>.
- [182] BOJOWALD, M.; BRAHMA, S. Minisuperspace models as infrared contributions. *Phys. Rev. D*, American Physical Society, v. 93, p. 125001, Jun 2016. Disponível em: <<https://link.aps.org/doi/10.1103/PhysRevD.93.125001>>.
- [183] LI, B.-F. et al. Preinflationary perturbations from the closed algebra approach in loop quantum cosmology. *Phys. Rev. D*, American Physical Society, v. 99, p. 103536, May 2019. Disponível em: <<https://link.aps.org/doi/10.1103/PhysRevD.99.103536>>.

- [184] BOLLIET, B. et al. Comparison of primordial tensor power spectra from the deformed algebra and dressed metric approaches in loop quantum cosmology. *Phys. Rev. D*, v. 91, n. 8, p. 084035, 2015.
- [185] LI, B.-F.; SINGH, P. On a close relationship between the dressed metric and the hybrid approach to perturbations in effective loop quantum cosmology. 6 2022.
- [186] GOMAR, L. C. et al. Cosmological perturbations in hybrid loop quantum cosmology: Mukhanov-sasaki variables. *Phys. Rev. D*, American Physical Society, v. 90, p. 064015, Sep 2014. Disponível em: <<https://link.aps.org/doi/10.1103/PhysRevD.90.064015>>.
- [187] CAILLETEAU, T. et al. Consistency of holonomy-corrected scalar, vector, and tensor perturbations in loop quantum cosmology. *Phys. Rev. D*, American Physical Society, v. 86, p. 087301, Oct 2012. Disponível em: <<https://link.aps.org/doi/10.1103/PhysRevD.86.087301>>.
- [188] GUIMARÃES, L. F.; FALCIANO, F. T. Viable curvaton models from the f_{nl} parameter. *Phys. Rev. D*, American Physical Society, v. 103, p. 063530, Mar 2021. Disponível em: <<https://link.aps.org/doi/10.1103/PhysRevD.103.063530>>.
- [189] VENNIN, V.; KOYAMA, K.; WANDS, D. Encyclopædia curvatonis. *Journal of Cosmology and Astroparticle Physics*, IOP Publishing, v. 2015, n. 11, p. 008–008, nov 2015.
- [190] BYRNES, C. T. et al. The hemispherical asymmetry from a scale-dependent inflationary bispectrum. *Journal of Cosmology and Astroparticle Physics*, IOP Publishing, v. 2016, n. 06, p. 025–025, jun 2016.
- [191] IJJAS, A.; STEINHARDT, P. J.; LOEB, A. Inflationary paradigm in trouble after planck2013. *Physics Letters B*, v. 723, n. 4, p. 261 – 266, 2013. ISSN 0370-2693. Disponível em: <<http://www.sciencedirect.com/science/article/pii/S0370269313003924>>.
- [192] GORDON, C. et al. Spontaneous isotropy breaking: A mechanism for cmb multipole alignments. *Phys. Rev. D*, American Physical Society, v. 72, p. 103002, Nov 2005. Disponível em: <<https://link.aps.org/doi/10.1103/PhysRevD.72.103002>>.

- [193] HIRATA, C. M. Constraints on cosmic hemispherical power anomalies from quasars. *Journal of Cosmology and Astroparticle Physics*, IOP Publishing, v. 2009, n. 09, p. 011–011, sep 2009.
- [194] FLENDER, S.; HOTCHKISS, S. The small scale power asymmetry in the cosmic microwave background. *Journal of Cosmology and Astroparticle Physics*, IOP Publishing, v. 2013, n. 09, p. 033–033, sep 2013.
- [195] NOTARI, A.; QUARTIN, M.; CATENA, R. CMB aberration and doppler effects as a source of hemispherical asymmetries. *Journal of Cosmology and Astroparticle Physics*, IOP Publishing, v. 2014, n. 03, p. 019–019, mar 2014.
- [196] AIOLA, S. et al. Microwave background correlations from dipole anisotropy modulation. *Phys. Rev. D*, American Physical Society, v. 92, p. 063008, Sep 2015. Disponível em: <<https://link.aps.org/doi/10.1103/PhysRevD.92.063008>>.
- [197] ERICKCEK, A. L.; KAMIONKOWSKI, M.; CARROLL, S. M. A hemispherical power asymmetry from inflation. *Phys. Rev. D*, American Physical Society, v. 78, p. 123520, Dec 2008. Disponível em: <<https://link.aps.org/doi/10.1103/PhysRevD.78.123520>>.
- [198] LYTH, D. H.; WANDS, D. Generating the curvature perturbation without an inflaton. *Physics Letters B*, v. 524, n. 1, p. 5 – 14, 2002. ISSN 0370-2693. Disponível em: <<http://www.sciencedirect.com/science/article/pii/S0370269301013661>>.
- [199] KENTON, Z.; MULRYNE, D. J.; THOMAS, S. Generating the cosmic microwave background power asymmetry with g_{NL} . *Phys. Rev. D*, American Physical Society, v. 92, p. 023505, Jul 2015. Disponível em: <<https://link.aps.org/doi/10.1103/PhysRevD.92.023505>>.
- [200] LYTH, D. H. Generating f_{NL} at $l \leq 60$. *Journal of Cosmology and Astroparticle Physics*, IOP Publishing, v. 2015, n. 04, p. 039–039, apr 2015.
- [201] ADHIKARI, S.; DEUTSCH, A.-S.; SHANDERA, S. Statistical anisotropies in temperature and polarization fluctuations from a scale-dependent trispectrum. *Phys. Rev. D*, American Physical Society, v. 98, p. 023520, Jul 2018. Disponível em: <<https://link.aps.org/doi/10.1103/PhysRevD.98.023520>>.

- [202] Hansen, F. K. et al. Isotropic non-gaussian gnl-like toy models that reproduce cosmic microwave background anomalies. *A&A*, v. 626, p. A13, 2019. Disponível em: <<https://doi.org/10.1051/0004-6361/201833698>>.
- [203] BYRNES, C. T. et al. Implications of the cosmic microwave background power asymmetry for the early universe. *Phys. Rev. D*, American Physical Society, v. 93, p. 123003, Jun 2016. Disponível em: <<https://link.aps.org/doi/10.1103/PhysRevD.93.123003>>.
- [204] ADHIKARI, S.; SHANDERA, S.; ERICKCEK, A. L. Large-scale anomalies in the cosmic microwave background as signatures of non-gaussianity. *Phys. Rev. D*, American Physical Society, v. 93, p. 023524, Jan 2016. Disponível em: <<https://link.aps.org/doi/10.1103/PhysRevD.93.023524>>.
- [205] HUANG, Q.-G. A curvaton with a polynomial potential. *Journal of Cosmology and Astroparticle Physics*, IOP Publishing, v. 2008, n. 11, p. 005, nov 2008.
- [206] ENQVIST, K. et al. Non-gaussian fingerprints of self-interacting curvaton. *Journal of Cosmology and Astroparticle Physics*, IOP Publishing, v. 2010, n. 04, p. 009–009, apr 2010.
- [207] LANGLOIS, D.; VERNIZZI, F. Mixed inflaton and curvaton perturbations. *Phys. Rev. D*, American Physical Society, v. 70, p. 063522, Sep 2004. Disponível em: <<https://link.aps.org/doi/10.1103/PhysRevD.70.063522>>.
- [208] ICHIKAWA, K. et al. Non-gaussianity, spectral index, and tensor modes in mixed inflaton and curvaton models. *Phys. Rev. D*, American Physical Society, v. 78, p. 023513, Jul 2008. Disponível em: <<https://link.aps.org/doi/10.1103/PhysRevD.78.023513>>.
- [209] BYRNES, C. T.; CORTÊS, M.; LIDDLE, A. R. Comprehensive analysis of the simplest curvaton model. *Phys. Rev. D*, American Physical Society, v. 90, p. 023523, Jul 2014. Disponível em: <<https://link.aps.org/doi/10.1103/PhysRevD.90.023523>>.
- [210] KAWASAKI, M.; KOBAYASHI, T.; TAKAHASHI, F. Non-gaussianity from curvatons revisited. *Phys. Rev. D*, American Physical Society, v. 84, p. 123506, Dec 2011. Disponível em: <<https://link.aps.org/doi/10.1103/PhysRevD.84.123506>>.

- [211] MEYERS, J.; TARRANT, E. R. M. Perturbative reheating after multiple-field inflation: The impact on primordial observables. *Phys. Rev. D*, American Physical Society, v. 89, p. 063535, Mar 2014. Disponível em: <<https://link.aps.org/doi/10.1103/PhysRevD.89.063535>>.
- [212] MOLLERACH, S. Isocurvature baryon perturbations and inflation. *Phys. Rev. D*, American Physical Society, v. 42, p. 313–325, Jul 1990. Disponível em: <<https://link.aps.org/doi/10.1103/PhysRevD.42.313>>.
- [213] LYTH, D. H.; UNGARELLI, C.; WANDS, D. Primordial density perturbation in the curvaton scenario. *Phys. Rev. D*, American Physical Society, v. 67, p. 023503, Jan 2003. Disponível em: <<https://link.aps.org/doi/10.1103/PhysRevD.67.023503>>.
- [214] LINDE, A. Chaotic inflation. *Physics Letters B*, v. 129, n. 3, p. 177 – 181, 1983. ISSN 0370-2693. Disponível em: <<http://www.sciencedirect.com/science/article/pii/0370269383908377>>.
- [215] ENQVIST, K. et al. The subdominant curvaton. *Journal of Cosmology and Astroparticle Physics*, IOP Publishing, v. 2009, n. 11, p. 003–003, nov 2009.
- [216] SEFUSATTI, E. et al. Constraining running non-gaussianity. *Journal of Cosmology and Astroparticle Physics*, IOP Publishing, v. 2009, n. 12, p. 022–022, dec 2009.
- [217] ENQVIST, K.; MULRYNE, D. J.; NURMI, S. Resolving primordial physics through correlated signatures. *Journal of Cosmology and Astroparticle Physics*, IOP Publishing, v. 2015, n. 05, p. 010–010, may 2015.
- [218] QUARTIN, M.; NOTARI, A. On the significance of power asymmetries in planck CMB data at all scales. *Journal of Cosmology and Astroparticle Physics*, IOP Publishing, v. 2015, n. 01, p. 008–008, jan 2015.
- [219] KANNO, S.; SASAKI, M.; TANAKA, T. A viable explanation of the CMB dipolar statistical anisotropy. *Progress of Theoretical and Experimental Physics*, v. 2013, n. 11, 11 2013. ISSN 2050-3911. 111E01. Disponível em: <<https://doi.org/10.1093/ptep/ptt093>>.

- [220] MARCOS-CABALLERO, A.; MARTÍNEZ-GONZÁLEZ, E. Scale-dependent dipolar modulation and the quadrupole-octopole alignment in the CMB temperature. *Journal of Cosmology and Astroparticle Physics*, IOP Publishing, v. 2019, n. 10, p. 053–053, oct 2019.
- [221] FERTIG, A.; LEHNERS, J.-L.; MALLWITZ, E. Ekpyrotic perturbations with small non-gaussian corrections. *Phys. Rev. D*, American Physical Society, v. 89, p. 103537, May 2014. Disponível em: <<https://link.aps.org/doi/10.1103/PhysRevD.89.103537>>.
- [222] FERTIG, A. et al. Converting entropy to curvature perturbations after a cosmic bounce. *Journal of Cosmology and Astroparticle Physics*, IOP Publishing, v. 2016, n. 10, p. 005–005, oct 2016. Disponível em: <<https://doi.org/10.1088/1475-7516/2016/10/005>>.
- [223] FONSECA, J.; WANDS, D. Primordial non-gaussianity from mixed inflaton-curvature perturbations. *Journal of Cosmology and Astroparticle Physics*, IOP Publishing, v. 2012, n. 06, p. 028–028, jun 2012. Disponível em: <<https://doi.org/10.1088/1475-7516/2012/06/028>>.
- [224] PINHO, E. J. C.; PINTO-NETO, N. Scalar and vector perturbations in quantum cosmological backgrounds. *Phys. Rev. D*, American Physical Society, v. 76, p. 023506, Jul 2007. Disponível em: <<https://link.aps.org/doi/10.1103/PhysRevD.76.023506>>.
- [225] BOHM, D. A suggested interpretation of the quantum theory in terms of "hidden" variables. i. *Phys. Rev.*, American Physical Society, v. 85, p. 166–179, Jan 1952. Disponível em: <<https://link.aps.org/doi/10.1103/PhysRev.85.166>>.
- [226] BOHM, D. A suggested interpretation of the quantum theory in terms of "hidden" variables. ii. *Phys. Rev.*, American Physical Society, v. 85, p. 180–193, Jan 1952. Disponível em: <<https://link.aps.org/doi/10.1103/PhysRev.85.180>>.
- [227] HOLLAND, P. R. The de Broglie-Bohm theory of motion and quantum field theory. *Phys. Rept.*, v. 224, p. 95–150, 1993.
- [228] MALIK, K. A.; WANDS, D. Adiabatic and entropy perturbations with interacting fluids and fields. *Journal of Cosmology and Astroparticle Physics*, IOP Publishing,

- v. 2005, n. 02, p. 007–007, feb 2005. Disponível em: <<https://doi.org/10.1088/1475-7516/2005/02/007>>.
- [229] COLEMAN, S.; WEINBERG, E. Radiative corrections as the origin of spontaneous symmetry breaking. *Phys. Rev. D*, American Physical Society, v. 7, p. 1888–1910, Mar 1973. Disponível em: <<https://link.aps.org/doi/10.1103/PhysRevD.7.1888>>.
- [230] BEZRUKOV, F.; SHAPOSHNIKOV, M. The standard model higgs boson as the inflaton. *Physics Letters B*, v. 659, n. 3, p. 703–706, 2008. ISSN 0370-2693. Disponível em: <<https://www.sciencedirect.com/science/article/pii/S0370269307014128>>.
- [231] BARVINSKY, A. O.; KAMENSHCHIK, A. Y.; STAROBINSKY, A. A. Inflation scenario via the standard model higgs boson and LHC. *Journal of Cosmology and Astroparticle Physics*, IOP Publishing, v. 2008, n. 11, p. 021, nov 2008. Disponível em: <<https://doi.org/10.1088/1475-7516/2008/11/021>>.
- [232] GARCÍA-BELLIDO, J.; FIGUEROA, D. G.; RUBIO, J. Preheating in the standard model with the higgs inflaton coupled to gravity. *Phys. Rev. D*, American Physical Society, v. 79, p. 063531, Mar 2009. Disponível em: <<https://link.aps.org/doi/10.1103/PhysRevD.79.063531>>.
- [233] LINDE, A. A new inflationary universe scenario: A possible solution of the horizon, flatness, homogeneity, isotropy and primordial monopole problems. *Physics Letters B*, v. 108, n. 6, p. 389–393, 1982. ISSN 0370-2693. Disponível em: <<https://www.sciencedirect.com/science/article/pii/0370269382912199>>.
- [234] ALBRECHT, A.; STEINHARDT, P. J. Cosmology for grand unified theories with radiatively induced symmetry breaking. *Phys. Rev. Lett.*, American Physical Society, v. 48, p. 1220–1223, Apr 1982. Disponível em: <<https://link.aps.org/doi/10.1103/PhysRevLett.48.1220>>.
- [235] BARENBOIM, G.; CHUN, E. J.; LEE, H. M. Coleman–weinberg inflation in light of planck. *Physics Letters B*, v. 730, p. 81–88, 2014. ISSN 0370-2693. Disponível em: <<https://www.sciencedirect.com/science/article/pii/S0370269314000616>>.
- [236] RACIOPPI, A.; RAJASALU, J.; SELKE, K. Multiple point criticality principle and Coleman-Weinberg inflation. 9 2021.

- [237] PETER, P.; PINHO, E. J. C.; PINTO-NETO, N. Gravitational wave background in perfect fluid quantum cosmologies. *Phys. Rev. D*, American Physical Society, v. 73, p. 104017, May 2006. Disponível em: <<https://link.aps.org/doi/10.1103/PhysRevD.73.104017>>.
- [238] VITENTI, S. D. P.; PINTO-NETO, N. Large adiabatic scalar perturbations in a regular bouncing universe. *Phys. Rev. D*, American Physical Society, v. 85, p. 023524, Jan 2012. Disponível em: <<https://link.aps.org/doi/10.1103/PhysRevD.85.023524>>.